Charnockite formation in southern India

Thesis

Charnockite Formation in Southern India

A thesis submitted for the degree of Doctor of Philosophy

by

David Hart Jackson B.A. Cantab.

Department of Earth Sciences
The Open University

January 1990

EX12

HIGHER DEGREES OFFICE

LIBRARY AUTHORISATION FORM

STUDENT: DAVID JACKSON SERIAL NO: _____

DEGREE: PhD

TITLE OF THESIS: Charnockite formation in southern India

I confirm that I am willing that my thesis be made available to readers and maybe photocopied, subject to the discretion of the Librarian.

SIGNED: David M Jackson DATE: 11th Jan 1990.

Abstract

A stepped heating gas extraction technique has been developed which is capable of isolating CO_2 released by fluid inclusions from that released by contamination and other sources. In some cases specific generations of inclusions may be extracted. This technique represents a significant advance in the measurement of carbon isotopes from fluid inclusions. Isotopic results are reproducible to ± 0.2‰ for gas-rich samples, but sample heterogeneity results in variable yield measurements (occasionally up to 200%).

The technique has been applied to charnockites and related rocks from South India to constrain the role of CO_2 in their petrogenesis. Results from a data base of 65 samples show that charnockites released more inclusion-CO_2 than did associated amphibolite facies gneisses, implying that CO_2 plays a significant role in charnockite formation.

Field observations and theoretical phase equilibria, suggest incipient charnockites (partially transformed gneiss) form by sub-solidus transformation (induced by influx of CO_2) and by melting (triggered by influx of mixed CO_2-H_2O). This melting reaction occurs at least 50°C below vapour-absent melting, so it may be an important mechanism for granulite and granite formation in the middle and lower crust. Massive charnockites (monotonous granulite) are believed to form mainly by direct crystallisation from a H_2O-poor, CO_2-rich melt.

$\delta^{13}C$ values support radiogenic and field evidence for at least two charnockite formation events in South India. The 2500 Ga event at the southern margin of the Archæan craton yields a range of $\delta^{13}C$ values (-4‰ to -13‰), tentatively interpreted as CO_2 derived from subducting sediments. The younger event (500 Ma) affects the southern blocks (of probable early Proterozoic age), and is characterised by a bimodal distribution of $\delta^{13}C$ values (-6‰ to -7‰ and -9‰ to -13‰). A sub-continental lithospheric source of CO_2 (transported by magmas associated with crustal extension) is suggested by the heavier values. The lighter isotopes result mainly from mixing between this mantle source and organic graphite, but inclusion capture during an earlier event cannot be ruled out in a few cases.

CO_2-rich fluids are found to propagate by advective fluid flow through a micro-hydraulic fracture mechanism. A detailed case study of local charnockite formation indicates that isotope and reaction fronts are diffuse, almost over the entire distance of fluid flow (60 m), and fluid/rock disequilibrium suggests that fluid-rock ratios must be treated with care.

Acknowledgements

I would like to thank the following for their help during this project:

Drs. Nigel Harris and Dave Mattey for initiating the project, excellent supervision in the field, lab., swimming pool, Stannage and other obscure locations.

Dr. M, Santosh for friendship and assistance both in the field and in Milton Keynes, for constant bullying and complete silence and for regular surprises by imaginative geopolitical manoeuvring.

Dr. S. Jayaram for help in the field, and to his family for limitless hospitality and curry.

Drs. Subramanian and Annamalai for assistance in the field.

Prof. K. Burke and Dr. K.V. (K-man) Krishnamurthy for turning a short-sighted eye at my crashing the Indo-US field symposium (1988).

The participants of the Indo-US field symposium (1988) for many helpful discussions, particularly Dave Pattison and Don Elsenheimer for lightening many long hours in the car.

Dr. C.T. Pillinger for use of laboratory facilities.

Monica Grady and Stuart Boyd for averting a number of disasters in the lab.

Nick Brough for assistance with probe analyses.

Andy Tindle, Dave Ormerod, Eira Parker and many others who have given advice on Macintosh usage.

Ian Chaplin *et al.* for thin section preparation.

Nigel Harris, Dave Mattey and Simon Inger for reviewing parts of this thesis.

El boys for using my unofficial taxi service, Tim for curries and smiles, Ma Davis for organisation and Monty Crear for constant reassurance that my thesis could not have been as much of a 'mare as his.

Janet for the cake.

My parents and family for their encouragement and support throughout this work and welcoming me home regularly with love and food.

Juliette for fun, friendship, distraction and support over the last 15 months and for beating me by 4 days!

CONTENTS

LIST OF FIGURES

LIST OF TABLES

LIST OF PLATES

Chapter 1

INTRODUCTION

"...I expect that the underplating mechanism, combined with partial-fusion reactions in the absence of fluids, will turn out to be a principal factor in granulite-facies metamorphism, growth and differentiation of the crust, and the origin of upper-crustal granitic rocks. In an even broader context, I believe that core-mantle boundary instabilities, mantle plumes, anomalous conductivity in the lower crust, continental rifting, flood basalt outpourings and major biological events will all eventually come to be linked with these lower crustal processes, operating on supracrustal rocks, in the same complex, discontinuous chain of events."

J.D.Clemens 16/11/89 (Nature).

1.1 THE GRANULITE FACIES

Charnockites, which are defined as 'orthopyroxene (hypersthene)-bearing rocks of broadly granitic chemistry' (Holland, 1900) form an integral part of many regional granulite facies terrains. In this thesis the term 'granulite' is simply used to describe any rock classed in the granulite facies. This definition is based on mineralogy rather than texture, but most fresh granulites preserve equidimensional, polygonal grains of all mineral species. Mineral assemblages from granulite facies rocks record temperatures of formation above 700°C over a wide range of pressures (5-12 kbars) (Harley, 1989). Although these pressures are consistent with granulite formation in the middle and lower continental crust, the stable crustal geotherm suggests temperatures of only 500°C - 600°C at the base of continental crust (Clark and Ringwood, 1964). This implies that recent granulites must have formed in tectonically active areas with additional heat input.

The majority of granulites exposed at the surface are in Precambrian shield areas, but some smaller young terrains are exposed by tectonic uplift on large faults or shear zones. Based on this distribution, it could be speculated that heat flow was higher in the Archæan and granulites were stable at the base of inactive crust. During the Archæan, when the majority of the continental crust may have been accreted (Taylor and McLennan, 1985), high radiogenic heat production would have enhanced melting of new continental crust and its re-entrainment into a rapidly convecting mantle. Stabilisation of the continental crust required rapid removal of heat-producing elements upwards by intracrustal differentiation. This differentiation would produce a refractory lower crust of granulite assemblages which may have been effective in limiting crustal resorption.

Traditionally zones of continent-continent collision have been considered the principal environments for granulite formation, but more recently both zones of continental extension (Sandiford and Powell, 1986) and continental arcs (Bohlen, 1987) have been suggested as alternatives. 'Arrested' mineral reactions sometimes permit construction of pressure-temperature-time (P-T-t) paths for metamorphic events. These paths do not uniquely characterise the tectonic setting, but have provided evidence from a variety of granulite terrains for formation in all three tectonic environments (Harley, 1989). Although constraining the tectonic environment of granulite formation is an interesting problem, this thesis is primarily concerned with the mechanism of granulite (and in particular charnockite) formation.

Assemblages in the amphibolite and granulite facies can co-exist at identical conditions of pressure and temperature (Janardhan *et al.* 1979), hence an increase in temperature alone may not be the major cause of stabilisation of granulite assemblages. The fundamental difference is that the ferro-magnesium minerals in amphibolite facies assemblages are hydrous (*eg.* biotite and/or hornblende) whereas those in granulites are anhydrous (*eg.* orthopyroxene and garnet). Although it has been known for sometime

that rocks of the granulite facies form under conditions of low water activity (Eskola, 1920), the identification of mechanisms responsible for the lowering of the water activity has been the subject of vigorous debate over recent years.

1.2 MECHANISMS OF GRANULITE FORMATION

Granulite facies metamorphism is not simply a culmination of increasing temperature, because mica and amphibole dehydration reactions intersect hydrous melting curves at low temperatures (650 - 700°C), so under conditions of granulite formation they are metastable with respect to melting (see Chapter 2 for a discussion of pertinent phase relations). In order to stabilise granulite assemblages the water activity in the system must be lowered and melting reactions inhibited. Three mechanisms have been suggested which may cause such a lowering of water activities in granulite facies environments:

1) Vapour-absent metamorphism: It has been suggested that metamorphism of already anhydrous rocks, in the absence of a fluid phase, will result in granulite facies assemblages (*eg.* Lamb and Valley, 1984).

2) Removal of water by extraction of a hydrous partial melt: This model proposes that formation of a partial melt within a rock (Fyfe, 1973) or passage of dry melts through the crust (Frost and Frost, 1987) will absorb pore water and lower water activities causing hydrous mineral breakdown.

3) Flushing with non-aqueous fluids: The water activity is lowered by dilution with a second fluid component, usually argued to be CO_2 (Newton *et al.* 1980).

Although the first of these models may be volumetrically important in the lower crust, where magmatic or polymetamorphic rocks will be anhydrous prior to

metamorphism, it does not help explain how previously hydrous rocks and supracrustal lithologies become granulite assemblages. Vapour-absent metamorphism can only result in transformation of assemblages from the amphibolite to the granulite facies if temperatures are sufficiently high for vapour-absent melting to occur, in which case mechanism (2) is also involved. Although field and geochemical evidence in support of each of these processes has been documented from different granulite terrains the relative importance of each mechanism remains uncertain. There is, however, general agreement that granulite production is inextricably bound up with fluid behaviour and closely linked to melting processes.

1.3 CHARNOCKITES: IGNEOUS OR METAMORPHIC?

The formation of charnockites may provide important constraints in trying to unravel the mechanisms involved in granulite formation, because their granitic and often undepleted chemistry, which is more akin to the melt fraction rather than the restite, precludes their formation by removal of a hydrous partial melt. Holland (1900)[1] described charnockites (with some reservation) as igneous rocks. This classification was widely believed until the beginning of this decade when subsolidus charnockite formation induced by massive influx of CO_2-rich fluids was advocated (Janardhan *et al.* 1979) and subsequently extended to granulites as a whole (Newton *et al.* 1980). This model was largely based on two pieces of evidence:

(1) The common occurrence of CO_2-rich fluid inclusions in granulite facies rocks and their absence from equivalent amphibolite facies rocks (Touret, 1971 and Hansen *et al.* 1984).

---

[1] Sir Thomas Holland coined the term "charnockite" after being shown the mausoleum of Mr. Job Charnock, an agent of the East India Company, who was buried in St. John's Church, Calcutta in 1692. Holland (a true geologist) was struck by the bizarre appearance and mineralogy of the tombstone, which was similar to the hypersthene-bearing rocks he was surveying at that time in Madras State. Holland named the rock "charnockite" in honour of the man said to be one of the founders of Calcutta. (Pichamuthu, 1972). Indian geologists are very proud of this tradition and regularly term any orthopyroxene-bearing rock "charnockite", so caution is required when studying the literature.

(2) Field evidence preserved in South India of structurally controlled charnockite forming in amphibolite gneiss, (on a centimeter scale) with no intrusive contacts and ghost gneissic foliation preserved (Pichamuthu, 1960). (These structures are termed 'incipient charnockites' in this thesis, in contrast with large areas (kilometer scale) of monotonous charnockite which are termed 'massive charnockites' see Chapter 3.)

More recently, calculations based on He fluxes have argued that insufficient carbon is released from the mantle to cause dehydration of the lower crust on a regional scale (O'Nions and Oxburgh, 1988). This, combined with the realisation that metamorphic rocks need not have a pore fluid, has moved opinion in favour of granulite formation in many terrains by partial melting under vapour-absent conditions. Where charnockites occur in such areas they are thought to be intrusive prior to or during the granulite facies event (*eg*. Valley and O'Neil, 1984). Nevertheless abundant CO_2 inclusions have been identified in charnockite bodies thought to have an igneous origin (*eg*. Konnerup-Madsen, 1979). These have been described as both solidus vapour phases (Konnerup-Madsen, 1979) and as forming much later during retrogression (Lamb *et al.* 1987).

Experimental petrology studies have shown that in liquids of granitic composition orthopyroxene is only a stable liquidus phase when low water contents (< 7 wt%) are present. Orthopyroxene (the diagnostic mafic mineral in charnockites) is not however a stable solidus phase even down to a_{H_2O} < 0.5 wt%, so in most plutonic rocks it is completely replaced by biotite or hornblende and is not observed (Naney, 1983). In order to stabilise orthopyroxene as a solidus phase CO_2 must be added to the system (Grant, 1986). In the presence of pure CO_2 complete crystallisation of a granitic magma will occur above 1000°C (Wendlandt, 1981) with orthopyroxene as the only ferro-magnesium phase. If the liquid co-exists with a mixed CO_2-H_2O vapour phase the solidus will be considerably lowered (to below 800°C) and the water component will preferentially dissolve in the liquid. Orthopyroxene and biotite will be the ferro-

magnesium solidus phases, their relative abundances dependent on the vapour phase composition (Grant, 1986).

1.4 AIMS OF THIS THESIS

Whether formation is a super- or sub-solidus process, CO_2 appears to be a critical variable which may determine the stability of charnockite assemblages. This study aims to evaluate the role of CO_2 in charnockite formation. Such an investigation is timely for two reasons:

(1) Recent theoretical advances and experimental results have provided new evidence pertaining to charnockite formation (*eg*. Peterson and Newton, 1989).

(2) Advances in hardware development and experimental techniques for analysing the stable isotopic composition of small samples may be applied to gas (CO_2) released from fluid inclusions. The sample size (100 mg of host mineral) allows dramatically increased sample control.

South India has been selected as a field area because the excellent quarry exposures allow the careful sample control required by this study. Field, petrological and geochemical studies which have already been accomplished (including an extensive reconnaissance study from the Open University) in selected areas of southern India, provide a good background for this more specialised study.

This thesis concentrates on the exceptionally preserved incipient charnockite formations, but due to their intimate temporal and spacial relationship the massive charnockites (which are volumetrically much more extensive) form an integral part of the study. Four principal aims have been identified for this thesis:

(1) Re-evaluation of possible mechanisms of charnockite formation in the light of recently published experimental data.

(2) Development of a stepped heating technique to release the contents of fluid inclusions for stable isotopic analysis.

(3) Application of the carbon isotope data obtained by this technique to evaluate the source of CO_2 and hence constrain possible mechanisms of charnockite formation.

(4) Investigation of the mechanism of movement of CO_2-rich fluids through high grade metamorphic lithologies using carbon isotopic compositions as a tracer.

During the progress of this study ideas have developed rapidly both in favour of and against influx of CO_2 and several long-standing myths have been dispelled. The final aim is to synthesise, from these developing ideas and the data presented in this thesis, a model for charnockite formation in South India.

Chapter 2

PHASE EQUILIBRIA STUDIES

2.1 INTRODUCTION

The equilibrium mineral assemblage present in a rock of given composition depends on the ambient pressure, temperature and activities of the fluid components. The pressure is a linear function of the depth of burial. Although the temperature is generally controlled by the regional heat flow and internal heat production, it can be buffered for short periods by endothermic mineral reactions. Both are externally buffered variables. The water activity can either be internally buffered, by mineral assemblages of coexisting hydrous and anhydrous phases, or, provided there is a sufficiently large reservoir, externally buffered, by a continual fluid influx from elsewhere. In unmetamorphosed or low grade metasediments near the surface it is easy to envisage such a reservoir but under amphibolite and granulite facies conditions it has been argued that (except locally) the water activity will be internally buffered (*eg*. Waters, 1988).

Mineral equilibrium reactions can be illustrated in pressure-temperature-water activity (P-T-a_{H_2O}) space. Fortunately there is a low mineral diversity in both the amphibolite gneisses and charnockites hence the number of relevant reactions is small and such plots are simple. In contrast the number of possible mineral reactions in the metapelite system can make such diagrams difficult to use (*eg*. Vielzeuf and Holloway, 1988). Despite the paucity of reactions, visualisation of the three dimensional system can be confusing, so projections on to P-T and T-a_{H_2O} planes are used for simplification.

It is of vital importance to distinguish between fluid-present and fluid-absent conditions. Fluid-present conditions occur when there is a continuous inter-connected

pore fluid with the fluid pressure equal to the lithostatic pressure, if these conditions are not met fluid-absent conditions exist. Thompson (1983) has argued that most metamorphic rocks at high grades, except those undergoing devolatilisation reactions, are unlikely to have a free fluid phase. Nevertheless both fluid-present and fluid-absent conditions will be discussed below.

The system of reactions relevant to charnockite formation are plotted in P-T-a_{H_2O} space for the potassium-magnesium-aluminium-silica-water-carbon dioxide (KMASH(CO_2)) system within the constraints of published experimental petrology data. KMASH(CO_2) has been adopted because the largest volume of experimental and most precisely constrained thermodynamic data exist for this system. In this discussion the solubility of CO_2 in granitic liquids is assumed to be negligible. The variety of models which have been proposed for charnockite formation are considered in the light of these phase constraints.

2.2 EXPERIMENTAL CONSTRAINTS ON PHASE EQUILIBRIA

2.2.1 Introduction

The reactions involving phases enstatite (en), phlogopite (ph), quartz (q), sanidine (Ksp), melt (l) and vapour (v) (considered to be a mixture of CO_2-H_2O with non-ideal behaviour (after Holloway, 1977)) are illustrated in P-T space (Figure 2.1). Of these reactions the most important to this discussion are the water saturated solidus [en], the vapour-absent melting reaction [v] and the subsolidus dehydration reaction [l]. [Ksp] has been experimentally determined (Bohlen *et al.* 1983 and Peterson and Newton, 1989a) but it is found to occur at higher temperatures than [en]. Hence under fluid-present conditions the rock will be buffered on [en] and will not usually reach [Ksp].

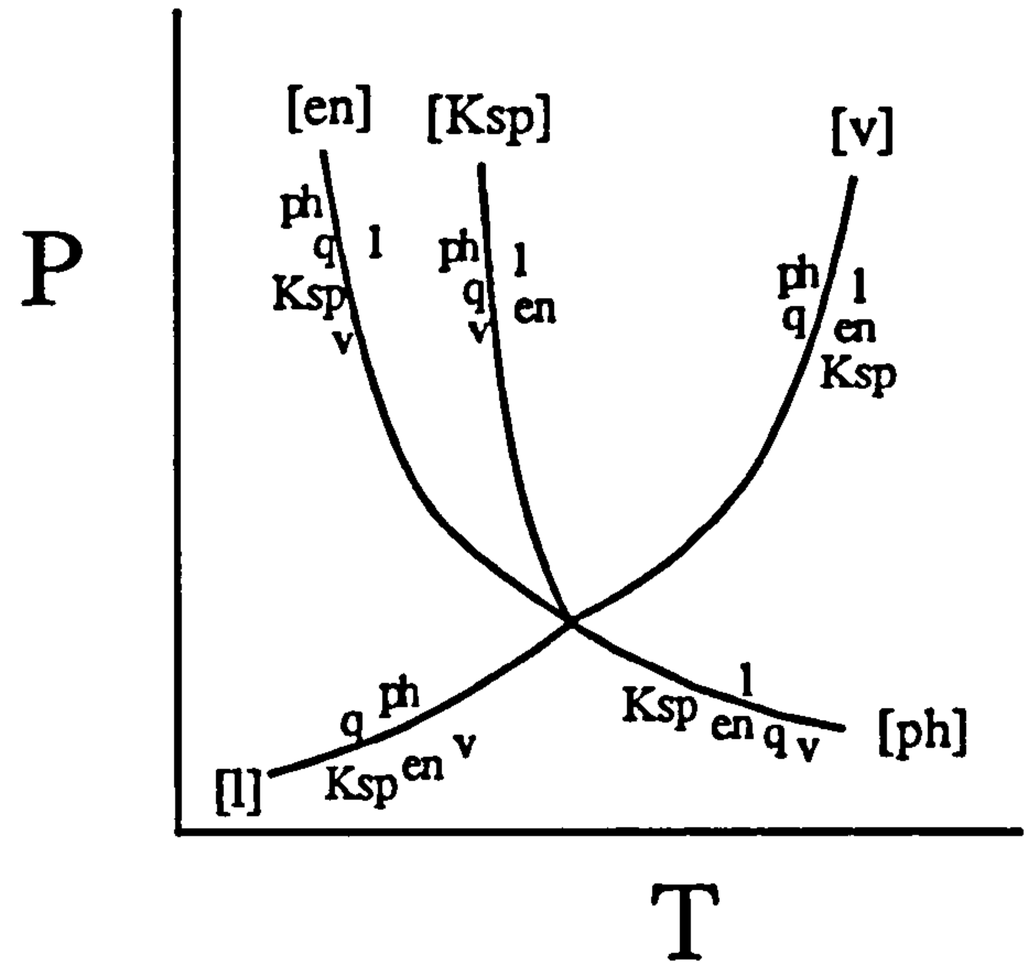

Figure 2.1. Schematic P-T plot showing relative positions of the reactions pertinent to charnockite formation in the KMASH system.

The role of K-feldspar in the fluid-absent melting reaction is uncertain. Peterson and Newton (1989a) distinguish a [v] (Ksp + ph + q = en + l) reaction from a [Ksp,v] (ph + q = en + l) reaction, using their experimental determinations the positions of the two curves are however indistinguishable, suggesting that the two reactions may be identical with K-feldspar not required as a reactant. Although Grant (1986) separates the two reactions at pressures below 4 kb and combines them into the [v] reaction (Figure 2.1) above this pressure, the following discussion of Wendlandt's (1981) experiments conclude that the thermal divide is invalid. Hence the [v] reaction q + ph = Ksp + en + l used in this discussion is the same as that measured by Bohlen *et al.* (1983) and preferred by Vielzeuf and Holloway (1988).

2.2.2 Vapour-absent conditions

Under vapour-absent conditions, the vapour phase is unavailable as a reactant (Figure 2.2). The subsolidus dehydration curve [l] has been experimentally determined by Wood (1976) and Peterson and Newton (1989a), these two estimates are in close agreement. The invariant point has been constrained experimentally to ± 25 bars and

±10°C (Wones and Dodge, 1977 and Peterson and Newton, 1989a). The [ph] curve is shown to emphasize the invariant point, but it is neither experimentally constrained nor strictly relevant to vapour-absent systems.

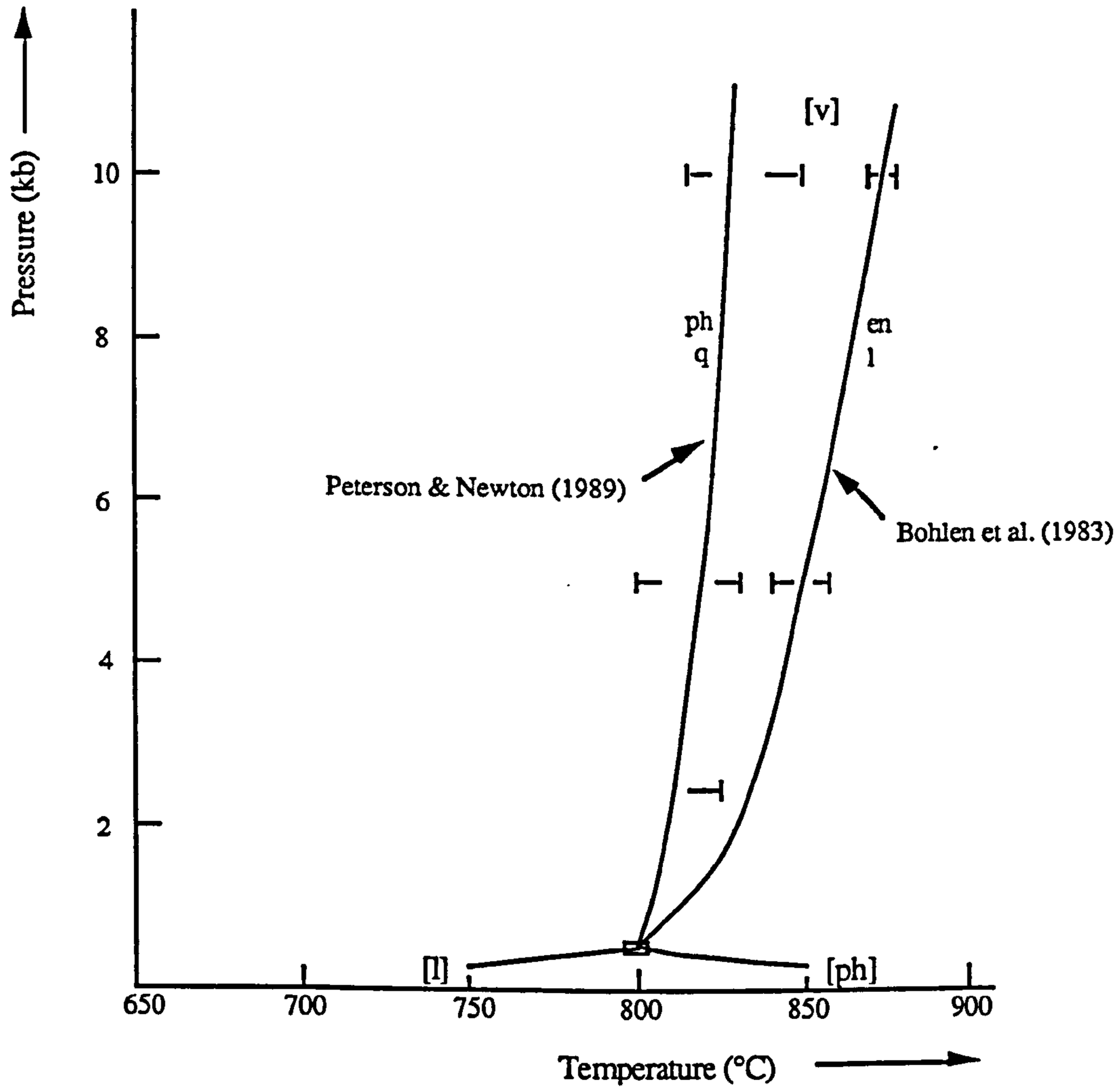

Figure 2.2. P-T section showing reactions in the KMAS system, constrained by experimental data from Wood, (1976), Wones and Dodge, (1977), Bohlen *et al.* (1983) and Peterson and Newton, (1989a).

The position of [v] is clearly the most important for high grade metamorphic rocks and it has been argued that reactions of this type that are most likely to dominate granite production in the lower crust (Clemens and Vielzeuf, 1987). Unfortunately the two attempts to constrain its position have yielded results differing by 30°C at 5 kb and about 50°C at 10 kb (Bohlen *et al.* 1983 and Peterson and Newton, 1989a). The latter authors attempted to explain their lower temperatures in terms of the effect of H_2 on the charge;

Bohlen *et al.* carried out their experiments with the reaction capsule surrounded by a jacket of hæmatite to ensure low f_{H_2}, whilst Peterson and Newton employed no such buffer. Luth and Boettcher (1986) conclude that the addition of H_2 to the water-saturated system will increase the solidus temperature, but this appears to be of little relevance to the vapour-absent system. Peterson and Newton (1989a) carried out control experiments with the hydrogen fugacity buffered, but found that changing f_{H_2} between 10^{-1} and 10^{2} had no perceptable effect on the temperature of the vapour-absent melting reaction. The temperature discrepancy in the results remains unresolved so both determinations have been plotted on Figure 2.2. Moreover at pressures typical of low pressure granulite formation (5 ± 1 kb), the difference between the two determinations (30°C) is smaller than the error involved with temperature estimates using Fe-Mg exchange geothermometry (± 50°C), so the experimental difference is not crucial. For high pressure granulites (P ≥ 10 kb) this experimental uncertainty is more significant.

2.2.3 Vapour-present conditions

In the vapour-present system an extra variable (a_{H_2O}) is introduced, which is controlled directly by the composition of the pore fluid (X_{H_2O}) when present. a_{H_2O} is also defined in the absence of a pore fluid by equilibrium mineral assemblages in which vapour is consumed or released. The phase equilibria diagram can be extended to P-T-a_{H_2O} space in the vapour-present system, but has been simplified to a T-a_{H_2O} plot at a constant pressure of 5 kb for this discussion (Figure 2.3).

No experimental determinations of the minimum melting curves [en] and [ph] have been made, hence its position is estimated from the data of Keppler, (1989), Peterson and Newton, (1989b) and Wendlandt, (1981). The brackets (1), taken from experimental results for the haplogranite-H_2O-CO_2 (KNASH-CO_2) system (Keppler,

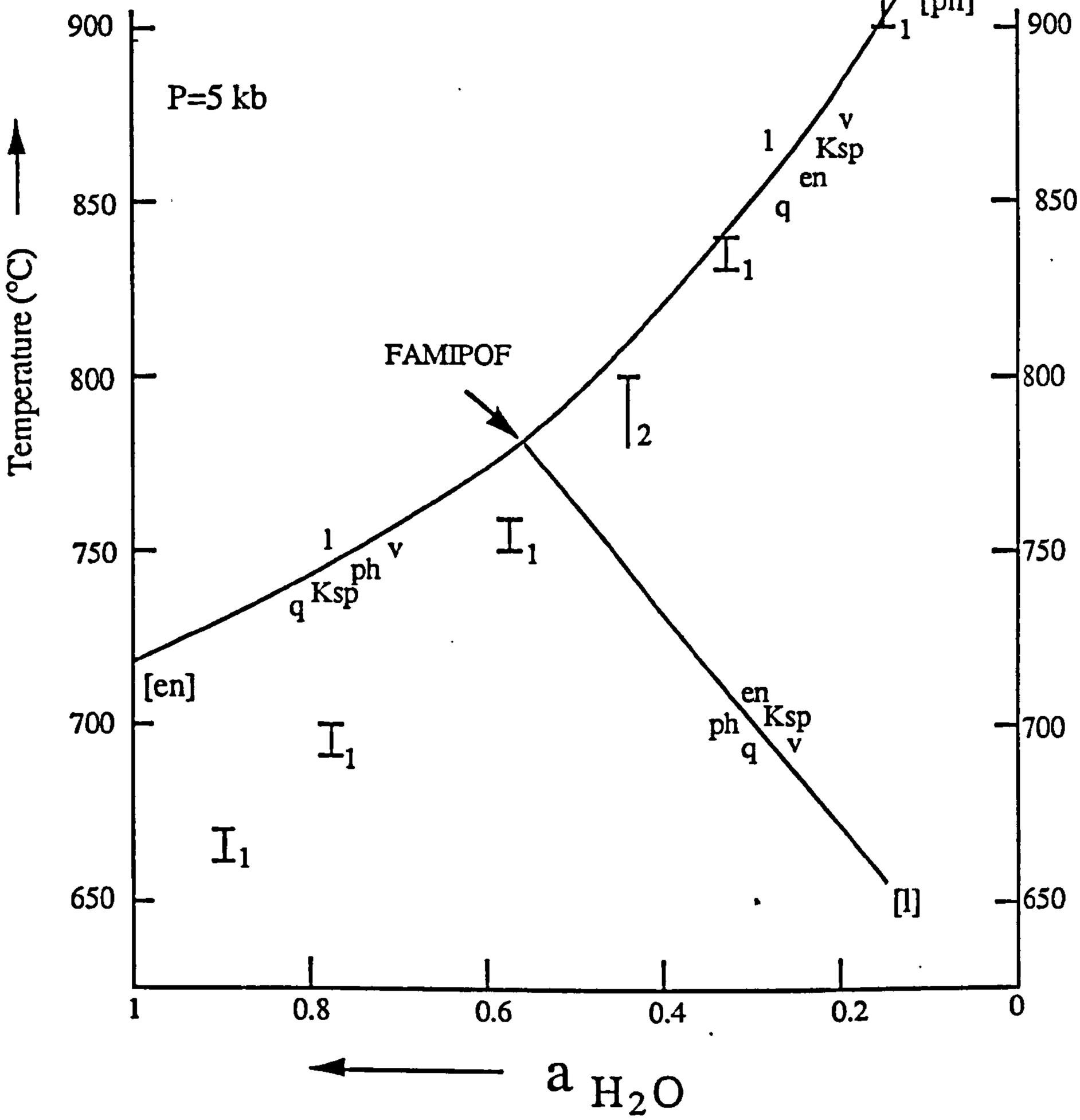

Figure 2.3. T-a_{H_2O} section (at 5 kb) illustrating the vapour-present melting and subsolidus reactions pertinent to charnockite formation in the KMASH-CO_2 system. The solidus curves are constructed from experimental data in [1]Keppler (1989), [2]Bohlen *et al.* (1983), Wendlandt (1981), Peterson and Newton (1989a) and the dehydration reaction is taken from the self-consistent database of Powell and Holland (1985a and b). See text for definition of FAMIPOF.

1989) are thought to provide minimum constraints on the [en] and [ph] curves (because sodium will reduce melting temperatures more than magnesium). In the KMASH-CO_2 system the [en] and [ph] melting curves have been experimentally determined for the pure H_2O and CO_2 endmembers at 720°C (Peterson and Newton, 1989b) and 980°C (Wendlandt, 1981) respectively. A further minimum constraint is applied by the experimental subsolidus determination of Bohlen *et al.* (1983) in the KMASH-CO_2

system. The subsolidus dehydration reaction [l] is calculated using the self-consistent data set of Powell and Holland (1985a and b). The only experimental constraint on this curve is from Bohlen *et al.* (1983) who give a bracket of 780 - 800°C for 5 kb and a_{H_2O} = 0.35, but from the available data (traces of reactions products are seen in the 780°C run) this bracket is strictly only a maximum temperature estimate.

The reaction at the invariant point (ph + q = l + en + Ksp) is the same as the [v] curve in Figure 2.1 and although the reaction occurs in the vapour-present system the vapour phase does not take part. The reaction has been termed vapour-absent melting (Clemens and Wall, 1981) and dehydration melting (Thompson, 1983). Both these terms are considered confusing; the former should only be applied to true vapour-absent conditions, whilst the latter implies a two stage process with the intermediate presence of a fluid phase. The term vapour-absent melting is preferred here for reaction [v] under vapour-absent conditions, but the coexistence of six phases at the invariant point only occurs if the water activity is internally buffered. Since this implies the presence of a free fluid phase, the term fluid-absent melting in the presence of fluid (FAMIPOF) is proposed.

The locus of the invariant point through P-T-a_{H_2O} space defines a line which is the minimum pressure and temperature at which the 'FAMIPOF' reaction is encountered for a given a_{H_2O}. The geometry of this line has been theoretically estimated by Clemens and Vielzeuf (1987). Experimental studies also place constraints on the location of this line (Wendlandt, 1981 and Peterson and Newton, 1989b). Both sets of experiments start with quartz, phlogopite ± sanidine and normally 50 wt% of a fluid of composition X_{H_2O} = 0.5. The reactions that occur in these experiments are easily interpreted with reference to Figure 2.3. The invariant point at low (≤ 6 kb) pressures is located at X_{H_2O} higher than 0.5, hence the first reaction encountered by the charge is [l] where enstatite forms at the expense of phlogopite. As the temperature is increased the fluid composition is buffered along [l] until the invariant point reached, when the FAMIPOF reaction occurs

and a melt phase is formed. The temperature constraints on this first appearance of melt have been measured at 2.5 kb, 3.5 kb and 6 kb by Peterson and Newton (1989b) and at 3 kb and 8 kb by Wendlandt (1981). Peterson and Newton (1989b) also report the fluid composition at the end of each run, from which it should be possible to constrain the P-T-a_{H_2O} variation of the invariant point. Unfortunately the results are variable; the lack of a hydrogen buffer may result in reduction of some of the CO_2 in the fluid, so these results are considered unreliable. From the heating paths recorded by the solid assemblages the invariant point is constrained to lie at $X_{H_2O} > 0.5$ up to at least 6 kb.

Figure 2.4 shows the line produced by joining the locii of the invariant points in P-T space for various water activities, the experimental data show a significant bending of this curve to lower temperatures above 2 kb. Also plotted are the phase relations for $a_{H_2O} = 1$ and [v] for vapour-absent conditions (dotted).

The identification of the 'FAMIPOF' reaction provides a reasonable interpretation of the experimental results without the need to speculate about Mg and CO_2 forming complexes to reduce the solidus temperatures (Newton and Peterson, 1989b). One important implication of Figure 2.4 which is particularly significant for subsequent discussions of charnockite formation, is that an influx of a small quantity of CO_2 into a vapour-absent biotite gneiss located between 760°C and 810°C at 5 kb can induce melting (see discussion below).

2.3 EFFECT OF OTHER COMPONENTS

The addition of other components to the KMASH-CO_2 system may effect the position of the phase equilibria in the ways discussed below. Addition of Fe, which partitions preferentially into orthopyroxene compared to biotite (*eg*. Janardhan *et al.*

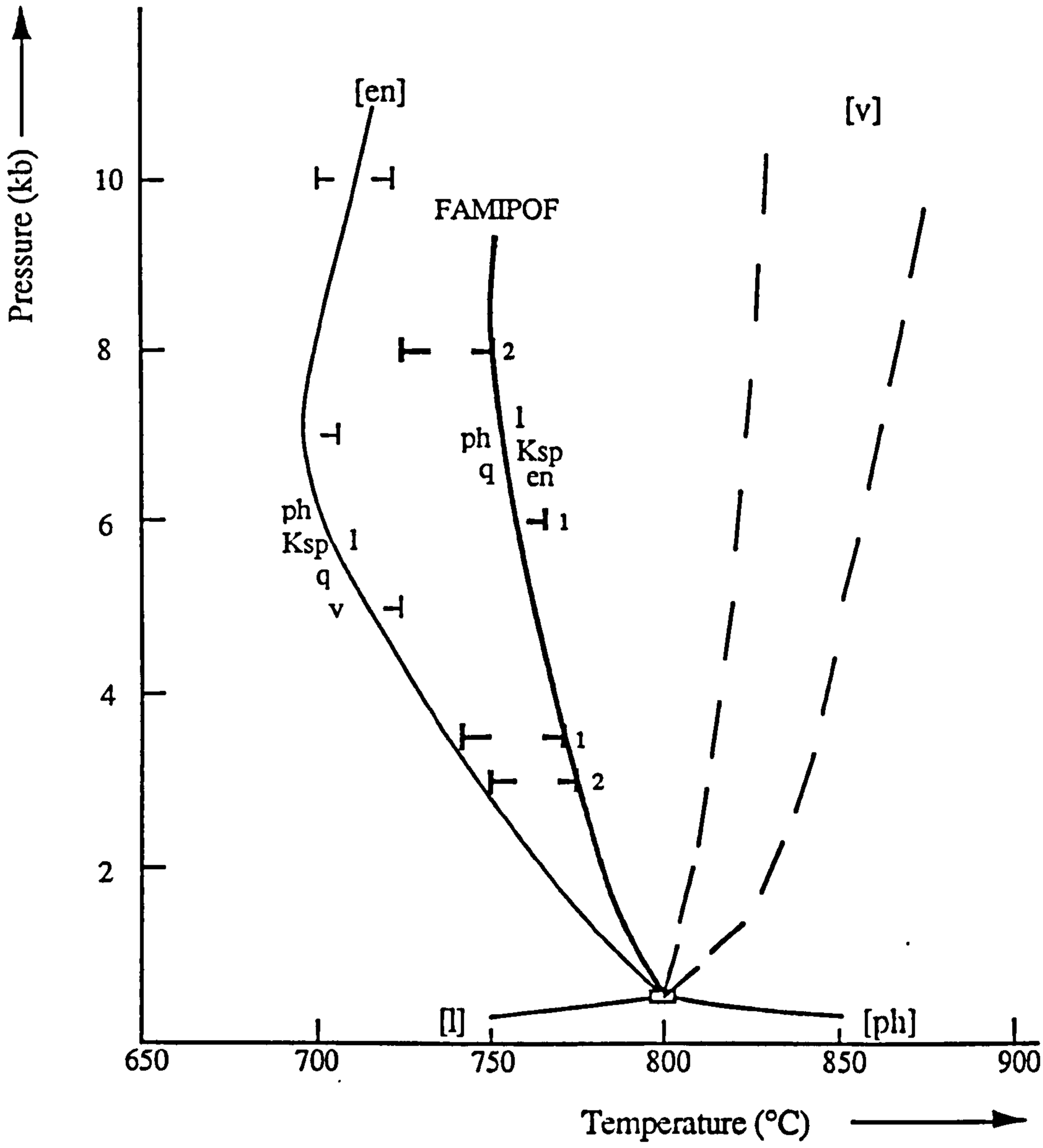

Figure 2.4. P-T section illustrating the position of the water-saturated solidus (data from Peterson and Newton, 1989a) and the locii of the invariant point (FAMIPOF) reaction for different water activities. The constraints on the FAMIPOF line are from (1) Peterson and Newton (1989b) and (2) Wendlandt (1981).

1982 and Grant, 1981), will expand the orthopyroxene stability field and displace the subsolidus [I] reaction to lower temperatures and higher water activities. This effect is illustrated in Figure 2.5 where the [I] reaction has been plotted for $X_{Mg(opx)} = 1.0, 0.6$ and 0.4 taken from Powell and Holland (1985a and b). Towards Fe-rich compositions the thermodynamic data become poorly constrained and the curves leśs accurate. In addition Fe is enriched relative to Mg in a melt phase thus displacing both vapour-

present and vapour-absent solidi to lower temperatures (MacRae and Nesbitt, 1980).

In contrast to this effect substitution of F and Ti into biotite increases its thermal stability and raises the solidus temperatures (*eg*. Valley *et al.* 1982 and Forbes and Flowers, 1978). Since neither of these elements are accepted into the orthopyroxene structure to any significant level, their presence will increase the phlogopite stability field inhibiting charnockite formation. Addition of plagioclase (Ca and Na) will have limited effect on subsolidus dehydration, but is likely to lower the solidi towards those plotted (Figure 2.3) for the haplogranite system (Keppler, 1989).

So far only reactions for a biotite gneiss have been considered. In some charnockite localities from southern India hornblende breakdown is also a charnockite-producing reaction (Janardhan *et al.* 1979). This reaction appears to occur at either lower temperature or higher a_{H_2O} than the biotite breakdown for some bulk compositions. Srikantappa *et al.* (1985) document the coexistence of biotite-bearing Al-poor compositions in which hornblende has been replaced by orthopyroxene, with more Al-rich rocks which are stable as biotite gneisses. Experimental determinations of the vapour-absent melting reaction for hornblende-bearing gneisses show that melting occurs 170°C higher than for biotite (and 80°C higher than for phlogopite) (at 5 kb) (Brown and Fyfe, 1970). No experimental determinations of melting or subsolidus dehydration curves are available for hornblende gneisses. The vapour-present melting curve is likely to be displaced to higher temperatures due to the lower solubility of Ca than K in granitic liquids. Determinations of the hornblende subsolidus dehydration curve, using analyses from Kabbaldurga quarry (Hansen *et al.* 1987) and the data base of Powell and Holland (1985a and b), suggest that hornblende breakdown will occur at higher water activities than biotite. Further evidence comes from crystallisation experiments, which show that stabilisation of hornblende over biotite requires higher water contents in the liquid (Naney, 1983).

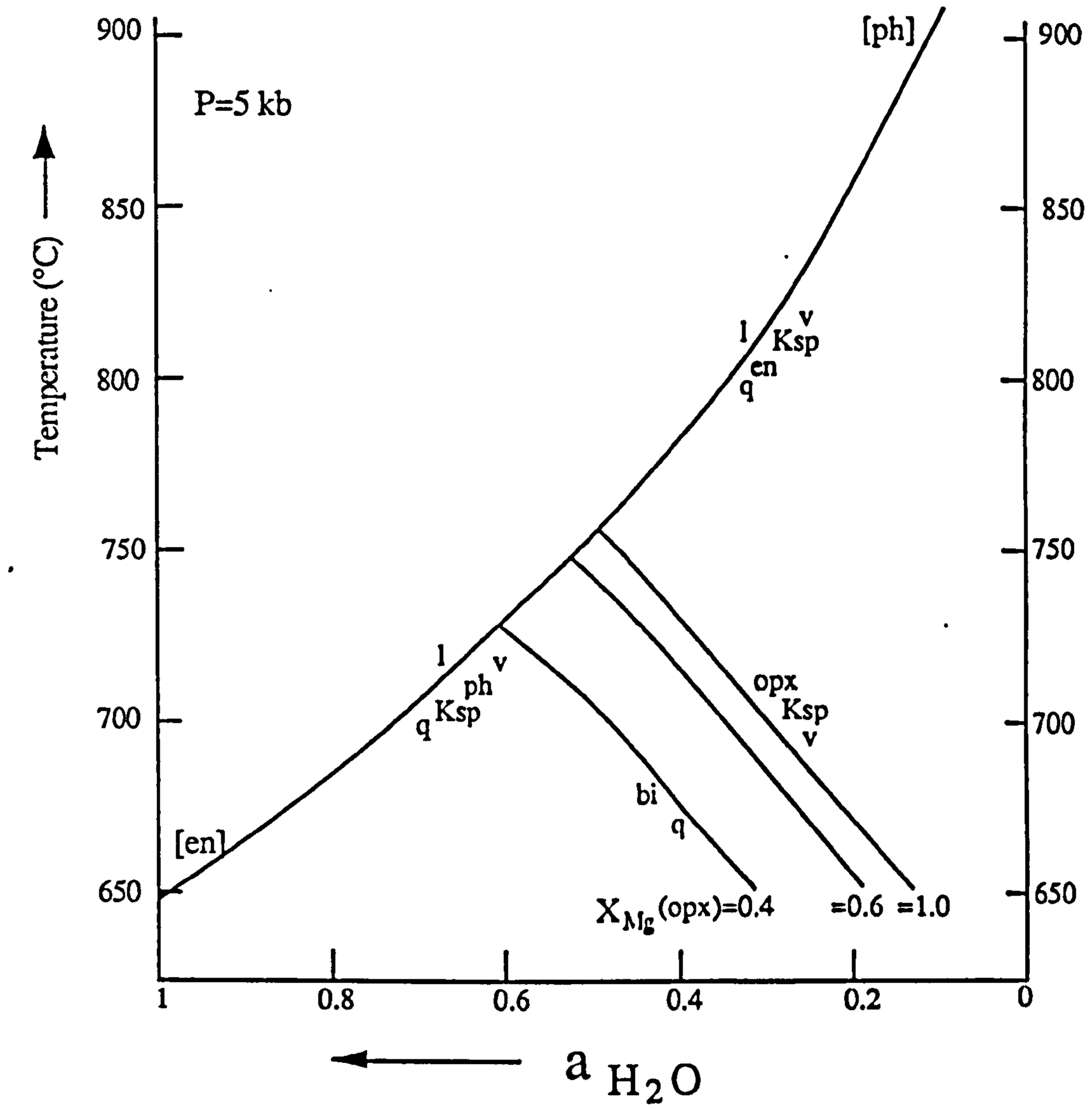

Figure 2.5. T-a_{H_2O} (5 kb) plot (after Figure 2.2) illustrating the effect on the subsolidus reaction of the addition of Fe, data taken from the self-consistent data base of Powell and Holland (1985a and b).

2.4 CHARNOCKITE FORMATION

2.4.1 Vapour-absent conditions

Figures 2.6a and b are duplicates of Figures 2.2 and 2.3 plotted to illustrate the different pressure-temperature-time (P-T-t) trajectories capable of producing charnockite assemblages. Figure 2.6a is initially considered in the vapour-absent system. Path (A1) is an isobaric heating path below the pressure of the invariant point. The first

reaction encountered along path (A1) is the subsolidus dehydration (charnockite-forming) reaction [l] and the granulite assemblage formed will be stable until the anhydrous melting curve is intersected. If path (A2) is followed the hydrated assemblage is stable until the vapour-absent melting curve [v] is encountered. This reaction will produce a melt and an anhydrous solid phase assemblage, so removal of the melt phase will leave a granulite assemblage (*eg*. Fyfe, 1973). Alternatively if the back-reaction is inhibited during recrystallisation, with no melt loss, a charnockite assemblage will result (Waters, 1988). Path (A3) is an isothermal decompression trajectory which cuts [l] and results in charnockite formation. Path (A1) is only capable of producing pyroxene hornfels and path (A3) is not followed by any normal metamorphic P-T-t paths. Path (A2) is the only one likely to produce a charnockite assemblage, but is not encountered until 790°C (Peterson and Newton, 1989a) or 850°C (Bohlen *et al*. 1983) at 5 kb.

2.4.2 Vapour-absent to vapour-present conditions

A vapour-absent biotite gneiss is stable until curve [v] is encountered, at 50 - 90°C above the FAMIPOF curve for pressures of 5 kb (Figure 2.4). Influx of a small quantity of fluid will then cause melting. This is illustrated in Figure 2.6b for a temperature of 780°C at 5 kb pressure. If the influxing fluid has a higher water activity than that of point B ($a^{B}_{H_2O}$), then on influx, the assemblage will appear in the melt stability field and melting will occur. This process may be important in melt genesis, but enstatite will not be produced and a charnockite assemblage will not result. If on the other hand the fluid has $a_{H_2O} < a^{B}_{H_2O}$ then the assemblage will appear in the enstatite stability field (in the case of pure CO_2 at point A). A sufficient fluid reservoir will transform all the phlogopite by the [l] reaction to enstatite and no melting will occur. If the fluid source is exhausted, leaving only the volume of pore fluid in the rock, the system becomes closed, the water activity will evolve to $a^{B}_{H_2O}$ and melting will occur.

The assemblage present when melting starts is already dominantly charnockitic, so charnockite is essentially formed by solid-state reaction.

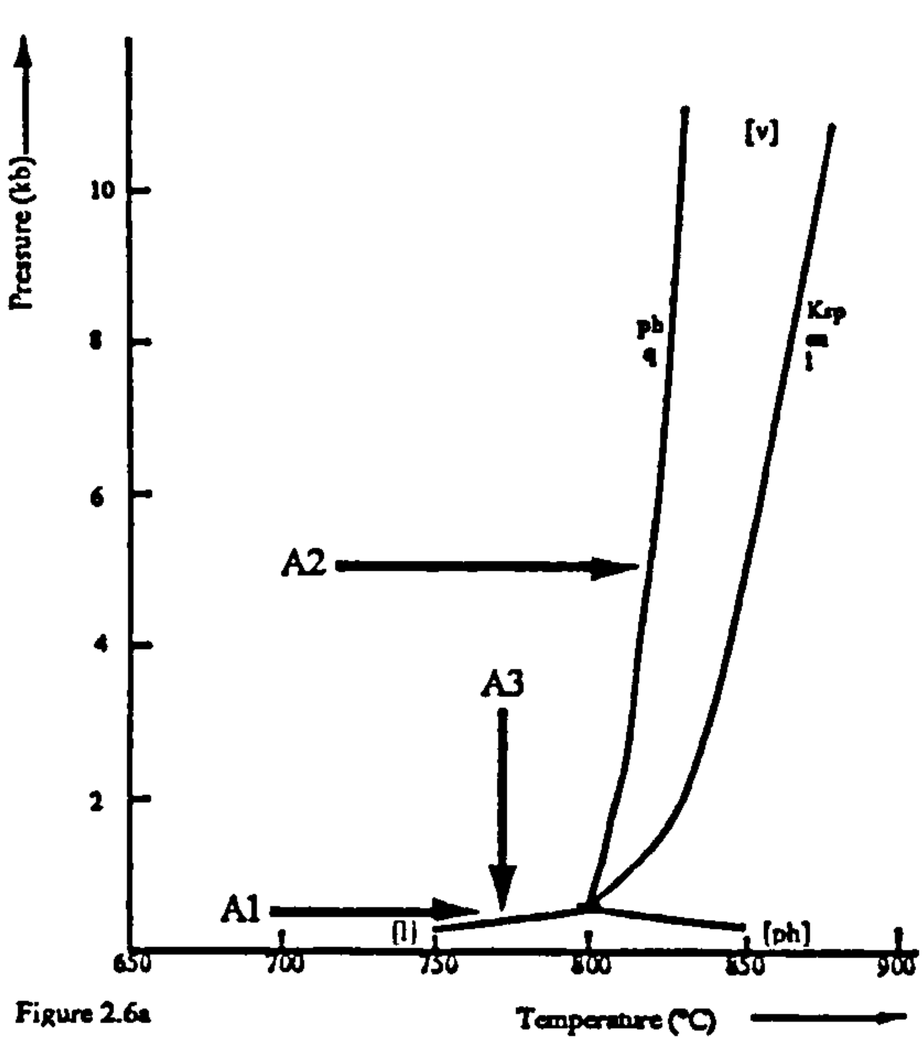

Figure 2.6a

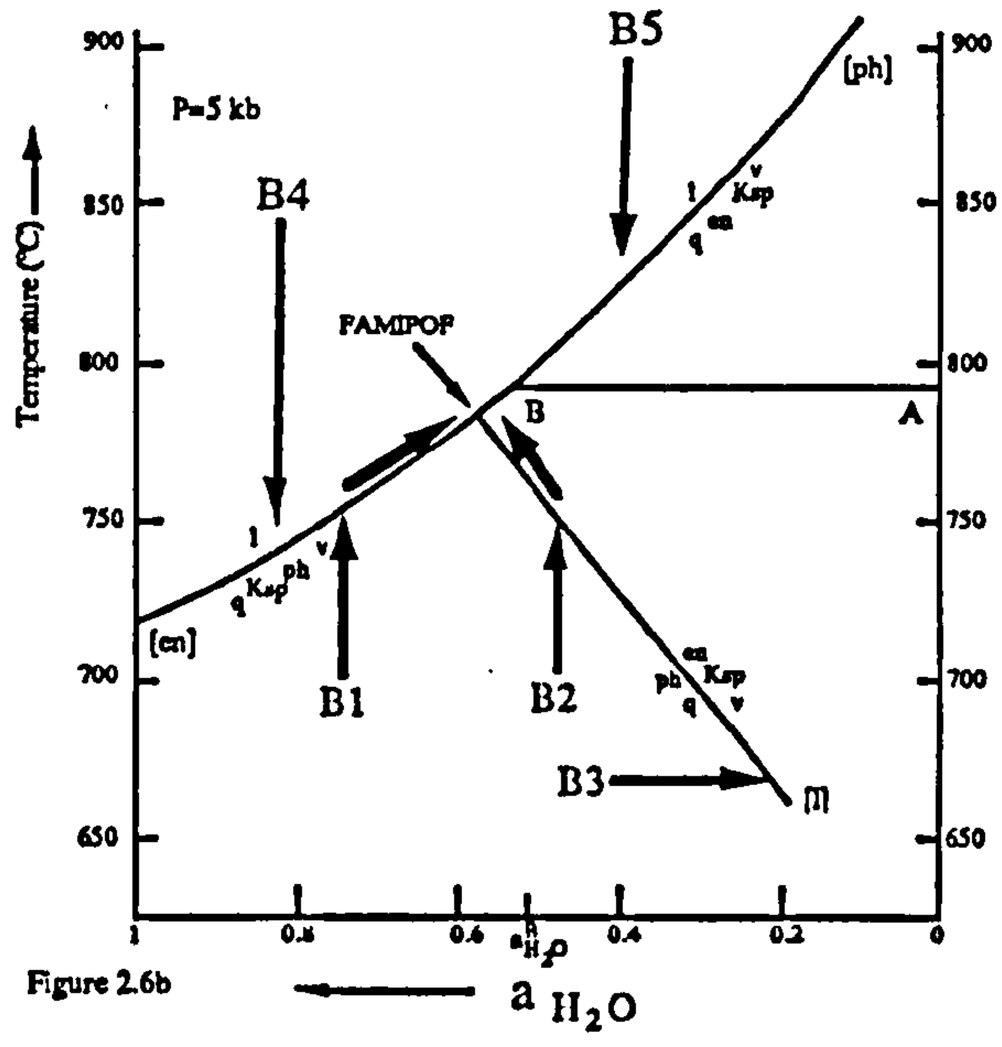

Figure 2.6b

Figure 2.6. P-T and T-a_{H_2O} sections at 5 kb to illustrate various metamorphic paths which can result in charnockite formation.

2.4.3 Vapour-present conditions

Phase relations and three possible metamorphic trajectories are illustrated for vapour-present conditions at 5 kb (Figure 2.6b). Path (B1) is for an internal pore fluid of water-rich composition. With increasing temperature the melting curve is intersected. If on the other hand the fluid is initially poor in water, heating path (B2), which intersects the subsolidus dehydration [l] reaction producing a charnockite assemblage, may be followed. If the temperature does not reach that of the invariant point, migmatite and charnockite will result from paths (B1) and (B2) respectively.

It is worth noting that the porosity of amphibolites and granulites is small (<1%) and unless there is constant input of fluid from a large reservoir, the pore fluid will rapidly become buffered by the solid and/or melt phases. For instance any pore fluid present will be used up in the melting reaction encountered on path (B1) before a large degree of

melt is produced. If the temperature continues to rise the water activity will be buffered along the melting curve to the invariant point where the FAMIPOF melting reaction will occur. Likewise for path (B2) the fluid composition will be internally buffered by the mineral assemblage before much enstatite has been produced. Continued temperature increase will result in the fluid composition buffering up the reaction curve, until the FAMIPOF reaction takes over. Similar considerations led Powell (1983) to the conclusion that, unless there is a continual external fluid flux, melting is inescapable-even at moderate granulite facies temperatures (780°C for 5 kb). Provided no melt is lost and the back reaction to phlogopite is prohibited, a charnockite assemblage may result from either path.

Path (B3) illustrates the condition of external buffering of the fluid phase by an isothermal influx of water-poor fluids. In this case the dehydration curve is intersected and a granulite assemblage produced. This is the path envisaged by Newton *et al.* (1980) for granulite formation by CO_2 influx. The abundance of anhydrous phases produced depends on both the abundance and composition of the influxing fluid.

2.5 MECHANISMS PROPOSED FOR CHARNOCKITE FORMATION

A variety of mechanisms have been suggested for charnockite formation (Table 2.1), these are discussed below with reference to Figures 2.6a and b.

2.5.1 Igneous processes

Although Holland's (1900) original theory that all charnockites form by direct crystallisation from a melt has been disproved in some instances by the identification of clear field evidence of a subsolidus transformation (Pichamuthu, 1960), a number of extensive charnockite bodies which lack field evidence of a solid state transformation may be interpreted as primary igneous rocks crystallising from a water-undersaturated

melt. The pertinent phase relations are described by Grant (1986) and are discussed in more detail in Chapter 3, where field evidence for their existence in southern India is presented. Two paths (B4 and B5) shown on Figure 2.6b are for identical melt compositions, high water activities will result in a biotite granite (B4), whereas low water activities may give a charnockite assemblage (B5). One method of lowering the water activity is by the addition of a CO_2-rich vapour phase.

Conditions	Model	Path	Reference
Igneous	Direct crystallisation from a water deficient magma	B5	Holland (1900)
Fluid-absent	Vapour-absent metamorphism of dry lithologies	A1	Lamb and Valley (1984)
	Melting/*in situ* recrystallisation	A1,B1,B2	Waters (1988)
Fluid-present	Influx of water deficient (CO_2-rich) fluids	B3	Janardhan *et al.* (1979)
	Isothermal decompression	A2	Srikantappa *et al.* (1985)
	Reduction in fluid pressure	-	Srikantappa *et al.* (1985)
	Internal fluid modification by graphite oxidation	B3	Hansen *et al.* (1987)
	H_2O removed/CO_2 added by passage of dry magmas	B3	Frost and Frost (1987)

Table 2.1 Models which have been proposed to explain charnockite formation and the paths for each on Figures 2.5a and b.

2.5.2 Vapour-absent processes

(a) Lamb and Valley (1984) have proposed vapour-absent metamorphism as mechanism for granulite formation. It has been described above, that, under vapour-absent conditions, amphibolite facies rocks are stable up to the (v) melting curve. Hence for this model to be correct the rocks must already have had an anhydrous mineral assemblage, *ie.* either magmatic rocks which originally crystallised under low water activities (*eg.* charnockites (Valley and O'Neil, 1984)), or rocks dehydrated by some previous metamorphic event. Since the precursor rock is already dehydrated the range of available mineral reactions is small, particularly for charnockitic rocks, the second metamorphic event will be preserved only by resetting of chemical and isotopic systems. Although this process may be volumetrically important in the lower crust it does not help to elucidate the original mechanism of charnockite formation.

(b) Partial melting by the vapour-absent dehydration reaction (or by the FAMIPOF reaction in the presence of a vapour phase), is a popular model for granulite production through removal of the melt phase (Fyfe, 1973). In order, however, to produce a charnockite all the melt must be retained in the source and the retrograde reaction must be inhibited. Waters (1988) documents the occurrence of such processes by field observations of charnockites forming as *in situ* partial melts in Namaqualand.

2.5.3 Vapour-present processes

(a) Flushing with non-aqueous fluids lowers the water activity enhancing dehydration by a simple dilution mechanism (Janardhan *et al.* 1979) and path (B3) on Figure 2.6b is followed. This mechanism has also been proposed for general granulite formation in the lower crust (Newton *et al.* 1980). Touret's (1971a and b) identification of the transition between dominantly H_2O fluid inclusions in amphibolites to dominantly CO_2 inclusions in the granulites from the Bamble region in S. Norway provides a major piece of evidence in favour of this model.

(b) Isothermal decompression (path (A3), Figure 2.6a) may cut [I] and cause subsolidus charnockite formation, although clearly either under vapour-absent conditions or high water activities this will happen at geologically unreasonable pressures. In vapour-present systems this process can be illustrated on Figure 2.6b. During decompression the invariant point (and the associated reactions [I] and [en]) will move almost isothermally to higher water activities (see locus of FAMIPOF on Figure 2.4). If the water activity is fixed by a constant pore-fluid composition, during decompression the subsolidus dehydration curve may intersect the position of the rock and charnockite formation will follow. Srikantappa *et al.* (1985) discussed this mechanism for charnockite formation in southern Kerala (see Chapter 3), but rejected it; nevertheless Ravindra Kumar and Chacko (1986) did favour this mechanism for some

south Keralan charnockites.

(c) A reduction in fluid pressure relative to lithostatic pressure has been favoured as a mechanism for charnockite formation in South Kerala (Srikantappa *et al.* 1985). This model involves opening cracks of some 5 km into which pore fluids are released, so the pore fluid pressure in the rock drops below the lithostatic pressure. This, it is claimed will reduce the water activity and cause dehydration. This model is unsound, because (by definintion) a pore fluid has a fluid pressure equal to the lithostatic pressure, otherwise it will not form a continuous grain boundary network. If the fluid pressure does drop then fluid-absent conditions will prevail and under such circumstances charnockite formation cannot occur without melting (**2.4.1**).

(d) Internal control of the fluid composition and hence the water activity by graphite oxidation (Hansen *et al.* 1987), will have the same effect on phase stability fields as influx of CO_2 from an external source and hence will also follow path (B3) on Figure 2.6b. Charnockite can be produced by this mechanism providing there is sufficient graphite in the rock and an increase in the oxygen fugacity occurs. Hollister (1988) suggests that changing the oxygen fugacity is unneccessary and a reaction between biotite and graphite to give CO_2 and enstatite and a melt may occur during decompression.

(e) Granitic melts dissolve up to 12% water (Bowen and Tuttle, 1950), so water-undersaturated melts will rapidly absorb pore water from rocks with which they interact, It has been suggested that this process will inhibit melting and cause solid-state charnockite formation (Frost and Frost, 1987). The process will be naturally enhanced by the extra heat input which is likely to accompany magmatic intrusion. If the rock is originally a biotite gneiss with a pore fluid of pure water, this process will simply cause vapour-absent conditions and inhibit both melting and charnockite formation (**2.4.1**). If on the other hand the pore fluid is initially mixed H_2O-CO_2 then removal of water will

cause a decrease of a_{H_2O} and path (B3) on Figure 2.6b will be followed, but through water removal rather than CO_2 influx (see below). Frost and Frost (1987) suggest that this process may be enhanced by the magmas exsolving CO_2 into the surrounding rocks.

Apart from an external influx of CO_2 all these processes imply that the water activity is internally buffered by the rock. Powell (1983) argues that if the rock is internally buffered then partial melting is inescapable, even in the absence of a free fluid phase, provided high enough temperatures are reached. This suggestion is confirmed by the review of phase relations in **2.4.2** and **2.4.3.** During prograde metamorphism the rocks will be buffered along dehydration equilibria paths which intersect melting curves before peak conditions are reached. In contrast the CO_2-flushing model can provide an external fluid buffer, but still the composition of the fluid co-existing with the solid assemblage is internally buffered by dehydration reactions, unless the buffering capacity of the rock is exceeded (*ie.* all the hydrous phases are destroyed). Hence all models imply internal fluid buffering unless a substantial influx of fluid has occurred.

2.6 CONCLUSIONS

One of the most important conclusions which can be drawn from this review is that the common assumption that vapour-absent conditions imply low water activities is incorrect. Low water activities can be achieved by two mechanisms: (1) under vapour-present conditions, where the pore fluid is diluted by non-aqueous fluids or (2) mineral phase equilibria provide an internal buffer to low a_{H_2O}.

This conclusion implies that subsolidus charnockite will not be formed under vapour-absent conditions. Charnockite formation can however occur under vapour-absent conditions by vapour-absent melting but this imposes the additional constraints of *in situ* recrystallisation and inhibition of the back reaction. Nevertheless Waters (1988) has

presented evidence from Namaqualand that such a mechanism has occurred. Under fluid-absent conditions temperatures must exceed 800°C (at 5 kb) for this process, but the FAMIPOF reaction will occur at the lower temperatures (750°C) (at 5 kb). This introduces the possibility that a fluid influx of any composition (even pure CO_2) into a vapour-absent amphibolite gneiss can induce melting.

It is proposed here that two major mechanisms exist for creating charnockite assemblages from amphibolite gneiss; the FAMIPOF reaction with *in situ* recrystallisation and modification of a pore fluid either externally (by CO_2 influx or dry magma passage) or internally (graphite oxidation) to water poor compositions. The critical factors in determining which mechanism occurs for a particular charnockite terrain is the maximum temperature reached (relative to that at which the FAMIPOF reaction occurs) and the availability of a pore fluid dilutant.

Chapter 3

CHARNOCKITE FORMATION IN SOUTHERN INDIA: FIELD, PETROGRAPHIC, GEOCHEMICAL AND FLUID EVIDENCE.

3.1 THE REGIONAL GEOLOGY OF SOUTH INDIA

Figure 3.1 is a simplified geological map which illustrates the broad tectonic and lithological relationships in the high-grade terrain of southern India. The area is divided into several major blocks by Proterozoic shear zones (Drury and Holt, 1980). The Moyar shear zone is identified as a major crustal suture with the terrains on either side having different affinities and ages. The geology of Sri Lanka is similar to that exposed in southern India and it has been suggested that they are part of the same block (Newton and Hansen, 1986).

The Northern block is an extensively studied Archæan granite-greenstone-gneiss terrain characterised by a series of elongate volcano-sedimentary supracrustals separated by tonalitic to trondhjemitic gneisses and intruded by post-tectonic granites. For a detailed description of the structure and geochemistry of the greenstone terrain the reader is referred to Wightman (1986). The banded gneisses, which are locally known as Peninsular gneiss, characterise the amphibolite grade and their formation has been resolved into several distinct episodes during a period of extensive magmatism between 3200 Ma and 2900 Ma (Table 3.1).

A prograde metamorphic sequence, from greenschist facies, in the north, to granulite facies in the south, formed about 2500 Ma (Table 3.1) and overprints earlier structures. This prograde sequence shows an increase in pressure and temperature conditions from 500°C and 3 kb in N. Karnataka (greenschist), through 700°C and 4.5 kb in the

Biligirirangan Hills and other areas just north of the Moyar suture zone (Harris and Jayaram, 1982, Harris *et al.* 1982, Raith *et al.* 1983, Hansen *et al.* 1984a and Raase *et al.* 1986). Although this apparent isothermal pressure increase in the granulite

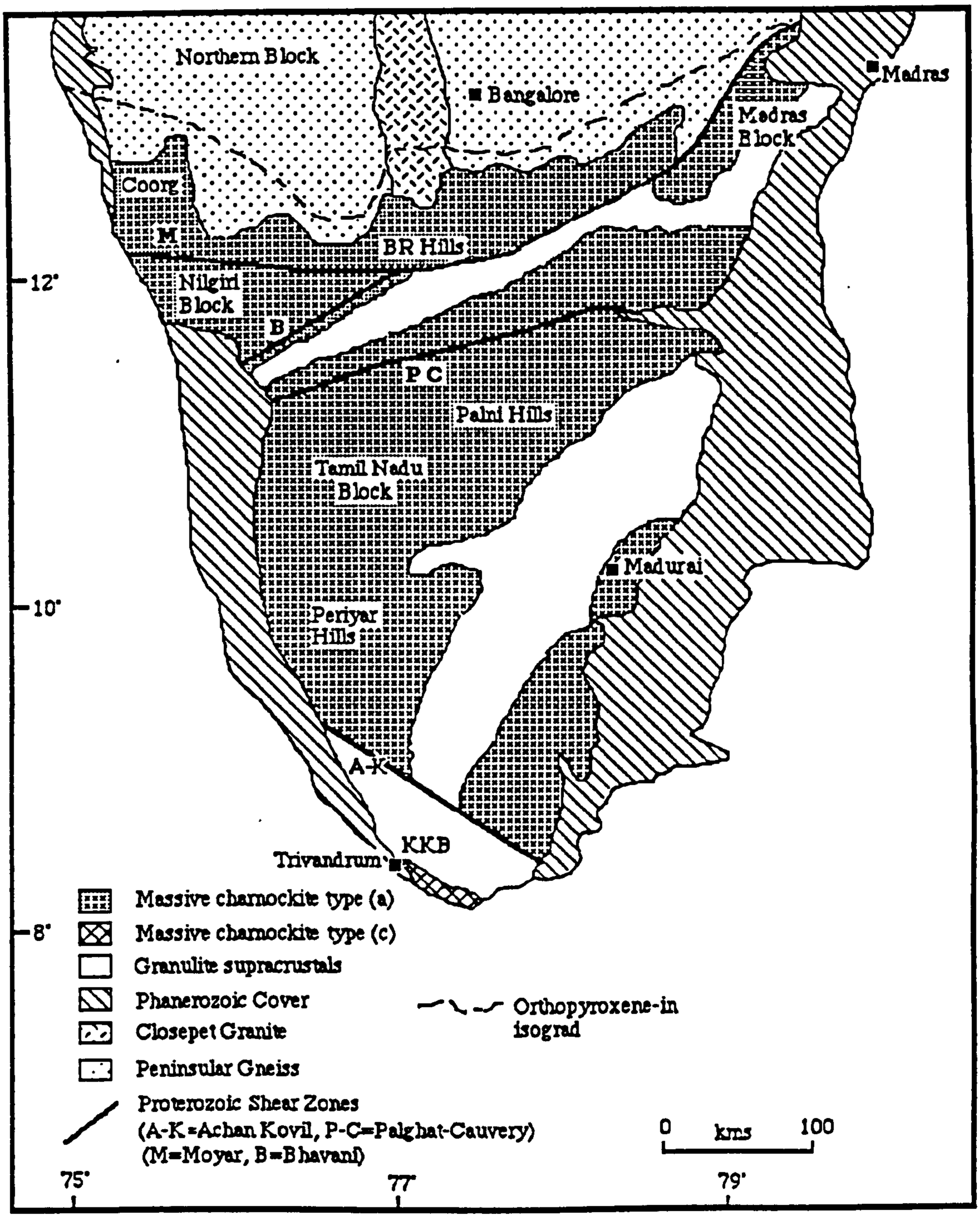

Figure 3.1. Summary geological map of southern India illustrating the broad lithological and tectonic relationships in the high grade terrain. (KKB = Kerala Khondalite Belt, BR=Biligirirangan Hills).

facies has been attributed to massive fluid upwelling (Drury *et al.* 1984) it is more likely to reflect the blocking temperature of Fe-Mg exchange thermometers (Harris *pers. comm.*, see also Frost and Chacko, 1989). The onset of the granulite facies is marked by a rather diffuse orthopyroxene isograd (Figure 3.1) (Subramanian, 1967) characterised by the first appearance of orthopyroxene, principally at the expense of hornblende (Janardhan *et al.* 1979). Along the isograd complex local relationships between amphibolite and granulite facies rocks are observed and although large tracts of amphibolite facies rock are still found to the south, the isograd marks the northern limit of granulite in southern India.

All the major structures in this block trend N-S, the most obvious is the large linear body of Closepet granite which follows this N-S lineation for 300 km, but peters out in the amphibolite-granulite transition zone. With increasing metamorphic grade there is a concomitant increase of deformation intensity southwards (Drury and Holt, 1980), but most stuctures are obliterated by the granulite facies recrystallisation. As the orthopyroxene isograd is approached, evidence of partial melting in the Peninsular gneiss is identified, but it appears to be arrested by the granulite recrystallisation (Friend, 1981).

The Northern block is cut at its southern margin by a major system of E-W trending shear zones. Drury *et al.* (1984) identified these as Proterozoic, and related them to a post-Cuddapah basin thrust (active between 1700 Ma and 700 Ma (Crawford and Compston, 1973)). The minimum age (700 Ma) of major shear movement is marked by later carbonatites and syenites which cross-cut the shear stuctures (Deans and Powell, 1968). The Moyar lineament is believed to be a major crustal suture, separating Proterozoic terrains to the south from Archæan terrains to the north (Raase *et al.* 1986).

Within and to the south of these shear zones are smaller Proterozoic blocks of predominantly granulite facies orthogneisses and metasedimentary sequences. The highlands in the west, including the Nilgiri, Palni and Periyar Hills (Figure 3.1), are extensive granulite facies orthogneisses of acid and intermediate composition consisting

North of Movar shear

Area	Rock type	Age (Ma)	Method	Geochronologist(s)
Karnataka	Peninsular gneiss	3080-3315	Rb-Sr (W.R.)	Beckinsale *et al.* 1982
		3000-3020	Rb-Sr (W.R.)	Bhaskar Rao *et al.* 1983
		2900-3200	Rb-Sr/Pb-Pb (W.R.)	Taylor *et al.* 1984
Karnataka	Granite	2522-2559	Rb-Sr (W.R.)	Beckinsale *et al.* 1982
	Granite	2605±18	Pb-Pb (W.R.)	Taylor *et al.* 1984
Kabbal	Granite/Gneiss	2529-2578	Pb-Pb (W.R.)	Taylor *et al.* 1988
	Charnockite	2844	U-Pb zircon	Buhl *et al.* 1983
	Gneiss/Granite	2515-2535	U-Pb zircon	Buhl *et al.* 1983
	Pegmatite	2500	U-Pb allanite	Grew and Manton, 1984
Krishnagiri	Charn/Gneiss/Granite	2463±72	Rb-Sr (W.R.)	Peucat *et al.* 1989
	Charn/Gneiss/Granite	2455±122	Sm-Nd (W.R.)	Peucat *et al.* 1989

South of Moyar shear

Madras	Charnockite	2580±95	Rb-Sr (W.R.)	Crawford, 1969
	Charnockite	2555±140	Sm-Nd (W.R.)	Bernard-Griffiths *et al.* 1987
Nilgiris	Charnockite	2615±80	Rb-Sr (W.R.)	Crawford, 1969
	Charnockite	2535	U-Pb zircon	Buhl, 1987
	Charnockite	2413±121	Rb-Sr (W.R.)	Peucat *et al.* 1989
	Charnockite	2578±72	U-Pb (W.R.)	Peucat *et al.* 1989
KKB	Charnockite	1930,540	U-Pb zircon	Buhl, 1987
	Khondalite	2100	Rb-Sr (W.R.)	Chacko, 1987
	Gneiss/Charnockite	>2000	Sm-Nd (W.R.)	Choudary *et al.* (in prep.)
Madurai	Granite/Gneiss	550±15	Rb-Sr (W.R.)	Hansen *et al.* 1985
Sri Lanka	Gneiss/Charnockite	536±6	Sr-Nd-Pb (W.R.)	Burton and ONions, 1988
	Gneiss/Charnockite	520±20	Sm-Nd (Garnet)	Burton and ONions, 1988
	Charnockite	1100/550	zircon ion probe	Kroner *et al.* 1986
	Charnockite	564±10	U-Pb zircon	Baur *et al.* 1987

Table 3.1 Geochronology related to granulite facies metamorphism in southern India and Sri Lanka. (W.R. = whole rock).

primarily of enderbites and charnockites (quartz, plagioclase, K-feldspar, orthopyroxene, garnet ± biotite). Granulite facies metamorphism of these massive charnockites (750 ± 40°C and 5 - 9 kb, Harris *et al.* 1982, Raase *et al.* 1986, Touret and Hansteen, 1988) is indistinguishable from their emplacement age around 2.5 Ga (Table 3.1).

The eastern side of Peninsular India from Madras through the Madurai plains (Tamil Nadu) to the Kerala Khondalite Belt (Figure 3.1) is dominated by granulite gneisses and supracrustal sequences. Deformed and interfolded acid and basic granulites are intercalated with a variety of metasedimentary units. Near Madras extensive field and geochemical studies have indicated that acid charnockites recrystallised under granulite facies conditions (780 ± 30°C, 7.1 ± 1 kb, Battacharya and Sen, 1986) with intense deformation soon after formation about 2.5 Ga (Table 3.1).

The large Tamil Nadu block between the Palghat-Cauvery and Achan Kovil shear zones has been studied in less detail, with only LANDSAT imagery (Drury and Holt, 1980) and reconnaissance studies by Wightman (1986) and more detailed mapping in selective areas (*eg.* Annamalai, 1988) giving a general outline of the geology. The supracrustal sequences consist of garnet-sillimanite gneisses, acid and basic meta-igneous units, banded iron formations and sparse calc-silicates metamorphosed to amphibolite and granulite facies (see Wightman, 1986).

To the south of Achan Kovil lies the well studied supracrustal terrain of the Kerala Khondalite Belt. Charnockites, garnet-biotite gneisses (locally called leptynites) and metapelites with sillimanite, cordierite and graphite (khondalites) are the major rock types although minor intercalated metabasite and calc-silicate units are reported (Srikantappa *et al.* 1985). Pressure and temperature conditions from this area show no regional trends and fall between 650 - 850°C and 5 - 6 kb (Chacko *et al.* 1987). The geochronological data are limited (Table 3.1), but granulite recrystallisation was

thought to occur at about 550 Ma on the basis of a zircon (Pb) lower intercept (Buhl, 1987) and Sm-Nd mineral ages (Choudry *pers. comm.*). Although the general structural trends in the area have been mapped as NW-SE by LANDSAT imagery (Drury and Holt, 1980), due to the dense forest outcrop is mainly confined to quarries and hills and very little is known of the small scale structural features.

The geological similarity between the Kerala Khondalite Belt and the Vijayan Complex in Sri Lanka (*eg*. Hansen *et al.* 1987) has led to the suggestion that they are part of the same terrain. Substantial geochronological work carried out in Sri Lanka suggests granulite metamorphism occurred at 500 - 550 Ma (Table 3.1), which appears compatible with the sparse data available from the Kerala Khondalite Belt. At the southern margin of this block there is an area of uniform massive chanockites which is thought to be part of a structurally distinct unit (Figure 3.1, also see 3.4).

3.2 CHARNOCKITE FORMATION IN SOUTHERN INDIA

Southern India has played a central role in the debate over the processes involved in charnockite formation since Holland (1900) first classified it as a distinct rock type. Initially the debate focused on whether charnockites were igneous or metamorphic in origin. Some charnockites show unequivocal evidence of forming by a subsolidus metamorphic transformation, but this evidence may not be applicable to all charnockite occurrences. In recent years the focus on the controversy has moved towards identifying the role (if any) of CO_2 in charnockite formation since its involvement was proposed by Janardhan *et al.* (1979). Again, due to the excellent field exposures, the evidence from southern India has played a leading part in this debate.

3.2.1 Igneous or metamorphic?

Following Holland's (1900) interpretation that charnockites were of igneous parentage there followed considerable debate as to their exact mode of origin. Howie (1955), using variation diagrams, attempted to prove the 'charnockite series' from Madras was a differentiated magma suite, but supported the view that they subsequently recrystallised under high-grade metamorphic conditions. Subramanian (1959) argued that the acid charnockites at Madras were intrusive into pre-existing basic granulites. Recognition of structural control on charnockite formation in amphibolite gneisses from Kabbaldurga (Pichamuthu, 1960) led to general acceptance that charnockites were metamorphosed rocks of igneous or sedimentary origin (*eg*. Cooray, 1969). There has recently been renewed speculation that some charnockites from southern India may be primary igneous rocks, following theoretical considerations of Grant (1986), calculations concerning the volume of CO_2 available O'Nions and Oxburgh (1988) and field observations made during the Indo-U.S. field symposium 'The deep continental crust of South India' (1988) (see Wickham, 1988).

3.2.2 Description

In the field charnockites are distinctive by their dark brown or green colouration and greasy lustre on fresh surfaces. According to Cooray (1969) these criteria invariably betray the presence of orthopyroxene, no examples of orthopyroxene-free green rock were recorded in this study. The green colouration has been attribute to tiny veins of chlorite and calcite (Howie, 1967) which may be retrogression products of orthopyroxene with CO_2 and H_2O fluids (Janardhan *et al.* 1982).

In this thesis charnockites are divided into two groups by the nature of their field relations. The term 'massive charnockite' is applied to acid and intermediate lithologies with charnockitic mineralogy (orthopyroxene and K-feldspar are the diagnostic

minerals) which form part of large areas of continuous granulite facies. In areas where charnockite is intimately associated with amphibolite facies rocks, normally occurring as veins and pods on a centimetre to metre scale, the term incipient charnockite is applied. In sub-solidus incipient charnockites orthopyroxene can either replace hornblende or biotite, with the former reaction taking place at higher water activities (2.3.4). Hence rocks of different bulk compositions may undergo transformation from gneiss to charnockite under different conditions and incipient charnockites may be found replacing biotite in a gneiss adjacent to a charnockitic rock completely devoid of hornblende. This chapter presents a review of published field, petrographic, fluid inclusion and geochemical data, supplemented by the author's field and petrographic observations, for both massive and incipient charnockites. In particular the evidence available to elucidate the role of CO_2 during the formation of charnockite will be examined. Although the massive and incipient charnockites are treated separately here, this is not intended to imply that their mode of formation in necessarily different.

3.2.3 The evidence

Despite numerous geochemical and theoretical studies, field observations often provide the best evidence for distinguishing which mechanism of charnockite formation is the most plausible for a particular area. For instance Waters and Whales (1984) document internal buffering of water activity by dehydration melting in the Namaqualand transition zone. Gradients of water activity between bands of different bulk composition are observed; iron-rich bands are migmatitic granulites and magnesium-rich bands are amphibolites with no evidence of partial melting.

Geochemical studies have added support to field based theories, but the results are often ambiguous. Extraction of a partial melt is supported by systematic depletions of large ion lithophile elements (LILE) in the residue with respect to the precursor. In the case of charnockite formation by partial melting and *in situ* recrystallisation, a variety of

case of charnockite formation by partial melting and *in situ* recrystallisation, a variety of effects may be seen. In the ideal case the melt forms and crystallises as discrete pockets having no interaction with the surrounding rock, here no element losses or gains should be detectable. In a more realistic case the melt may be enriched in LILE (and other elements) from the surrounding rocks, but equally elemental losses may occur with late stage aqueous fluid release.

Extraction of water from the pore fluid by passing anhydrous magmas will deplete the rock of LILE, but should leave rare earth element (REE) trends unfractionated. Displacement of water by influx of CO_2 may have a similar effect, but the CO_2 may bring (or remove) a variety of elements (including some LILE and REE) which dissolve by forming carbonate complexes. In contrast internal modification of the fluid composition should not cause much element movement, unless there is an overall fluid loss or gain. Attempts to quantify any of these processes are hazardous because the mechanisms involved and mobilisation effects of the fluids are not fully understood.

Evidence of the fluid characteristics at the time of charnockite formation come either from mineral assemblages which equilibrated in the presence of a fluid phase or directly from fluids entrapped in inclusions during granulite formation (Touret, 1971). In order to use evidence from fluid inclusions to characterise the fluid phase present at peak conditions it must be assumed that the inclusions were trapped during charnockite formation and they have not suffered loss, gain or modification since their entrapment. These assumptions are discussed in 5.3.

3.3 INCIPIENT CHARNOCKITE AT THE ORTHOPYROXENE ISOGRAD

The field relations displaying a complex association between amphibolite and granulite (incipient charnockite) provide the strongest evidence of a metamorphic origin for at least some charnockite. Incipient charnockite structures have been reported from

a number of worldwide granulite terrains; southwest Greenland (Wells, 1979), southwest Sweden (Hubbard, 1978), northwest Norway (Heier, 1960), California (Compton, 1960), Adirondacks (Cartwright, *pers. comm.*), Laramy (Frost *et al.* 1989) and Sri Lanka (Hansen *et al.* 1987). They are most extensively studied in the quarry exposures in South India.

Holland (1900) having identified and classified the massive charnockites of the type area near Madras as intrusive rocks became uncertain when studying incipient charnockites near Salem (Figure 3.3a). He described transgressive tongues of charnockite eminating from a large charnockite mass into the amphibolite gneiss, but in places a ghost gneissic foliation was traceable through the charnockite. Holland reported that "*no previously established criterion of igneous intrustive relationships can account for this phenomenon*". There is still no established criterion which classifies this type of structure as intrusive, in fact this observation is the major evidence for incipient charnockites having a metamorphic origin.

The incipient charnockite outcrops in South India can be divided into two groups; those which occur around the orthopyroxene isograd in the Northern block and those which occur to the south of (and in) the Proterozoic shear zone systems. This division in not only on spacial grounds but is also based on different reactions as outlined in **3.1.** It is therefore possible that the two types of incipient charnockites formed at different ages and are perhaps the result different processes. This review of incipient charnockite formation is divided into two parts, the first deals with those found in the Northern Block and the second those to the south of the Moyar shear zone.

3.3.1 Field relations in the Northern Block

The majority of studies from this area have been carried out in the quarry complex at Kabbaldurga (Figure 3.3a), where incipient charnockites were first identified

(Pichamuthu, 1960). Similar structures have been reported from many localities in the region between the orthopyroxene-in isograd and the onset of massive charnockite. Although the structures were first documented by Rama Rao (1940) incipient charnockite was not recognised as a prograde granulite formation until Pichamuthu (1960) discovered charnockitic patches and pods forming within the Peninsular gneiss in the quarries at Kabbaldurga. After futher work at Kabbaldurga and to the south around the margins of the BR Hills, Pichamuthu (1965 *pp.* 124) described the field relations as follows:

"*The relationship between the biotite gneiss or hornblende-biotite gneiss and charnockites, is clearly noticeable because of their contrasting colours and textures: the gneiss is light-coloured, foliated and highly contorted, while the charnockite is brownish green, coarsely crystalline and greasy looking. Some of the elongated charnockite patches transect the foliation directions of the gneiss* (Plate 3.1), *while some of the pods of charnockite which have formed in situ still retain traces of the original gneissic foliation passing through them* (Plate 3.2). *Where the transformation of gneiss into charnockite is complete, the gneissic foliations end abruptly on one border of the charnockite and continue from the opposite side.*"

Although this description sums up the major field evidence in support of a metamorphic origin for charnockite, further pertinent observations have been made, in particular on the field relationships between gneiss, charnockite and granite. Ramiengar *et al.* (1978) noted that the gneiss in incipient charnockite localities often showed evidence of migmatisation (Plate 3.3), with leucocratic segregations and contorted deformation. Charnockite recrystallisation is superimposed on normal gneiss and migmatite alike. They also noted blotchy charnockitic overprint of a massive granodiorite with feeble foliation. The Peninsular gneiss contains numerous amphibolite enclaves thought to be disrupted basic dykes (Ramiengar *et al.* 1978) and where the contact between the two lithologies is cut by a 'charnockite vein', the gneiss is transformed to charnockite and the ampibolite to a pyroxene granulite. At Kabbaldurga these authors note charnockite 'tree structures' in which a vein of

charnockite not only cross cuts the gneissic foliation but also spreads out along it producing a branching effect.

Plate 3.1. Veins of incipient charnockite cross-cutting the gneissic fabric at Kabbaldurga.

Around some charnockite patches a thin (< 30 cm) pink microcline-rich aplitic gneiss layer is developed. This layer is gradational into both the charnockite and gneiss, so formation due to potassium migration has been suggested (Ramiengar *et al.* 1978). Late aplite veins are observed cutting both the charnockite and migmatite, but alaskitic veins carrying coarse hypersthene crystals also cross cut early migmatite structures. Friend (1981 and 1983) carried out a more detailed field investigation at Kabbaldurga into the relative timing of migmatisation, charnockite formation and granitic intrusion. He suggests that the Closepet Granite is a polyphase intrusive body, often showing coarse pink K-feldspar development which he cited as evidence for K-metasomatism during a late stage of granite crystallisation. Friend interprets the migmatite structures in the Peninsular gneiss as the beginning of a melting episode from which the granites were derived, although evidence for large scale movement of melt is not obvious.

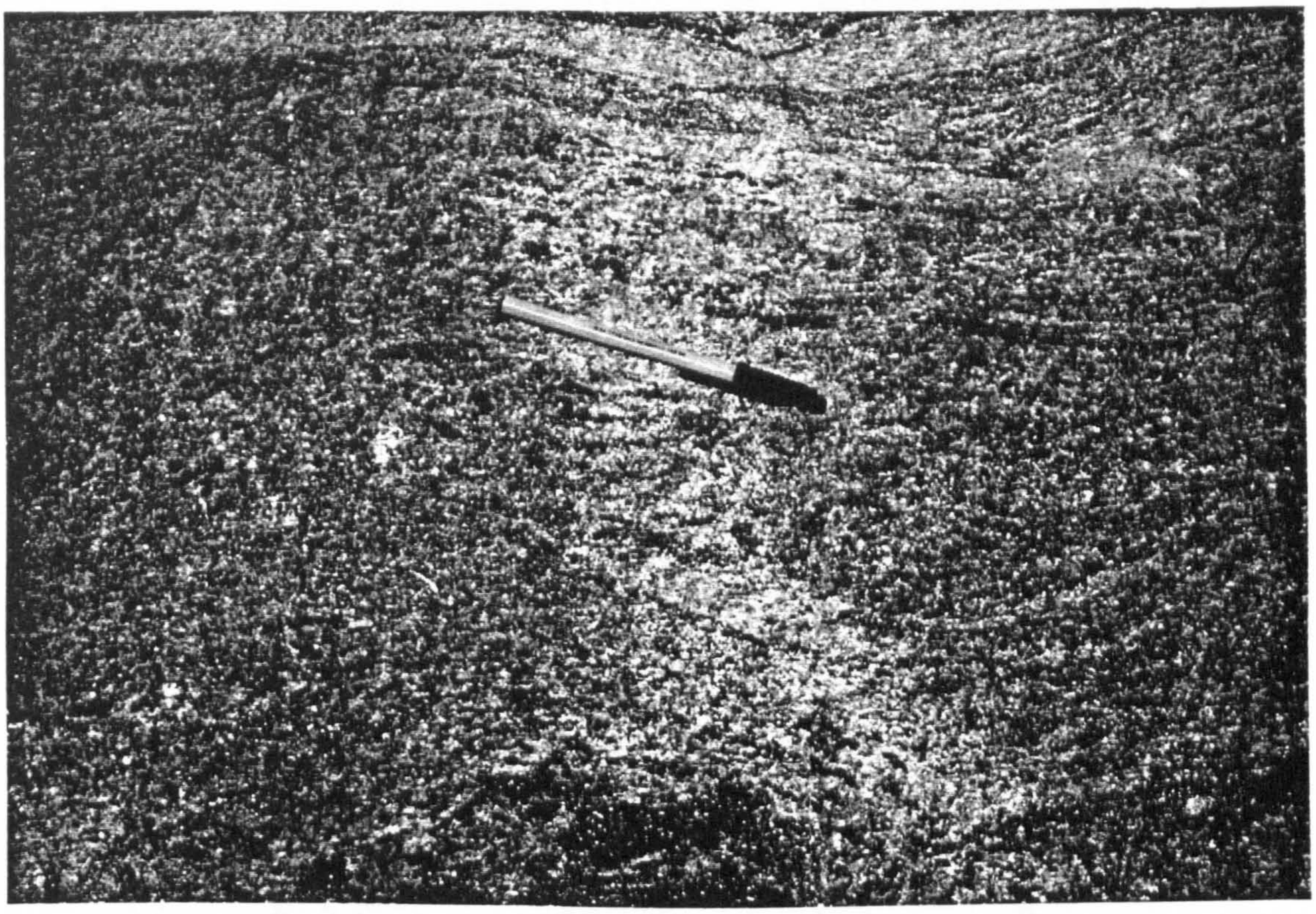

Plate 3.2. Incipent charnockite formation with relict gneissic foliation preserved within the charnockite (Satnuru).

Plate 3.3. Heavily migmatised Peninsular gneiss from an incipient charnockite locality (Coorg).

His observations are illustrated in Figure 3.2 which is reproduced from Friend, Figure 7, (1983). Patchy charnockite develops in both the gneiss and granite, and veins of charnockite cross-cut gneissic structures (Plates 3.4 and 3.5). Veins and sheets of granite cut patches of charnockite in the gneiss, but are themselves cut by charnockitic (hypersthene-bearing) granitic veins. The identification of these 'charnockite' veins which have clear intrusive relations to the surrounding rock is important, as it confirms that igneous charnockites exist in the area. The field relations imply that whether a magma crystallises as a granite or a charnockite may depends on the composition of the vapour phase associated with it.

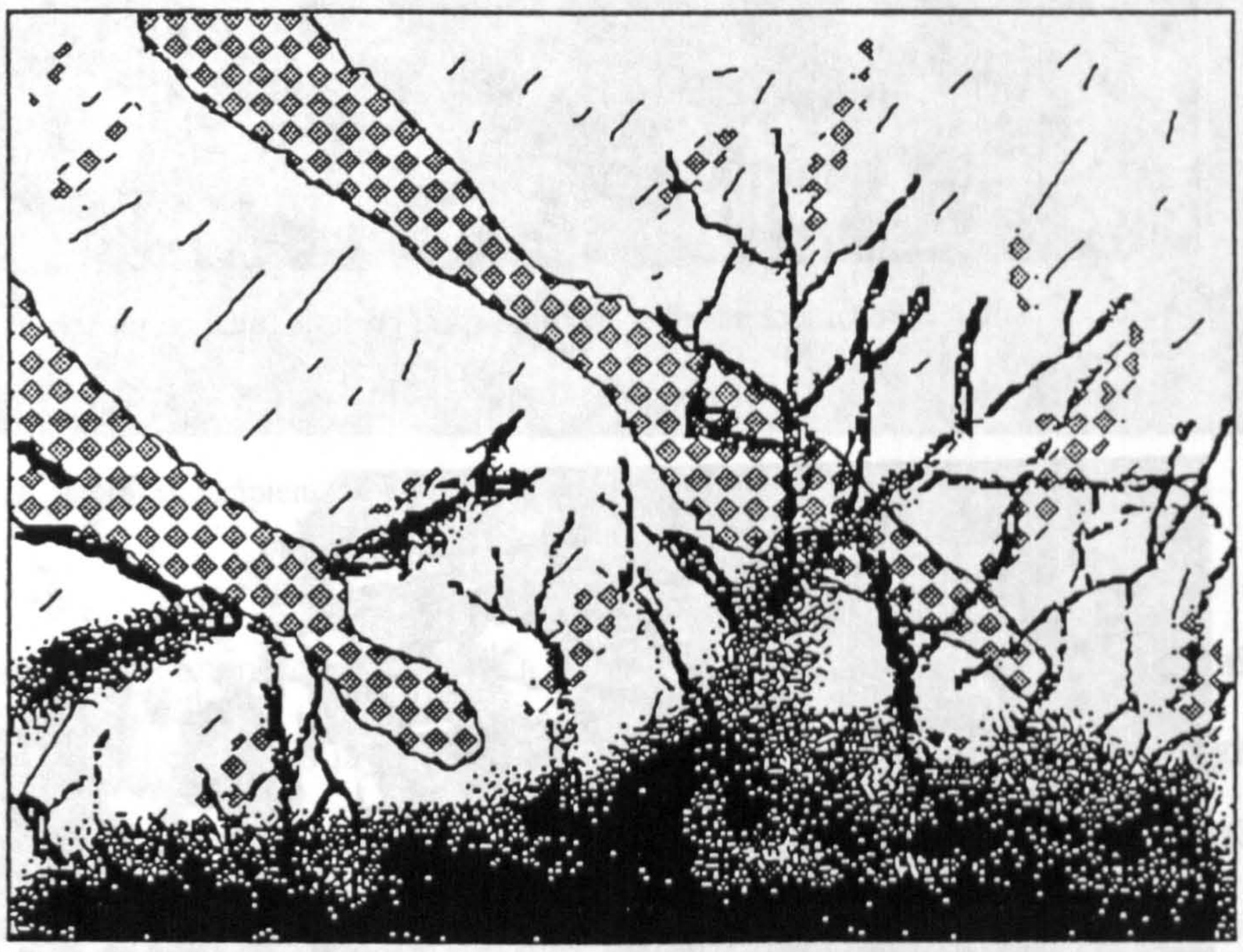

Figure 3.2 Reproduced from Friend (1983) Figure 7, "Schematic representation of the manner of charnockite development and the relationships of granite at Kabbaldurga quarry: Dashes - Peninsular gneiss; diamonds - Closepet granite; black - charnockite.

Janardhan *et al.* (1979) argued that the intimate association of charnockite and gneiss on the centimetre scale was not due to changes of temperature or pressure, but must represent a fluid controlled process. Charnockite formation in shear zones, along lithological boundaries and in 'tree structures' provide very strong evidence for such a

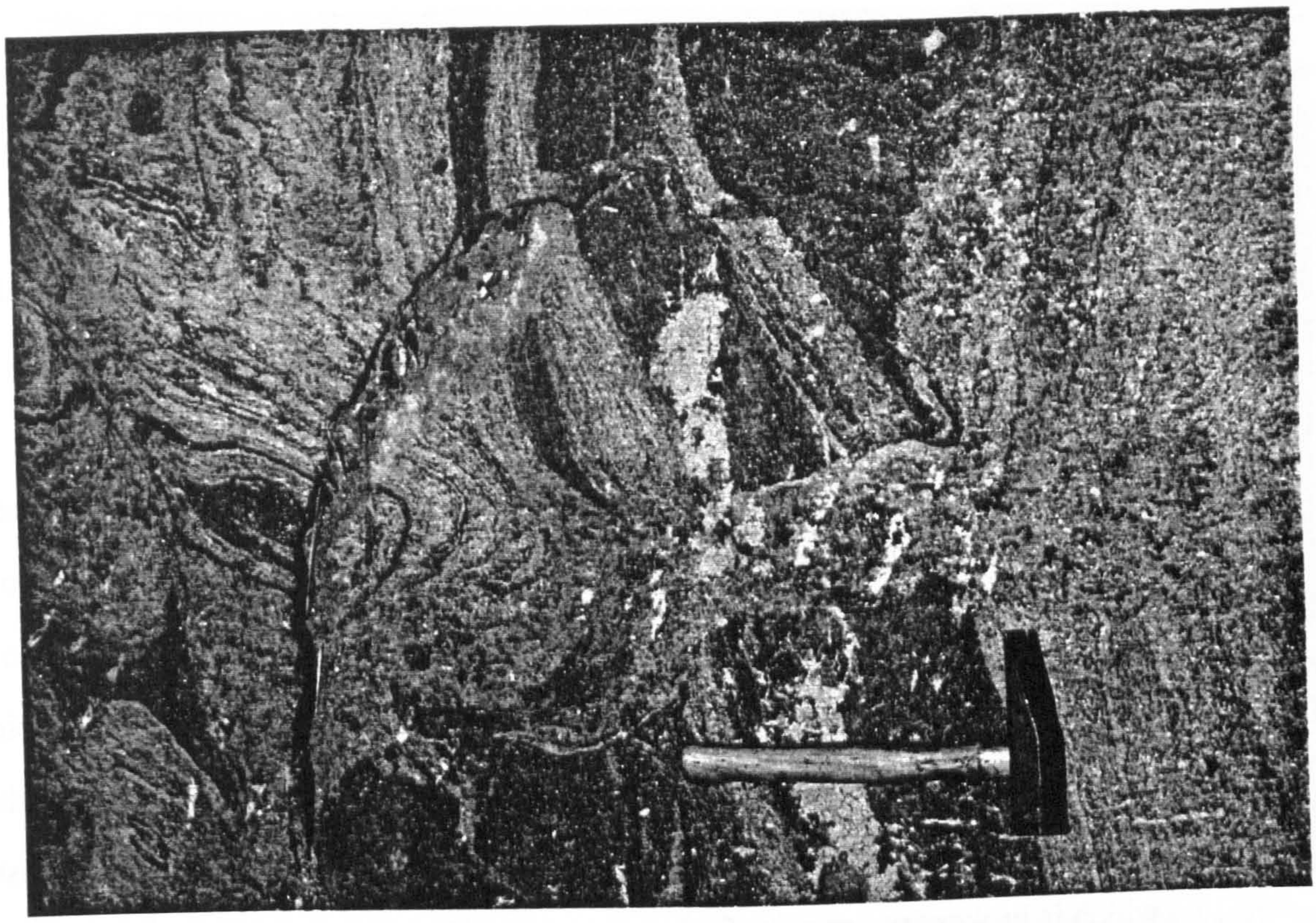

Plate 3.4. Charnockite intrusion cross-cutting both gneissic and basic layers (Kabbaldurga).

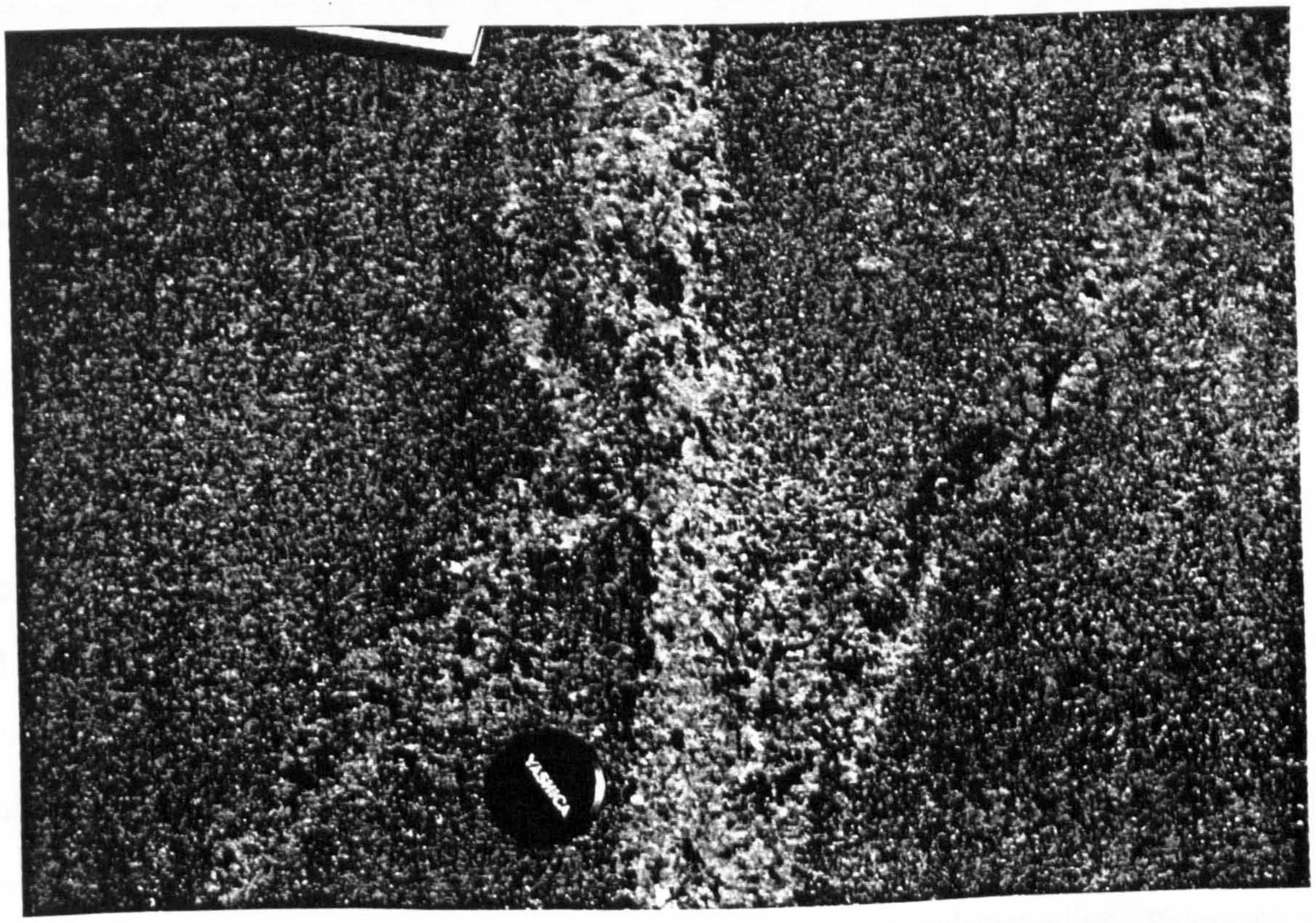

Plate 3.5. Intersecting pegmatite veins cross-cutting Peninsular gneiss, the earlier vein has a charnockitic mineralogy, suggesting charnockite formation by direct igneous crystallisation (10 km southwest of Kabbaldurga).

fluid controlled process. Due to its presence in fluid inclusions and the existence of grain margin calcite, carbon dioxide was invoked as the major fluid component. Friend (1983) suggested that the water released by the dehydration reaction pervades ahead of the CO_2 causing migmatite formation and melting in the gneisses, hence explaining the contemporaneous nature granitic magmatism and charnockite formation.

Plates 3.6 and 3.7 show orthopyroxene 'spots' growing in both the gneiss and leucosome segregations in a 'porphyroblastic manner'. This effect is not easily explained either by partial melting or CO_2 influx because the orthopyroxene growth does not appear to be related to a charnockite recrystallisation. Nevertheless it is suspected that a change in pore fluid composition was responsible, albeit after the major deformation episode. Plate 3.8 shows coarse charnockite forming within a basic dyke, which is broken into angular fragments suggesting brittle behaviour, this is unlike most basic dyke occurrences which exhibit plastic deformation. The process causing this phenomenon is poorly understood but it is tentatively suggested that CO_2 flooded into this vapour-absent area, at sufficiently high temperatures for the FAMIPOF reaction to occur. Consequently melting with its associated volume increase caused rapid expansion and fracturing of the basic lens.

3.3.2 Petrography and geochemistry

Since its recognition, based on field criteria, as the prograde transition from amphibolite to granulite, incipient charnockite at the orthopyroxene isograd has been the subject of many petrographic and geochemical studies. These were primarily carried out to document the changes which accompany the transition and assess whether this type of process is capable of generating the geochemical characteristics of large granulite terrains.

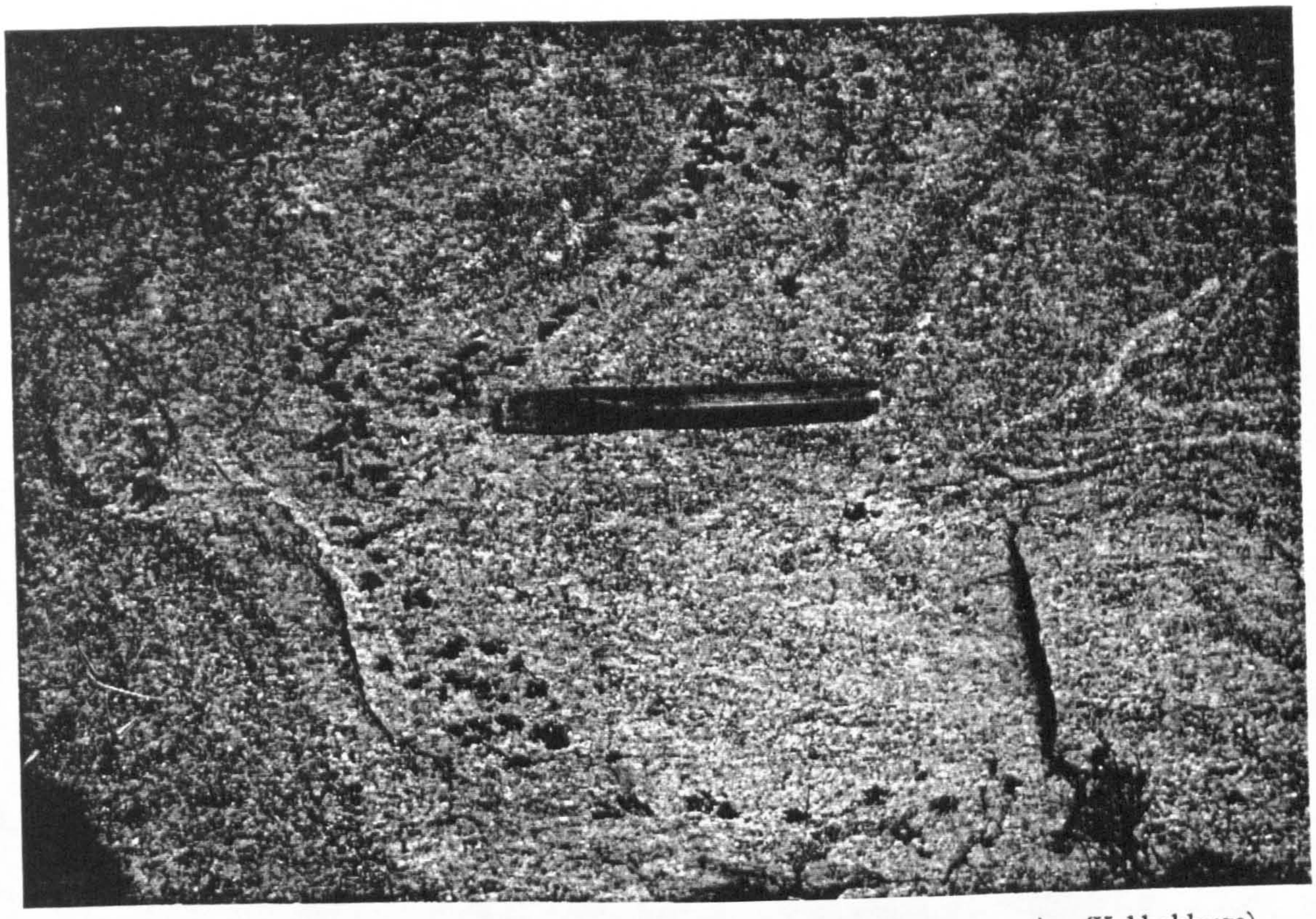

Plate 3.6. Orthopyroxene crystals growing in a conformable partial melt segregation (Kabbaldurga).

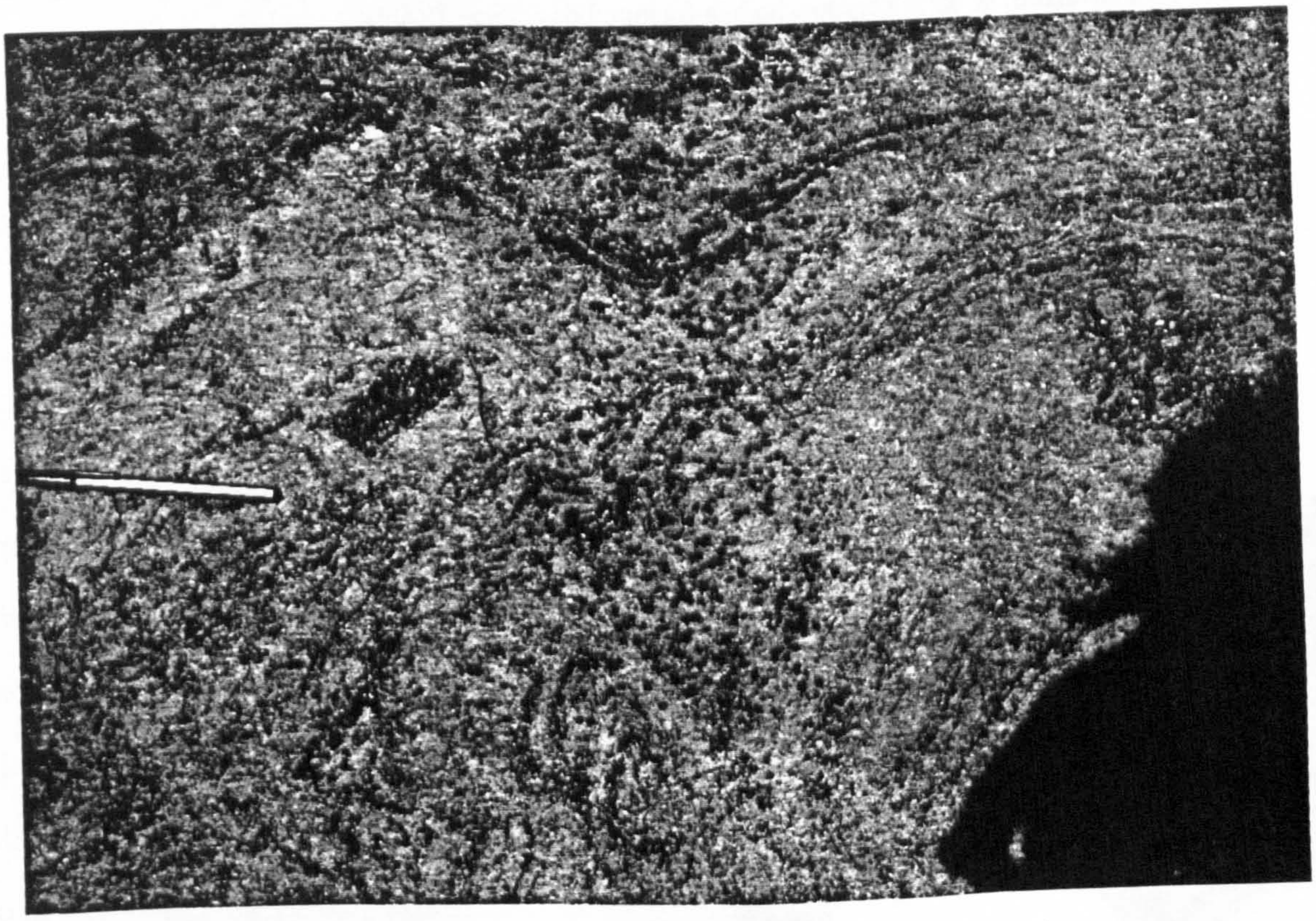

Plate 3.7. Orthopyroxene 'porphyroblasts' growing in amphibolite gneiss after deformation (Kabbaldurga).

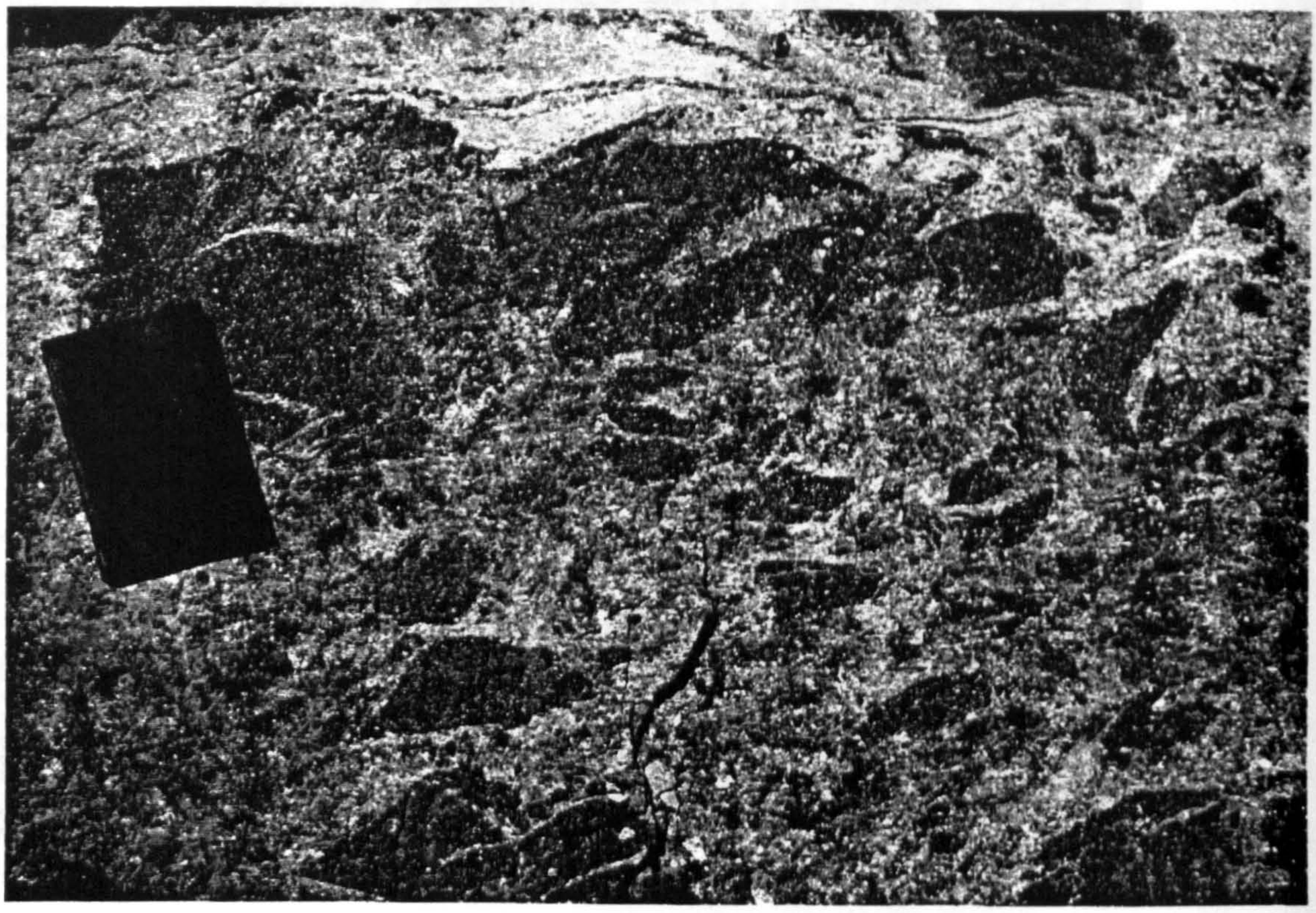

Plate 3.8. Coarse charnockite in a fractured basic lens. (Kabbaldurga)

Early petrographic observations identified that the reaction essentially involved orthopyroxene replacing biotite and hornblende (Pichamuthu, 1953). Occasional examples of grains of biotite and hornblende being overgrown by orthopyroxene have been identified to establish the prograde nature of the transformation, although examples of the retrogade replacement of hypersthene by biotite and hornblende are more common. The Peninsular gneiss has tonalitic to trondhjemitic composition (Condie *et al.* 1982) and consists of quartz, microcline, plagioclase, biotite and hornblende with common accessories magnetite, apatite, ilmenite, and zircon (Plate 3.9). The charnockite has a similar composition (Janardhan *et al.* 1982), although silica enrichment has occasionally resulted in more granitic chemistry (Stähle *et al.* 1987). Gneiss and charnockite have a similar mineralogy but the appearance of large pleochroic grains of orthopyroxene is accompanied by increases in quartz and microcline and decreases in biotite, hornblende and plagioclase abundances (Plate 3.10).

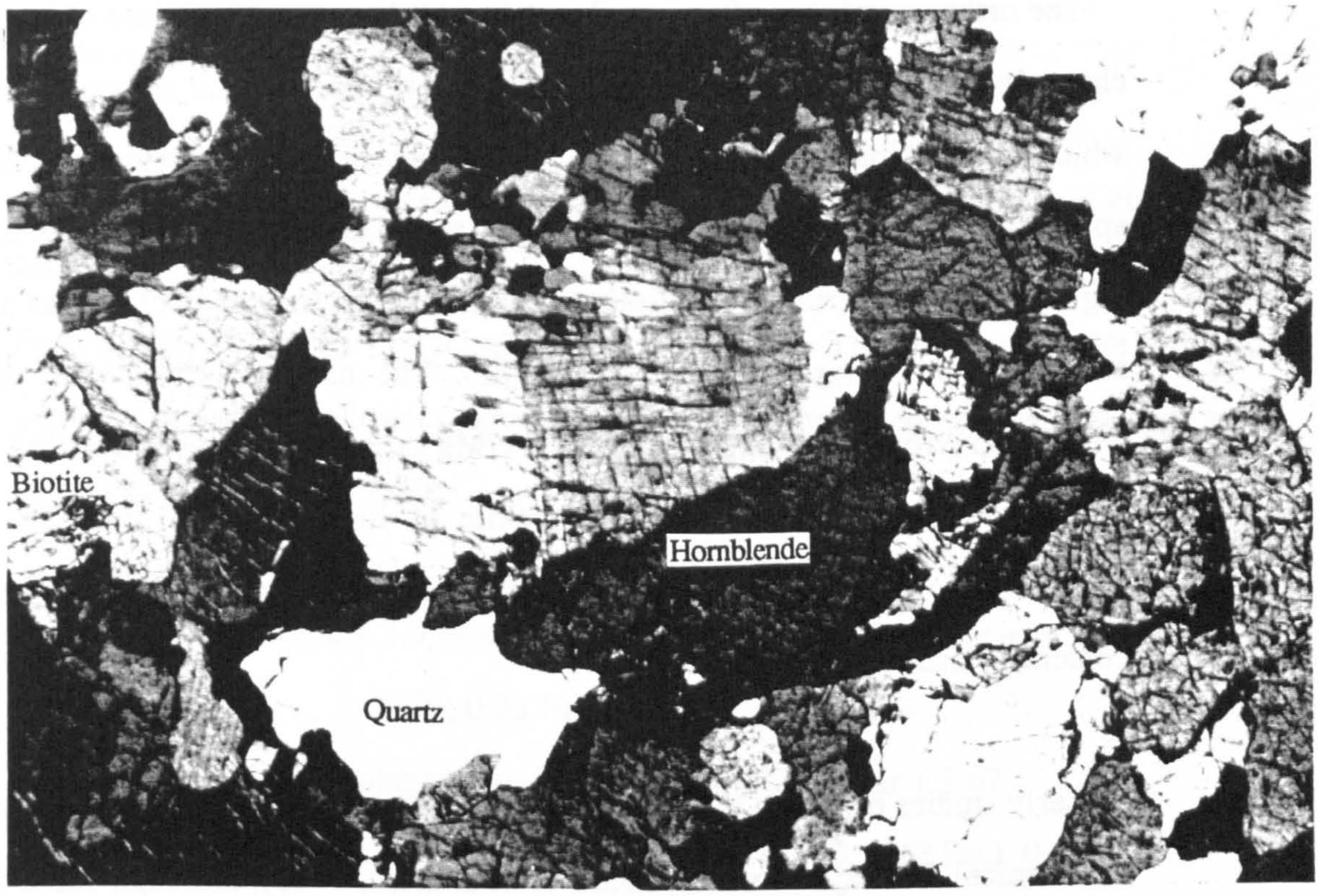

Plate 3.9. Photomicrograph of Peninsular gneiss from Kabbaldurga in cross polars, showing predominantly hornblende, quartz and microcline, plagioclase and biotite are also present (sample KA2). Plate is 3.5 mm across.

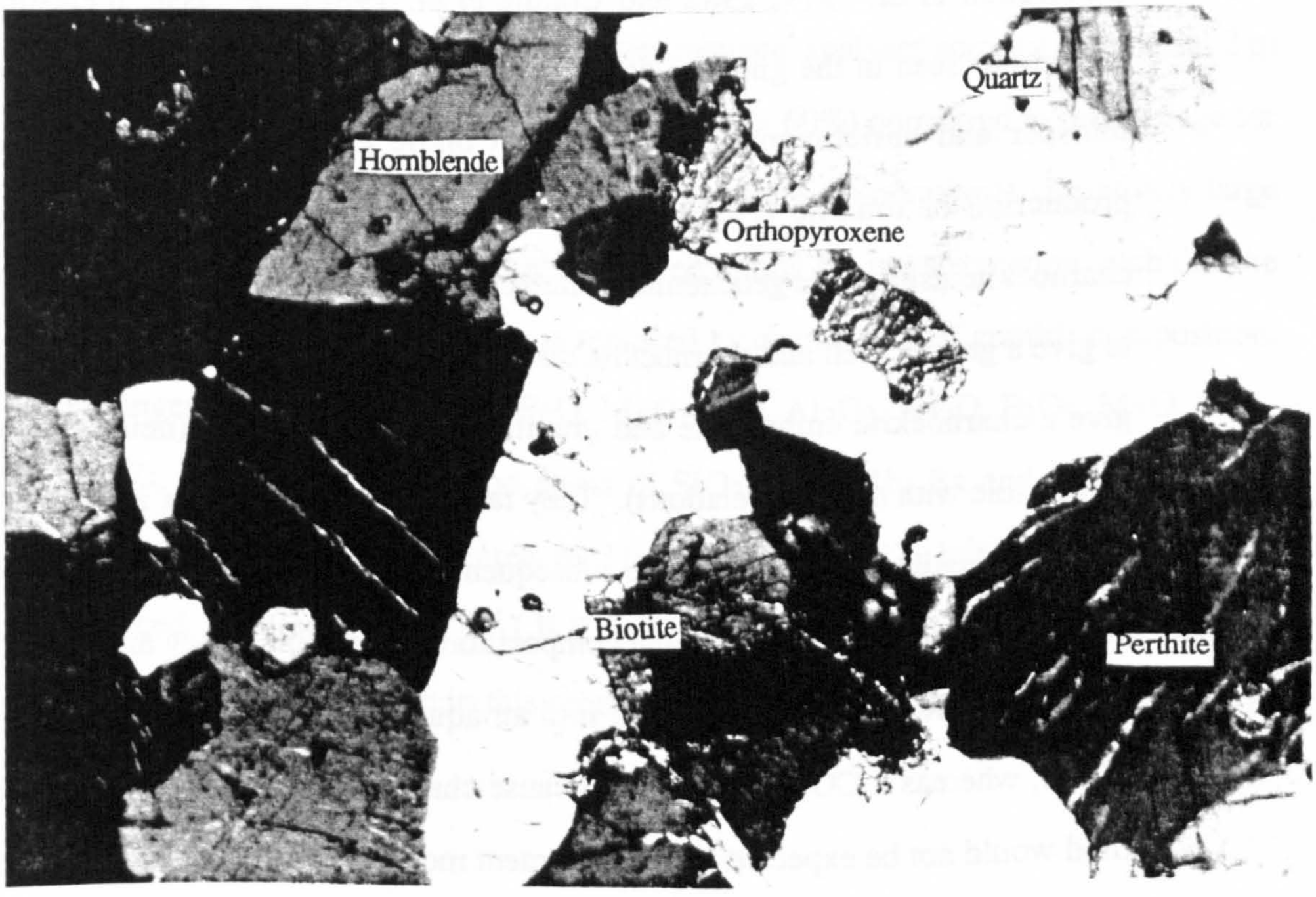

Plate 3.10. Photomicrograph of incipient charnockite from Kabbaldurga (KA5) in cross polars, showing co-existing biotite, hornblende and orthopyroxene. Recrystallisation and grain size coarsening compared to the gneiss (Plate 3.9) is obvious. (Plate is 3.5 mm across).

The orthopyroxene is often heavily retrogressed to a turgid mixture of hæmatite and clay minerals, associated with this orthopyroxene retrogression are small green veins which lace feldspar and quartz grains. The chemistry of the feldspars does not change appreciably during charnockite formation; the alkali feldspar is microcline which regularly shows perthitic exsolution of albite, whilst the plagioclase has a constant composition of An_{25-35} (Condie *et al.* 1982). The mafic minerals are all rich in iron with orthopyroxene having the highest Fe/Mg ratio (Janardhan *et al.* 1982). Biotite appears to be stablised in the charnockite by high Ti and F contents, whereas hornblende occurs mainly as a retrogressive mineral (indicated by its very low F content) (Janardhan *et al.* 1982).

Early studies of whole rock geochemistry suggested the transformation was nearly isochemical for major, trace and REE (Pichamuthu, 1965), although some small and irregular depletions of K_2O, Rb and Th in the charnockite have been reported (Janardhan *et al.* 1979, 1982 and Condie *et al.* 1982). Potassic-metasomatism is sometimes seen in the gneisses around veins of charnockite with development of K-feldspar and enrichment of the LILE. Condie *et al.* (1982) tried to model the production of tonalite (Peninsular) gneiss, granitic gneiss (Closepet granite) and charnockite using their geochemical characteristics. Both partial melting of the gneiss to give a granite melt and charnockite restite, and crystallisation of a tonalite magma to give a charnockite cummulate and granitic liquid are rejected (neither of which are compatible with the field relations). They favour partial melting of a tholeiite parent to give the tonalite gneiss and invoke subsequent metasomatism to form charnockite and granite gneisses, depending on the composition of the fluid. They argue that elements such K and Rb will be partitioned into an aqueous fluid and can granitise areas of gneiss, whereas a CO_2-rich fluid will cause charnockite formation. Such a CO_2-rich fluid would not be expected to cause element mobility. Early geochemical analyses of gneiss and charnockite showed an isochemical change, supporting the CO_2 infiltration

pairs of gneiss and charnockite have revealed such depletions (Hansen *et al.* 1987, Stähle *et al.* 1987).

Hansen *et al.* (1987) report analyses of five close pairs of gneiss and charnockite and detect subtle changes in whole rock chemistry. They document decreases in CaO, Fe_2O_3, MgO, Y and Rb and increases in SiO_2 and Na_2O during charnockite formation and they derive the following equation for the reaction based on a system open to all components except aluminium:

hornblende + 1.3 biotite + 1.24 quartz + 0.82 magnetite + (4.23 SiO_2, 0.38 Na_2O) added from fluid =

1.49 plagioclase (An_{21}) + 1.43 K-feldspar + 3.67 orthopyroxene + 0.57 ilmenite + (1.44 CaO, 2.12 FeO, 0.58 MgO, 2.3 H_2O/F, 0.41 O_2) removed by fluid.

Stähle *et al.* (1987) obtained a suite of geochemical analyses across a continuous 2 m section (which is surprisingly rich in charnockite (> 60%) compared to the average for the quarry at Kabbaldurga < 5% charnockite (author's observation)). Relatively large variations in whole rock chemistry are recorded during the transformation, such that the gneiss of granodioritic composition is replaced by charnockite of granitic composition. The changes, which show loss of FeO, MgO, CaO, Al_2O_3, Na_2O, P_2O_5, MnO, TiO_2, Zn, V, Zr and Y to the fluid and gains of SiO_2, K_2O, Rb, Ba and Sr, are broadly consistent with those documented by Hansen *et al.* (1987) but significantly more pronounced. The enrichment of LILE and change to granitic compositions strongly suggests that the charnockite in this section has a melt composition and is an intrusive phase.

Stähle *et al.* (1987) and Jiang *et al.* (1988) present oxygen isotopic analyses for gneisses and charnockites from Kabbaldurga which all lie in the range 6.9 - 8.0‰

(w.r.t. SMOW). The charnockites are on average only 0.2‰ heavier, which Stähle *et al.* (1987) attribute to the higher abundance of quartz and K-feldspar (^{18}O-enriched phases) in the charnockite. These results either indicate that there has not been enough fluid to alter the rock's isotopic signature or that the fluid and rock had similar initial isotopic compositions.

3.3.3 Fluid characteristics

Hansen *et al.* (1984) studied the fluid inclusions across a N-S traverse in southern Karnataka (≈ 50 km) from amphibolitic gneiss through incipient charnockites (at Kabbaldurga) to massive charnockites. Two major fluid inclusion generations were identified in quartz and felspar grains, both occurring as fracture-bound arrays. The charnockites are dominated by trails of pure CO_2 inclusions, in contrast to the amphibolite gneisses which mainly contain arrays of mixed CO_2-H_2O inclusions or pure H_2O inclusions. In the charnockite the texturally early trails of pure CO_2 inclusions often terminate within grains, suggesting entrapment before recrystallisation was complete. The later trails are dominated by H_2O with mixed CO_2-H_2O inclusions only occurring where the two generations intersect. Occasional isolated H_2O inclusions are believed to have survived the charnockite forming event, preserving an earlier fluid regime.

Microthermometric measurements on the pure CO_2 inclusions reveal a considerable spread of densities from each locality and sometimes a distinct bimodality, which is probably due to partial re-equilibration by inclusion volume changes during decompression (**5.3**). The densities generally record pressures slightly below those measured using mineral barometers. There is, however, a significant trend of increasing density southwards into the massive charnockites which directly correlates with other barometry estimates (see Figure 5.3a). This trend provides evidence for peak entrapment of the fluids, so their contents provide reliable indications of the fluids

which accompanied charnockite formation.

Hansen *et al.* (1984) also use mineral equilibria on the charnockite assemblage orthopyroxene-quartz-biotite-K-feldspar to estimate the water activity and constrain a_{H_2O} to 0.1 - 0.35. The calculation was performed assuming the pure Mg end-members in the mafic minerals, addition of Fe, Ti or F to the system will stabilise biotite to higher water activities. $X_{H_2O} = 0.35$ is about the proportion of water which may be undetected in a CO_2-rich inclusion and Hansen *et al.* (1984) report observing this quantity of water in a few irregular large inclusions.

3.3.4 Conclusions

Many of the field relations suggest that the gneiss-charnockite transformation was effected by the influx of CO_2-rich fluids along zones of enhanced permeability, such as shears and lithological boundaries. This hypothesis is supported by mineral equilibria, which constrain the water activities to low values, and the contents of fluid inclusions which illustrate a predominance of CO_2 in the charnockite and H_2O in the gneiss. Most studies have emphasised the isochemical nature of the transformation, indicative of a sub-solidus fluid controlled transformation, but in more heavily charnockitised areas considerable element mobility has been suggested. The element mobility observed is, however, more easily explained as FAMIPOF melting of the gneiss to a sufficient degree to permit melt mobility. Field structures support these conclusions, with evidence for some of the incipient charnockites formed by a sub-solidus transformation and others, with intrusive contacts, probably crystallised from a mobile melt.

The contemporaneous granitic intrusions and partial melting provide an additional complication. The model, proffered by Friend (1983), argues for a wave of H_2O-rich fluids, causing migmatisation, to preceed the CO_2-rich fluids, which cause charnockitisation and arrest the melting. This hypothesis is however unable to account

for the intrusive veins of charnockite. An alternative model involves the Peninsular gneiss being initially vapour-absent, at a temperature near to that of the FAMIPOF invariant point. Influx of a variety of CO_2-H_2O fluid compositions from the nearby granite to the gneiss can cause a variety of effects including wet melting and granite formation, subsolidus charnockite formation or FAMIPOF melting leading to igneous charnockite formation. This model will be discussed in more detail (Chapter 7) when a greater understanding of the source of CO_2 and mechanism of its movement through and interaction with the gneiss has been gained from the carbon isotope study presented in Chapters 5 and 6.

3.4 INCIPIENT CHARNOCKITE FROM SOUTH OF PALGHAT-CAUVERY SHEAR ZONE

To the south of the Palghat-Cauvery shear zone, the highland areas consist of massive charnockite and lowland areas are dominated by supracrustals. Amphibole, the characteristic mineral of the amphibolite facies, is absent (except retrogressively) from all acid and intermediate rocks and biotite is the only hydrous phase present. In the supracrustal areas alumina-poor lithologies, form massive charnockites (3.4), whereas alumina-rich metasediments are biotite gneisses (Ravindra Kumar and Chacko, 1986). Despite preservation of incipient charnockite formation in biotite gneiss the whole area has been described as in the granulite facies due to the absence of amphibole (Srikantappa *et al.* 1985). Although it has also been identified in a few localities in the Tamil Nadu block (Figure 3.3), incipient charnockite is most common in the Kerala Khondalite Belt. Santosh (1987) reports the petrologic and fluid characteristics of the minor unit of cordierite gneisses in the Kerala Khondalite Belt adjacent to the Achin Kovil shear zone. These outcrops although not strictly incipient charnockites provide important evidence for the tectonic regime during charnockite formation.

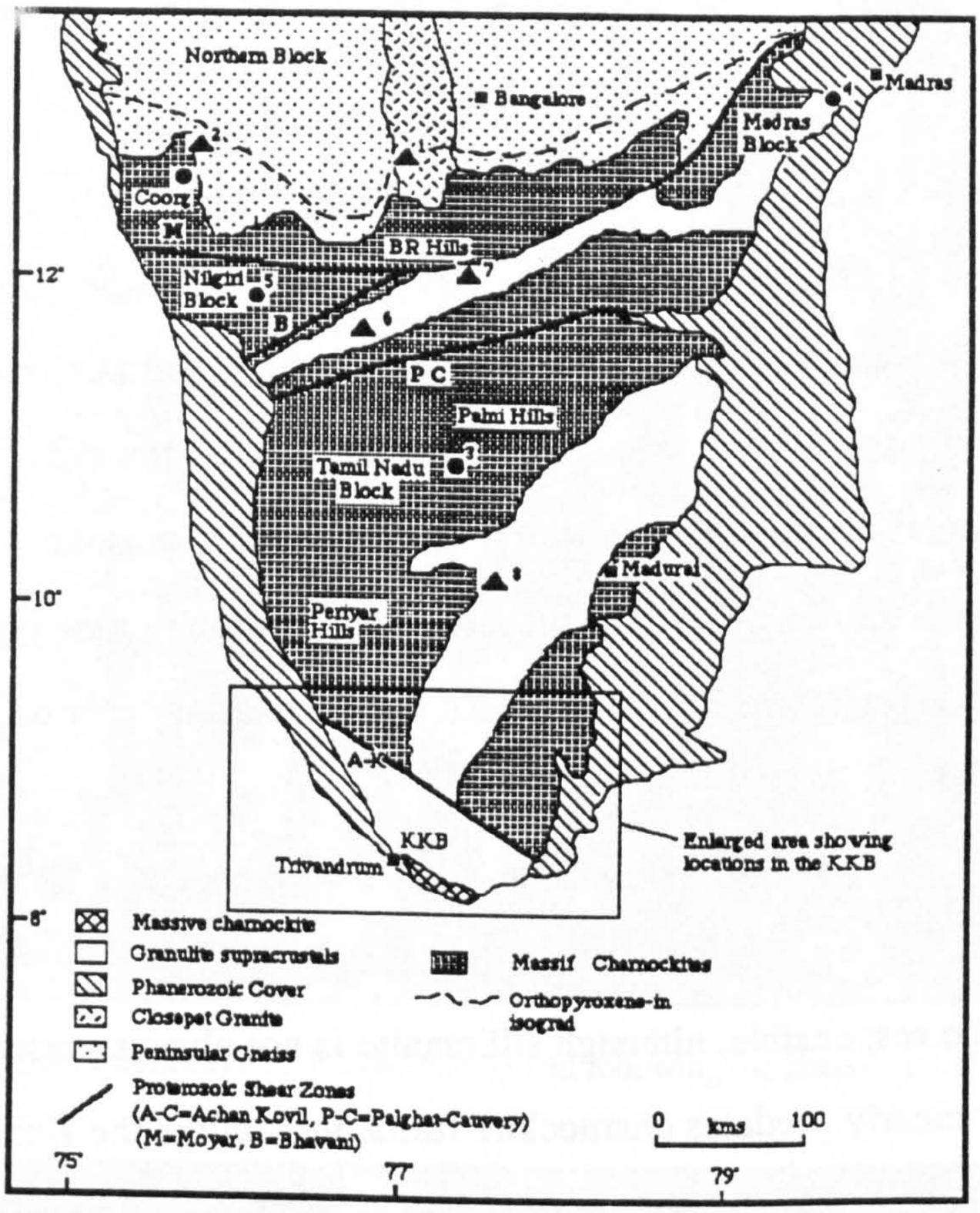

Figure 3.3a. Map showing the incipient charnockite localities (filled triangles) and massive charnockite localities (filled circles), investigated in this study. 1=Kabbaldurga; 2=Coorg; 3=Palni Hills; 4=Madras; 5=Nilgiri Hills; 6=Koddakad; 7=Salem; 8=Andipatti (see Appendix B for sample description).

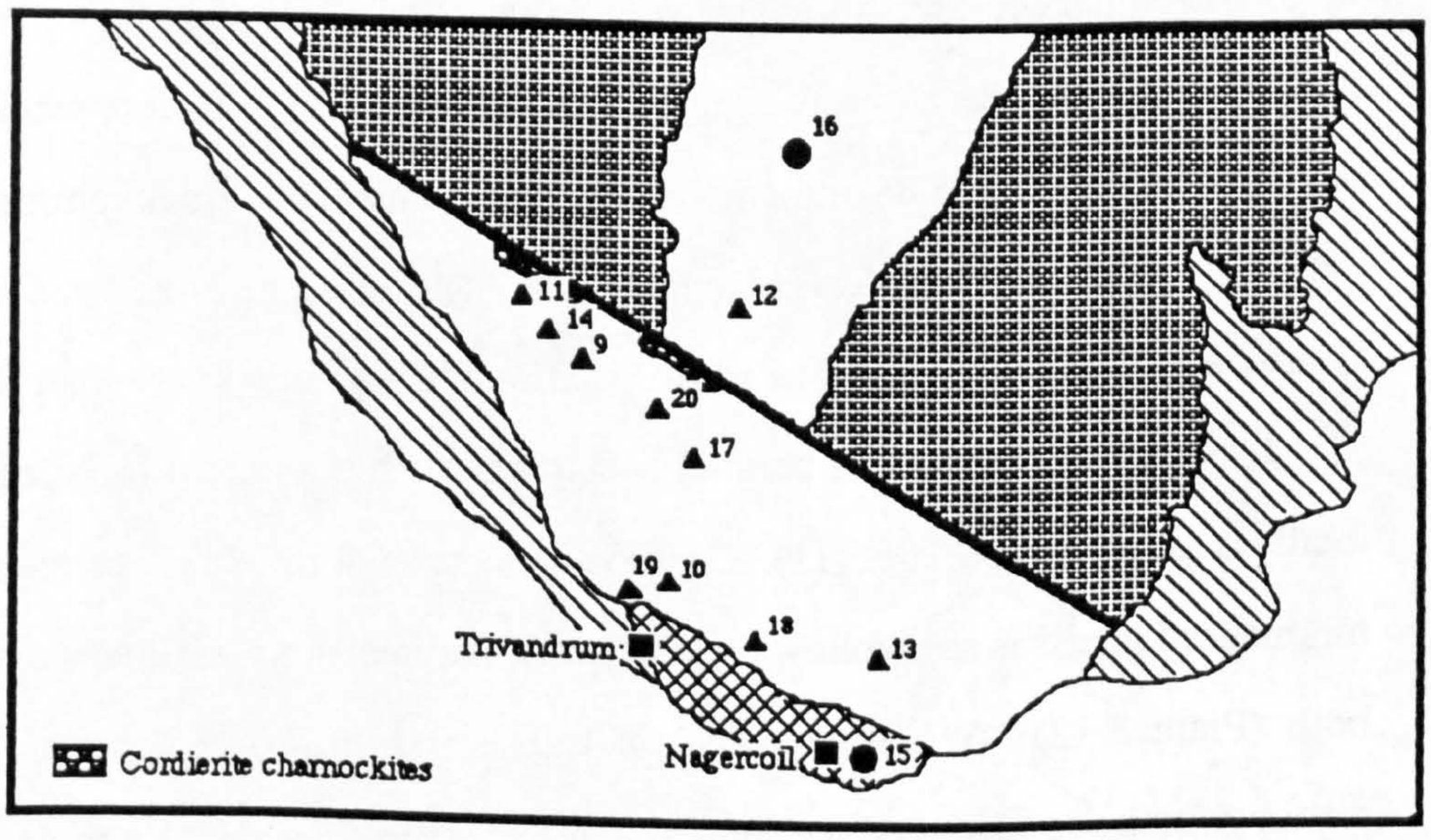

Figure 3.3b. Enlarged simplified geological map of the Kerala Khondalite Belt (KKB) (symbols are the same as Figure 3.11a), showing incipient charnockite localities studied in this thesis. 9=Kottavatom, 10=Manali, 11=Kalanjur, 12=Kuttalam, 13=Panaikkudi, 14=Kadamakad, 15=Kottaram, 16=Rajapalayam, 17=Ponmudi, 18=Nuliyam, 19=Mannantala, 20=Kadakaman.

3.4.1 Field relations

Incipient charnockite is commonly preserved in the garnet-biotite ± graphite gneiss (leptynite) lithologies. These gneisses exhibit structural variations from a faint foliation to migmatitic structures; all of which are sometimes over-printed by incipient charnockite. In some areas large leucocratic segregations of quartz, feldspar and garnet are found. Srikantappa *et al.* (1985) argue for a subsolidus origin for such lenses, although the composition of the leucosome and their morphology in the field suggests anatexis (*eg.* Plate 3.12). A vapour-absent melting reaction of the type observed in metapelites

biotite + sillimanite + quartz = garnet + K-feldspar + liquid

(*eg.* Waters, 1988)

may be responsible, although sillimanite is not always present. This migmatisation event clearly predates charnockite formation, unlike the Kabbaldurga-type incipient charnockite which has a close genetic relationship with partial melting (Friend, 1983).

Charnockite occurrences were initially reported from Panaikkudi and Ponmudi (Holt and Wightman, 1983 and Ravindra Kumar *et al.* 1985), but comprehensive studies have since documented more than one mode of incipient charnockite formation from a variety of quarries in the Kerala Kondalite Belt (Srikantappa *et al.* 1985 and Ravindra Kumar and Chacko, 1986). The most common morphology shows patches and bands of charnockite forming both parallel to and across the gneissic foliation partially or totally obliterating it (Plate 3.11). Charnockite is often formed in shear zones and in the migmatised gneiss is seen following leucocratic and melanocratic layers or cross-cutting both (Plate 3.12). Where charnockite transects biotite-free leucocratic pods the orthopyroxene is observed forming at the expense of garnet (Ravindra Kumar and Chacko, 1986). In general garnet is destroyed during charnockite formation (Hansen *et al.* 1987). Srikantappa *et al.* (1985) conclude that

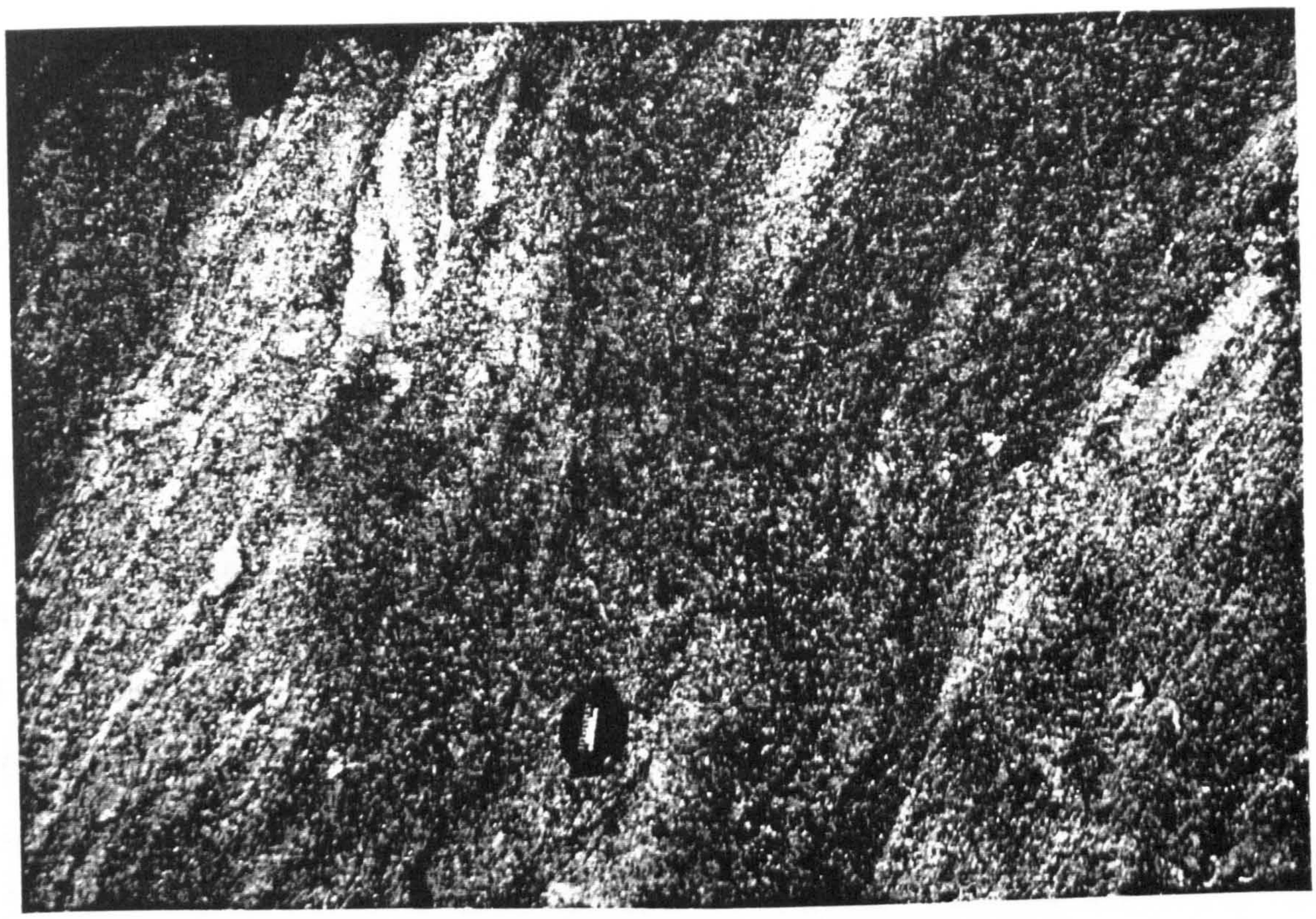

Plate 3.11. Incipient charnockite both cross-cutting and following the gneissic foliation at Ponmudi.

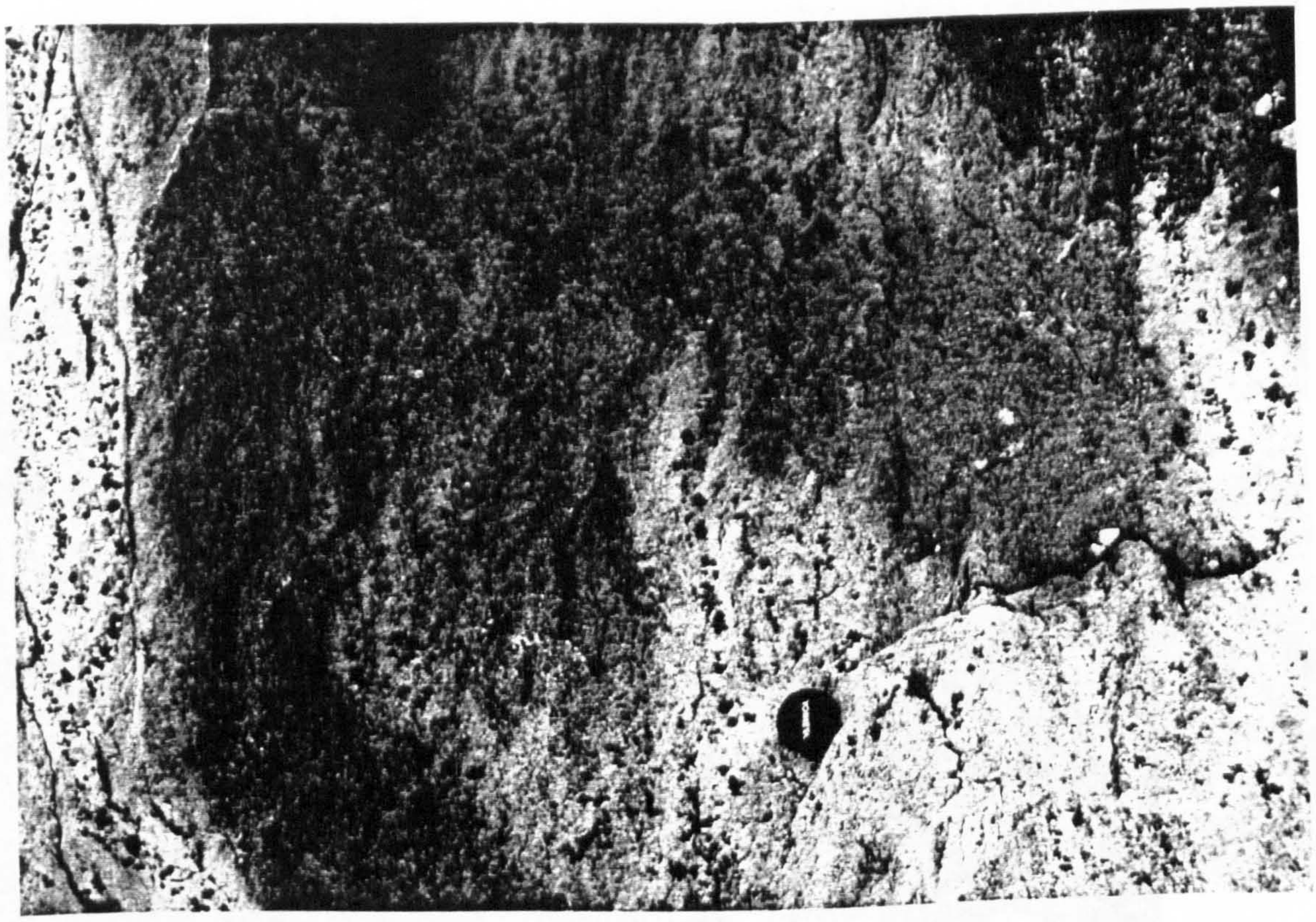

Plate 3.12. Charnockite post-dating migmatisation. It is seen both warping around the melt leucosome and cross-cutting it in a shear zone (Kadamakad).

charnockite forms preferentially in two steeply dipping planes (N30E and S70E) which they interpret as conjugate fracture surfaces (Plate 3.13). They also illustrate a quarry where the charnockitisation is approaching completion with only rafts of gneiss remaining.

Ravindra Kumar and Chacko (1986) describe two other modes of charnockite formation; one is associated with calc-silicate and the other with granitic intrusives. Where calc-silcate lithologies occur they are mantled by coarse-grained charnockite (Ravindra Kumar and Chacko, 1986 and author's observation), this provides convincing evidence that at least some charnockite formation is due to a locally-derived CO_2 influx-driven transformation (Plate 3.14). Further discussion of this type of charnockite formation is presented in Chapter 6 which is a case study of such an occurrence.

Plate 3.13. Incipient charnockite forming along oriented directions at Mannantala.

Plate 3.14. Coarse charnockite forming around a pod of calc-silicate material (Kadakaman).

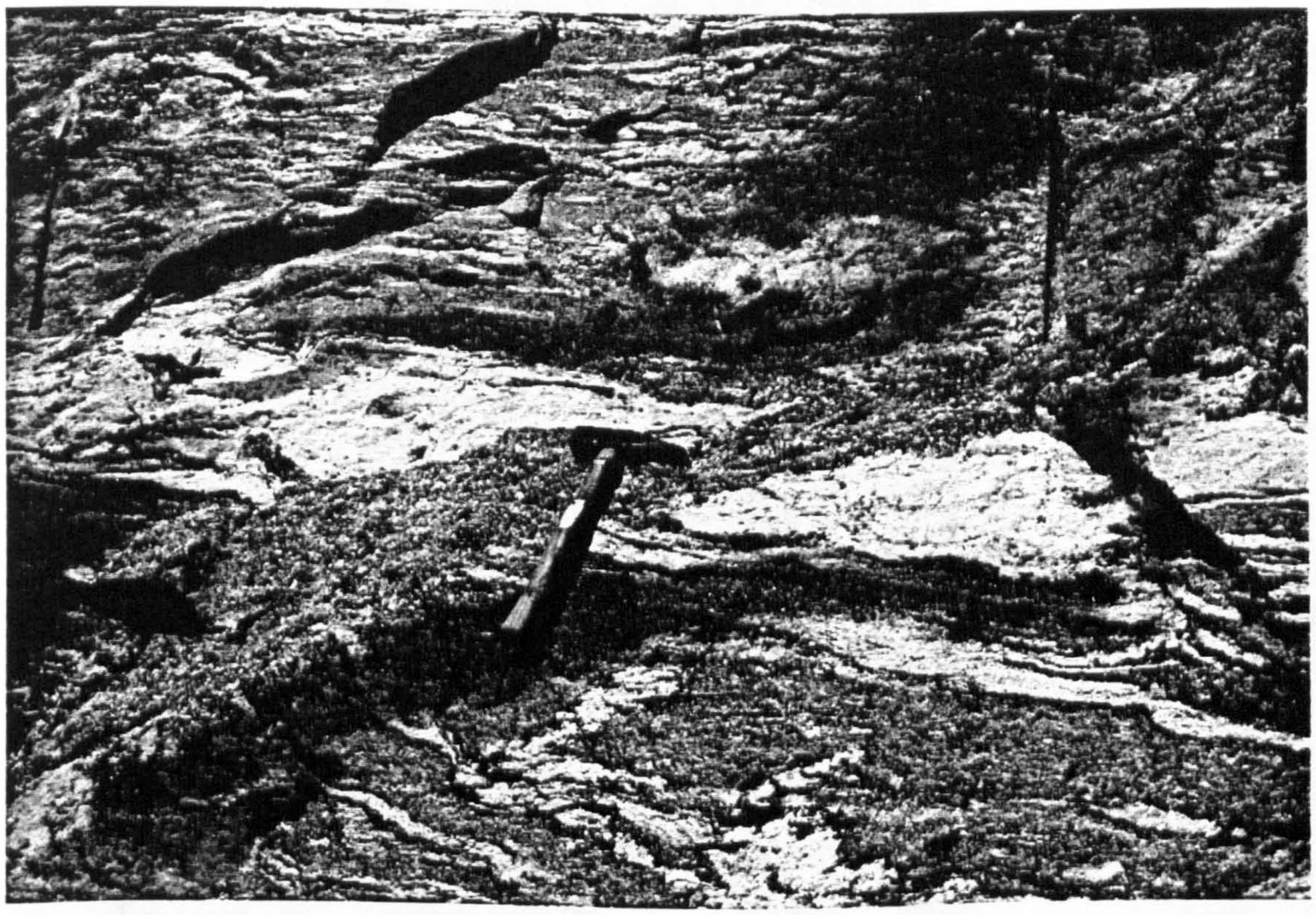

Plate 3.15. Charnockite forming as rims around a granitic intrusive. CO_2 brought with the intrusion pervades the surrounding rock, dehydrating it. Partial retrogression of the charnockite was caused by water released on final crystallisation of the magma (Kalanjur).

Ravindra Kumar and Chacko (1986) interpret charnockite rims around granitic dykes (Plate 3.15) and veins around brittle fractures (Plates 3.16a and b) as decompression phenomina. Such locations provide both enhanced fluid flow pathways and a possible transport mechanism, so an influx of CO_2 cannot be discounted. Although the field relations in the KKB are all compatible with charnockite formation by influx of CO_2, alternative explanations which deserve consideration include decompression (Ravindra Kumar and Chacko, 1986), pore fluid release (Srikantappa *et al.* 1985) and internal fluid buffering (Hansen *et al.* 1987).

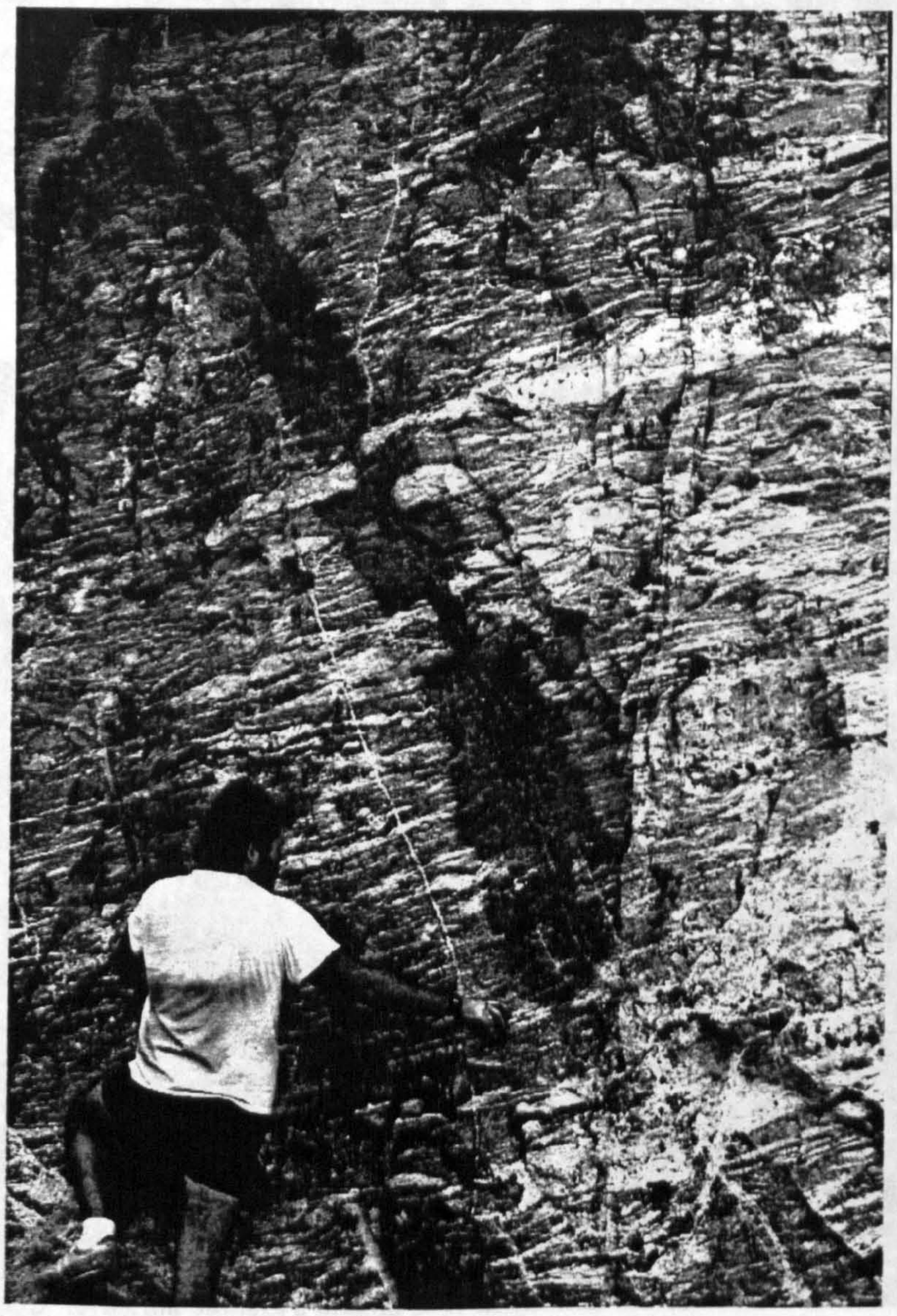

Plate 3.16a. Charnockite forming around a crack which provided an easy fluid pathway (Kalanjur).

Plate 3.16b. Charnockite forming around conjugate fractures (Andipatti).

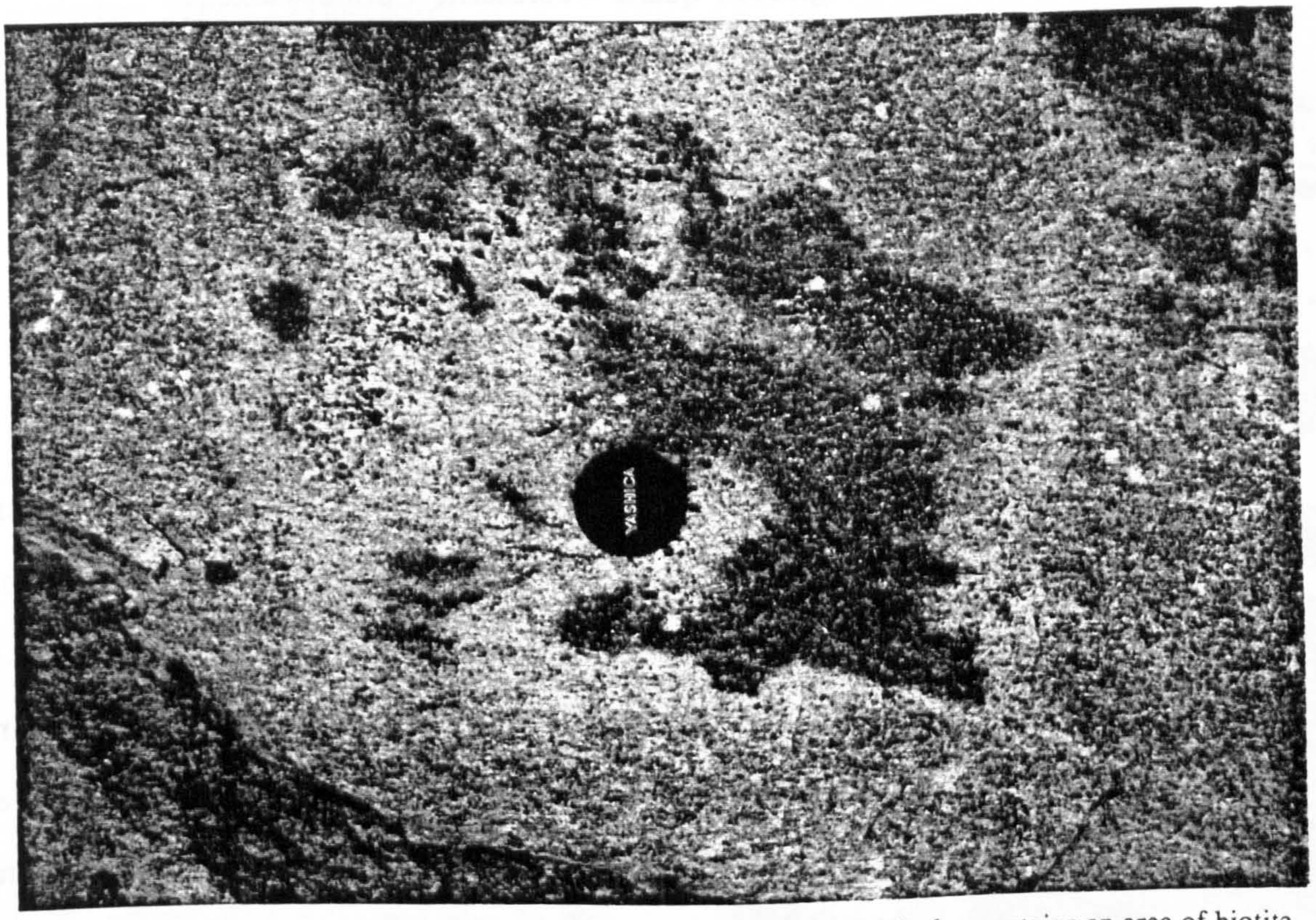

Plate 3.17. Charnockite formation in a bleached area of gneiss which also contains an area of biotite-pegmatite (on the left), suggesting element mobility and a strong possibility of a partial melting mechanism (Mannantala).

In some localities (*eg.* Kottavatom and Mannantala) graphite-bearing gneisses, which have not undergone an earlier migmatisation episode, have incipient charnockite forming as isolated pods surrounded by a bleached rim. Although these pods are often oriented (Plate 3.13), the gneissic foliation is completely obliterated and occasionally both charnockite and pegmatite formations are preserved within the same bleached patch (Plate 3.17). These instances suggest charnockite formation may be associated with melting, although no melt migration has occurred.

The cordierite gneisses to the south of the Achin Kovil shear zone (Figure 3.3b) provide reaction textures indicative of decompression. These include symplectic intergrowths of cordierite and hypersthene (± K-feldspar) forming in and around garnet and garnet break down to cordierite (Santosh, 1987). He interprets these structures as suggesting the reaction

garnet + quartz = cordierite + orthopyroxene

whilst symplectite preservation suggests rapid uplift. These rocks have the green greasy appearance of charnockites, but blue cordierite patches make their pelitic compositions distinctive.

3.4.2 Petrography and geochemistry

Hornblende is absent from the area, so the charnockite formation process is not identical to that at the orthopyroxene isograd. The precursor gneiss consists of garnet, biotite, plagioclase, K-feldspar, quartz, ilmenite, apatite, zircon and sometimes graphite and pyrrhotite (Plate 3.18). This oxide mineralogy is suggestive of relatively reducing conditions in the gneiss; under such conditions graphite precipitation would be expected to accompany an large influxes of CO_2 (Lamb and Valley, 1984). Although graphite is coarsely recrystallised in the charnockite, an increase in its abundance is generally not obvious (see Chapter 5).

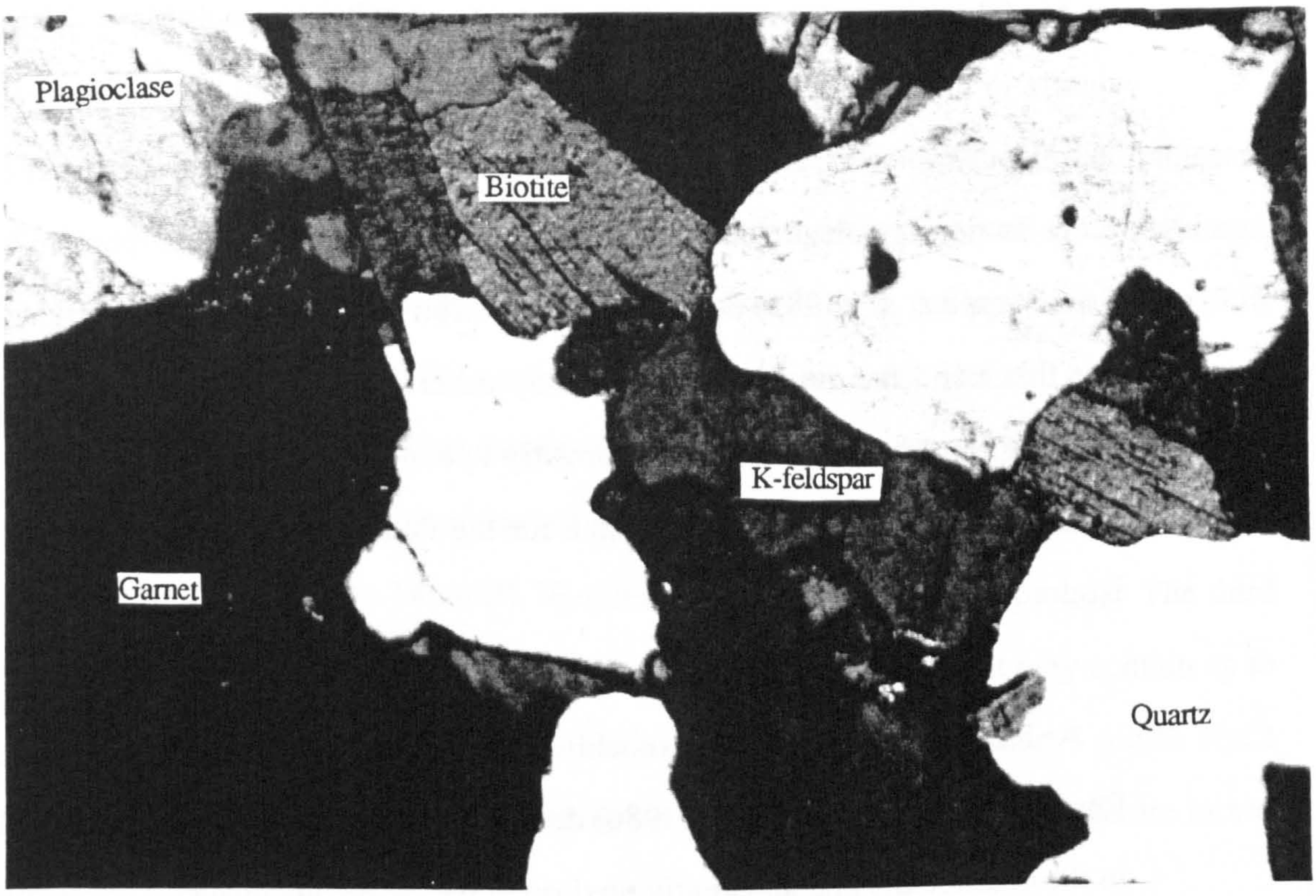

Plate 3.18. Photomicrograph of a garnet-biotite gneiss from Kalanjur in cross-polarised light. The large isotropic grain in the lower left is garnet. Low birefringent minerals are quartz, K-feldspar and plagioclase. Plate is 2.23 mm across.

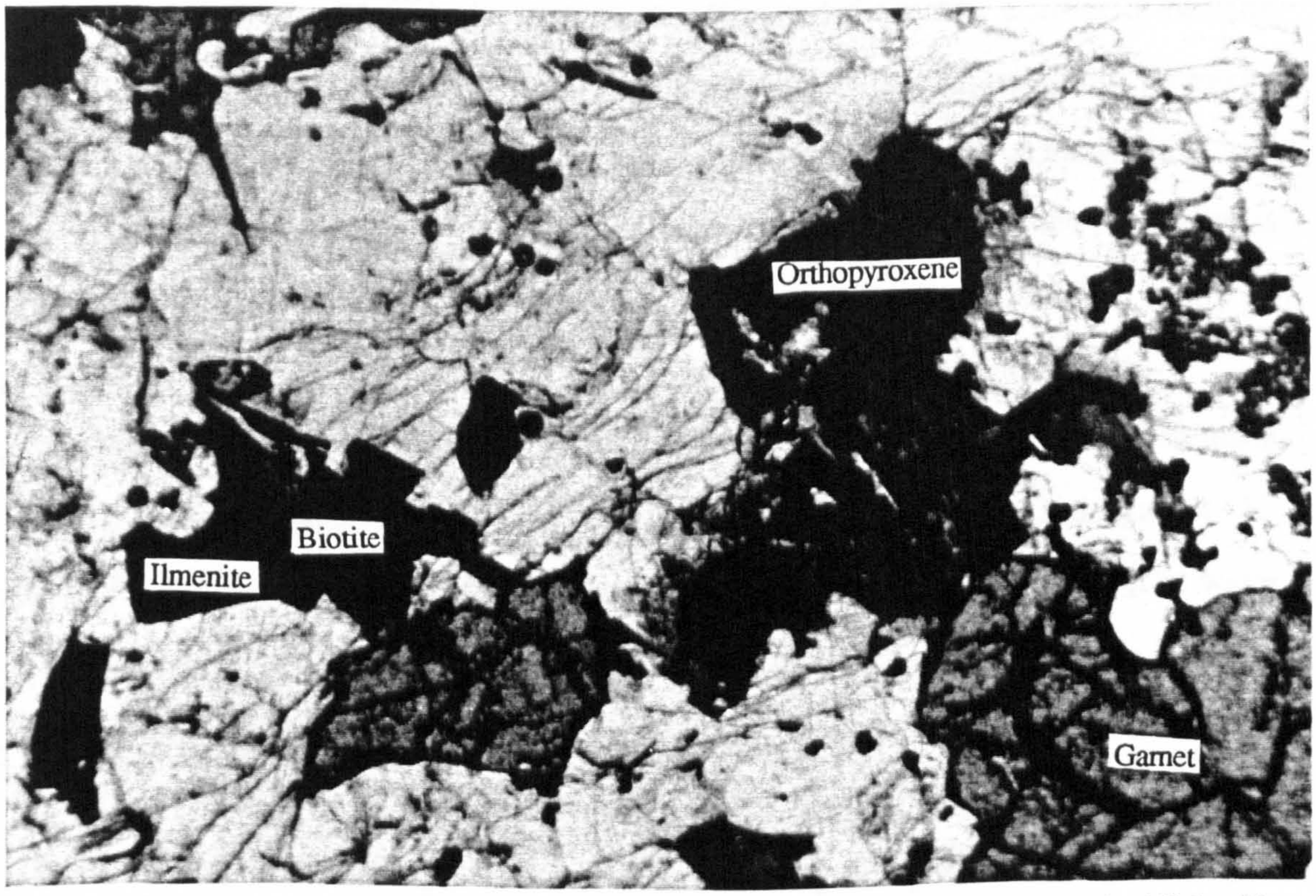

Plate 3.19. Photomicrograph of an incipient charnockite from Kalanjur in plain polarised light. The orthopyroxene which is present is heavily retrogressed and biotite grains are corroded. The opaque phase is ilmenite formed during biotite breakdown. Plate is 3.5 mm across.

Modal analyses document a decrease in the abundance of biotite, garnet and perhaps quartz in the charnockite and an increase of K-feldspar and orthopyroxene (Ravindra Kumar and Chacko, 1986 and Hansen *et al.* 1987) (Plate 3.19). Across the transition there is no significant change in mineral chemistry or minor phase abundances. Srikantappa *et al.* (1985) document a small iron enrichment in the charnockitic biotite but this trend has not been recorded by other studies (*eg.* Hansen *et al.* 1987 and Chapter 6). The mafic mineral chemistry is controlled by the bulk rock composition which is generally richer in iron than for the Peninsular gneiss at the orthopyroxene isograd.

At Kalanjur (Plate 3.15) charnockite forms at the margins of intrusive acidic dykes. Ravindra Kumar and Chacko (1986) document a shift towards more calcic plagioclase in the charnockite and apparently no drop in the biotite abundance. These observations led to the suggestion of decompression charnockite formation by the reaction

garnet + quartz + Na-plagioclase = orthopyroxene + Ca-plagioclase.

This does not explain the enrichment in LILE in the charnockite (Ravindra Kumar and Chacko, 1986), which is suggestive of an input of fluid from the granite.

Whole-rock geochemistry suggests that the gneiss to incipient charnockite transformation is essentially isochemical, with only minor enrichments and depletions (Srikantappa *et al.* 1985, Hansen *et al.* 1987). Unlike at the orthopyroxene isograd there is no LILE depletion. Consequently various closed system models have been proposed to explain these modes of incipient charnockite formation. The $\delta^{18}O$ of both charnockites and gneisses is reported to be identical at 10.3‰ (Jiang *et al.* 1988 and Raith *et al.* 1989), which is claimed to preclude the influx of large volumes of mantle derived CO_2 ($\delta^{18}O \sim 8‰$).

3.4.3 Fluid characteristics

The evidence gleaned from fluid inclusions in the Kerala Khondalite Belt indicate a more complex fluid phase than the CO_2-H_2O binary system observed at Kabbaldurga. Klatt *et al.* (1988) find four principal types of inclusions in the incipient charnockite localities of South Kerala. The earliest phase present are a few isolated briny-aqueous inclusions believed to be relicts that have survived metamorphism. CO_2-rich inclusions which occur in several sets of healed microfractures are the dominant type. These sometimes contain up to 14 mol% N_2 (identified by Micro Raman probe). The third type of inclusions are N_2-rich and are reported to be free of CO_2 but may contain up to 16 mol% CH_4. Trails of small H_2O inclusions containing less than 4 mol% NaCl denote the youngest generation. Only where these intersect CO_2-rich trails are mixed CO_2-H_2O inclusions found.

Two generations of CO_2 inclusions are reported from the cordierite-bearing charnockites; early scattered and later array bound types, as well as arrays of mixed CO_2-H_2O inclusions (Santosh, 1987). The mineral assemblage is only stable at low values of a_{H_2O} and the cordierite contains abundant CO_2 entrapped in the channelways (Santosh *et al.* in prep.).

Chacko *et al.* (1987) estimate the water activity in the Kerala Khondalite Belt using equilibrium assemblages in both khondalites (biotite - quartz - sillimanite - garnet - K-feldspar) and charnockites (biotite - quartz - K-feldspar - orthopyroxene). The water activities derived from the two lithologies are identical and relatively uniform throughout the area ($a_{H_2O} = 0.27$). In this study they take into account the Fe-Mg solid solution yielding more reliable results than earlier estimates (Hansen *et al.* 1984). No systematic variation of a_{H_2O} with either bulk Fe-Mg composition or Ti activity is detectable. These observations led the authors to conclude that the water activity must

have been buffered externally by an influx of water-poor fluids.

3.4.4 Conclusions

Incipient charnockites from south of the Moyar shear zone are fundamentally different from those preserved at the regional orthopyroxene-in isograd. The charnockite forming reaction involves orthopyroxene replacing biotite (or garnet) in contrast to hornblende. Charnockite formation, although sometimes related to intrusives, is not contemporaneous with migmatite formation in the gneiss. Some incipient charnockites from the Kerala Khondalite Belt exhibit structures which suggest that they may be *in situ* partial melts, no charnockite melt mobility is observed, and no element mobility has been documented from the Kerala Khondalite Belt incipient charnockites.

The incipient charnockite formations from south of the Moyar shear zone can be divided into six major groups, based on the divisions outlined by Ravindra Kumar and Chacko (1986).

(1) Charnockite formation around calc-silicate lithologies.

(2) Charnockite formation around pegmatites and cracks.

(3) Patchy charnockite formation in graphite-bearing gneiss, with evidence for melting.

(4) Patchy charnockite formation in graphite-bearing gneiss, without evidence for melting.

(5) Charnockite associated with cordierite formation.

(6) Charnockite formation in zones of enhanced permeability, in the absence of graphite.

Models, outlined in **2.5**, which have been proposed to explain some of these charnockite formations include:

(a) Influx of CO_2-rich fluids.

(b) Isothermal decompression.

(c) Internal fluid modification by graphite oxidation.

(d) Melting/*in situ* recrystallisation.

(e) H_2O removed/CO_2 added by passage of dry magmas.

None of these possibilities can be ruled out in the light of the field relations and data reviewed above, although the ubiquitous presence of CO_2-rich inclusions in general supports the mechanisms related to modification of the pore fluid composition. The field evidence confines the applicability of some models to certain localities (*eg*. model (c) requires the presence of graphite in the gneiss), but does not rule out the possibility of model (a) being important in all localities. The metasedimentary origin of the Kerala Khondalite Belt has resulted in the presence of graphite- and carbonate-bearing units, both of which are intimately associated with charnockite formation. The presence of these carbon-bearing phases makes this area ideal for a detailed carbon isotope study to constrain the sources of CO_2 and differentiate between the various models.

3.5 MASSIVE CHARNOCKITE

The massive charnockites exposed in southern India are particularly interesting because considerable doubt exists as to whether there is sufficient CO_2 available in the lower crust or mantle to dehydrate such large areas by carbonic fluid flushing (*eg*. O'Nions and Oxburgh, 1988). Three types of massive charnockite are distinguished in this thesis;

(a) large charnockite massifs which form much of the highlands to the south of the orthopyroxene isograd.

(b) aluminous-poor lithologies in supracrustal sequences which are devoid of hornblende but often have biotite coexisting with orthopyroxene.

(c) massive 'granitic' charnockites in the Nagercoil region (Figure 3.3b) which display igneous field relations.

In each of these types retrogression to bleached biotite-gneiss is seen around cracks or pegmatitic intrusions, a phenomenon also associated with deformation and shear zones. The bleaching can often be seen spreading out along the foliation, suggesting a fluid controlled process (Plate 3.20). The petrology, geochemistry and fluid characteristics of this retrogression are outlined at the end of each section.

3.5.1 Field relations

Pichamuthu (1965) distinguished a 'granulitic' type of charnockite with granoblastic equant texture but gneissic foliation or migmatitic structures, from a 'granitic' type with coarse xenoblastic texture and no lineation. Weaver (1980) and Janardhan *et al.* (1982) suggest that the former had a gneissic precursor and the latter a granitic one. Weaver working in the Madras charnockite area (type b) extended this by suggesting the granite was formed by migmatisation of the gneiss under water-rich conditions, but the process was arrested prior to large scale melt separation by an influx of CO_2-rich fluids.

Plate 3.20. Hydrous retrogression of charnockite to biotite-gneiss due to influx of water given off granitic intrusives (Andipatti).

Type (a)

These massive charnockites are mainly free from supracrustal lithologies but commonly have basic inclusions which are thought to be disrupted sills and dykes. In the Northern block the Biligirirangan Hills massif appears to be the culmination of the regional increase in metamorphic conditions. The Nilgiri massif is surrounded on two sides by Proterozoic shear zones in which retrogression of the charnockite by hydrous fluid infiltration has been documented (Drury and Holt, 1980 and Allen *et al.* 1985). The regional relationship between the massifs in the west of Tamil Nadu block and the supracrustal sequences is unknown, but a tectonic contact is considered the most probable.

Type (b)

The massive charnockite horizons in the supracrustal sequences extend from the Madras block through the Tamil Nadu block and into the Kerala Khondalite Belt (Plate 3.21). They form conformable horizons in the sequences, but often display original intrusive relations to basic granulites and metapelite lithologies (Subramanian, 1959 and Sen, 1974). They are variably deformed to give a gneissic foliation, these structures are best exposed on weathered surfaces (Sen, 1974) (Plate 3.22).

Type (c)

These massive charnockites have a coarse xenoblastic ('granitic') texture and, despite the presence of biotite, no clear foliation. The only examples of this type of massive charnockite were found in the Nagercoil area, which is identified as a separate unit by Srikantappa *et al.* (1985) and is associated with layered anorthositic, syenitic and noritic complexes. The relationship between this area and the Kerala Khondalite Belt is unknown. The main evidence for an igneous origin comes from field studies in a quarry near Kottaram where xenoliths of metapelite can be found in the massive charnockite (Plate 3.23) with coarse orthopyroxene-bearing veins intruding these xenoliths.

Plate 3.21. Massive charnockite with basic pods which were probably disrupted sills or dykes, (basic autoliths in a charnockite magma is an alternative) (near Andipatti).

Plate 3.22. Weathered surface of a massive charnockite at Madras picking out gneissic foliation.

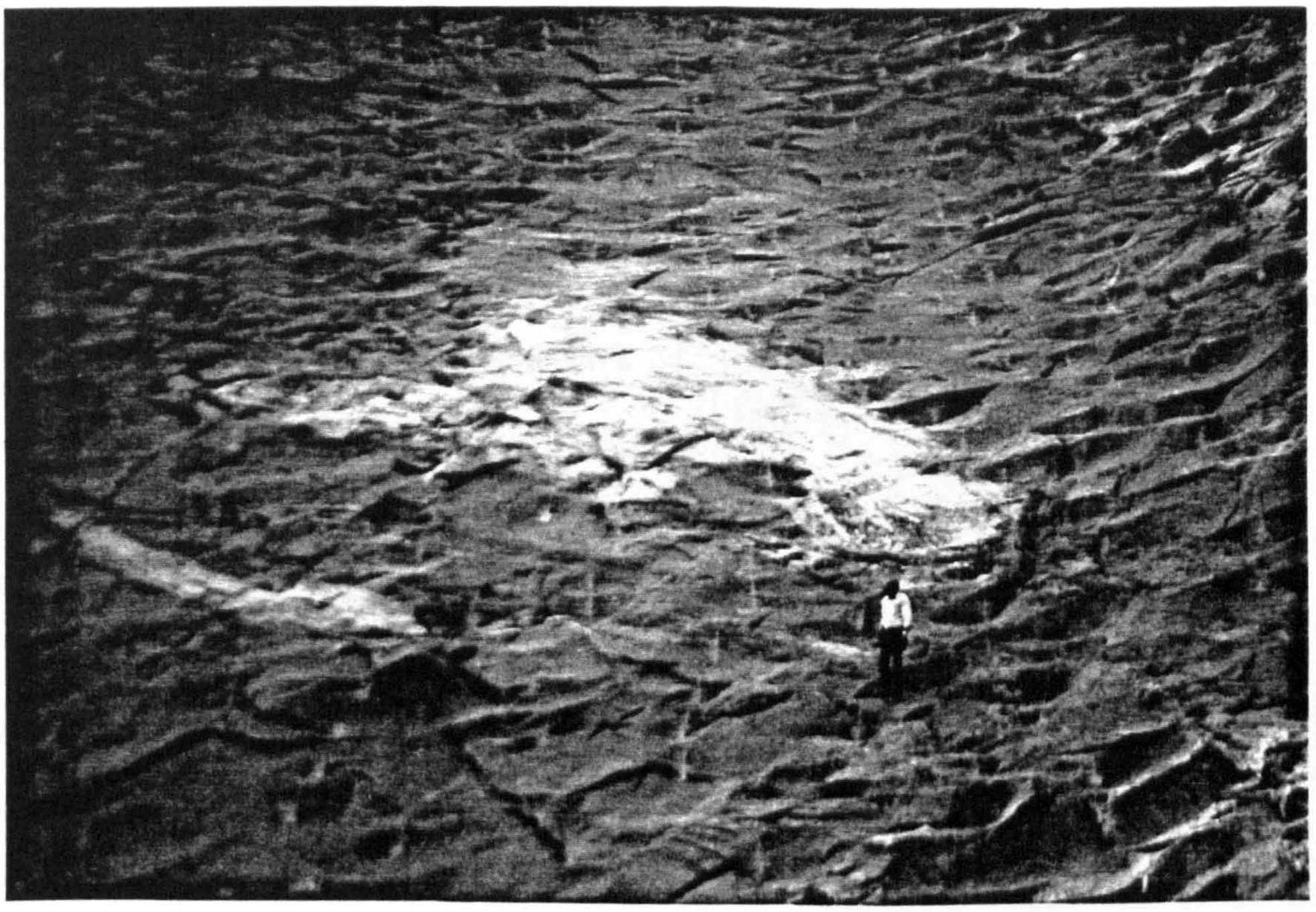

Plate 3.23. Metapelite xenoliths in massive charnockite magma (Kottaram).

3.5.2 Petrography and geochemistry

Type (a)

Geochemical and petrographic work has been carried out in the BR and Nilgiri Hills mainly as comparison to the incipient charnockite formations at the orthopyroxene isograd (Janardhan *et al.* 1982 and Condie and Allen, 1984). Hydrous minerals have been identified as retrogressive phases on the basis of their low flourine contents (Janardhan *et al.* 1982), although primary biotite has been reported in some localities (*eg.* Touret and Hansteen, 1988). Plate 3.24 illustrates orthopyroxene and hornblende in textural equilibrium from a massive charnockite in the Palni Hills, suggesting that they were both stable at peak conditions. A primary igneous origin for such massive charnockites may reconcile this observation with the low flourine contents of the amphibole. Garnet is often present and orthopyroxene is generally less retrogressed than in the incipient charnockites. Associated with this is a grey, rather than dark green, coloration which is attributed to less chlorite/calcite veins, probably because pore

water has been completely removed from the rock during granulite formation. In general the mineral chemistry reflects higher pressures (8-10 kb) (and temperatures), compared to the incipient charnockites further north (5-6 kb).

The bulk composition of the Nilgiri charnockites suggest their protolith was tonalitic to granodioritic, Raith *et al.* (1988) suggest low temperature sea-water alteration prior to metamorphism caused unusual oxygen and strontium isotopic ratios but no details are given. U-Pb, Sm-Nd, Rb-Sr whole rock isochron data is unable to distinguish between the time of protolith formation and metamorphism (Buhl, 1987, Peucat *et al.* 1989). In general the massif charnockites show depletions of LILE and REE which are typical for granulites. They contain low abundances of U, Th, Rb, Cs and light REE and hence have high K/Rb ratios (Janardhan *et al.* 1982), a strong Pb depletion has also been recorded (Condie and Allen, 1984).

Type (b)

Geochemical studies on the Madras charnockites have been used to argue against Holland's (1900) suggestion that the charnockites were intrusive rocks, although, as in the Nilgiris, Sm-Nd whole rock geochronology is unable to separate the ages of the protolith formation from granulite facies metamorphism (Bernard-Griffiths *et al.* 1987). The charnockites have very fractionated REE patterns, typical of Archæan gneisses, which is attributed to igneous processes in formation of the protolith. Atypically they are enriched in the alkali elements (Rb, Ba, K and Na/K), an effect attributed to metasomatism by potassic fluids which did not effect the REE signatures (Weaver, 1980 and Bernard-Griffiths *et al.* 1987).

Both 'granitic' and 'granulitic' types of charnockite are exposed; the former being of granitic composition and the latter varying from tonalite to quartz monzonite. The two types are also distinguished by the lack of any primary hydrous phases in the 'granitic' type in contrast to the common presence of biotite in the 'granulite' type.

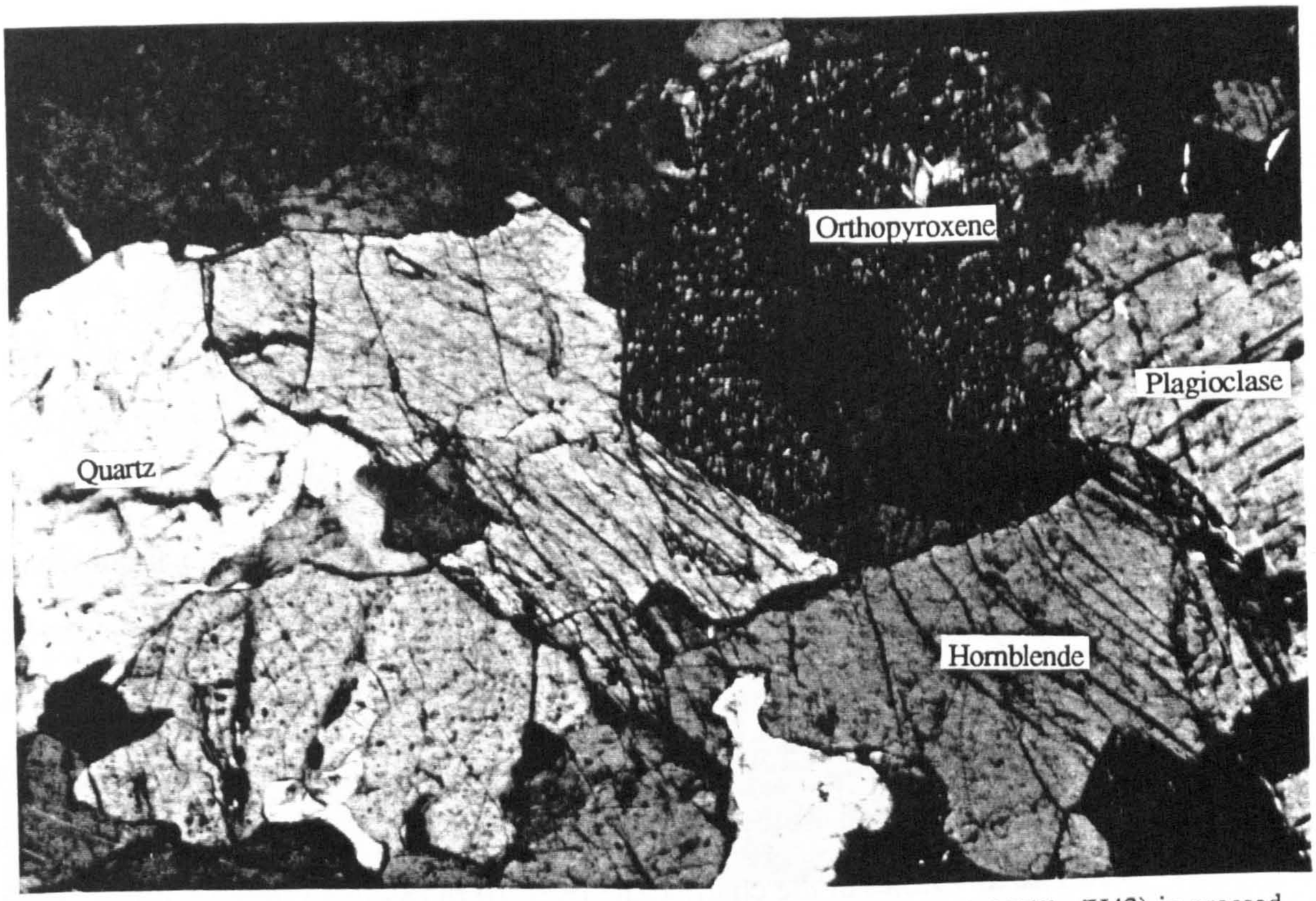

Plate 3.24. Photomicrograph of massive charnockite (type a) from the Palni Hills (H43) in crossed polars, showing orthopyroxene and hornblende in textural equilibrium with quartz and feldspar. Plate is 3.5 mm across.

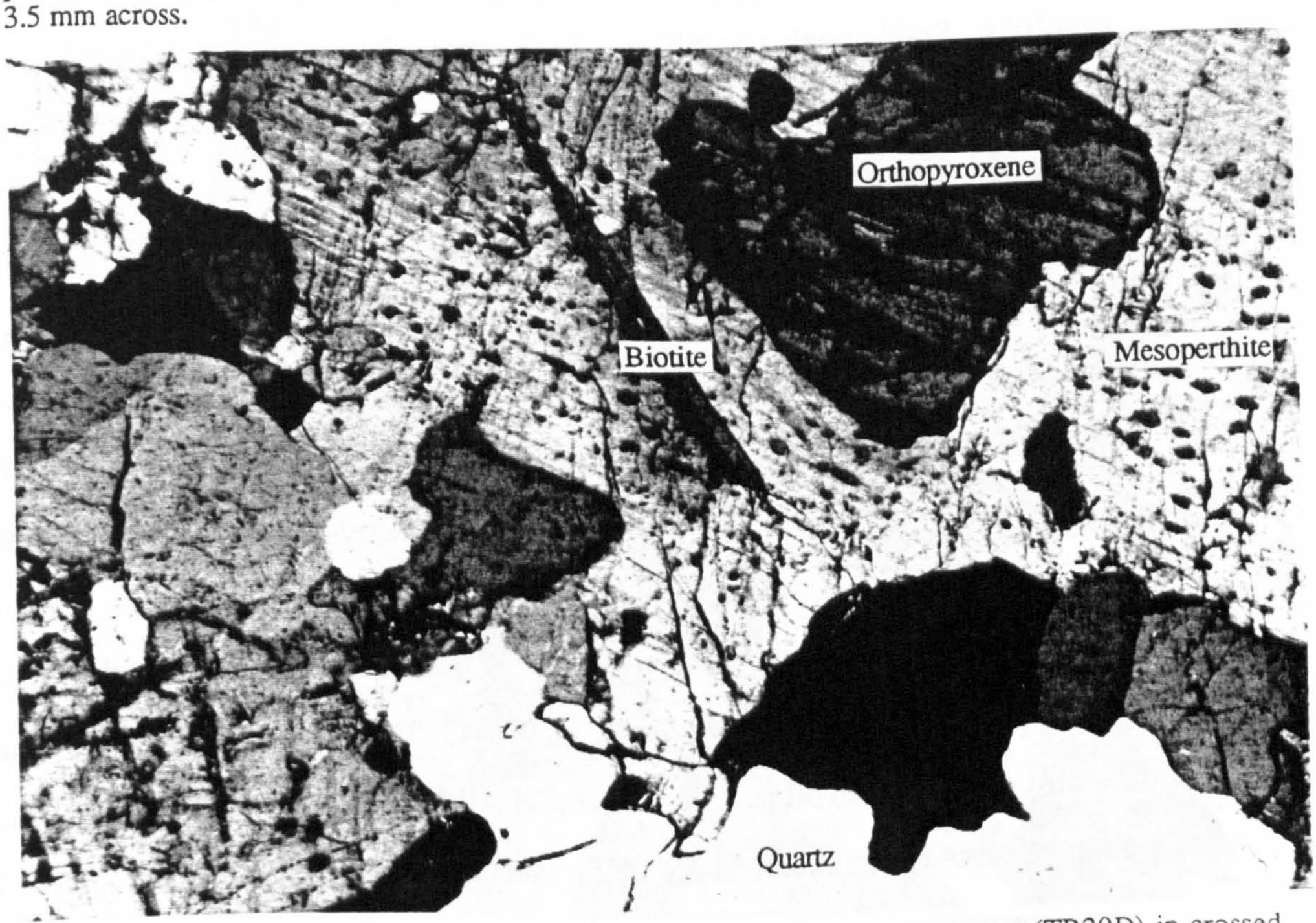

Plate 3.25. Photomicrograph of massive charnockite (type c) from Kottaram (TR20D) in crossed polars, showing orthopyroxene, a needle of biotite, quartz and a large grain of mesoperthite. Plate is 3.5 mm across.

Type (c)

The massive charnockites at Kottaram are dominated by quartz, mesoperthitic feldspar, plagioclase and orthopyroxene (Plate 3.25). Biotite is present in lower abundances than orthopyroxene and accessory phases of ilmenite, apatite and zircon are common. Graphite is absent. The geochemistry which has been published for the massive charnockites from the Nagercoil area show that they have a wide range in SiO_2 (56-72%), and linear trends between SiO_2 and Al_2O_3, FeO, MgO and CaO (Srikantappa *et al.* 1985). These charnockites also have a high Na_2O content and show clear affinities to differentiated calc-alkaline rock suites, which is compatible with a primary igneous origin. In the quarry at Kottaram the metapelite xenoliths appear to be digested by the charnockite. Support for this observation comes from the decrease in abundance of garnet away from the xenoliths, with garnet-free charnockite exposed 1-2 km away. Whole rock oxygen isotopic compositions decrease away from the metapelite from +12.1‰ to +9.0‰ in the charnockite over 20 m (Santosh, *unpub. data*). Evidence for intrusion during a decompressional regime comes from the mineralogy in the metapelite xenoliths. Stable peak assemblages in the mafic layers appear to be spinel - garnet - sillimanite - biotite (Plate 3.26), but in some areas a decompression reaction between garnet and spinel, producing cordierite is preserved (Plate 3.27).

The bleaching retrogression which occurs around pegmatite and intrusive veins in type (a) massive charnockites, is a high temperature effect with biotite and hornblende seen as overgrowths around orthopyroxene in thin section. The retrogressive nature of the hydrous minerals is confirmed by their low flourine contents (Janardhan *et al.* 1982). The bleaching involves considerable major element changes although trace element variations are surprisingly small. SiO_2 abundance increases whilst FeO, MgO and CaO decrease, but the low levels of Rb, U, Th, Pb and REE are only partly and variably restored (Janardhan *et al.* 1982 and Allen *et al.* 1985). The latter authors show an increase in the volatile content in the bleached areas, an equivalent volatile increase was observed in prograde incipient charnockite.

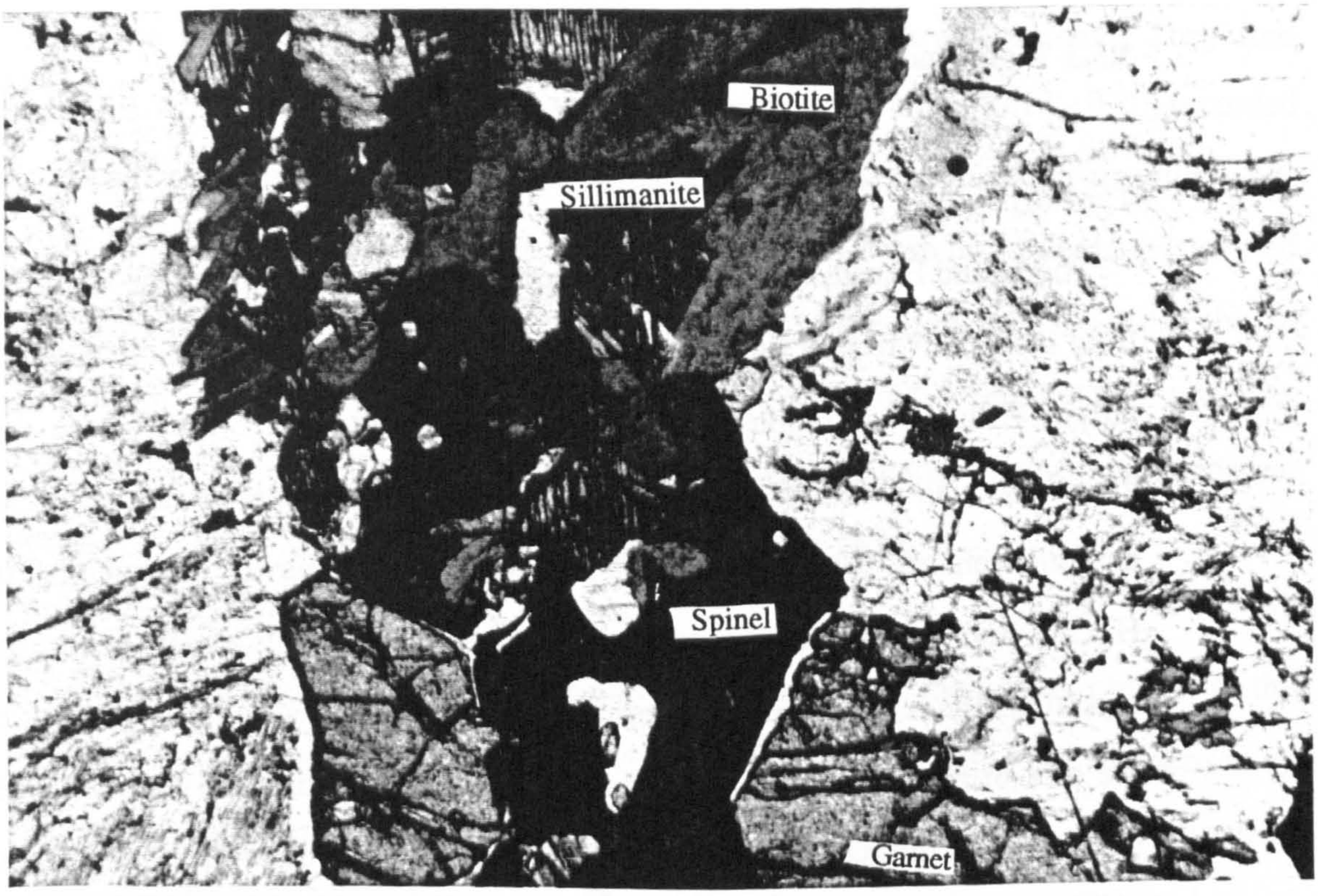

Plate 3.26. Photomicrograph of sample TR20B, taken from a metapelite xenolith within the Kottaram (type c) massive charnockite, showing a peak mafic assemblage of spinel - garnet - sillimanite - biotite. Plate is 2.75 mm across.

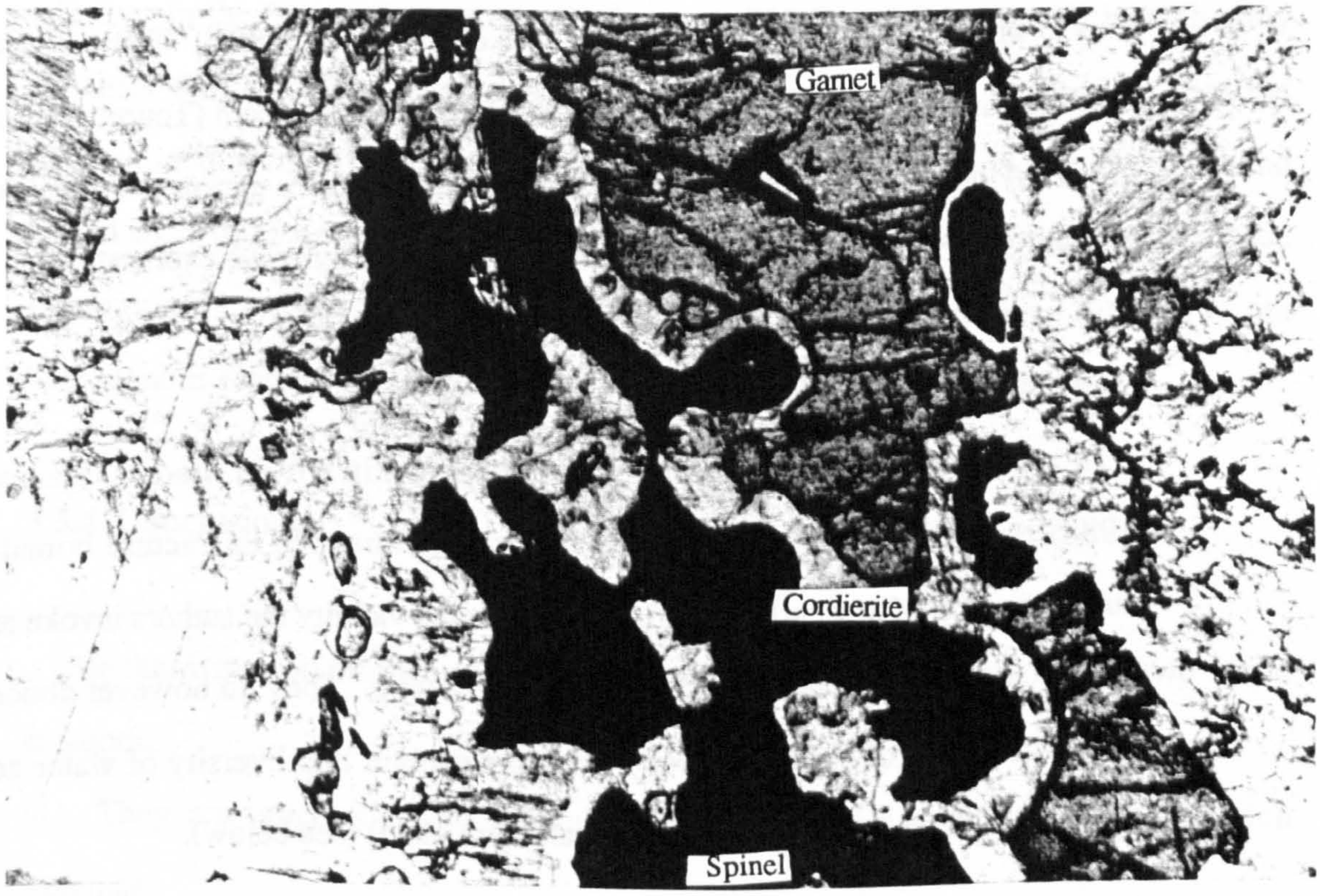

Plate 3.27. Photomicrograph of sample TR20B, taken from a metapelite xenolith within the Kottaram (type c) massive charnockite, showing decompression reaction between garnet and spinel to form cordierite. Plate is 2.23 mm across.

3.5.3 Fluid characteristics

Type (a)

Touret and Hansteen (1988) have made a very detailed study of the solid phases and fluid inclusions from a single hand specimen collected from Doddabetta quarry in the Nilgiri Hills. They report pure CO_2 inclusions from garnet, plagioclase and quartz grains, with no evidence either from freezing point or micro Raman probe studies of any other phases. Up to 20% of a 'pure' CO_2 inclusion may be occupied by 'invisible' H_2O which preferentially wets the inclusion walls, its presence during early crystallisation is indicated by the primary phlogopite crystals. The inclusions in garnet are of a primary scattered nature and decrease in abundance from core to rim. The inclusions in quartz crystals appear to be related to a discrete kinematic event but predate the latest deformation and annealing event. The inclusion densities are all high and increase with entrapment order (deduced on textural grounds) from garnet (1.00 gcm^{-3}) through plagioclase (1.06 gcm^{-3}) to quartz (1.12 gcm^{-3}). These observations are explained as peak entrapment during an isobaric cooling path (Touret and Hansteen, 1988). A decrease in the water content of inclusions from garnet to quartz due to its removel by primary biotite crystallisation provides an alternative explanation.

Type (b)

In a preliminary study on the massive charnockites from Madras, Hansen *et al.* (1988) report pure high density CO_2 inclusions entrapped in fracture bound arrays. Due to the lack of any carbon-bearing phases in the vicinity the authors invoke an influx of CO_2-rich fluids from an unknown external source. They do however conceed that fluid heterogeneity on the outcrop scale may explain the diversity of water activities recorded in different units (Battacharya and Sen 1986) (see below).

Battacharya and Sen (1986) and Sen and Battacharya (1988) have used mineral phase equilibria in charnockite and metapelite assemblages to estimate the water

activities in the Madras and Satnuru (south of Kabbaldurga) regions. They find contrasting results from the two areas; at Satnuru the same a_{H_2O} (0.13 - 0.20) recorded by both charnockites and metapelites whilst at Madras the charnockites record a_{H_2O} = 0.23 - 0.34 and the metapelites give a_{H_2O} = 0.10 - 0.16. From these results it is argued that the fluid composition at Madras was internally buffered by partial melting, but at Satnuru it was externally buffered by influx of CO_2-rich fluids. The findings at Madras cannot rule out an influx of CO_2, in sufficient quantity to cause charnockite formation but not to overcome the internal buffering ability of the rocks.

Santosh (1985 and 1986) reports three generations of inclusions present in the massive charnockites (type b) of the KKB. The earliest generation is characterised by scattered high density pure CO_2 inclusions with two subsequent generations of secondary fracture-bound inclusions. The earlier of these contains pure CO_2 and mixed CO_2-H_2O inclusions, whilst the younger contains dominantly H_2O inclusions with low salinity. In the former the variety of mixtures of H_2O and CO_2 present in each array suggests that the fluid captured was not homogeneous. It is possible that the 'schematic' diagrams (Figure 3 in Santosh 1985) of the inclusions are inaccurate and mixed inclusions only occur where early carbonic and late aqueous arrays intersect. Alternatively, if the observations are genuine and the entrapped fluid was not homogenous then the microthermometric studies carried out are invalid.

3.5.4 Conclusions

Mechanisms for producing massive charnockites can be divided into two broad catagories:

(1) They are igneous bodies crystallising directly from water-deficient CO_2-rich magmas.

(2) They form by a regional extension of the incipient charnockite formation processes described above.

Clear evidence for an igneous origin of type (c) massive charnockites exists, but such localities appear to be of very limited extent. Grant (1986) describes the crystallisation order of granitic liquids in the presence of a H_2O-CO_2 fluid phase (with most of the water component dissolved in the melt) and concludes that the relative abundances of orthopyroxene and biotite/amphibole which result depends on the abundances of CO_2 and H_2O.

It could be argued that types (a) and (b) massive charnockites also crystallise directly as igneous charnockite because protolith and metamorphic ages are generally indistinguishable. The preservation of gneissic foliation and depleted geochemistry argue against this possibility, although a depleted lower crustal protolith may be expected and subsequent granulite facies deformation may obliterate the igneous textures. An alternative possibility is that massive charnockite formation is simply an extension of the process described at the orthopyroxene isograd (Newton *et al.* 1980 and Weaver 1980). When extensive volumes of CO_2 are involved, complete dehydration occurs which leaves the massive charnockites depleted in LILE without dramatic changes in the bulk chemistry. Although neither of these mechanisms can be dismissed, the strong possibility of charnockitic melt formation in some incipient charnockite localities argues that massive charnockites, which generally form at higher temperatures and pressures, are unlikely to form without melting except perhaps in the presence of a continual flux of pure CO_2.

Chapter 4

ANALYTICAL TECHNIQUES FOR FLUID INCLUSION EXTRACTION

4.1 FLUID INCLUSION EXTRACTION

4.1.1 Introduction

The stable isotopic composition of a metamorphic fluid can be diagnostic of its source. Since the fluid present during metamorphism is no longer preserved in the pore space, analysis of either the host rock or gas released from fluid inclusions can be used to constrain its isotopic composition. Deducing fluid characteristics from isotopic analysis of solid phases with which the fluid phase has interacted depends on assumptions related to the attainment of isotopic equilibrium and a knowledge of both the initial isotopic composition of solid phases and the equilibrium fractionation between solid and fluid (*eg*. Baker and Fallick, 1988). Assuming fluid inclusions have remained closed systems since the time of entrapment (5.3), direct analysis of fluid released from inclusions should be more reliable to interpret. This method has not been employed extensively because of the analytical problems involved in measuring the small volume of fluid trapped in inclusions. Nevertheless fluids have been extracted from their host inclusions for stable isotopic analysis by vacuum grinding and thermal decrepitation techniques (*eg*. Hoefs and Touret, 1975). The merits and short comings of both these techniques are discussed below, followed by a description of the method adapted for this study, which is designed to overcome the major problems encountered by previous studies.

4.1.2 Thermal decrepitation

Thermal decrepitation relies on the thermal expansion of the fluid within the inclusions to build up sufficient internal pressure to overcome the constraining strength of the host mineral. When this point is reached decrepitation will occur and the inclusion's contents will be released into cracks propagating from the inclusion. If decrepitation cracks intersect grain surfaces and high enough temperatures are used this method has the potential to release all the fluid and provide reliable yield measurements (see below).

Nevertheless if high temperatures are required to cause decrepitation, reactions between gaseous phases and with mineral grains may alter the composition of the gases released. For instance under given f_{O_2} conditions CO_2 and H_2O will react to produce a variety of other species including CO, H_2 and CH_4 (*eg*. Gerlach and Nordlie, 1975). Such reactions have an associated isotopic fractionation. Another problem with thermal decrepitation is that high temperatures can cause gas release from sources other than fluid inclusion decrepitation. For instance carbon dioxide can be released from the thermal breakdown of calcite, oxidation of graphite and combustion of organic contamination as well as from fluid inclusions. Careful sample preparation and analytical protocols can overcome some of these problems.

4.1.3 Vacuum grinding

Vacuum grinding ruptures the inclusions during mechanical crushing of the host mineral grains and avoids the problem of gas release from sources other than fluid inclusions. Crushing methods which have been tried include repeated dropping of a ball-bearing (Barker and Sommer, 1973), mechanical crushing within a stainless steel section of the vacuum line (Kreulen, 1980) and use of a screw action press (Mattey *et al*, 1989).

Vacuum grinding results in small and unreproducible yields for two major reasons. Firstly, the crushing process is inefficient; for example crushing experiments were carried out as part of this study (**4.4.2**) on 1 mm grains, after crushing the residue, when inspected under a microscope, consisted of 50 - 100 μm grains. The majority of fluid inclusions which have a diameter ≤ 10 μm would be preserved intact in this residue. Secondly, crushing creates a large increase in surface area and these new reactive surfaces are believed to adsorb gas very rapidly (Piperov and Penchev, 1973). Figure 4.1 which is reproduced from Barker and Torkelson (1975) shows how CO_2 is adsorbed onto the surface of quartz during crushing. In those experiments where crushing has been used to release fluid from inclusions large samples have been required (see Table 4.1).

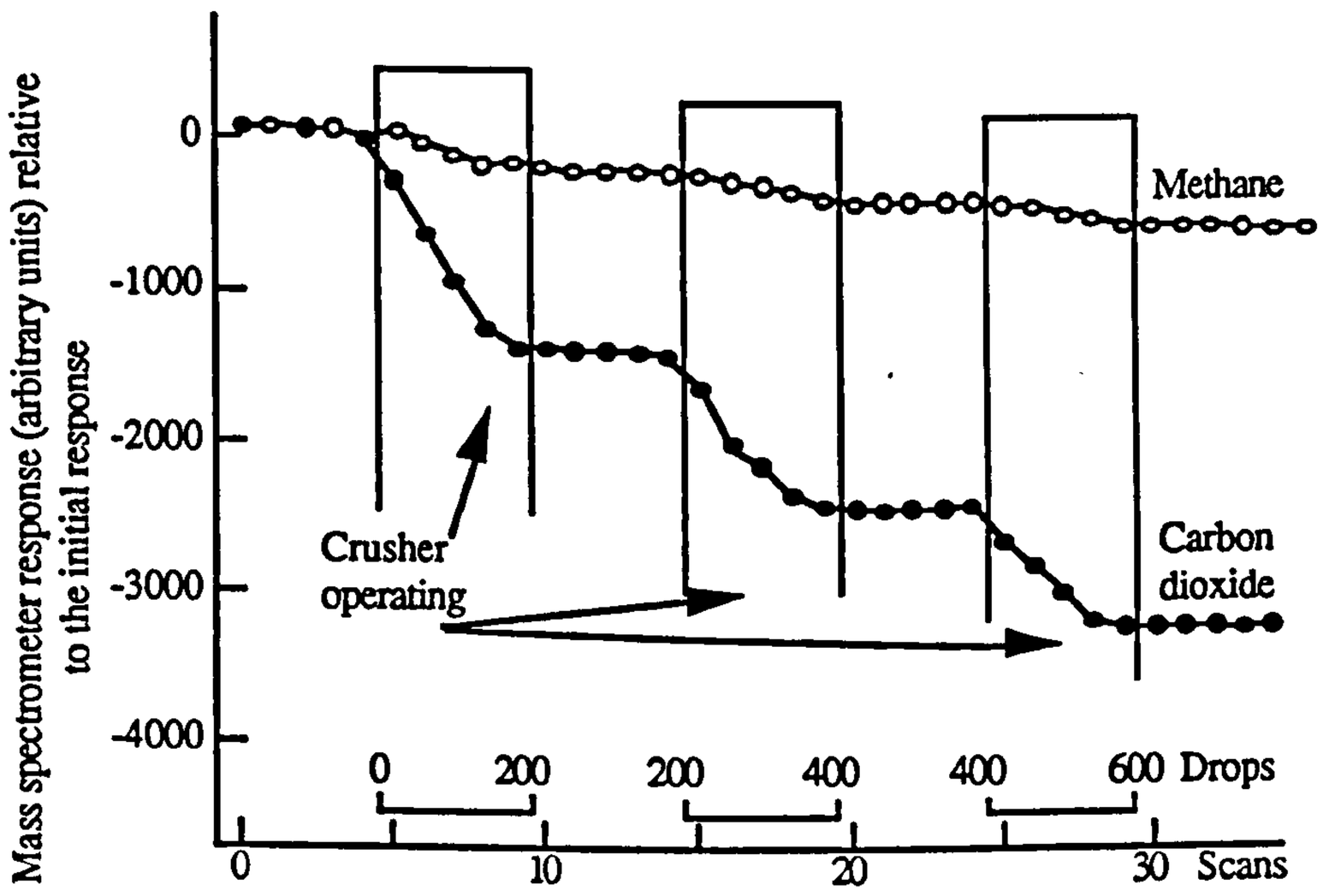

Figure 4.1. Figure 2 from Barker and Torkelson (1974) showing how CO_2 (and methane) is rapidly adsorbed on to the newly created surfaces of quartz grains during crushing.

4.1.4 Previous studies

Previous attempts to extract CO_2 fluids from inclusions in high grade rocks for isotope analysis are listed in Table 4.1. Most of these studies use quartz separates, with

samples of 5 - 308 g required to release sufficient gas for analysis. Use of such large samples not only considerably increases the possibility of sample contamination by the

Author	Area	Method	Sample size	Rock type	Yield	$\delta^{13}C$
Hoefs and Touret (1975)	Bamble, Noway	Heat (1000°C)	5-20 g	Quartz Segregations	-	-4.5 to -22‰
Pineau *et al.* (1981)	Bamble, Norway	3 Step Heat	?	Whole rock	7-52 ppm	-14 to -24‰
Kreulen (1980)	Naxos	Crushing	50 g	Quartz Segregations	1-660 ppm	1 to -13‰
Lamb (1988)	Adirondacks, USA	(a)3 Step Heat (b)Crushing	45 g 308 g	? ?	58 ppm -	-5.5 to -7.9‰ -5.1 to -7.4‰
*Vry *et al.* (1988)	Worldwide	Heat (1050°C)	0.2-0.8 g	Cordierite	0.3-1.9 wt%	0.7 to -35‰

Table 4.1. Summary of previous studies from high grade terrains which have extracted the fluids from their host inclusions for isotopic analysis. * Cordierite has large channelways which readily trap CO_2 molecules and it is this gas rather than inclusion-trapped CO_2 which is released and analysed by Vry *et al.* (see 5.4.3 for further discussion of these results).

presence of other carbon bearing phases (*eg.* Lamb (1988) reports only 80% quartz in his sample), but usually restricts sampling to quartz-rich veins and segregations. These interconnecting vein systems cross-cut structures formed at peak conditions (Hoefs and Touret, 1975) and probably represent late fluid escape channels rather than sampling the peak metamorphic pore fluid.

A wide range of isotopic compositions of the gas released is characteristic of several of these earlier studies (Table 4.1) and interpretation of these results has been problematic. The technique described below has been adapted to overcome the problems encountered by vacuum crushing and single step thermal decrepitation. In particular the use of small sample sizes was considered of vital importance so that mineral grains could be separated from samples with average bulk rock mineralogy rather than from later veins. To minimise contamination problems a low blank extraction line connected directly to the mass spectrometer was adopted and a stepped thermal decrepitation procedure was used to separate genuine fluid inclusion release from contamination and CO_2 released from other sources.

4.2 THE MASS SPECTROMETER

The mass spectrometer available for this study was a conventional V.G. ISOGAS SIRA 24 (*SIRA*), the operating specification of which places limits on sample size. This instrument analyses the sample gas by making five comparisons with the same volume of a calibrated reference gas, the isotopic composition of the sample is then calculated relative to the international P.D.B. standard. The *SIRA* is designed to give high precision measurements, to an accuracy of ± 0.02‰, using a major beam current of > $1x10^{-9}$ A (equivalent to > 4 μgC as CO_2 frozen into the inlet cold finger). Typical fluid inclusion releases are less than 4 μgC per extraction step and most isotopic measurements have been made using 0.2 - 3 μgC. It was therefore necessary to investigate the accuracy of *SIRA* analyses for ion beam currents (I_m) in the range $1x10^{-9}$ A to $5x10^{-11}$ A.

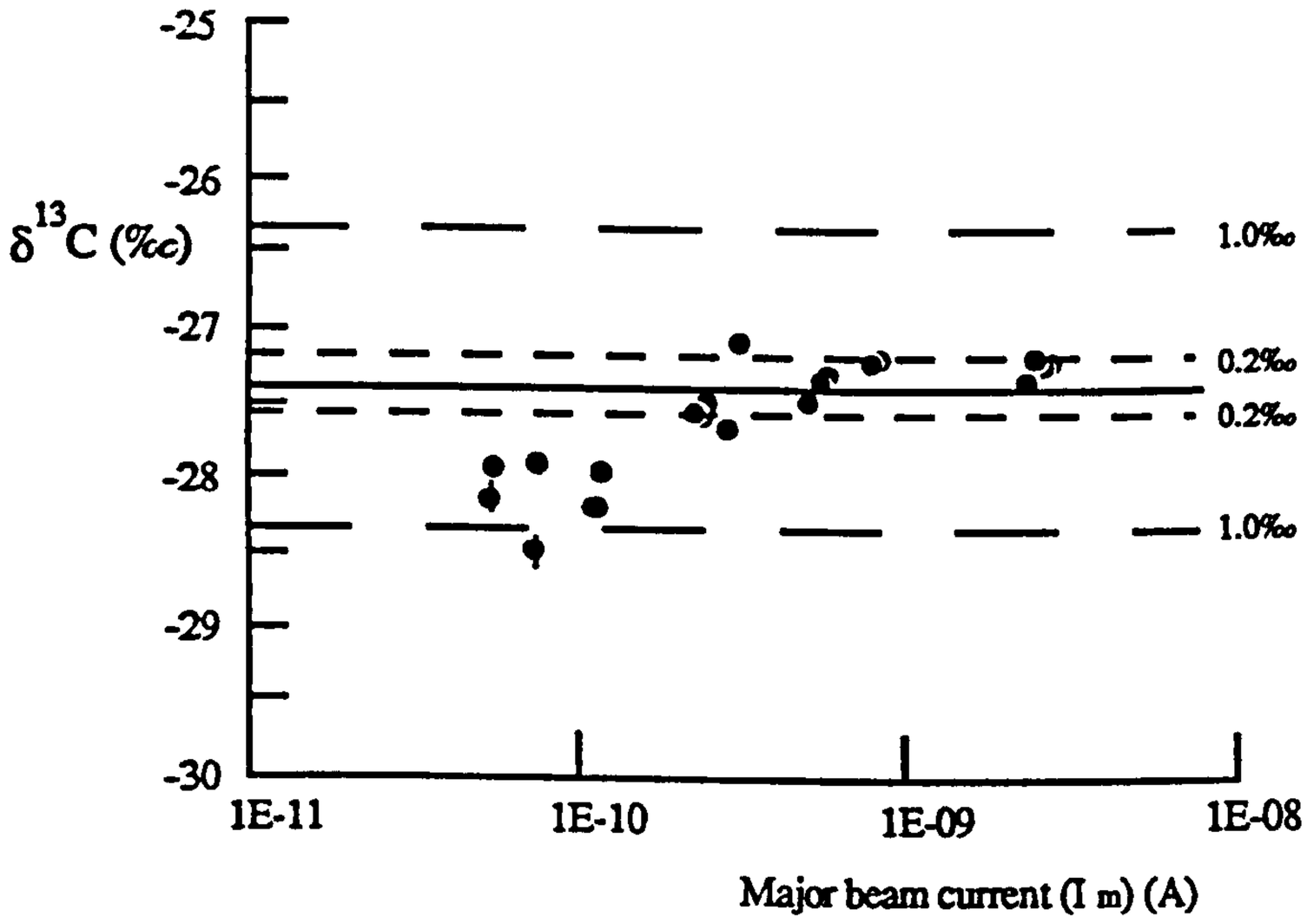

Figure 4.2. Graph showing the accuracy of isotope analyses of small samples of CO_2 performed on the *SIRA*. Samples with a major beam current down to $2x10^{-10}$ A have accuracies better than 0.2‰. The internal error on each measurement is within the size of the point except where an error line is shown. (Solid line is the true value ($\delta^{13}C$=-27.395‰), fine dotted line is 0.2‰ accuracy, coarse dotted line is 1.0‰ accuracy).

Zero enrichment analyses (with standard gases in the sample and reference inlets, with $\Delta\delta^{13}C$ = 14.108‰, ie. typical of the difference between standard gas and that released from fluid inclusions) over a range of values for I_m from $2x10^{-9}$ A to $5x10^{-11}$ A (Figure 4.2) were performed. On each measurement the accuracy is better than ±0.2‰ down to $I_m = 2x10^{-10}$ A (equivalent to 400 ngC), and better than ±1.0‰ as low as $5x10^{-11}$ A (40 ngC). Most fluid inclusion release steps (see **5.2.1**) fall within the ±0.2‰ accuracy field. These results imply that the error generated by the mass spectrometer is probably insignificant compared to the error which comes from the stepped heating procedure itself (**5.2.2**).

4.3 GAS EXTRACTION

4.3.1 Sample preparation

CO_2-rich fluid inclusions from charnockites in southern India have an average diameter of 10 μm and contain pure CO_2 of density 1.0 gcm^{-3}. The gas released from about 3000 - 4000 such inclusions is required to provide a suitable quantity of CO_2 for isotopic analysis. It has been found that samples of 50 - 150 mg normally consisting of 20 - 40 mineral grains of 0.5 - 1 mm grain size, evolve sufficient gas from each extraction step for analysis. The maximum sample size (≈ 150 mg) was constrained by the size of the sample vessel (quartz tube with an internal diameter of 4 mm **4.3.2**). Samples occupying more than 0.75 cm vertical height in the combustion vessel were avoided because a thermal gradient between the centre and edges of the sample may have resulted in broadened of the thermal release profile.

The mineral separates were hand picked from a crushed, washed and sieved rock under a binocular microscope, each grain was checked for purity and lack of solid inclusions. (Use of small samples has the advantage that this process is not unduely long and tedious, which may induce poor sample control).

The mineral separate was subjected to an ultrasonic cleaning procedure before being loaded into the vacuum extraction line. Mattey *et al.* (1989) discuss the merits of various tested procedures designed to remove as much surficial contamination as possible. They conclude that for basalt glasses a simple five minute ultrasonic wash in an organic solvent immediately prior to loading gives the best results, dichloromethane was favoured in their study. They avoid an initial acid wash, unless needed to remove carbonate, because the acid appears to activate grain surfaces, increasing atmospheric adsorption. In charnockite samples carbonate veinlets are common and although great care was exercised during optical separation, an initial ultrasonic wash with 0.1 M HCl was used as a precaution. This was followed by similar washes in distilled water and dichloromethane, with the sample being left to dry over night in a dust-free oven at 100°C, before being weighed to ± 0.01 mg in a clean environment and loaded in to the vacuum line. Although minimised, the sample is exposed to the atmosphere prior to loading for long enough to adsorb some organic contamination onto its surface.

4.3.2 The glass line

The glass extraction line illustrated in Figure 4.3 is based on the system described by Swart *et al.* (1983). The line is designed to contribute a very low and reproducible blank level and has a background pressure typically better than $5x10^{-6}$ Torr. It is constructed from pyrex glass (outer diameter (o.d.) = 8 mm, internal diameter (i.d.) = 6 mm) except in the high temperature areas where quartz glass (o.d.= 6 mm, i.d.= 4 mm) is used. Two types of furnace, insulated and non-insulated, are employed on the elevated temperature fingers. Insulated furnaces, which can attain temperatures of 1300°C, are used on the sample and Pt fingers (Figure 4.3). Uninsulated furnaces, which consist of wire spirals wound onto quartz glass fingers, can change temperature rapidly (*ie.* 850°C to 450°C in 90 secs) and are used for generating pure O_2 from copper oxide.

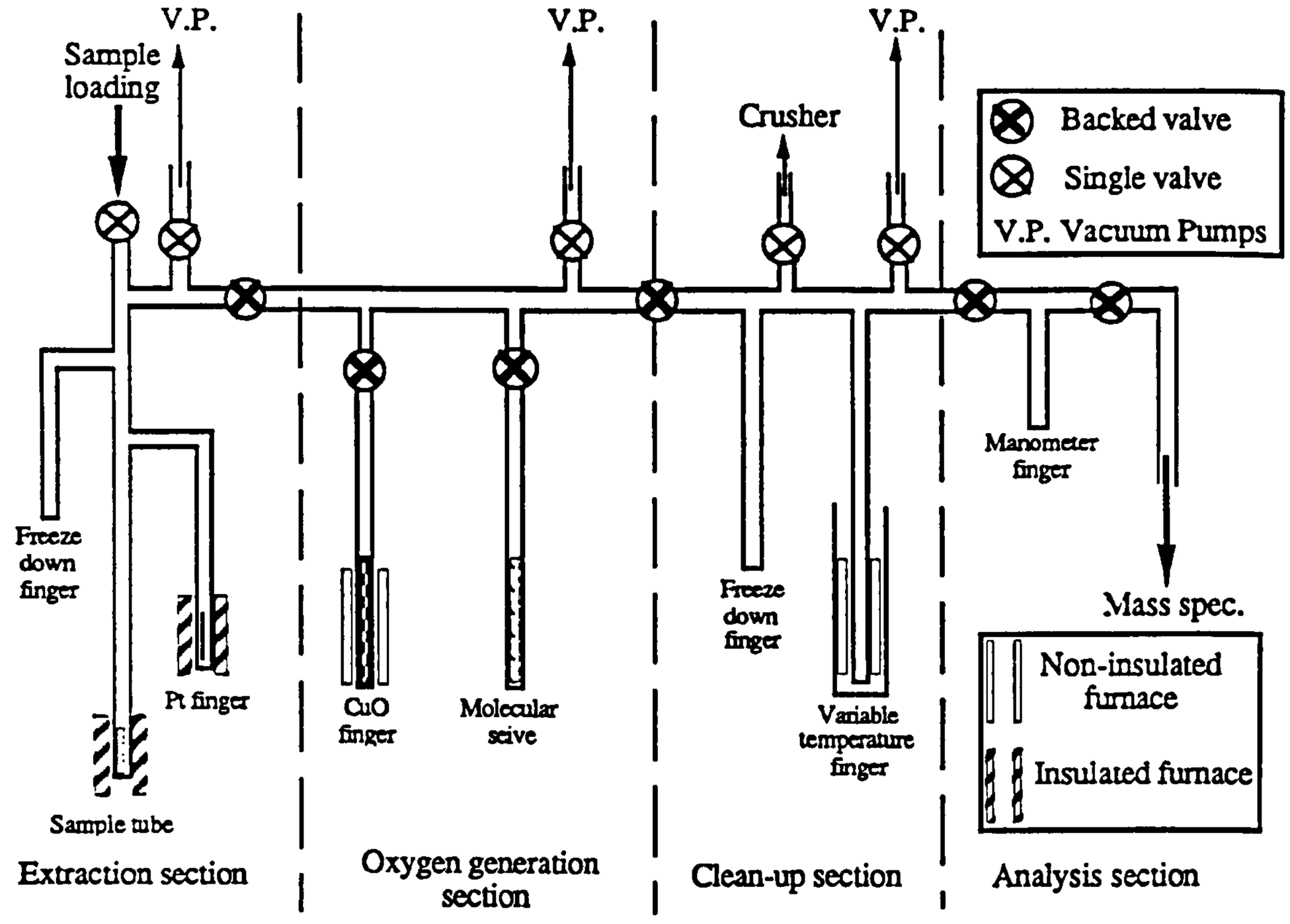

Figure 4.3. Diagram of the glass extraction line, see text for discussion.

The possible sources of blank contamination include valve leakage, a dirty sample vessel, the CuO finger and the molecular sieve. By using double 'O'-ring valves (Young's Scientific Glassware, London), with a backing line between the atmosphere and the sample handling section, which is kept at high vacuum, valve leakage is minimised. Baking the sample vessel at 1200°C, CuO at 450°C and molecular sieve at 150°C for at least twelve hours before each sample extraction minimises the blank contribution from these sources. The blank from the extraction line has been measured in a number of experiments involving no sample (**C.1.1**). When a normal loading procedure and pump down time was employed the blank was typically < 20 ng of carbon for each 100°C pyrolysis step up to 1200°C, and < 50 ng for the initial combustion steps, with barely sufficient gas being collected over a whole experiment for isotopic analysis. Procedural blanks using pre-baked (1200°C) crushed quartz glass subjected to normal cleaning procedures released ≈ 100 ng of carbon for the early combustion steps and ≈50 ng from subsequent pyrolysis steps (**C.1.1**).

The glass line is divided into four sections (Figure 4.3). The sample was loaded into the extraction section and the gas liberated was collected in a liquid nitrogen trap. Any non-condensible gases were removed at this stage. Although CO and CH_4 may be present, CO is not reported to be a constituent of fluid inclusions, and if it occurs it is thought to be formed from the breakdown of CO_2 on the hot Pt during the pyrolysis steps (Boyd, 1988). The presence of a liquid nitrogen trap which continually freezes down CO_2 as it is released minimises this effect.

CH_4 has been reported as a fluid inclusion constituent from several KKB localities, albeit from different generations than those in which CO_2 fluid inclusions predominate. As such it may have a different source and unrelated isotopic composition, so it was excluded from isotope analysis with the CO_2. To verify that CH_4 was not converted to

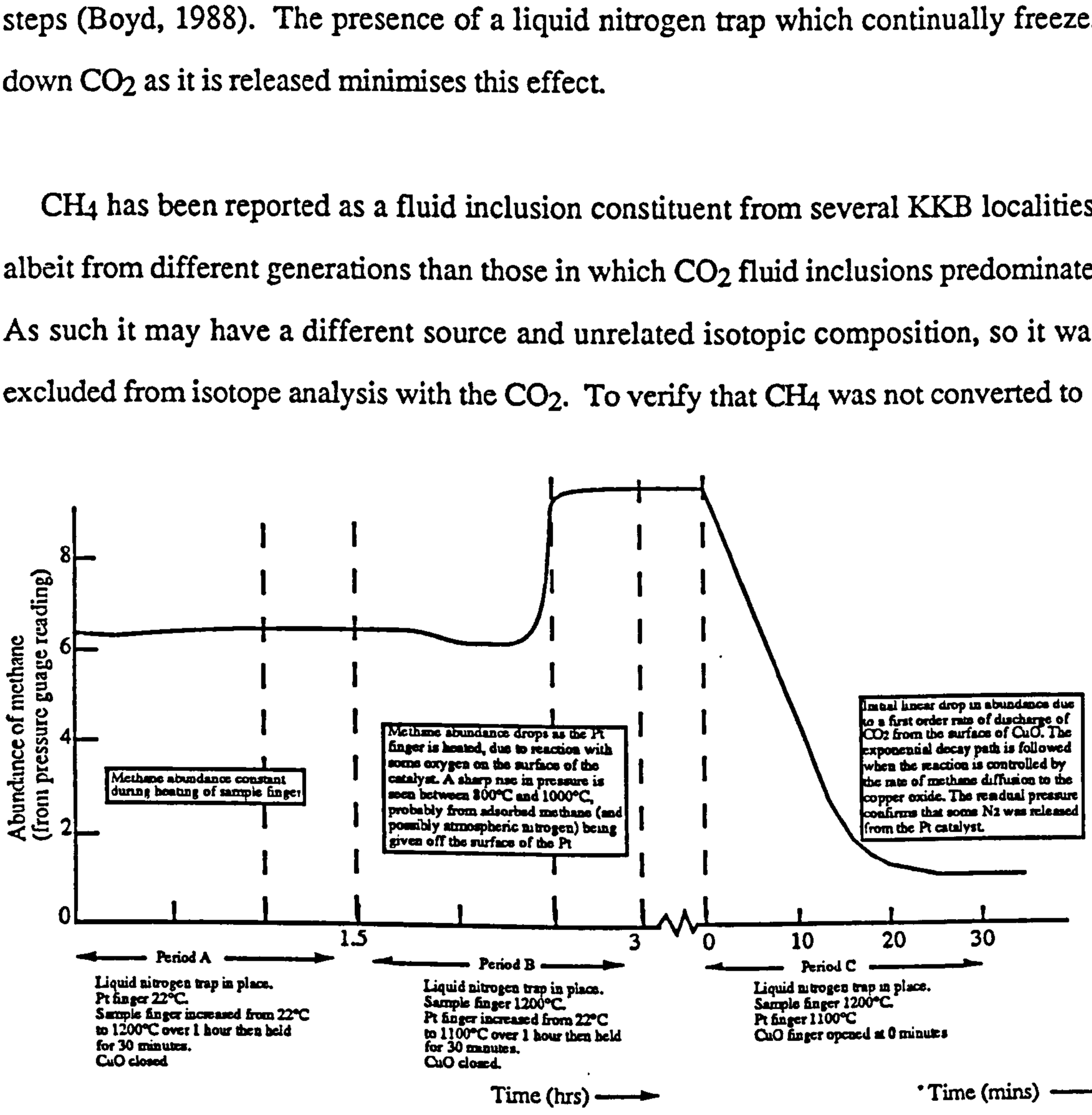

Figure 4.4. Results of an experiment to investigate the behaviour of methane in the extraction line. Methane is stable with the sample vessel and Pt finger at 1200°C and 1100°C respectively in the absence of oxygen, but is rapidly oxidised on the surface of CuO at 450°C. *Note the change of time scale for the latter part of the experiment.

CO_2 in the presence of hot Pt under vacuum conditions, an experiment using pure CH_4 was conducted, the results of which are shown in Figure 4.4. In the presence of cold or hot Pt the CH_4 is stable, but is rapidly converted to CO_2 when opened to CuO at 450°C. During all pyrolysis steps the CuO finger was kept isolated from the sample vessel.

Condensible gas species were transferred to the 'clean up' section where CO_2 was separated from other species (predominantly water) in a variable temperature cold finger. The abundance of CO_2 given off each step was measured by capacitance manometry to ± 5% and then passed into the mass spectrometer for isotopic analysis.

4.4 PROCEDURES ADOPTED IN THIS STUDY

4.4.1 Stepped heating

Stepped heating can be used for two purposes; firstly to separate contamination from indigenous material (Chang *et al.* 1974) and secondly to differentiate between gas released from different sources within the sample (Becker and Clayton, 1975). A stepped heating procedure was adopted in this study for both of these reasons; primarily to remove organic contamination, but also to attempt to distinguish gas release from different generations of fluid inclusions.

The temperature step interval adopted was a compromise between counteracting factors. To obtain the best discrimination of gas sources a small step size is ideal, but it is necessary to limit the number of steps to reduce both the amount of sample required and the time taken to perform the extraction. Although most experiments in this study used a 100°C step size, two experiments with 50°C steps were performed (**5.2.6**).

The sample was loaded into the pre-baked quartz sample vessel and initially degassed to less than 10^{-5} Torr (about 45 mins). Combustion in about 500 Torr of pure oxygen for 30 minutes at 300°C and/or 400°C was conducted to remove any remaining organic surface contamination (Desmarais, 1986, Mattey *et al.* 1989). The gas extraction was then carried out by a stepped heating process under pressure conditions of less than 10^{-5} Torr in the combustion section. Each temperature step lasted for 30 minutes, a liquid nitrogen finger was constantly present to freeze out any condensible gas species. The temperature was increased rapidly at the beginning of each step (approximately 5 minutes). Care was exercised to keep the temperature constant during each step, but sometimes drift of ± 5°C was unavoidable, particularly at high temperatures. For most of the analyses in this study extra time was taken between each step for transferring the gas to the 'clean up' section (Figure 4.3) and evacuating the sample vessel back to below 10^{-5} Torr. The procedure was refined by transferring the gas just before the end of 30 minutes and evacuating the sample vessel for the next step to start exactly 30 minutes after the previous one. This modification was introduced to allow analysis of the stepwise release to be performed with greater confidence.

4.4.2 Vacuum grinding

Crushing experiments were attempted in this study as a means of verification of the results obtained by stepped heating. A small volume, low-blank screw action crusher was employed to minimise the sample size required (see Mattey *et al.* 1989). The crusher was connected directly to the glass extraction line (Figure 4.3) to allow cleaning and analysis of small gas samples with a low blank contribution. The results of these experiments are given in **5.2.4**, but crushing always gave a low yield even in gas-rich samples for the reasons outlined in **4.1.3.**

4.4.3 Graphite abundance analysis

In Chapter 6 an estimate of the graphite abundance in the rock is an important parameter in modelling fluid flow. Conventional elemental abundance determination techniques (such as neutron activation analysis) do not analyse for carbon, so an alternative method had to be devised. Being ductile and occurring as large flakes the graphite is likely to smear on the surfaces of the crusher used to powder the rock, so the abundance estimate will be a minimum value. The technique employed was a stepped combustion, with each step carried out in about 500 Torr of pure oxygen, on 4 - 6 mg of a powdered whole rock. The same gas extraction procedure as described above was followed, with the gas released between 900°C and 1200°C collected as being derived from the oxidation of graphite.

Chapter 5

CARBON ISOTOPE CHARACTERISTICS OF FLUID INCLUSIONS FROM SOUTH INDIA.

5.1 INTRODUCTION

The change from water to carbon dioxide dominated fluid inclusion assemblages when passing from amphibolite to granulite facies terrains (Touret, 1971) continues to be one of the major pieces of evidence cited in favour of a massive influx of CO_2 into the lower crust (Newton *et al.* 1980). A number of alternative hypotheses which imply that the CO_2 inclusions are incidental to granulite formation, have also been advanced to explain this observation (Table 5.1). In ascertaining the role of CO_2 in granulite formation it is of paramount importance to determine the source of the fluids. In particular differentiation between local crustal and external (possibly mantle) sources will constrain the scale over which CO_2-influx can cause dehydration and stablisation of the lower crust.

	Reference	Origin of CO_2-rich inclusions
1	Hoefs and Touret (1975)	Juvenile (mantle) source.
2	Ormaasen (1977)	Solidus vapour compositions.
3	Ashwal (1978)	CO_2 evolved from proximal intrusion.
4	Glassley (1983)	Decarbonation of carbonate-bearing lithologies.
5	Hansen *et al.* (1987)	Oxidation of graphite.
6	Hollister and Burruss (1976)	Diffusional loss of H_2 from mixed inclusions.
7	Konnerup-Madsen (1977)	Dehydration of CO_2-H_2O fluid by retrogression of orthopyroxene.
8	Crawford and Hollister (1986)	Selective entrapment of immiscible fluid phases.
9	Lamb *et al.* (1987)	Late stage CO_2-rich fluid trapped during uplift.
10	Hollister (1988)	Selective leakage of H_2O from mixed inclusions.

Table 5.1. Possible origins of CO_2-rich fluid inclusions in high grade rocks.

Although hypotheses 6-10 (Table 5.1) explain how 'secondary' CO_2-rich inclusions may have be produced, they do not constrain the source of the CO_2 which is a more

important problem in charnockite genesis. The stable isotopic composition of CO_2 derived from different sources may be distinct. Oxygen has proved to be of limited use in southern India (Stähle *et al.* 1987, Jiang *et al.* 1989). Provided that isotopic equilibration between fluid and rock is rapidly attained, the ubiquitous presence of oxygen in crustal rocks will ensure that the CO_2 will soon lose its distinctive oxygen isotopic signature. Carbon, on the other hand, is relatively scarce in the lower crust, confined to minor carbonate- and graphite-bearing lithologies. For this reason the carbon isotopic composition of CO_2 released from inclusions was selected as the most likely method of constraining the origin of the fluid.

The analytical procedure described in Chapter 4 has been applied to gneiss-incipient charnockite pairs and massive charnockites from a variety of localities across southern India. The results are presented in this chapter and the constraints they impose on the source of CO_2 in the various areas of South India are discussed. Initially, to justify the validity of the results, evidence that the fluid inclusions were captured during charnockite formation and are released during stepped heating is presented. All the carbon isotopic compositions discussed in this chapter are in the conventional $\delta^{13}C$ notation with respect to the Pee Dee Belemnite (P.D.B.) standard:

$$\delta^{13}C=\{\frac{[^{13}C/^{12}C]_{sample}}{[^{13}C/^{12}C]_{standard}}-1\}\times 1000.$$

5.2 STEPPED HEATING RELEASE

5.2.1 Description

The results from stepped heating experiments are illustrated on 'stepwise plots', Figure 5.1 shows a simple example. Both the isotopic composition and the abundance of the gas released over each temperature interval are illustrated on these plots. Blank contamination was discussed in Chapter 4 and shown to be low, so the analyses

presented here have not been blank corrected. It should be noted that the background isotopic composition derived from the glass line is around -25‰ so temperature steps with very low yields (< 50 ngC) give isotopic signatures between this value and that of the genuine release. The stepped heating procedure was adopted to distinguish between gas released by fluid inclusion decrepitation and by other sources (contamination, carbonate and graphite are possible). It was also hoped that where more than one inclusion generation existed, this experimental procedure may distinguish between them.

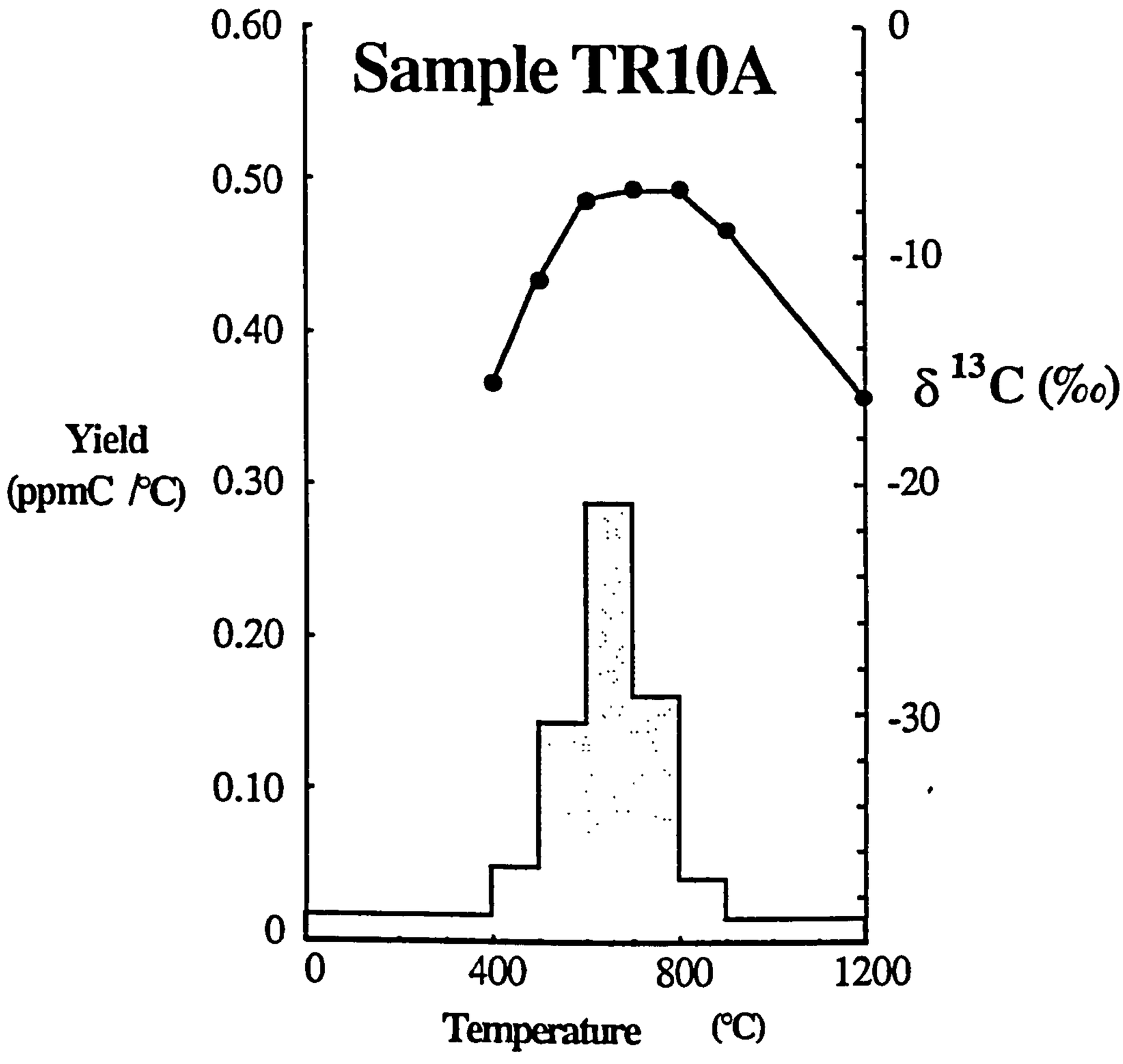

Figure 5.1. The stepped heating results are graphically illustrated for easy comparison between samples. The yield of CO_2, calculated as ppm/°C (these units allow direct comparison independently of sample size) is plotted as a histogram, and refers to the left hand axis. The solid line joining points is the isotopic composition of the CO_2 released at each step and refers to the right-hand axis. Sample TR10A from Kalanjur (KKB).

In most samples the release profile is relatively simple with only one major peak (Figure 5.1). Carbon released by the combustion steps at 300°C and 400°C is isotopically light ($\delta^{13}C$ values ranging from -30‰ to -25‰) and represents adsorbed organic contamination. With increasing temperature, carbon yields increase sharply to form a single maximum release of isotopically heavier CO_2 in the 500-800°C range. Above 800°C carbon yields rapidly diminish with essentially all the CO_2 released by 1000°C. Extraction of the isotopic composition of the fluid inclusion-CO_2 from such plots involves some subjectivity. In simple case with large releases (*eg.* Figure 5.1) an isotopic plateau is reached for two or more temperature steps and the $\delta^{13}C$ value can be taken directly. In samples from which small volumes of gas are released and a plateau is not reached, the isotopically heaviest component may not be effectively separated. In this study either the heaviest isotopic value or the weighted average over two or three steps (for broad releases) is taken. Inherent to all isotopic analysis is a decrease in the reliability of the results for smaller gas releases.

5.2.2 Reproducibility and source separation

The reproducibility of the stepped heating results was tested by running duplicate analyses on samples SH/QF/3 (incipient charnockite from Ponmudi), TR10A (gneiss from Kalanjur) and KA5 (incipient charnockite from Kabbaldurga) (Figure 3.3). The results are given in Appendix C and illustrated on Figures 5.2a, b and c, with the profiles from each locality superimposed for easy comparison. It can be seen that the reproducibilty of the isotopic composition is good to ± 0.5‰, but the yield can vary by 50% (and sometimes by even more in gas-poor samples). This range in yields is expected from the sample heterogeneity induced by using only 10-20 mineral grains. The yield is strongly dependent on the number of inclusion trails that intersect the mineral grains being analysed. Optical observation confirms that while some grains contain no inclusion trails, others have many intersecting trails.

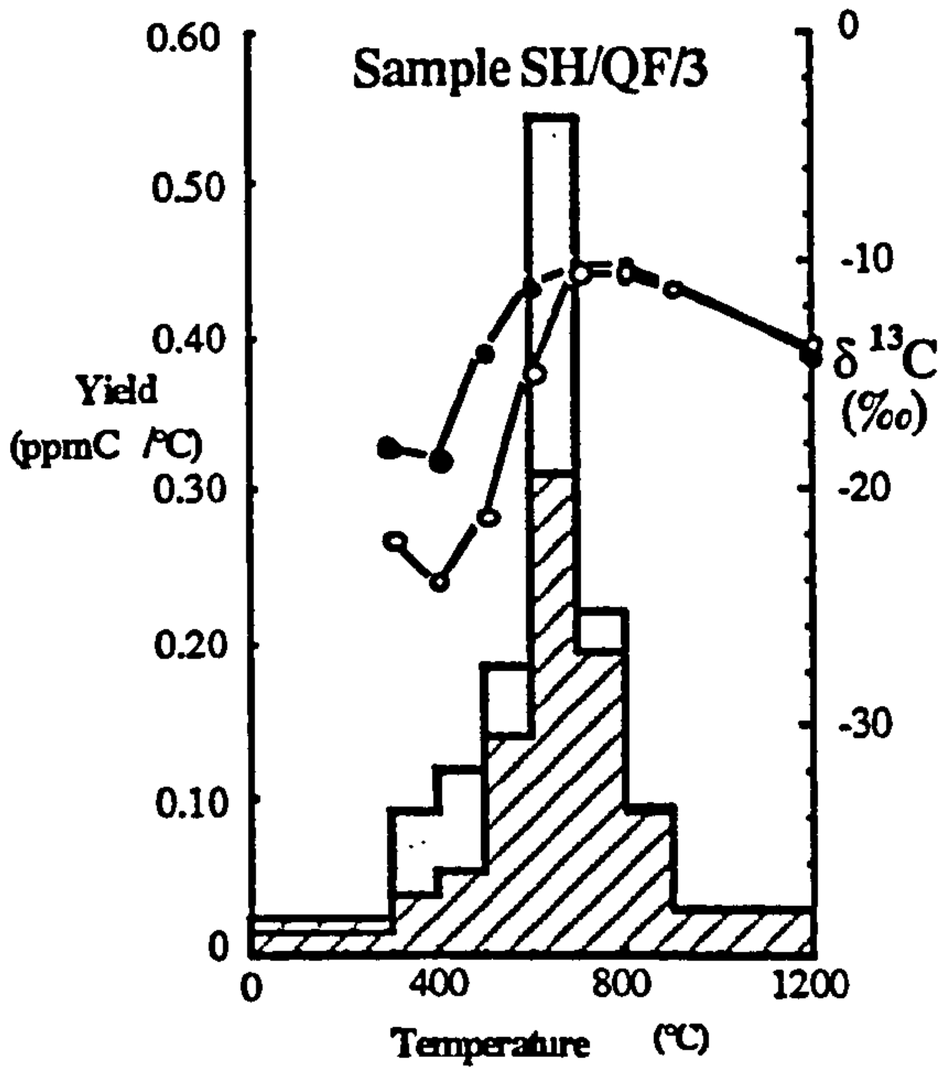

Figure 5.2a

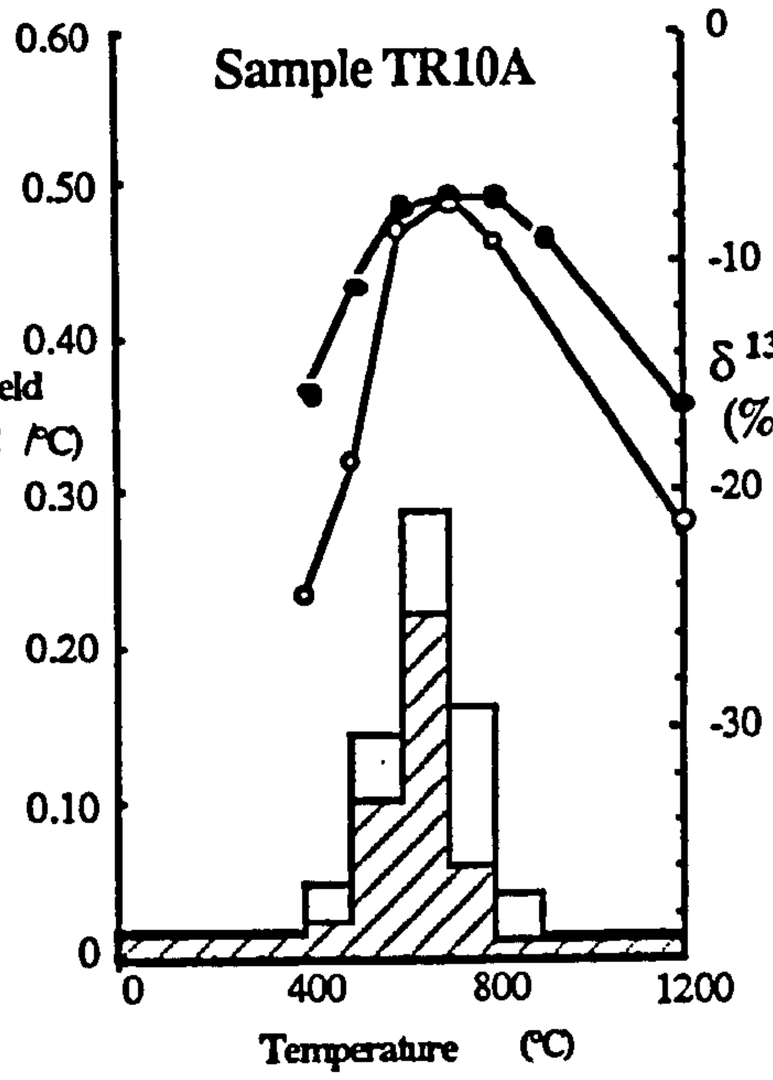

Figure 5.2b

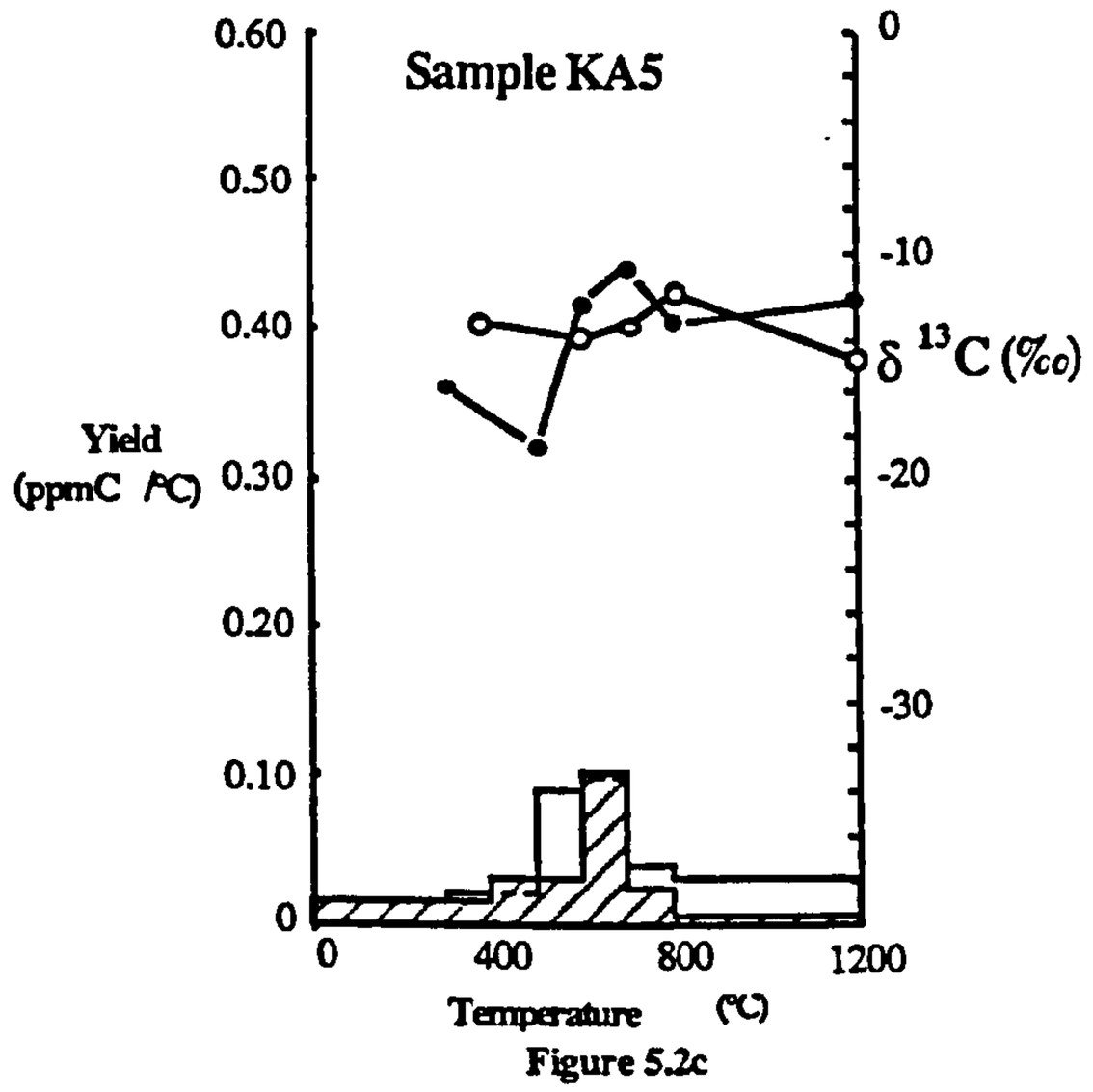

Figure 5.2c

Figure 5.2. Three duplicate analyses from incipient charnockites (SH/QF/3-Ponmudi charnockite, KA5-Kabbaldurga charnockite) and a gneiss (TR10A-Kalanjur charnockite) to test the reproducibility of stepped heating experimental results. Here, and in subsequent diagrams, shaded histograms correspond with filled circles; hatched histograms correspond with open circles.

5.2.3 Fluid inclusion decrepitometry

The use of the stepped heating results depends on verification that the major release is indeed from fluid inclusions and that this release is clearly distinct from carbon derived from other sources. The temperature at which a fluid inclusion decrepitates (T_d)

depends on several variables including inclusion shape and size, fluid composition and density, entrapping mineral structure and grain size. Consequently it is arguable whether T_d can give any quantitative information about conditions of inclusion formation; for instance Roedder (1984, pp. 266) states "*I must admit my personal bias against the use of decrepitation data in any quantitative connotation*".

Theoretical attempts to model the T_d of fluid inclusions have assumed spherical inclusions which decrepitate when their internal pressure exceeds that required to break the constraining force (the strength of the entrapping material) (*eg.* Bodnar *et al.* 1989). A calculation of T_d for a pure CO_2 inclusion with a density of 1 gcm^{-3} (typical for inclusions in incipient charnockite from S. India) is given below.

The tangential stress (σ_{rt}) at a distance r from the centre of a spherical inclusion (radius R) is given by:

$$\sigma_{rt} = -\frac{P}{2} x \frac{R^3}{r^3}$$

where P is the internal pressure in the inclusion.

For decrepitation to occur the internal pressure must exceed the confining force at the surface of the inclusion *ie.* R = r. If the retaining force is assumed to be the tensile strength of the quartz matrix (7000 psi. for clear fused quartz) (Handbook of Chemistry and Physics 66th Edition), then the internal pressure required to cause decrepitation is about 1 kb. From Figure 5.11 this gives a T_d of 100°C. This type of calculation is clearly over simplified and is independent of inclusion diameter, a parameter shown to be one of the major controls on T_d (Bodnar *et al.* 1989). The tensile strength of clear fused quartz may also be considerably weaker than quartz formed and 'annealed' at metamorphic conditions over several million years.

Bodnar *et al.* (1989) carried out a decrepitation study of hydrous fluid inclusions synthesized under metamorphic conditions (700°C, 7 kb). They found that although

inclusion shape had a minor effect on T_d, inclusion size was the dominant factor. Based on their synthetic inclusion data and observations made by Leroy (1979) and Swanenburg (1980) Bodnar *et al.* (1989) derived an empirical equation

$$P = 4.26D^{-0.423}$$

relating inclusion size (D) to internal pressure required to cause decrepitation (P). Using this relationship on 10 μm inclusions an internal pressure for decrepitation of 1.5 - 2 kb is derived, from Figure 5.11 this is equivalent to a T_d = 200 - 300°C. Swanenburg's (1980) study of natural carbonic inclusions from the Bamble granulites may be of greater relevance to this study than synthetic water inclusions. An approximate relationship derived from his data gives pressures of 3 - 3.5 kb equivalent to 400 - 500°C (Figure 5.11) for 10 μm fluid inclusion decrepitation.

Jackson *et al.* (1988b) and Santosh *et al.* (in prep.) report decrepitation temperatures measured by optical observation for carbonic inclusions in granulites from the Kerala Khondalite Belt. A strong correlation between the stepped heating release and inclusion decrepitation was observed (Figure 5.3). Most fluid inclusion decrepitation 'events' were observed to occur between 500°C and 700°C, although at these temperatures it was suspected each individual decrepitation 'event' corresponded to the rupturing of a number of inclusions. These observations provide strong evidence that fluid inclusions release their contents during stepped heating over the 500 - 800°C temperature range.

In summary, theory predicts low temperatures for fluid inclusion decrepitation (<200°C), but optical observations of synthetic inclusions suggest temperatures of 400 - 500°C are required. It is probable that carbonic inclusions captured and 'annealed' at granulite facies conditions may not decrepitate until 600 - 700°C. Optical observations of inclusion decrepitation confirm that the stepped heating 'peak release' is derived from fluid inclusion decrepitation.

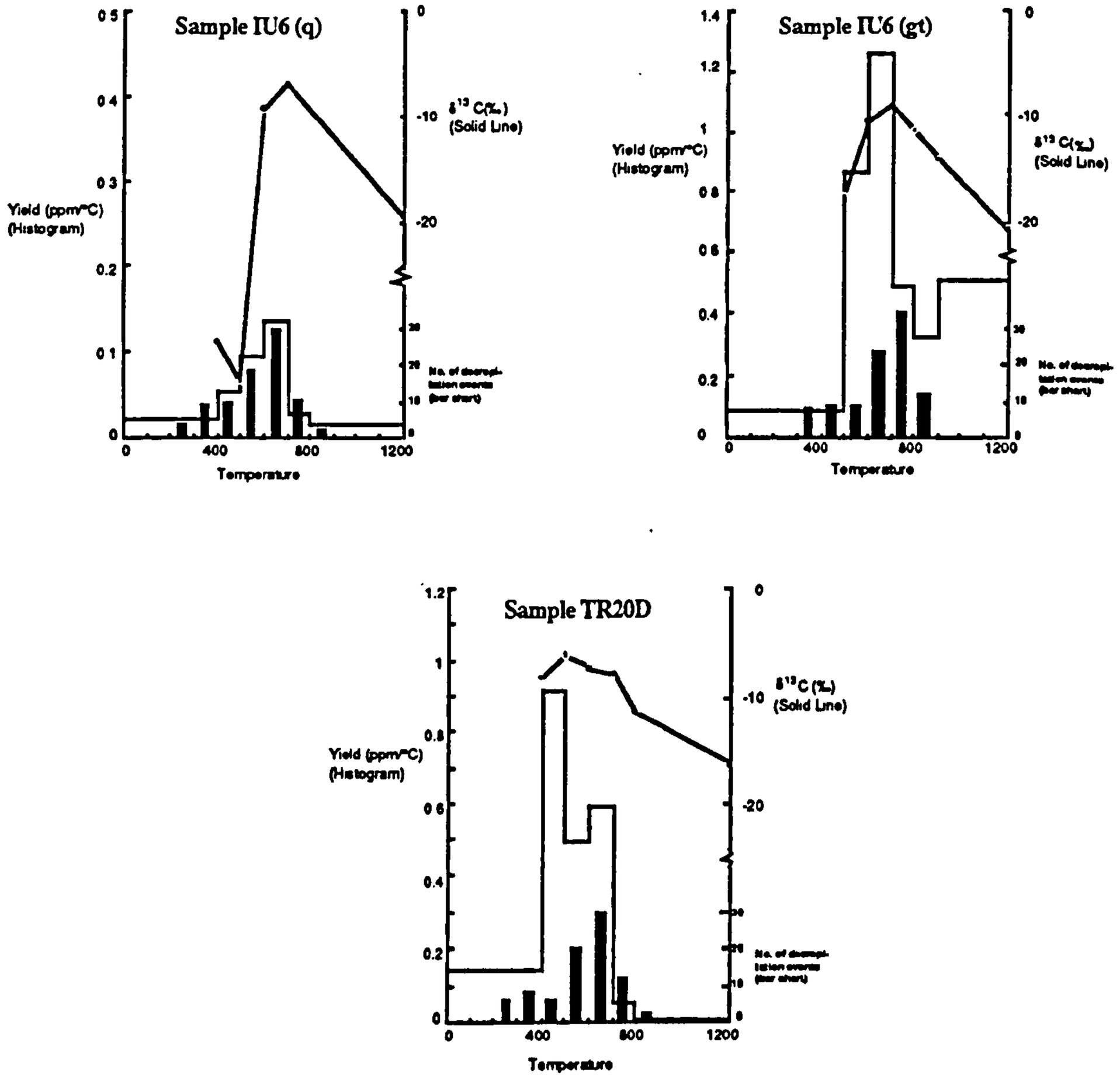

Figure 5.3. Reproduced from Figure 2 in Jackson *et al.* 1988b. "Optical heating stage decrepitation observations, super-imposed on stepwise plots for massive charnockite samples. The lower half of the right-hand scale now refers to the bar chart and is calibrated as the number of decrepitation events observed over that temperature interval. Fig. 2a is a quartz sample from Doddabetta in the Nilgiris (IU6 (q)), Fig. 2b is a garnet sample from the same locality (IU6 (gt)) and Fig. 2c is a quartz sample from a massive charnockite near Kottaram in South Kerala (TR20D)."

5.2.4 Other sources of carbon

Despite the good correlation between optical decrepitation and stepped heating release, it is worth considering whether other sources of carbon may contaminate the fluid inclusion release.

a) Graphite

Graphite combusts in the presence of oxygen at 800-1000°C (Grady, 1982). Only two samples (IU6 (gt) and TR27B) gave a major release at high temperatures, both clearly distinct from the fluid inclusion release (Figure 5.4). These experiments were carried out under pyrolysis conditions, so reaction between graphite and silicate matrix is suspected to account for carbon released at temperatures above 1000°C. Samples IU6 and TR27B, although from different environments, are both thought to have formed under conditions of high CO_2 flux and may have trapped reduced carbon in the mineral matrix or as tiny inclusions during growth. In TR27B reducing conditions are signified by large graphite flakes (see Chapter 6), whereas in the first sample no graphite was found, but early reducing conditions may have been buffered to more oxidising conditions by massive CO_2 influx. A stepped heating method has been successfully adopted for determining the abundance of graphite (released between 900°C and 1200°C) from a powdered rock sample (Chapter 6).

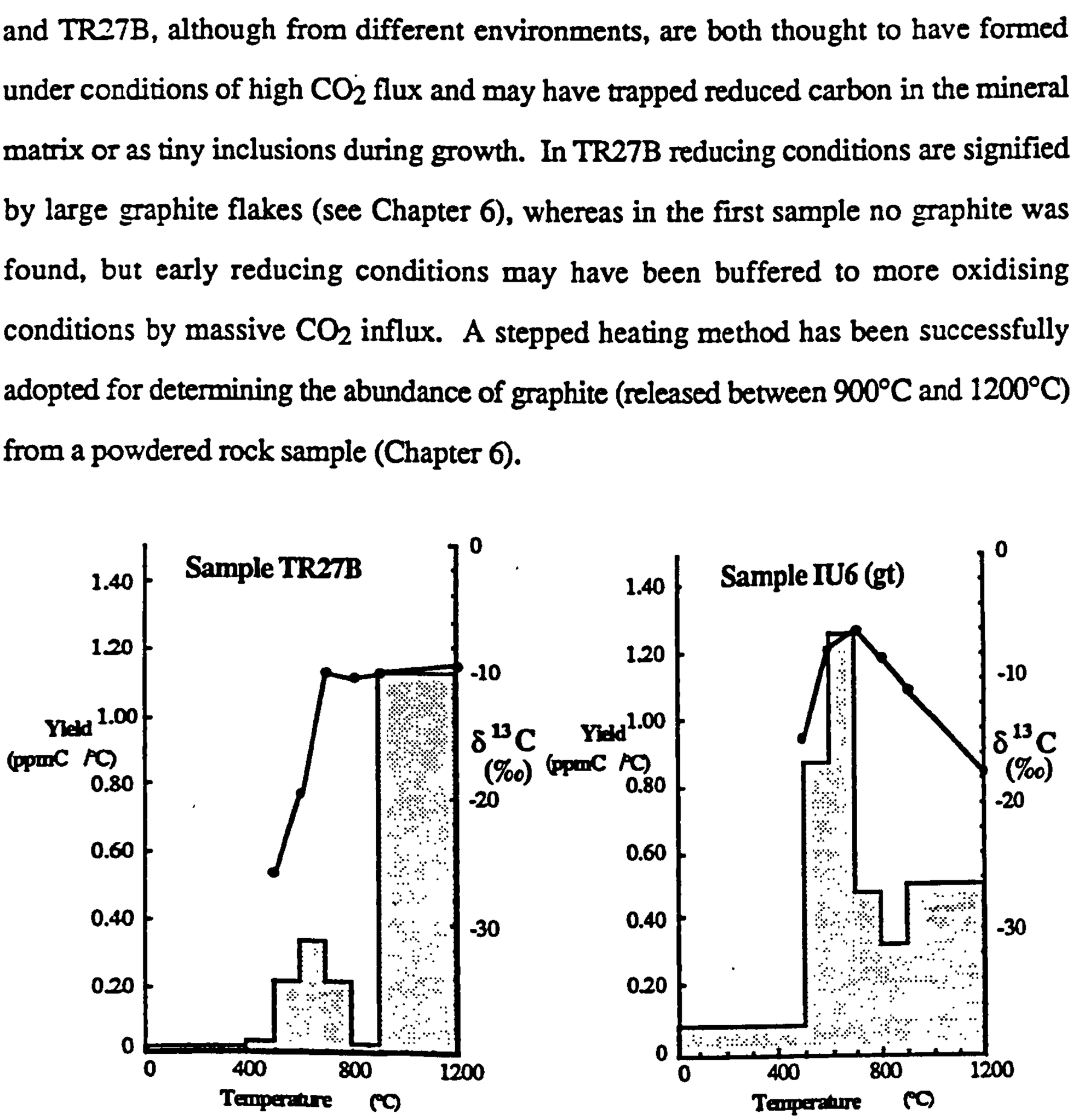

Figure 5.4. Stepwise plots for two samples (TR27B-Nuliyam calc-silicate and IU6 (gt)-Doddabetta charnockite) which show large carbon releases at high temperatures, attributed to come from reduced matrix carbon. Results given in C.1.10 and C.1.3.

In sample IU6 (gt) the inclusion-CO_2 and 'matrix' carbon appear to be in approximate isotopic equilibrium (assuming the carbon is graphite) for 700-800°C (Bottinga, 1969). In sample TR27B the isotopic signatures for inclusions and 'matrix' carbon are roughly equal, suggesting disequilibrium, a phenomenon discussed further in Chapter 6.

b) Carbonate

Carbonate breaks down in the 500°C to 700°C temperature range (Grady, 1982) and is a potential source of contamination to the fluid inclusion release. Veinlets of chlorite and calcite occur in the charnockite giving the rock its characteristic green colour (Howie, 1967). These veinlets have been used as evidence of a CO_2-rich fluid influx (Friend, 1981). They have been identified by cathodoluminescence as a wide spread phenomenon in some granulite terrains and have been interpreted as forming during retrogression by a late influx of H_2O-CO_2 fluids (Morrison and Valley, 1988). The veins must indeed form well below peak metamorphic conditions because the chlorite compositions suggest waning temperatures (<500°C) (Janardhan *et al.* 1982). Nevertheless, since the green colour of incipient charnockites is derived from these veins, they cannot be present in the surrounding gneiss, so the difference in the rock's fluid content must be preserved since the time of charnockite formation, perhaps entrapped as fluid inclusions. During uplift the inclusions, particularly in cleaved minerals, may rupture or leak releasing fluids which react with orthopyroxene forming clay minerals, hæmatite and chlorite-calcite veins. The observation that when veins transecting feldspar or orthopyroxene cross a quartz grain they change into a trail of CO_2-H_2O inclusions (Morrison and Valley, 1988), confirms this suggestion.

The rock appears to have acted as a closed system since charnockite formation (see 5.3), so in the absence of other carbon-bearing phases, any late calcite formed in veinlets should have an isotopic composition identical to the original CO_2 entrapped in fluid inclusions. CO_2 released from this vein calcite during stepped heating will not

invalidate conclusions drawn from the isotopic composition of the gas. Nevertheless care was exercised to avoid grains with green colouration. The yield of CO_2 obtained during a single temperature step over the 'peak release' range (6 μgC) can be derived either from the decrepitation of 4000 CO_2-rich inclusions with a diameter of 10 μm or one grain of calcite with 0.2 mm grain size. The experiments described below were performed to try to evaluate the contribution of carbonate breakdown to the peak release. A summary of the results is given in Table 5.2 and they are discussed below.

Experiment (1).

Mineral separates were crushed in the screw-crusher connected to the extraction line (Figure 4.3) and the residue was subjected to stepped heating. Gas released from these experiments was compared with that from the uncrushed sample to identify a drop in yield during stepped heating. This experiment had the added advantage that the gas released during crushing could also be isotopically analysed. Results from samples TR20D and IU10A (see C.1.6 and C.1.8) are plotted on Figure 5.5.

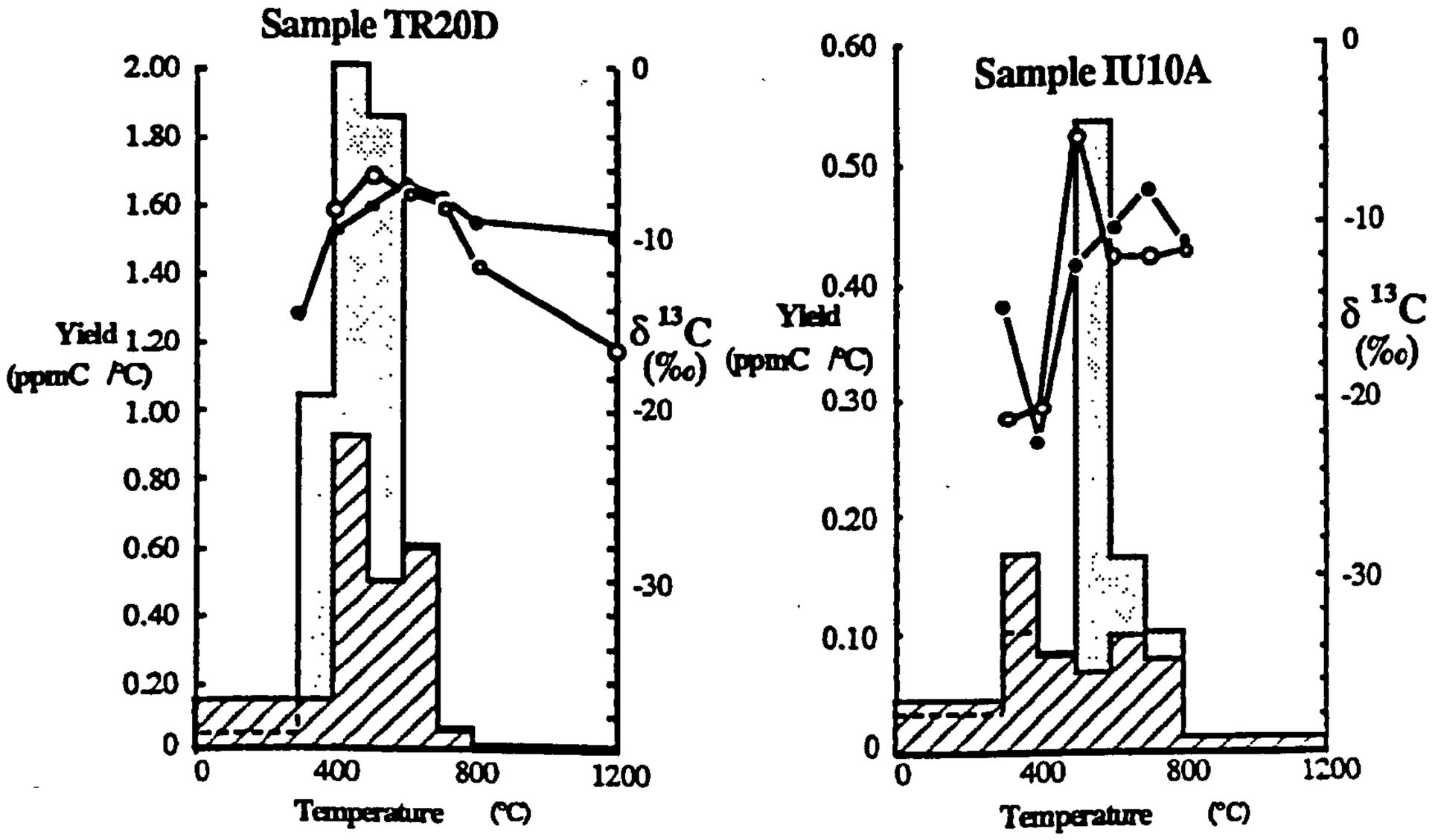

Figure 5.5. Stepwise plots illustrating a comparison between quartz samples from Kottaram charnockite (TR20D) and Ponmudi charnockite (IU10A) which have been stepped heated (hatched histogram and open circles) and crushed first then stepped heated (shaded histogram and filled circles). Surprisingly, a larger yield is obtained from the pre-crushed sample in both cases.

Unfortunately the problems associated with sample crushing, discussed in **4.1.3,** were encountered by these experiments and sufficient gas for isotope analysis was only released during crushing of one of the samples. Inspection of the residue after crushing indicated that the small gas release may not be due to gas adsorption but to crushing inefficiency, because the residue was normally whole grains (50-200 μm) rather than a fine powder. The peak yields obtained from the subsequent stepped heating experiments were in both cases more than 200% that of the uncrushed sample. This surprising result can only be attributed to sample heterogeneity and implies that no meaningful conclusions can be drawn. This variation in yield is substantially larger than that measured by replicate analyses in **5.2.2.** It is interesting to note however that the peak release in TR20D occurs at 500°C, which is below the temperature for carbonate breakdown. The isotopic composition of the gas obtained by crushing TR20D is 2‰ heavier than the peak obtained by stepped heating. The reason for this discrepency is unknown, although the small abundance of gas released by crushing may render the isotope measurement inaccurate.

	Experiment	Samples	Crush		Stepwise (peak)		Acid extraction	
			Yield (ppm)	$\delta^{13}C$	Yield (ppm)	$\delta^{13}C$	Yield (ppm)	$\delta^{13}C$
1	Crush and stepwise	TR20D	6.2	-4.7‰	384	-6.8‰	-	-
		IU10A	0.7	N.D.	69.4	-8.1‰	-	-
2	Powder and stepwise	IU10A	-	-	47.3	-5.6‰	-	-
		IU13A	-	-	51.8	-6.7‰	-	-
		SH/QF/CS	-	-	2 wt%	0.7‰	-	-
3	Acid extraction	IU10A (q)	-	-	-	-	400	-10.7‰
		IU10A (gt)	-	-	-	-	175	-8.4‰
		IU13A (q)	-	-	-	-	500	-1.7‰
		TR27E (gt)	-	-	-	-	85	N.D.

Table 5.2. Results of crushing, stepped heating and acid extraction experiments to evaluate the contribution of carbonate to the fluid inclusion peak release. Results given in **C.1.5, C.1.6, C.1.7** and **C.1.8.**

Experiment (2).

A further experiment entailed grinding quartz separates from samples IU10A and IU13A by pestle and mortar, and analysing the resulting powder by a stepped heating extraction. A large organic contamination peak was obtained at low temperatures (Figure 5.6), but the peak release abundances had dropped in both cases. In sample IU10A this abundance decrease was minor, but more than 50% for sample IU13A. The stepped heating on this second sample was carried out using 50°C intervals to try to provide better resolution between the contamination and fluid inclusion release. Optical inspection of the powder showed that grains up to 10 μm in diameter were still present; these grains may contain abundant small inclusions (1 μm) which could have contributed 50% of the original release.

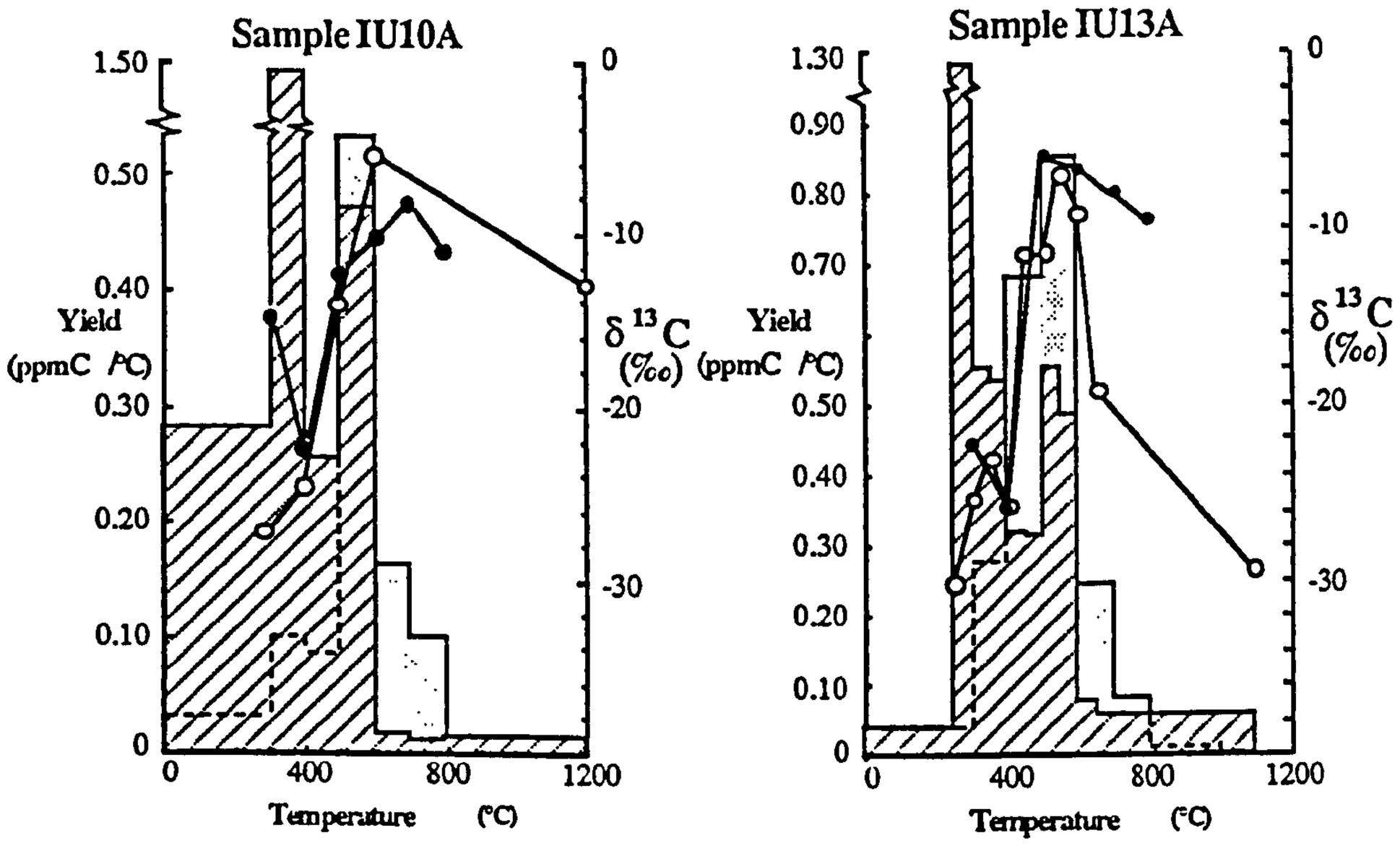

Figure 5.6. Comparison between stepwise releases for quartz separates (from Ponmudi (IU10A) and Kottavatom (IU13A) charnockites) as whole grains (shaded histograms/filled circles) and after powdering (hatched histograms/open circles). A large low temperature contamination peak is developed for the powdered samples, but the peak release is reduced.

For comparison a sample of calc-silicate from Kadakaman (SH/QF/CS), powdered in a similar fashion, was treated to a stepped heating experiment (Figure 5.7). The release profile is sharp, with essentially all the gas being given off during the 600°C and

700°C temperature steps. It is concluded from this experiment that any release obtained below 600°C or above 700°C is not derived from carbonate breakdown, although a degree of uncertainty remains for releases in the 600°C-700°C range.

Experiment (3).

Acid extraction of carbonate was also performed on three powdered mineral separates. The releases from some samples were again surprising because the yields were consistently greater than the yields obtained by stepped heating. The blank for the acid extraction procedure was measured to be high (3.2 µg, equivalent to 5-35% of the yields from powdered mineral separates), so the results from these experiments are difficult to interpret until the procedural blank is more accurately constrained.

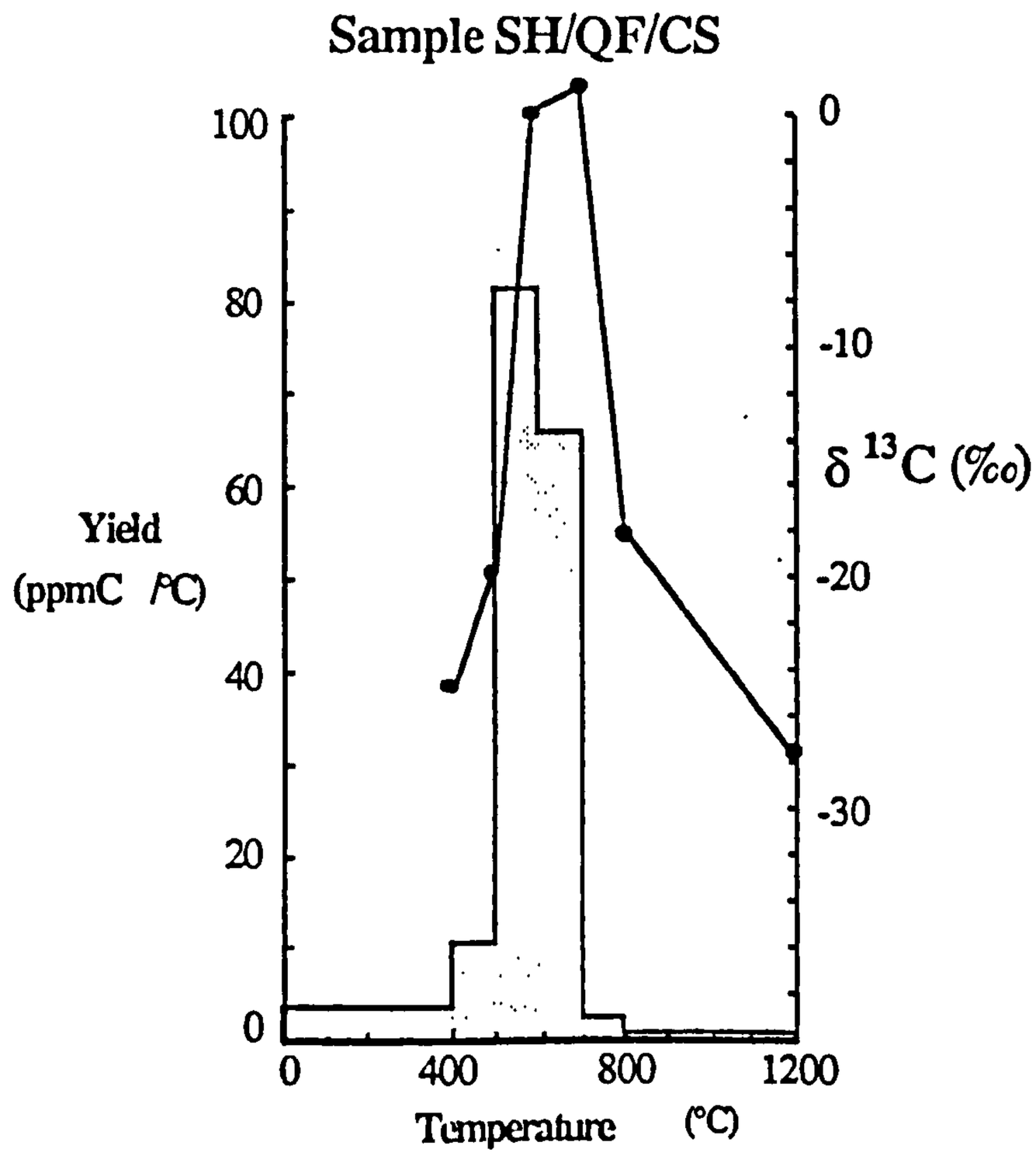

Figure 5.7. Stepped heating experiment on sample SH/QF/CS (Kadakaman, KKB) of powdered calc-silicate to compare the release pattern for carbonate with that obtained from fluid inclusions.

In conclusion a contribution to the peak carbon release from a carbonate component cannot be eliminated. Nevertheless care during mineral separation and acid leaching should ensure that the samples are carbonate-free. Large yields of CO_2 in the 500-800°C temperature range obtained from samples of gneiss which have no chlorite-calcite veining also confirms that carbonate is not a major source of contamination to the fluid inclusion release.

5.2.5 Stepped heating extraction from minerals other than quartz

An important verification of the stepped heating technique is to obtain correlatable results from stepped heating of coexisting minerals. Fluid inclusions have been reported from garnet and feldspar grains as well as quartz from southern Indian localities (Touret

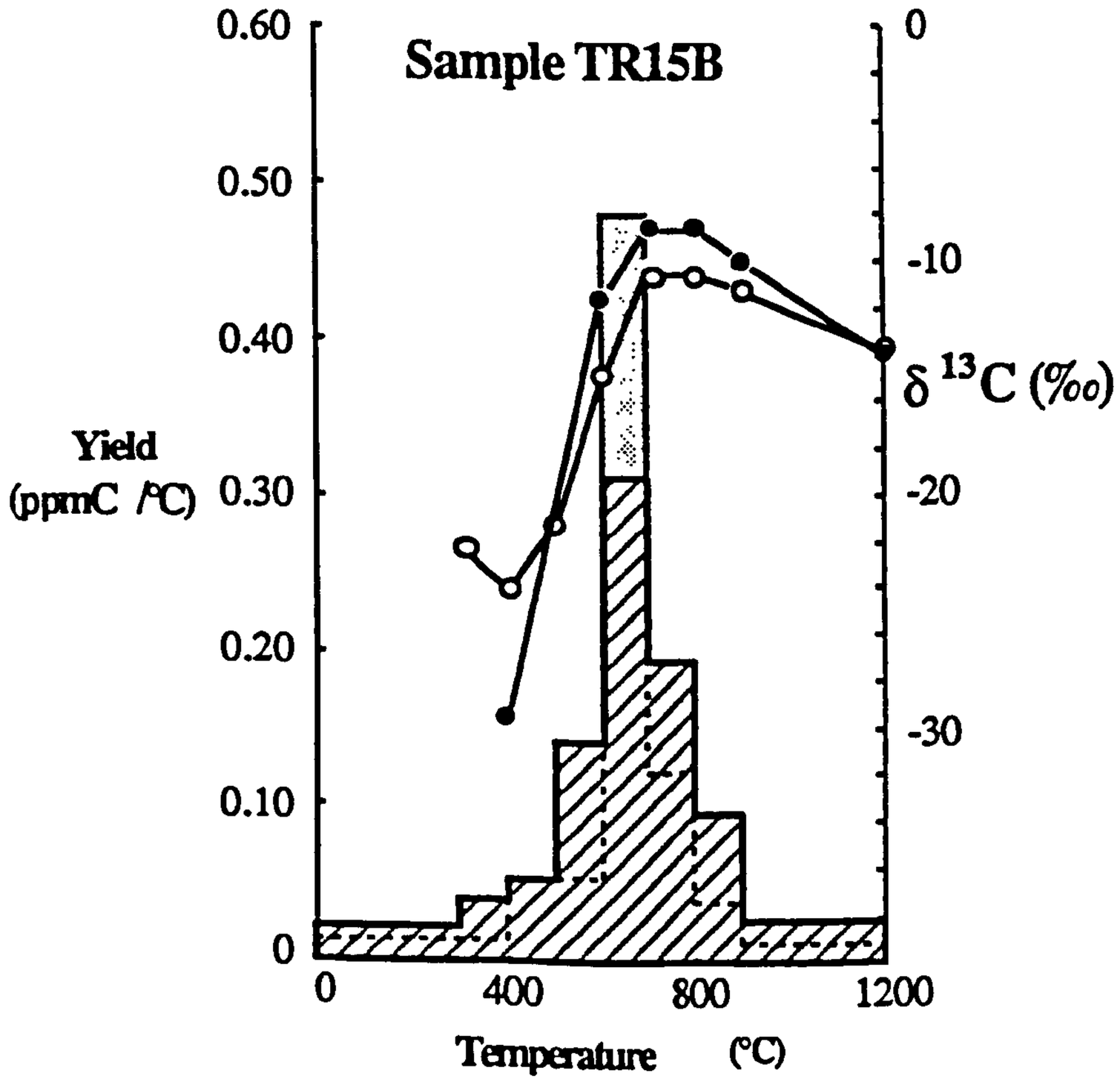

Figure 5.8. Superimposed stepwise release profiles for garnet (shaded histogram/filled circles) and quartz (hatched histogram/open circles) separates from the same sample of charnockite from Ponmudi. The profiles are very similar suggesting inclusion decrepitation temperature is strongly dependent on formation conditions. Results given in C.1.8.

and Hansteen, in press, Hansen *et al.* 1984). Feldspars were not favoured for this study because in charnockite samples they are often pervaded by green (calcite-bearing) veins, particularly along cleavage planes. The presence of cleavage also enhances fluid inclusion leakage during uplift. Garnet which has no cleavage and regularly contains large fluid inclusions was considered potentially more useful.

Eight quartz-garnet pairs from a variety of samples were measured to compare the release profiles and look for any systematic differences. The stepped heating profiles are generally similar for the two minerals (*eg*. Figure 5.8). This similarity corroborates the suggestion in **5.2.2** that fluid inclusion decrepitation temperature depends strongly on the entrapment conditions and is largely independent of the trapping material. When the peak release yields and isotopic compositions are plotted (Figure 5.9) dissimilarities between quartz and garnet releases in both yields and isotopes are observed.

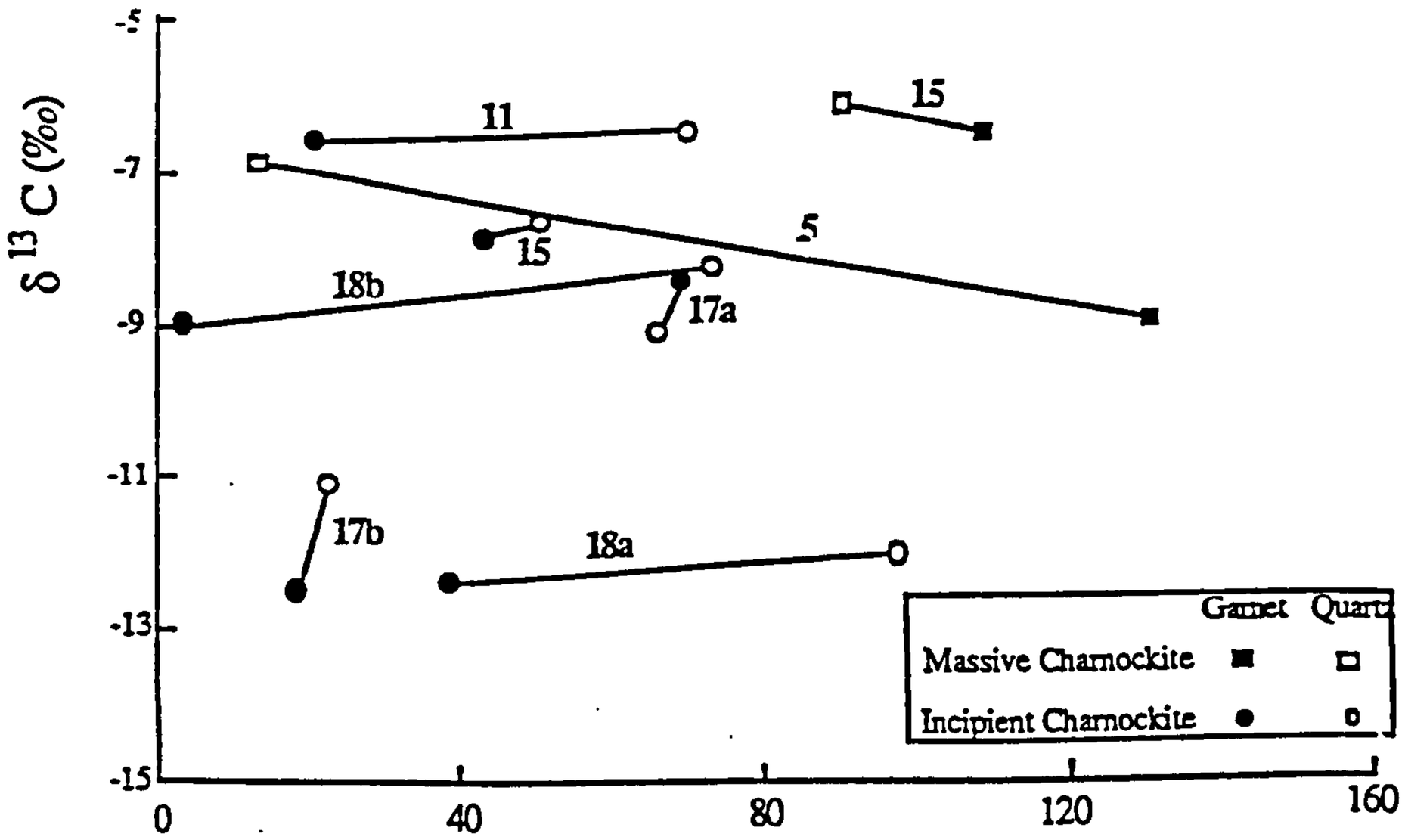

Figure 5.9. Yield of CO_2 against isotopic composition over the peak release interval for garnet and quartz separated from the same samples, see discussion in the text. Sample numbers refer to locations given on Figure 3.3a and b (5=Doddabetta (Nilgiris); 15=Kottaram; 11=Kalanjur; 17a=Ponmudi charnockite; 17b=Ponmudi gneiss; 18a and b=Nuliyam charnockites (KKB)).

These disparities may be explained by considering the massive charnockites separately from the gneiss/incipient charnockite pairs. In the two examples of massive charnockite the garnet releases more gas than the quartz. The converse is true for gneiss/incipient charnockite samples (except for the Ponmudi charnockite). If the massive charnockites either crystallise or recrystallise within the garnet stability field in a CO_2-rich environment, then fluid will be trapped during garnet growth. As crystallisation continues, the CO_2 may either be diluted by water or escape from the rock, so late crystallising quartz will entrap less CO_2.

In contrast during incipient charnockite formation the garnet is consumed, probably does not recrystallise and will capture little fluid. So it may be capable of preserving fluids from before the charnockite-forming event. Quartz is however thoroughly recrystallised to coarser grains, so any pre-existing inclusions are expelled and the ambient fluid at the time of charnockite-formation is trapped. This implies that the isotopic signature of CO_2 entrapped in quartz and garnet in incipient charnockite localities may be different. The implications of the absolute values will be discussed in **5.6**.

Finding an explanation for the change in isotopic composition between CO_2 entrapped in quartz and garnet from massive charnockites is more problematic, unless another carbon-bearing phase is present. Primary carbonate (reported by Touret and Hansteen, 1988 at Doddabetta) or graphite (see **5.2.4**), derived from a CO_2-rich fluid, would be isotopically lighter than the CO_2 (Bottinga, 1969), so the remaining CO_2 will become isotopically heavier. The CO_2 entrapped by early crystallising garnet will be isotopically lighter than the late crystallising quartz and the garnet may provide a more reliable estimate of the original isotopic composition of the CO_2.

5.2.6 Can fluid inclusion generations be distinguished?

The samples analysed in this study can be divided into three groups based on the shape of their stepwise releases. Some correlation between these release patterns and optical observations of fluid inclusion distribution can be drawn. Table 5.3 describes the rock types, stepwise releases and fluid inclusion characteristics indicative of each of these groups.

Group	A	B	C
Rock types	(1) Graphite-free gneiss/ incipient charnockites. (2) Type (a) massive charnockites (*eg.* Coorg, Nilgiris and Palni Hills). (3) Garnet from graphite-bearing incipient charnockites (Ponmudi and Nuliyam).	(1) Graphite-bearing gneiss/incipient charnockite. (2) Type (b) massive charnockites (*eg.* Madras and KKB).	(1) Type (c) massive charnockites (Kottaram) (2) Two miscellaneous samples from the Nigiris and a KKB graphite-bearing incipient charnockite (Kottavatom).
Stepwise plot profile	Simple unimodal release, normally peaking between 500°C and 800°C (*eg.* Figure 5.1).	Profile dominated by major 500-800°C release, with a minor release of isotopically heavy carbon at 300-400°C, The second release is superimposed on the contamination release and cannot be quantitatively assessed. (*eg.* Figure 5.2a)	Bimodal release profile with yield peaks at 500 and 700°C. Although small variations are seen the isotopic composition of CO_2 from both releases is essentially identical.
Optical fluid inclusion observations	Two generations (primary and 'pseudo-secondary') of biphase (CO_2-H_2O) fluid inclusions, both trapped during charnockite formation. (refs. 1 and 2).	Mainly pure CO_2 fluid inclusions, with a later generation of mixed N_2-CH_4 inclusions tentatively correlated with the low temperature release (CH_4 converted to CO_2 in oxygen on the hot Pt catalyst). (ref. 3)	Two generations of CO_2 rich inclusions. Pure high density CO_2 and later array-bound mainly pure CO_2 with lower densities. Decrepitation temperatures optically observed at Kottaram confirm that these generations give rise to recorded peaks. (ref. 4).

Table 5.3. Charnockites and related rocks from southern India divided into three groups on the basis of their stepped heating release patterns and fluid inclusion characteristics, to illustrate that in some cases stepped heating is capable of differentiating between generations of fluid inclusions. References: 1= Hansen *et al.* (1984); 2 = Touret and Hansteen, (1988); 3 = Klatt *et al.* (1988); 4 = Santosh *et al.* (in prep). Kottaram = 15 on Figure 3.11b.

To investigate the possibilities discussed above more fully one sample from a massive charnockite (IU6 (gt)) (Group A, Table 5.3) and one sample from a graphite-bearing incipient charnockite (IU10A) (Group B, Table 5.2) enjoyed the delights of a stepped heating experiment conducted with 50°C temperature intervals (Figure 5.10). In these experiments it was hoped to provide better resolution of the main peak and to

distinguish between the low temperature fluid inclusion and contamination releases. These samples were selected because their respective 100°C stepped heating experiments yielded interesting results; IU6 (gt) showed the high temperature 'graphite' release described in **5.2.4** and IU13A gave a prominent release of heavy carbon at 500°C as well as the normal release at 600-700°C.

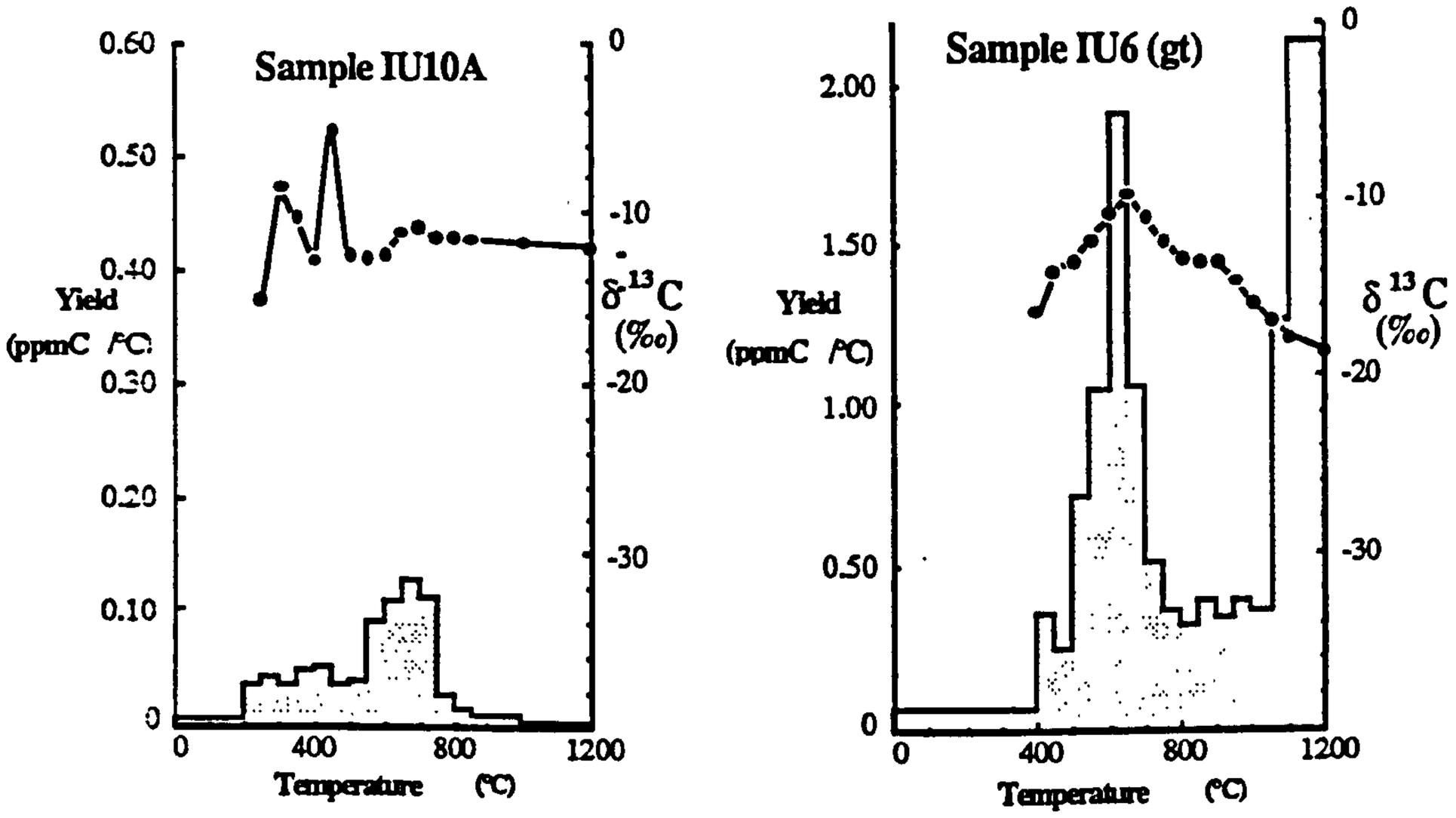

Figure 5.10. Release profiles for two 50°C stepped heating experiments, one (IU10A) showing releases at low (300°C and 450°C) temperatures, the other (IU6 (gt)) showing a high temperature release (see also Figure 5.4). Results given in **C.1.9.**

Sample IU6 (gt) has been discussed in **5.2.4** with reference to the high temperature (>1050°C) release. Of interest in this section is the lack of any low temperature release besides that of organic contamination at 400°C and 450°C. The tail from the main fluid inclusion release is superimposed on this contamination release and the isotopic composition of the CO_2 is of an intermediate value. The abundance and isotopic composition of the gas in the main release reaches a peak at 650°C and then drops on a mixing line towards the 'graphite' release at higher temperatures. Although this is a gas-rich sample the experiment confirms that the 100°C stepwise is capable of adequately resolving the fluid inclusion release from other carbon sources.

Sample IU10A was selected for an equivalent 50°C stepped heating experiment because inspection of the 100°C profile (Figure 5.5) shows a clearly defined release of heavy carbon at 500°C before the main release starts. This experiment provides a suitable contrast to that for sample IU6 (gt) because, although no high temperature release is found, detail is picked out over the low temperature range. The experiment was started at 200°C in the hope of removing the organic contamination before any fluid inclusion release.

A normal fluid inclusion release was observed peaking at 700°C, but two further peaks were detected, characterised by high yields and heavy isotopes at 300°C and 450°C. The 450°C release can be correlated with the heavy carbon observed during the 100°C experiment. The lower temperature peak appears to have been masked by the contamination release in the earlier (100°C) experiment. These low temperature releases may be from decrepitation of later generations of fluid inclusions and are not resolved during a 100°C experiment, nevertheless they do not interfer with the peak release for fluid inclusions entrapped during charnockite formation, so results obtained by 100°C experiments are not effected.

5.3 FLUID ENTRAPMENT CONDITIONS

The use of CO_2 entrapped in fluid inclusions to investigate granulite formation processes presupposes that the inclusions contain remanents of fluids captured during the granulite formation event. The conventional evidence in support of this peak entrapment of fluids comes from correlating the density of the fluid with P-T conditions of metamorphism estimated from solid phase equilibria (Figure 5.11) (Touret and Bottinga, 1979).

Fluid inclusions from single grains and even single arrays seldom all have identical densities. Lamb *et al.* (1987) argued that fluid densities do record their conditions of

entrapment, which implies they were captured at various times during the retrograde pathway. The presence of different density inclusions within a single trail negates this possibility. A more likely explanation is that the inclusions have changed volume during uplift and hence the density of the entrapped fluid is modified. Sterner and Bodnar (1989) have experimentally studied the effects of re-equilibration during retrograde metamorphism on water inclusions in quartz. They conclude that 3-50 μm inclusions subjected to a pressure differential of 1.0-1.5 kb will change their shape and volume, so the internal fluid pressure can revert to within 1 kb of the external pressure.

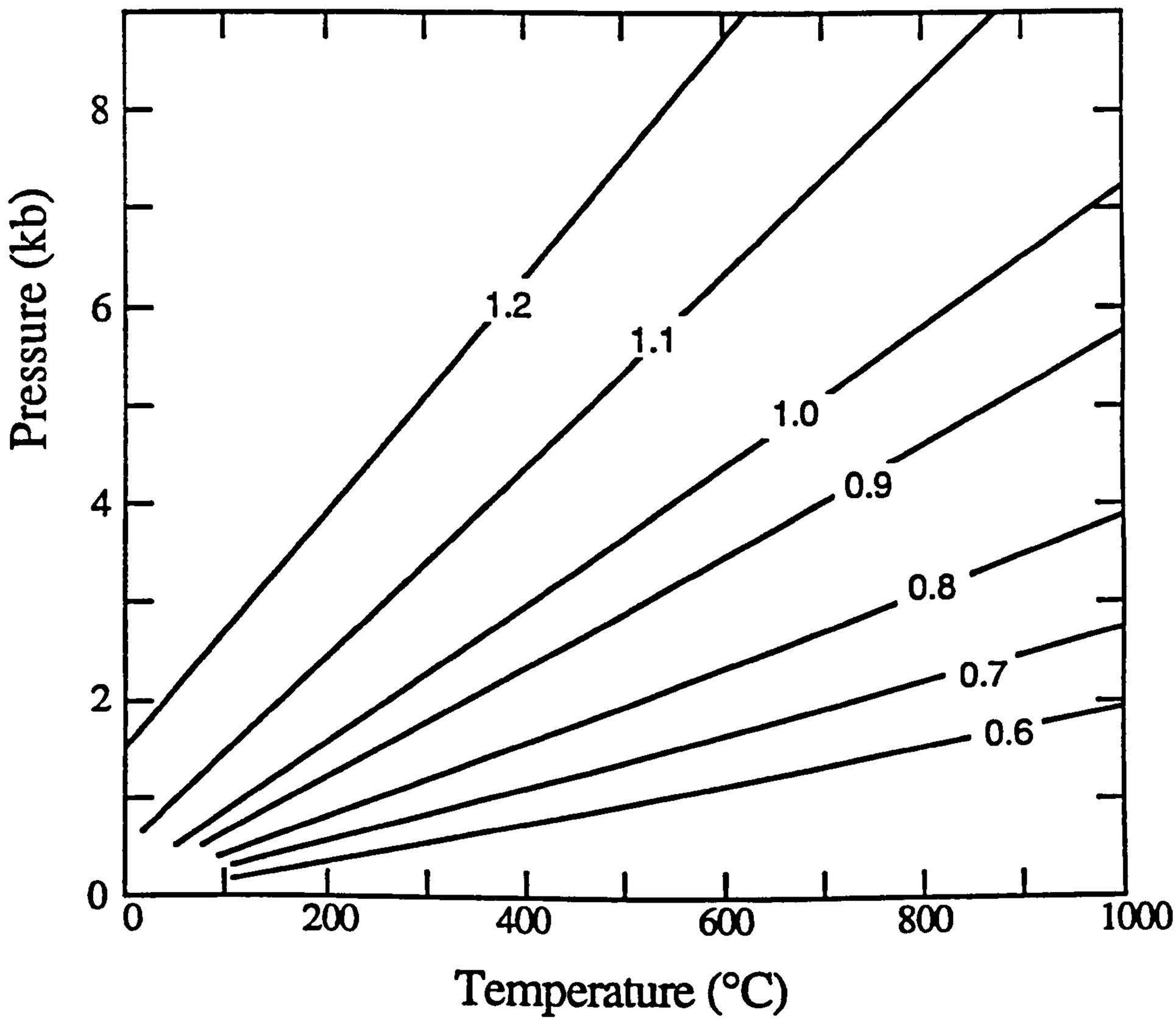

Figure 5.11. Isochore diagram for pure CO_2 (values on isochores show fluid density in gcm^{-3}): The density of fluid is measured by its homogenisation temperature, each density defines an 'isochore' (lines of constant volume) in P-T space (plotted using the modified Redlich-Kwong equation (Kerrick and Jacobs, 1981)). If the isochores intersect the P-T conditions calculated by solid phase thermobarometry, the inclusions may have been captured under those conditions, they may also have been captured anywhere in P-T space defined by that isochore. It has recently been shown that inclusions readily change their volume (Sterner and Bodnar, 1989), hence conclusions based on fluid density measurements alone are often unreliable (see text).

Nevertheless the majority of inclusions remain as closed systems with no change to their original compositions, hence if peak entrapment can be verified by other means the contents of the inclusions should be an accurate reflection of the pore fluid composition at their time of formation.

Peak fluid entrapment has been verified in a number of studies by very careful optical fluid inclusion observation. For instance, relevant to charnockite formation in South India are studies by Touret and Hansteen (1988) and Hansen *et al.* (1984) (see discussion in **3.5.3** and **3.3.3** respectively) who confirm peak entrapment on textural grounds and by using other corroborative evidence. Touret and Hansteen (1988)

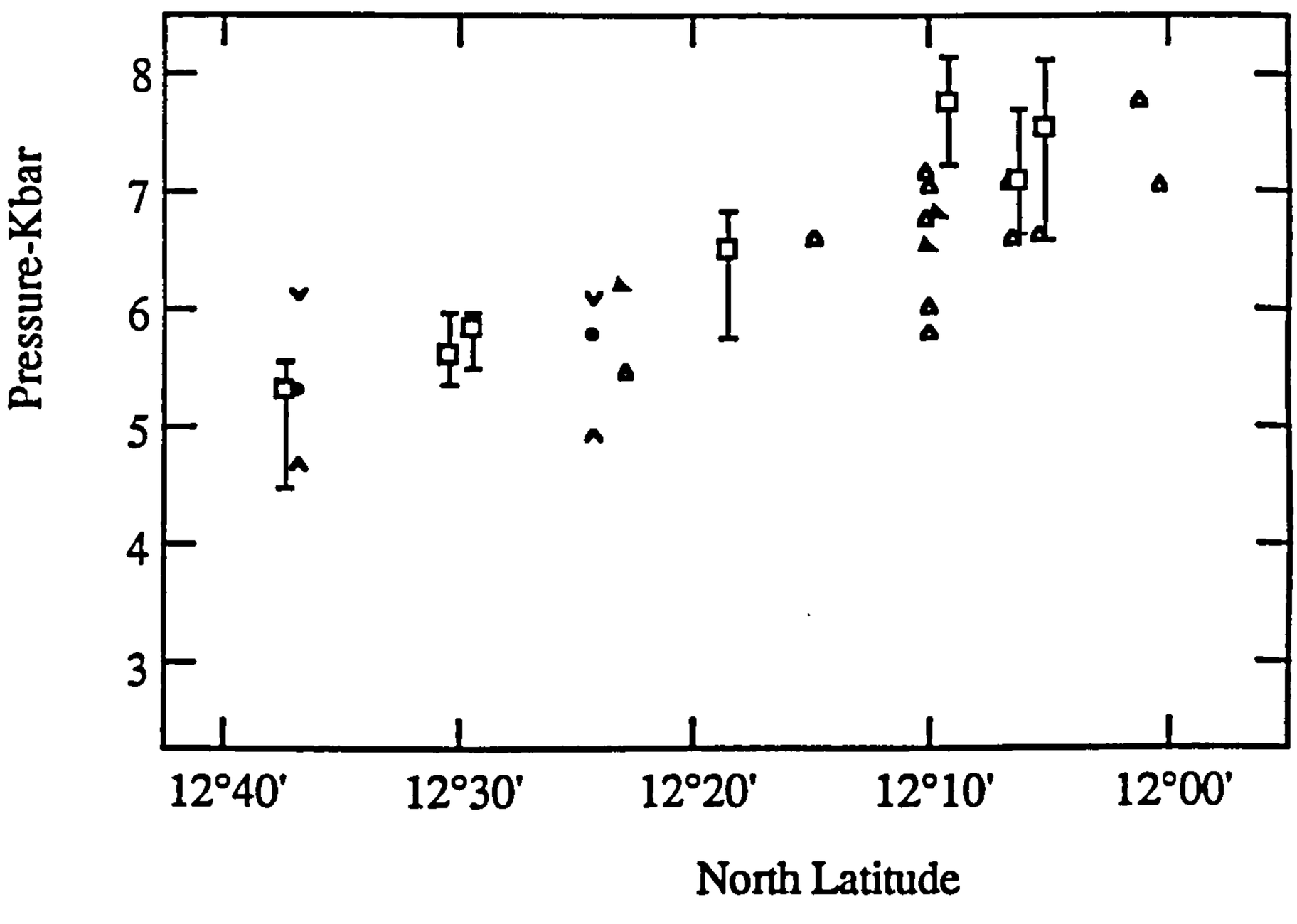

Figure 5.12a. Reproduced from Hansen *et al.* (1984b) showing the correlation between pressure estimates from fluid inclusion inclusions and solid phases. "Palaeo-pressures of late Archæan metamorphism in the granulite facies transition region, calculated from the assemblages garnet-opx-plagioclase-quartz (*open triangles*), garnet-cpx-plagioclase-quartz (*filled triangles*), garnet-sillimanite-plagioclase-quartz (*filled circles*, Harris and Jayaram, 1982), and garnet-sillimanite-cordierite-quartz (*Downward-pointing arrowheads* for $P_{H_2O} = P_{total}$ and *upward-pointing arrowheads* for $P_{H_2O} = 0$. Cordierite compositions from Harris and Jayaram, 1982). Shown also are palaeo-pressures calculated from measured densities of CO_2 inclusions (*open squares with error bars*). The plot shows that the transition region is an apparently unbroken depth profile."

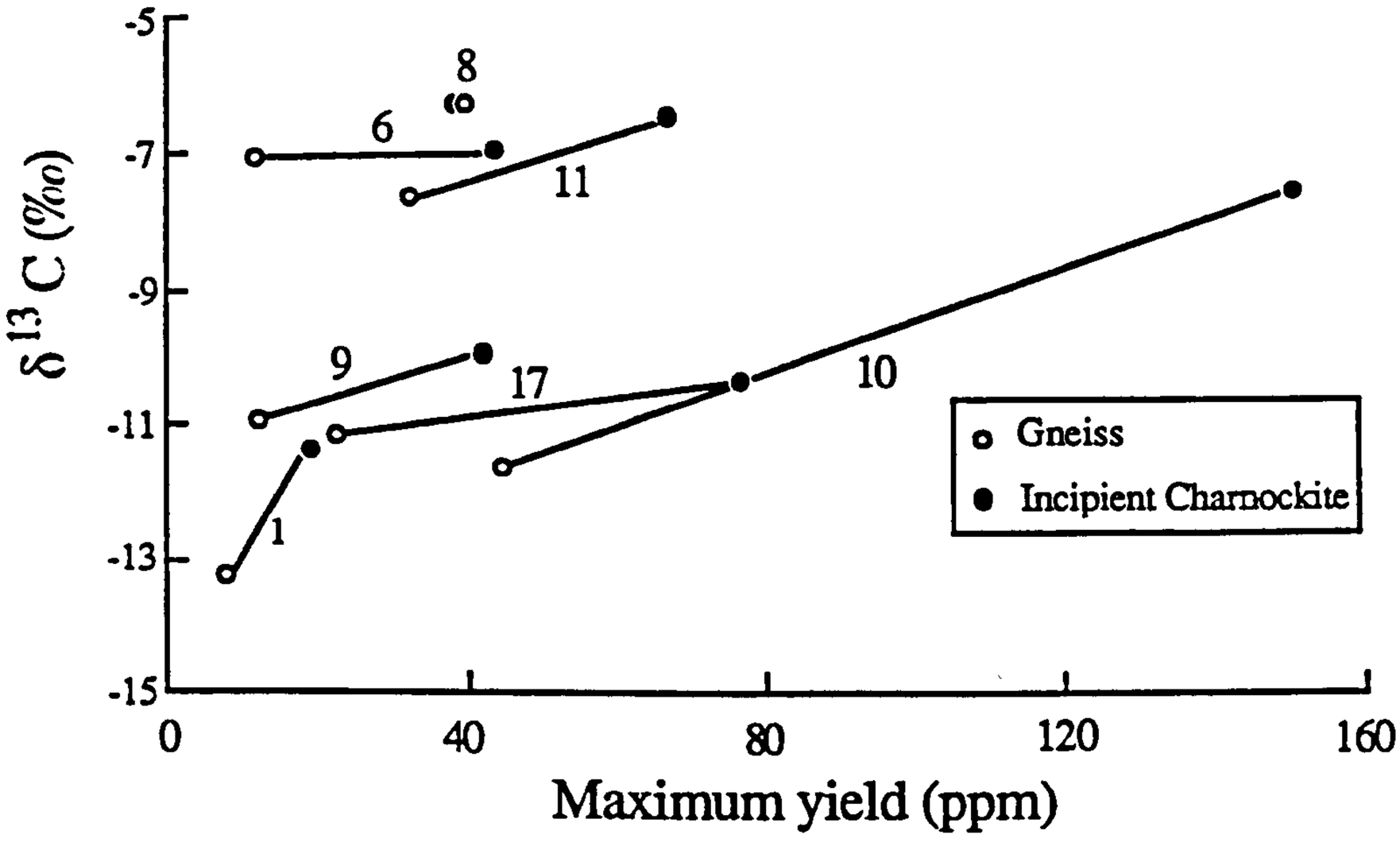

Figure 5.12b. Plot of yield against isotopic composition of CO_2 released from quartz separates in gneiss-incipient charnockite pairs over the peak release interval. In all but one case there is a sharp increase in both isotopic composition and yield in the charnockites. Sample numbers from Figure 3.3b (1=Kabbaldurga; 6=Koddakad; 8=Andipatti; 9=Kottavatom; 10=Manali; 11=Kalanjur; 17=Ponmudi).

chart fluid density variations in different minerals and compare them with solid phase equilibria to obtain entrapment orders. Hansen *et al.* (1984) investigate changes in fluid inclusion density over a metamorphic gradient across the orthopyroxene isograd from north of Kabbaldurga to the Biligirirangan Hills (Figure 3.3a) and find results which are consistent with solid phase geobarometric estimates (Figure 5.12a).

An alternative line of evidence for entrapment during charnockite formation in southern India comes from the abundance data obtained from stepped heating experiments (Figure 5.12b). This shows peak release results for sets of incipient charnockite-gneiss pairs. In all but one case (Andipatti, where gneiss and charnockite were sampled from the same hand specimen a few centimetres apart) there is a significant increase in the abundance of CO_2 in the charnockite over the gneiss, ranging up to 400%. This observation confirms the conclusions of Chapter 3, that in general incipient charnockite formation was caused by a change in pore fluid to compositions

richer in CO_2. If the fluid was retrogressive, pervading the rock after charnockite formation no such systematic difference between gneiss and charnockite would be expected. It is therefore probable that charnockite formation and fluid entrapment were synchronous events. There are two possibilities to explain why the charnockite contains more CO_2 than the adjacent gneiss. The most obvious is that the pore fluid was richer in CO_2, but it is possible that during charnockite recrystallisation inclusions were readily trapped in the growing minerals. Even if the second of these possibilities is true, inclusion capture must have occurred at the time of charnockite formation.

5.4 POSSIBLE SOURCES OF CO_2

There has been considerable speculation on the source of the CO_2 preserved in fluid inclusions in the charnockites. Those workers who support CO_2 as the cause of granulite formation have to invoke a large reservoir, whilst local sources may be sufficient for those who argue that the CO_2 is merely coincidental to granulite formation. The possible sources can be divided into two broad groups; the mantle and the crust, the isotopic compositions of which each are reviewed separately below.

5.4.1 The mantle

There are two environments in which large volumes of volatiles may flux from mantle to continental crust.

1) Above subduction zones. Evidence for fluid movement comes from the geochemistry of subduction related volcanism and calc-alkaline magmatism which has been affected by volatiles derived from the subducting slab (*eg*. Brophy and Marsh, 1986).

2) Continental rifting environments. High mantle fluid fluxes have been recorded in these regions using He isotope studies (O'Nions and Oxburgh, 1988).

3) Continental collision zones have been suggested for granulite formation (*eg*. Drury *et al.* 1984), but it is difficult to envisage a mechanism for transporting fluids from the mantle into the middle crust in such settings.

Estimates of the carbon isotopic composition of the mantle can be obtained indirectly from a number of sources. It should be borne in mind that the subcontinental lithosphere (most important in this study) may have been isolated from the rest of the convecting mantle since its formation (Richardson *et al.* 1984). Nevertheless $\delta^{13}C$ values obtained for MORB samples (typical of sub-oceanic mantle) show a similar range of values to carbonatites and kimberlites which sample the sub-continental mantle. Javoy *et al.* (1986), Mattey (1987) and Boyd (1988) provide excellent reviews of mantle carbon isotopic systematics (for further details readers are referred to these works), their findings are presented here on a cartoon (Figure 5.13), with points of interest commented on.

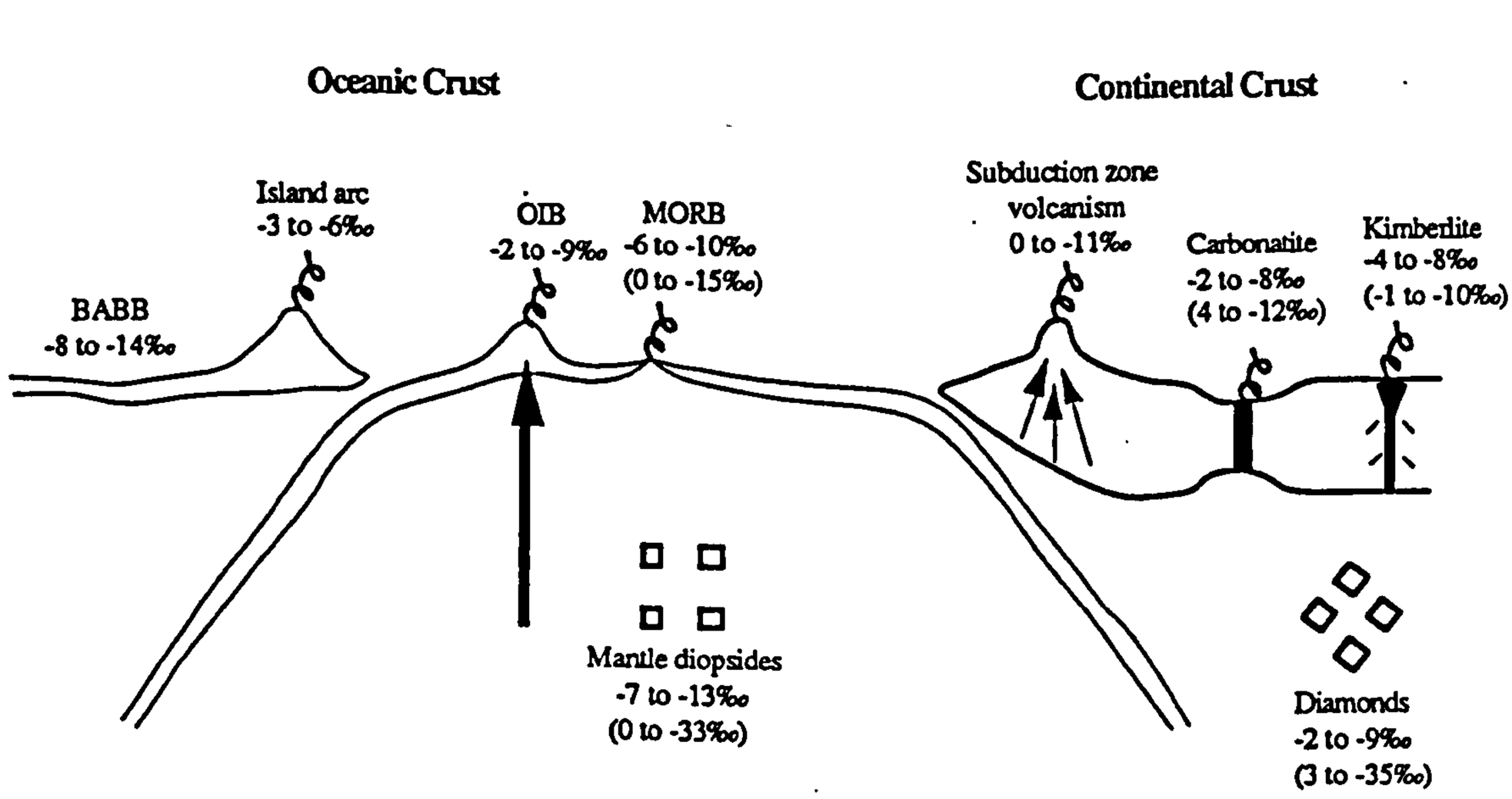

Figure 5.13. Cartoon illustrating the isotopic compositions of mantle-derived carbon measured in a variety of different environments, data from Javoy *et al.* 1986, Mattey, 1988 and Boyd, 1988 (and references therein). Where applicable the peak of the range of measured values is given (> 80%) with the entire range in parentheses.

The bulk of the determinations of the carbon isotopic composition of the mantle came from MORB glasses, carbonatites, kimberlites, mantle diopsides and diamonds.

The majority of the results fall between -2‰ and -9‰ with a sharp peak consisting of about 70% of the analyses between -5‰ and -8‰. This range is normally quoted as typical for mantle carbon, but it is still unclear whether this reflects a primordial signature or whether it is controlled by recycling a mixture of organic and carbonate sediments by subduction. The MORB values which sample broad areas of sub-oceanic mantle show considerable uniformity, with 85% of values having $\delta^{13}C$ between -6‰ and -10‰. The subcontinental mantle also shows a major peak within this range, but the spread of data is considerably broader (+3‰ to -35‰) covering the entire range of commonly occurring crustal carbon. It has been suggested that this large range, preserved mainly in morphologically 'unusual' diamonds reflects original isotopic heterogeneity at the time of the earth's accretion (Deines *et al.* 1986), but may attest to an unknown mechanism of diamond formation at depths of greater than 500 km (Boyd, 1988).

The carbonatite and kimberlite (and hence diamond) sources only sample certain, perhaps unusual, tectonically active areas, but these are also the most likely areas for flooding of CO_2 from mantle to continental crust and for charnockite formation. In contrast to the sub-continental lithosphere there are very limited data available for carbon isotopic compositions above subduction zones, in which CO_2 gas emissions from volcanic vents provide the only measured data. Considerable variation is sometimes found (4‰) from a single volcano, but other volcanoes release isotopically uniform CO_2 (Javoy *et al.* 1986). Although they attribute this variation to fractionation between vapour phase-CO_2 and CO_2 dissolved in magma, it has recently been shown that the isotopic fractionations involved are small (about 2‰, Mattey *et al.* 1989) and variation in the isotopic composition of carbon released by subducted sediments provides an alternative hypothesis. From the sparse data available no clear correlation between isotopic composition and distance from the subduction zone can be determined. The broad agreement between the composition of these gases and other mantle samples lends support to the carbon recycling theory.

In conclusion the mantle's carbon isotopic signature is well constrained below stable or rifting continental crust at -5‰ to -8‰, but above subduction zones considerable variation may be expected between 0‰ and -12‰.

5.4.2 The crust

In the crust carbon is stored in two principal states; as oxidised carbonate and as reduced organic matter. Although wide ranges of isotopic compositions exist for both of these carbon reservoirs at their time of formation, most organic carbon has $\delta^{13}C$ between -20‰ and -40‰ and carbonate between -10‰ and +10‰ (with mean and mode at 0‰). Geodynamic calculations have suggested that, for both the bulk overall crust and the crust recycled through subduction, carbon-bearing phases are present in proportions such that the average crustal $\delta^{13}C$ is identical to the mantle (-5‰ to -8‰) (Javoy *et al.* 1986). Nevertheless the two isotopically distinct crustal sources of carbon are distinguishable from mantle values, hence in some circumstances the $\delta^{13}C$ value may be diagnostic of the source of CO_2. It has been widely suggested that carbon with intermediate values could have been derived either from the mantle or from a mixed crustal source.

It is important to the investigation of granulite formation to examine the effects that metamorphism has on the isotopic composition of these carbon-bearing phases. As organic matter is metamorphosed its hydrogen to carbon (H/C) ratio tends towards zero, becoming pure graphite at temperatures greater than about 500°C (McKirdy and Powell, 1974). This process occurs by loss of methane, which is isotopically light, so the remaining graphite becomes isotopically heavier. Nevertheless where a high proportion (>5-10%) of graphite is present (without carbonate) in granulite facies rocks light isotopic signatures (-20‰ to -30‰) are commonly preserved (*eg.* Weis *et al.* 1981). Although Lamb and Valley (1984) predict that precipitation of graphite will occur when

CO_2 is influxed into a rock below the quartz-magnetite-fayalite (QMF) buffer, the effect has only recently been documented in the formation of 1 μm graphite films around mineral grains (Frost *et al.* 1989). Most, if not all, coarse disseminated graphite flakes in metasediments form by recrystallisation of sedimentary organic matter (Weis *et al.* 1981) (but see 6.5.3). Graphite flakes present in magmatic intrusions are normally of primary igneous origin.

The majority of sedimentary carbonates have $\delta^{13}C$ between -2‰ and +2‰ (Schidlowski *et al.* 1975) and in lithologies with > 40% carbonate these values are commonly preserved into the granulite facies (*eg.* Valley and O'Neil, 1984). Decarbonation reactions, which are confined to calc-silicates and narrow metasomatic margins of marble units, give off isotopically heavy CO_2, driving the remaining carbonate to isotopically lighter values. Even at its most efficient (by a Rayleigh volatilisation process) this will only cause substantial (> 5‰) fractionations when more than 90% of the original carbonate has been destroyed. Consequently although 5% carbonate in a regional metamorphic terrain is potentially a sufficient source for CO_2 to cause charnockite formation (Glassley, 1983), the average isotopic composition of the released CO_2 will have a distinctive signature of ≥ 0‰. It is impossible to produce large volumes of isotopically light (< -5‰) CO_2 from initially normal (0 ± 2‰) carbonate.

Crustally-derived CO_2 with intermediate isotopic compositions (-5‰ to -10‰) can only be produced from mixed carbonate and organic sources. Valley (1986) presents a review of isotopic exchange between coexisting carbonate and graphite, showing how isotopic exchange increases with metamorphic grade. Under granulite facies conditions the equilibrium fractionation (achieved by most samples) is 2.5‰ to 3.5‰. So with increasing metamorphic grade the isotopic difference between coexisting carbonate and graphite diminishes. The absolute isotopic composition of two such phases depends on their initial compositions and more importantly their relative abundances. Most of the cases which have been analysed are from graphitic marbles (> 75% carbonate) in which

the isotopic composition of the carbonate is virtually unchanged with the graphite tending towards -3‰ (Valley, 1986). To produce intermediate values the rock must initially have equal abundances of oxidised (carbonate) and reduced (graphite) carbon. It is only in rare graphite-rich, carbonate-poor calc-silicate lithologies that crustal rocks can generate 'mantle-type' compositions under closed system conditions. Such lithologies are unlikely to be sufficiently abundant in the majority of granulite terrains to produce the required volume of CO_2 with an isotopic composition in the same range as mantle derived CO_2. It is worth noting, that although this rock type may be rare, calc-silicates and the margins of carbonate bodies are documented as areas of strongly channelised fluid flow (Yardley, *pers. comm.*).

A carbon-bearing fluid phase which can move freely between lithologies makes intermediate isotopic compositions more accessible. If a fluid ($\delta^{13}C = 0‰$) is released from a carbonate lithology and subsequently interacts with graphitic sediments then an intermediate isotopic composition may result. In such a case, fluids with a full range of isotopic compositions between 0‰ and -20‰ would be expected rather than a cluster between -5‰ and -8‰. This is confirmed by the large volume of carbon isotope data available from Naxos.

This island consists of a metamorphic sequence (420°C to 690°C at 5 - 7 kb) of marble dominated metasediments with intercalations of carbonate and graphite-bearing schists (Jansen and Schuiling, 1976). The marbles generally retain their depositional isotopic compositions (Rye *et al.* 1976), but an even spread of $\delta^{13}C$ between +5‰ and -16‰ has been reported for CO_2-rich fluid inclusions sampled in quartz segregations (Kreulen, 1980). Of these the positive values are derived from dolomite-rich layers and those below -5‰ from graphite-rich schists (Kreulen, 1980). The remaining measurements from graphite/carbonate schists show a range of values between -1‰ and -5‰, these have been interpreted as mixing between a mantle source (-5‰) and the local marbles (Kreulen, 1980). A reinterpretation suggests that this scenario is incompatible

with other geological evidence and local mixing between carbonate and graphite with a skew towards the composition of the dominant marbles is more likely (Jansen *et al.* 1989).

Valley (1986) reviews isotopic studies in metamorphic aureoles and illustrates mixing trends between sedimentary carbonate and magmatic fluids on a $\delta^{13}C$ - $\delta^{18}O$ plot. In such high level intrusives there will be very little dissolved CO_2 hence these trends principally reflect oxygen isotopic mixing with magmatic water. Although decarbonation reactions are considered to be the main cause of light carbon enrichment, some mixing with an isotopically light fluid of mixed crustal and mantle origin may occur. Despite the possibility of mixing crustal sources of carbon, intermediate (-5‰ to -8‰) isotopic signatures in deep crustal terrains of largely igneous provenance are considered to be diagnostic of a mantle source.

5.4.3 Carbon isotope studies from granulites

Baker and Fallick (1989) analysed the isotopic compositions of the margins of marble bodies across an amphibolite to granulite facies terrain (N.W. Norway). The amphibolite facies marbles preserved their original isotopic compositions (about +8‰) but a spectacular trend towards -7‰ was observed in the graphite-free margins of carbonates in the granulite facies (with > 50% carbonate remaining). The authors conclude that interaction with an isotopically light fluid caused these shifts. The close proximity of a mangerite-charnockite suite of intrusive rocks provides a mechanism for transportation of large volumes of CO_2 from the mantle into the crust probably during a crustal extension event.

Several attempts have been made to determine the isotopic composition of a CO_2-rich fluid which has equilibrated with granulite facies rocks. Techniques employed include analysis of CO_2 direct from fluid inclusions (Hoefs and Touret, 1975, Pineau *et al.*

1981, Kreulen, 1980 and Lamb, 1988), CO_2 trapped in cordierite channelways (Vry *et al.* 1988) and the carbonate component in scapolite (Hoefs *et al.* 1981 and Blattner, 1976). The results of the studies (Figure 5.14 and 5.15) show a cluster of values between -5‰ and -8‰, although in three of the studies the authors have argued that these fluids result from late stage influxing after the peak conditions and are often preserved as carbonate in microfractures; a feature common to many granulites (Hoefs and Touret, 1975, Pineau *et al.* 1981, Hoefs *et al.* 1981). It is generally agreed that these fluids are ultimately derived from a mantle source. Of more speculative origin are texturally early fluid inclusions (Hoefs and Touret, 1975 and Pineau *et al.* 1981) and the carbonate component in some scapolites (Hoefs *et al.* 1981) which show lighter isotopic values -10‰ to -25‰. It has been suggested that these are crustally-derived fluids, rich in an organic carbon component, which date from earlier in the metamorphic history (Pineau *et al.* 1981 and Hoefs *et al.* 1981).

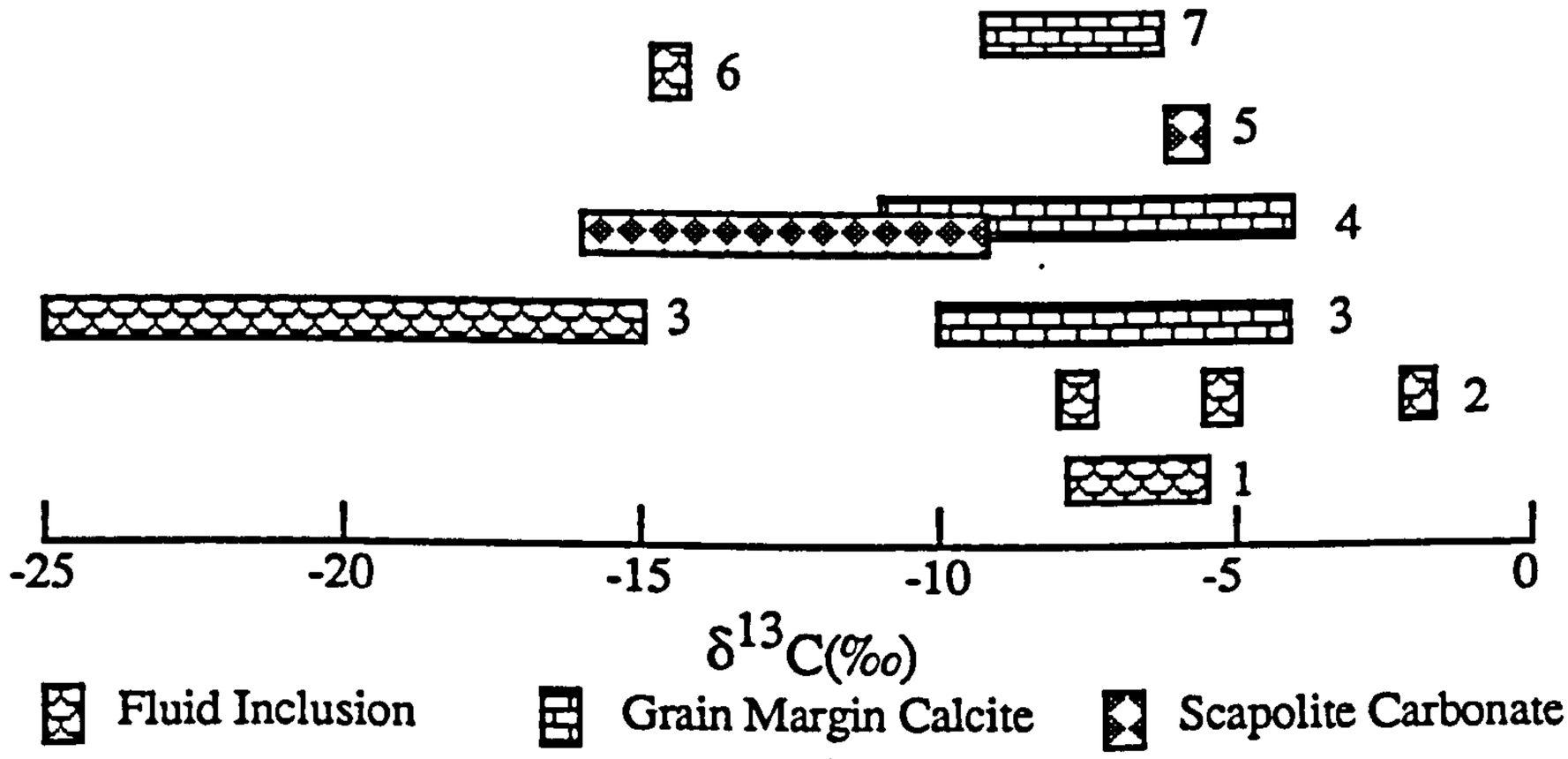

Figure 5.14. Plot showing the $\delta^{13}C$ values obtained from sources other than marbles, calc-silicates and graphite in granulite facies terrains. References and location of study: 1=Lamb (1988)-Adirondacks; 2=Santosh (1988)-S. India; 3=Hoefs and Touret (1975) and Pineau *et al.* (1981) reviewed in Javoy *et al.* (1986)-Bamble (S. Norway); 4=Hoefs *et al.* (1981)-S. Tanzania; 5=Blattner (1976)-New Zealand; 6=Coolen (1982)-S. Tanzania; 7=Stähle *et al.* (1987)-S. India.

The cordierite channel CO_2 data (Vry *et al.* 1988) show a wide spread of $\delta^{13}C$ values from -40‰ to -6‰. When their $\delta^{13}C$ data is plotted against yield of CO_2 (Figure 5.15) a significant trend can be observed towards -6‰ with higher CO_2 contents. This trend

is consistent with a mixing relationship between early organic-dominated crustal fluids and a mantle fluid, assuming that CO_2 can be retained in the cordierite channels from peak conditions (Vry *et al.* 1988).

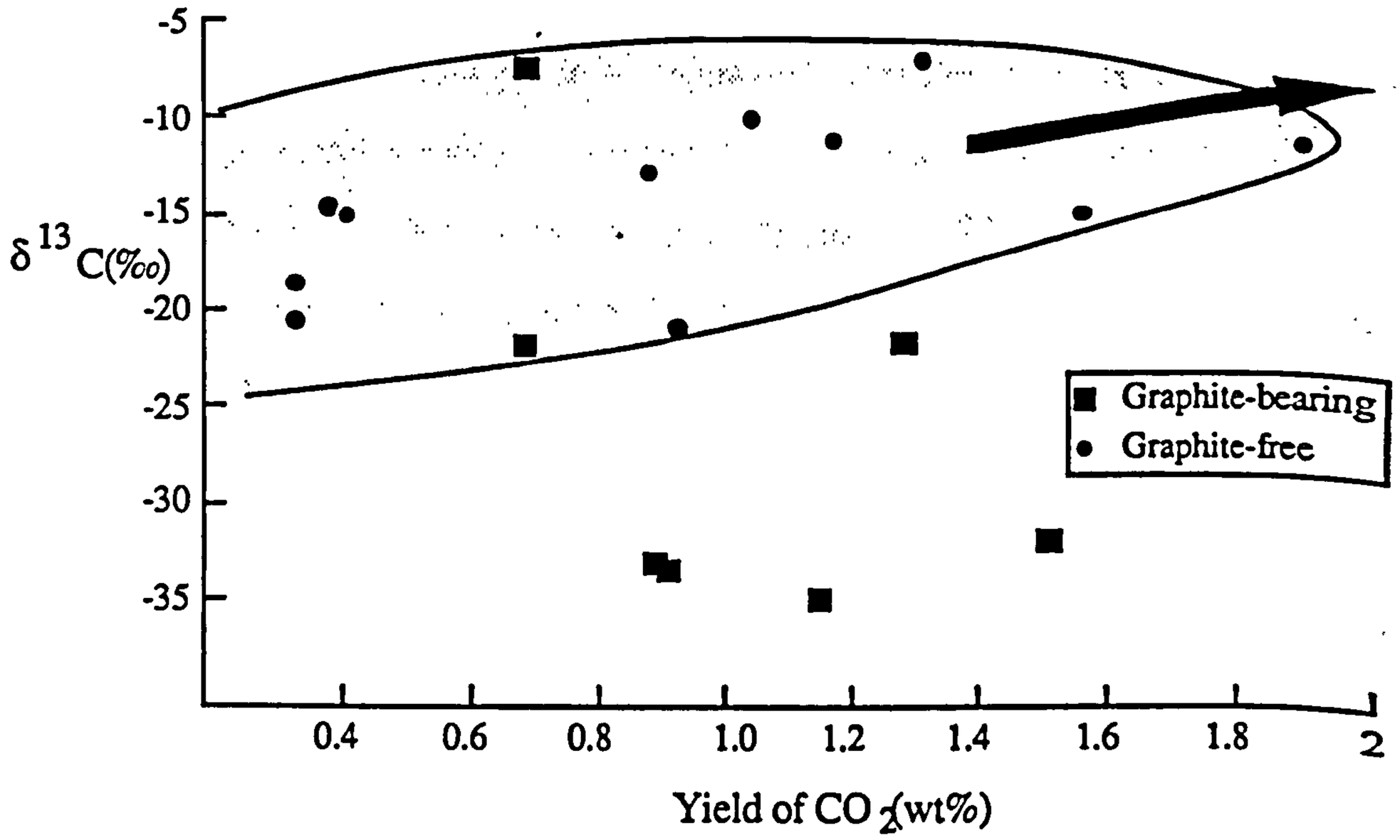

Figure 5.15. Plot of yield against $\delta^{13}C$ taken from the data in Vry *et al.* (1988). In graphite-free samples there is a clear trend towards typical sub-continental mantle values, this trend contradicts Vry *et al.*'s conclusion that the data show no evidence for influx of CO_2 from the mantle. Caution is required in interpreting these data until potential local carbon sources are evaluated in each case.

In conclusion, where an interaction with large volumes of CO_2-rich fluid can be demonstrated in granulite facies terrains most isotopic determinations are consistent with the fluid being derived from 'isotopically normal' sub-continental mantle. Early fluid retained through granulite conditions appear to be crustally derived with organic carbon rather than carbonate being the dominant source.

5.5 CHARNOCKITE FORMATION IN SOUTH INDIA AT 2.5 GA

Well constrained geochronological evidence indicates extensive crustal growth and associated granulite facies metamorphism between 2500 Ma and 2600 Ma (Buhl, 1987 and Peucat *et al.* 1989). The metamorphism effected the southern margin of the

Archæan Northern block, to the north of the Moyar suture zone, but also involved accretion of blocks of charnockitic rocks which record no earlier history (Nilgiri Hills and Madras block). The massive charnockites of the Palni and Periyar Hills from the south of the Palghat-Cauvery shear zone (Figure 3.1), which are geologically similar, may have formed during this same episode, but no radiogenic age constraints are available.

The carbon isotopic compositions obtained for CO_2 released from fluid inclusions in the charnockites and related rocks formed at this time are illustrated in Figures 5.16 and 5.17, data are given in Table 5.4. In Figure 5.16 a poorly constrained trend can be identified with isotopically heavier CO_2 being derived from samples richer in CO_2. Peninsular gneiss analysed from areas north of Kabbal and Coorg (more than 50 m, and probably 10 km from the nearest charnockite) contained no CO_2, so an isotopic

Locality	Sample No.	Lithology	Mineral	ppm C	$\delta^{13}C$ (‰)
Kabbaldurga[1]	KA2	Gneiss	quartz	7.7	-13.3
	KA4	Charnockite	quartz	16.5	-11.9
	KA5	Charnockite	quartz	18.8	-11.4
Satnuru[1]	SA3	Charnockite	quartz	69.9	-9.4
Palni Hills[2]	146061	Charnockite	quartz	72.8	-6.8
	H43	Charnockite	quartz	21.2	-10.9
Nilgiri Hills[2]	I685	Charnockite	quartz	60.8	-9.0
	IU6	Charnockite	quartz	13.6	-6.9
	IU6	Charnockite	garnet	125.9	-9.0
Coorg[1]	I633	Gneiss	quartz	3.2	-9.4
	CO8D	Charnockite	quartz	20.7	-7.5
Coorg[2]	I648	Charnockite	quartz	66.5	-4.4
Madras[3]	MA5A	Charnockite	quartz	42.4	-8.9

Table 5.4. Abundance and isotopic composition from 'peak release' carbon in gneiss-incipient charnockite pairs and massive charnockites from the 2.5 Ga metamorphic event. See Figure 3.13 and Appendix B for sample localities and details. Data for quartz from CO_2 released over the 600°C to 800°C peak release temperature interval. [1]=incipient charnockite localities; [2]=Type (a) massive charnockites; [3]=Type (b) massive charnockite.

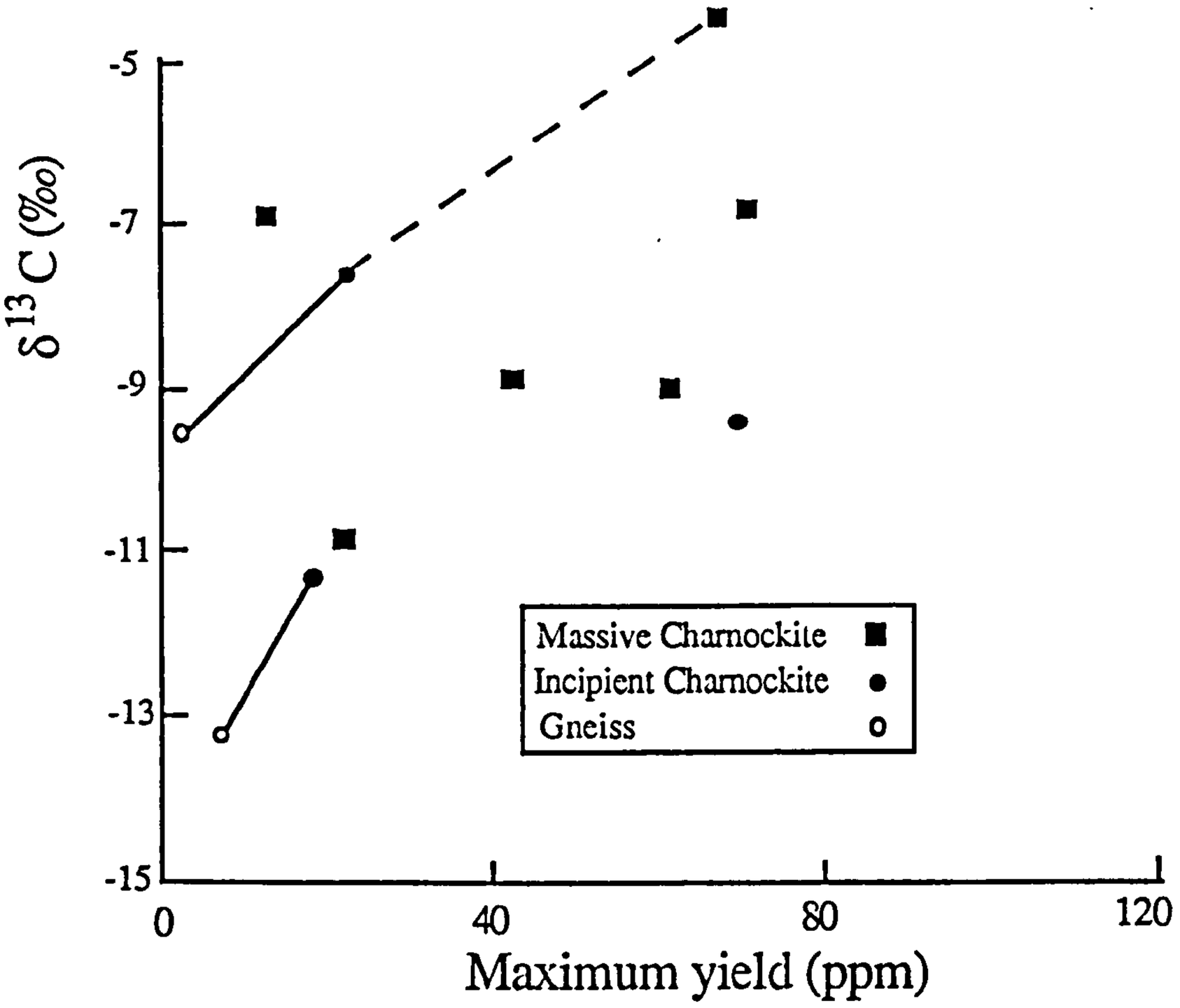

Figure 5.16. Plot of $\delta^{13}C$ against yield over the peak release interval from stepped heating experiments on gneisses, incipient and massive charnockites metamorphosed in the 2.5 Ga event.

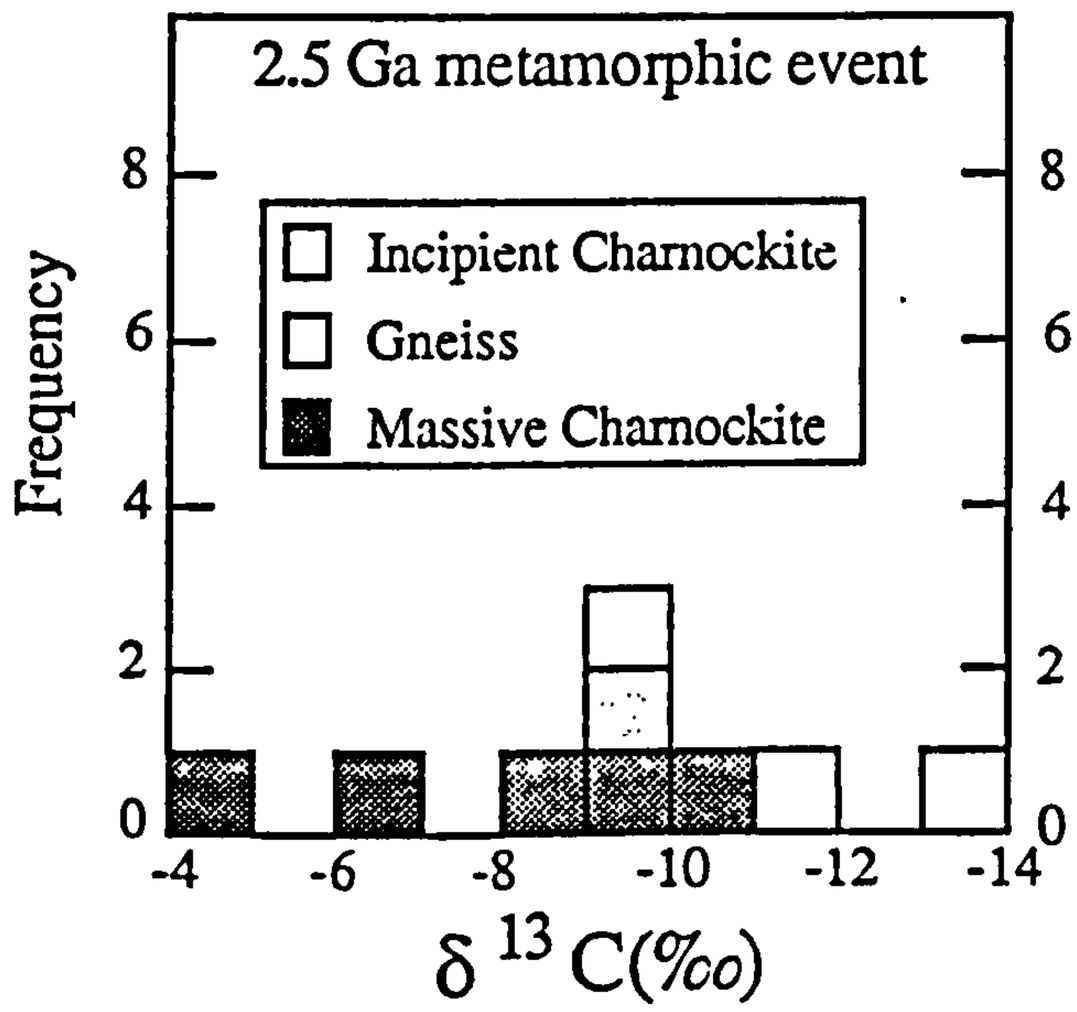

Figure 5.17. Histogram of frequency of $\delta^{13}C$ for quartz separates for samples given in Table 5.4.

composition prior to influx could not be determined. Although this precludes estimates of fluid influx abundances, it suggests that any measured isotopic compositions will be genuine influx values, rather than reflecting a mixed composition.

The samples illustrated on Figure 5.16 cover a large geographical area in which the relative positions of the blocks, at their time of formation, is unknown. The isotopic compositions for this area show an spread of $\delta^{13}C$ values between -4‰ and -13‰. The reasons for this diversity of results can only be speculated. It is possible that the CO_2 is derived locally in each case from crustal sources; natural heterogeneity of organic or carbonate lithologies may have given rise to the variation in isotopic compositions. Alternatively CO_2 derived from a homogenous source may have isotopically exchanged with such a variety of carbon-bearing lithologies during its passage through the crust. Metasedimentary horizons are found in both the Archæan terrain and occasionally in the accreted blocks, but they are rare and thought to be incapable of generating the required volumes of CO_2. The evidence for rapid crustal growth from Nd isotopic systematics (Peucat *et al.* 1989), the paucity of metasediments in the massive charnockites (type a) and the wide range of carbon isotopic compositions leads the author to suggest crustal accretion occurred during a period of subduction on the margin of the Archæan craton at this time.

Isotopic measurements on subduction related volcanic gas emissions cover the same range of isotopic compositions as observed for the CO_2 inclusions in the charnockites. The two processes postulated to control the $\delta^{13}C$ of the release CO_2 (sedimentary carbon release and dissolved CO_2 - free CO_2, **5.4.1**), are both likely to be depth dependent. The position of charnockite formation in relation to the subduction zone may be the factor which controls the isotopic composition of the carbon released into the overlying crust.

5.6 CO_2 TO THE SOUTH OF THE PALGHAT-CAUVERY SHEAR ZONE

5.6.1 Introduction

Although evidence is starting to emerge for a granulite facies event around 500 Ma (Hansen *et al.* 1985 and Buhl, 1987) in the Tamil Nadu block and KKB, the earlier history of this area is very poorly constrained with model ages between 1900 Ma and 2100 Ma reported (Chacko, 1987 and Choudry *et al.* in press). Available age data do not constrain charnockite formation to a single period in this area, but isotopic data from Sri Lanka strongly support a 500 Ma charnockite forming event (Burton and O'Nions, 1989 and Kroner *et al.* 1989). The carbon isotopic data collected for charnockite formation to the south of the Palghat-Cauvery shear zone (except the massive charnockites of the Palni and Periyar Hills) are discussed together in this section.

Figures 5.18 and 5.19 show the 'peak release' isotopic composition of CO_2 plotted against the yield and as a histogram. The first point of interest to be noted from Figure 5.18 is that all the incipient charnockites contain more (up to 400%) CO_2 than their precursor gneisses. Despite the variations observed in some samples this consistent effect is believed to be a real result and illustrates that CO_2 is intimately involved in charnockite formation. Moreover the isotopic values also illustrate a consistent trend towards heavier values in the charnockite compared with the associated gneiss. In contrast to the Peninsular gneiss, CO_2 was released from all gneissic samples analysed from the KKB.

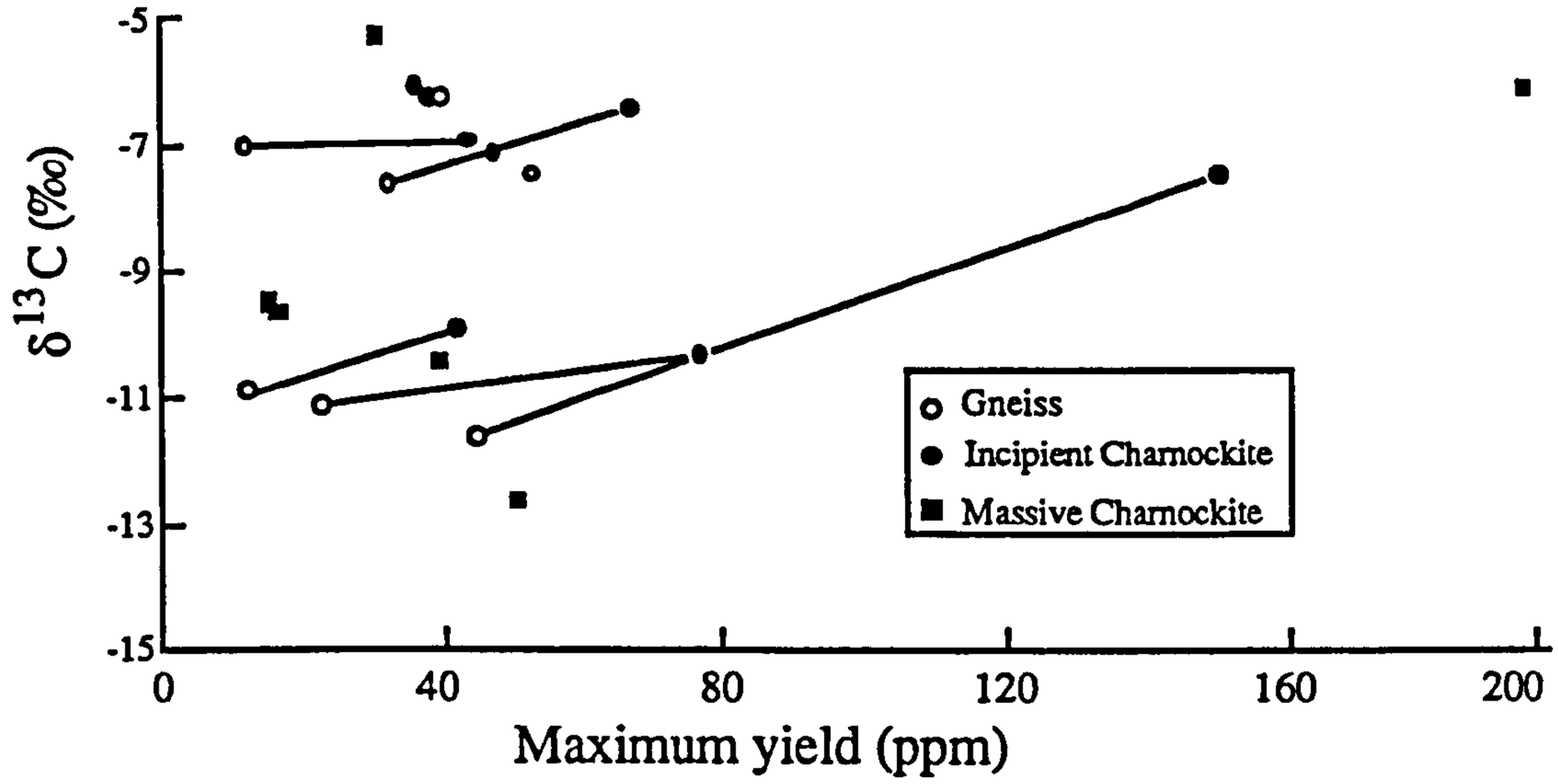

Figure 5.18. Plot of $\delta^{13}C$ against yield over the peak release range during stepped heating for gneiss, incipient and massive charnockite samples from south of the Palghat-Cauvery shear zone.

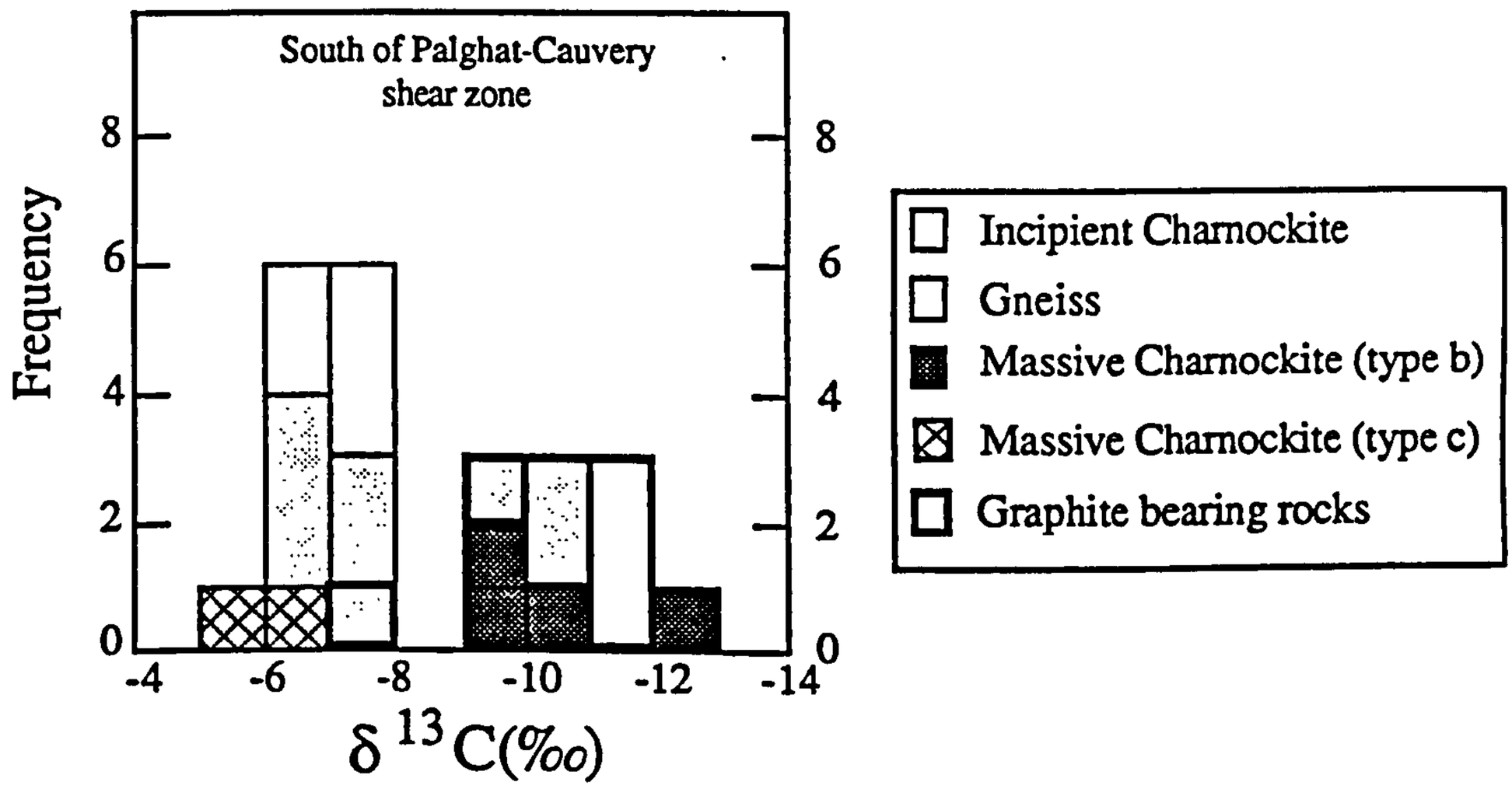

Figure 5.19. Histogram of frequency of $\delta^{13}C$ for quartz separates from samples given in Table 5.5.

5.6.2 Graphite-free localities

Figure 5.19 shows a distinct bimodality of isotopic compositions, with a cluster of analyses in the -5‰ to -8‰ range and a distinct group between -9‰ and -13‰. The first of these groups consists of (type c) massive charnockites (and metapelites) from Kottaram (Figure 3.11b) and graphite-free incipient charnockites and gneisses. In Chapter 3 incipient charnockite forming in graphite-free localities was mainly identified

Incipient Charnockite localities

	Locality	Sample No.	Lithology	Mineral	ppm C	$\delta^{13}C$ (‰)
6	Koddakad[1]	PC6A	Gneiss	quartz	11.7	-7.1
		PC6C	Charnockite	quartz	43.8	-7.0
8	Andipatti[1]	AN11A1	Gneiss	quartz	39.8	-6.3
		AN11A2	Charnockite	quartz	38.3	-6.3
9	Kottavatom[2]	SH/QF/12	Gneiss	quartz	12.0	-11.0
		SH/QF/12	"	graphite	-	-11.5
		SH/QF/11	Charnockite	quartz	42.2	-10.0
		SH/QF/11	"	graphite	-	-11.3
10	Manali[2]	SH/QF/6	Gneiss	quartz	44.6	-11.7
		SH/QF/5	Charnockite	quartz	150.2	-7.6
11	Kalanjur[1]	TR10A	Gneiss	quartz	32.0	-7.7
		TR10A	"	quartz	44.6	-7.1
		TR10D	Charnockite	quartz	66.9	-6.5
		TR10D	"	garnet	22.1	-6.7
13	Panaikkudi[2]	146060	Charnockite	quartz	45.6	-7.3
17	Ponmudi[2]	SH/QF/3B	Gneiss	quartz	22.4	-11.2
		SH/QF/3B	"	garnet	19.2	-12.6
		SH/QF/3B	"	graphite	—	-19.7
		SH/QF/3	Charnockite	quartz	76.7	-10.4
		SH/QF/3	"	quartz	50.4	-10.3
		TR15B	"	quartz	66.4	-9.1
		TR15B	"	garnet	70.2	-8.5
		TR15B	"	graphite	—	-18.1
12	Kuttalam[1]	146057	Charnockite	quartz	38.5	-6.2

Massive Charnockite localities

8	Andipatti[3]	146059	Charnockite	quartz	17.8	-9.6
10	Manali[3]	SH/QF/4	Charnockite	quartz	48.8	-12.4
20	Kadakaman[3]	SH/QF/10	Charnockite	quartz	38.9	-10.7
16	Rajapalayam[4]	146058b	Charnockite	quartz	16.5	-9.5
15	Kottaram[4]	TR20A	Charnockite	quartz	31.8	-5.2
		TR20B	Metapelite	quartz	49.6	-7.7
		TR20B	"	garnet	42.9	-7.8
		TR20D	Charnockite	quartz	200.1	-6.2
		TR20D	"	garnet	236.2	-6.2

Table 5.5. Abundance and isotopic composition from 'peak release' carbon in gneiss-incipient charnockite pairs and massive charnockites from south of the Palghat-Cauvery shear zone. Locality numbers from Figure 3.3b (see Appendix B for sample details). Data for quartz and garnet from CO_2 released over the 600°C to 800°C peak release temperature interval and graphite bulk analyses. [1]=Graphite-free; [2]=Graphite-bearing; [3]=Type (b) massive charnockite; [4]=Type (c) massive charnockite.

along cracks and related to granitic intrusives. The isotope data are consistent with the CO_2 in both, these incipient charnockites and the Kottaram massive charnockites (type c), having a single magmatic source, with characteristic sub-continental mantle signatures. The igneous suite, described in Chapter 3, of which the Kottaram charnockites are part, are indicative of continental rift magmatism. The decompression mineral reactions recorded during incipient charnockite formation (Santosh, 1987) are consistent with rapid uplift on the Achan Kovil shear zone (compatible with extensional tectonics). Such continental rifting environments are often the settings for carbonatitic magmatism; which has been identified in Tamil Nadu during this period (Subramanian, 1983). This 600-800 Ma event includes alkali granites and graphite-bearing syenites which indicate that mantle carbon was available, at least to intrusive rocks (Santosh and Drury, 1988). It is concluded that charnockite formation occurred, both super- and subsolidus during continental rifting with the input of large volumes of CO_2 from a mantle source. Basic melts carrying dissolved CO_2 may have formed at the base of attenuating crust and been emplaced into higher crustal levels providing a vector for upward movement of mantle-derived CO_2.

5.6.3 Massive charnockite (type b) localities

The remaining data on Figure 5.19 which have isotopic compositions between -10‰ and -13‰ are from graphite-bearing incipient charnockites and gneisses and intercalated (type b) massive charnockites (graphite-free). Limited field evidence is available to constrain the relative timing of massive charnockite (type b) and incipient charnockite formation with contacts between massive charnockite and gneiss only being exposed in a few localities. In one such locality (Manali) incipient charnockite and orthopyroxene-bearing quartz segregations were observed forming in the (graphite-bearing) gneiss along its contact with a massive charnockite. The most obvious explanation suggests that the contact was an enhanced fluid pathway, which allowed access to externally-derived fluids. This hypothesis is supported by the isotopic compositions of inclusion-

CO_2 from quartz separates from each lithology. The gneiss and massive charnockite preserve $\delta^{13}C$ values of -11.7‰ and -12.4‰ respectively, whilst the incipient charnockite (sampled from an orthopyroxene-bearing quartz segregation) records $\delta^{13}C$ = -7.6‰, close to the composition of externally derived fluid in graphite-free localities.

This evidence argues in favour of massive charnockite formation prior to the incipient charnockite 'event' and probably contemporaneous with gneiss formation and migmatisation in the Kerala Khondalite Belt. Isotopic compositions of massive charnockites suggest either equilibrium with organically-derived CO_2 from the gneiss, or an external source isotopically distinct from that associated with incipient charnockite formation. A tentative comparison may be drawn between these results are those documented for the Bamble region (Hoefs and Touret, 1975 and Pineau *et al.* 1981). In the Bamble granulites early CO_2-rich inclusions are isotopically lighter than those entrapped during the waning of granulite conditions. A similar effect is suggested for the Kerala Khondalite Belt, where earlier gneisses and massive charnockites have lighter isotopic compositions than the incipient charnockites formed during uplift.

5.6.4 Graphite-bearing localities

Two explanations can be advanced for the shift to isotopically heavier values during charnockite formation in these localities:

1) Internal production of isotopically heavy CO_2.

2) Influx of externally-derived, isotopically heavy CO_2.

The carbon isotope systematics associated with these two processes are illustrated as cartoons in Figure 5.20. With a source of CO_2 and clear evidence of external influx causing charnockite formation in the area, the second possibility is an attractive model even in the graphite-bearing localities, with the isotopic composition of the fluid being

buffered to lighter values by the graphite. The isotopic shift towards mantle values in the incipient charnockites compared to gneisses supports this hypothesis.

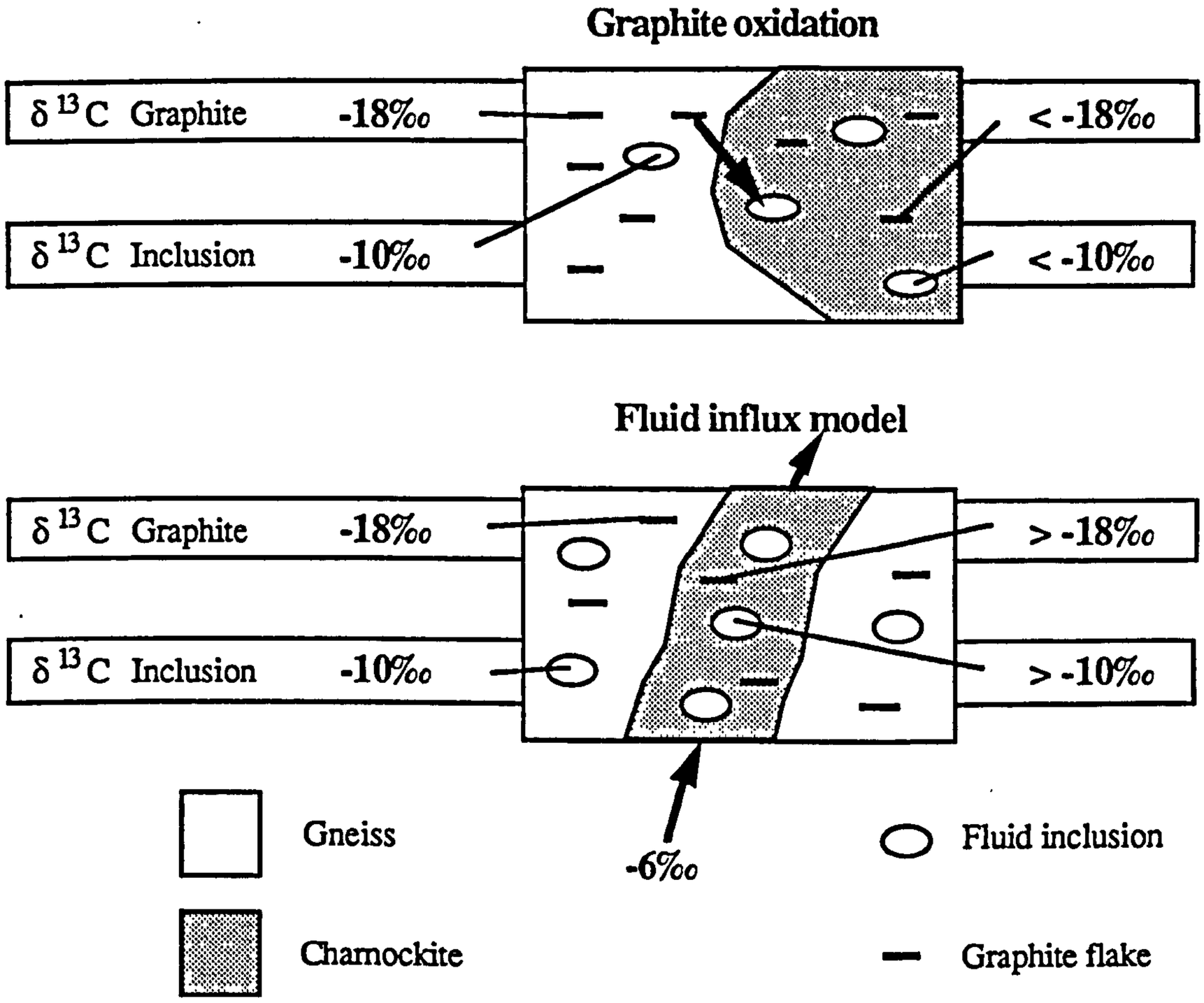

Figure 5.20. Cartoon illustrating the isotopic changes expected for graphite and inclusion-CO_2 for both an internal graphite oxidation source and external (mantle) source for CO_2. See text for discussion.

To distinguish between these possibilities graphite flakes from both gneisses and charnockites from Ponmudi and Kottavatom were analysed. The graphite in both cases also shows a shift to heavier values in the incipient charnockite (Table 5.4). This appears inconsistent with the graphite oxidation model (Figure 5.20), but the presence of trails of mixed N_2 - CH_4 inclusions (Klatt *et al.* 1988) suggest that methane may be an important carbon-bearing phase. Methane is isotopically lighter than both graphite and CO_2, hence a reaction of the type:

Graphite + Water (as fluid or in biotite) = Methane + Carbon dioxide

may result in isotopically light methane and heavy graphite and CO_2. A simple mass balance calculation, based on the isotopic fractionations between these phases (at 700°C) of $\Delta_{CH_4 - Gr} = -2‰$ and $\Delta_{CO_2 - Gr} = +7‰$ (Bottinga, 1969) can be used to test the plausibilty of this reaction. Unless CO_2 and CH_4 are produced in greatly disproportionate amounts (requiring a change in bulk oxygen fugacity) the resultant CO_2 will be heavier and the CH_4 and graphite both isotopically lighter. So it is concluded that influx of CO_2 from an external source is required by the isotopic data in all localities (except perhaps those with calc-silicate horizons, see Chapter 6).

5.6.5 Fluid abundances

The abundance of CO_2 fluid required to effect the transformation from gneiss to charnockite can be estimated by a phase equilibrium approach. From the data in Hansen *et al.* (1987) and that given in Table 6.3 one mole of a typical biotite from a gneiss from the Kerala Khondalite Belt contains 0.6 mol of H_2O (and 0.4 mol of F/Cl). If it is assumed that average gneisses contain 5% (by volume) biotite (Table 6.2 and Hansen *et al.* 1987) then 3.4×10^{-3} cm^3 of water is released from the complete destruction of the biotite in 1 cm^3 of gneiss (molecular weight of biotite = 430, density of biotite = 0.3 gcm^{-3} and the molar volume of water at these conditions = 16.02 cm^3).

While some biotite remains the fluid composition is buffered on the dehydration equilibrium curve (*eg.* point B on Figure 6.6) and the fluid composition at this point controls the abundance of CO_2 required to cause complete biotite destruction. Newton (1986) used a conservative estimate of $X_{H_2O} = 0.1$, from Figure 2.5 it is seen that even for pure phlogopite at 700°C $X_{H_2O} = 0.2$ is more reasonable. For more realistic biotite compositions (*eg.* $X_{Mg} = 0.4$) (data in Hansen *et al.* 1987 and Table 6.3) $X_{H_2O} = 0.5$ is obtained for 700°C (Figure 2.5). This value implies that the volume of CO_2 required to cause complete destruction of the biotite is equal to the volume of water released from that biotite. 0.0034 rock volumes of pure CO_2 (equivalent to about 0.1 wt%) is required

in this case. This quantity of CO_2 would be liberated by oxidation of only 0.027 wt% graphite. Such a decrease in graphite abundance would neither be detected optically nor by the experimental method described in **6.5.3.**

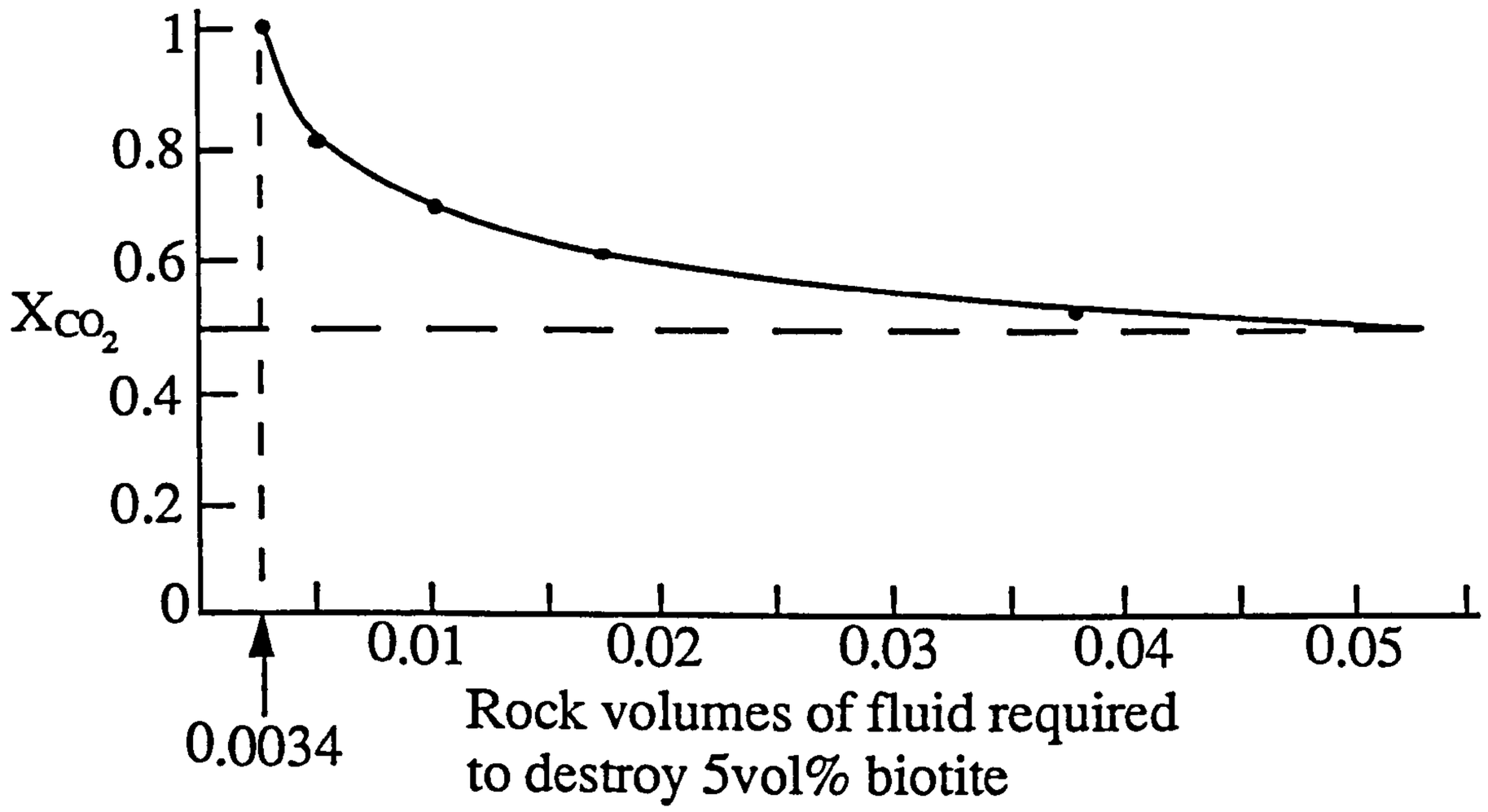

Figure 5.21. Plot showing the abundance of fluid, in rock volumes, required to destroy 5vol% biotite in a gneiss for different compositions of influxing fluid. This is plotted for $X_{Mg} = 0.4$ in orthopyroxene, the graph should be modified for other compositions.

This value, which uses more realistic rock chemistry, is a factor of 10 lower than that derived by Newton (1986). Figure 5.21 illustrates how the abundance of fluid required to cause complete destruction of 5% (by volume) biotite varies with its influx composition. It should be noted that most incipient charnockites investigated in southern India still contain some biotite, so Figure 5.21 only gives maximum fluid volume estimates. Harris and Bickle (1989) derive an estimate for a fluid-rock rock ratio, from the rate of propagation of a charnockite reaction front through the gneiss. They assume an influx fluid composition with X_{CO_2} only 0.05 above the equilibrium value, the fluid-rock ratio (0.08) obtained using the same assumption (local fluid-rock equilibrium) is similar to that from Figure 5.21 for these conditions. A further discussion of the significance of fluid-rock ratios is presented in **6.6.** In Chapter 2 it was argued that hornblende breakdown occurred at higher water activities, so the

abundance of CO_2 required to cause incipient charnockite formation in Peninsular gneiss localitites is lower than the estimates above.

5.7 CONCLUSIONS

The stepped heating technique described in Chapter 4 can successfully distinguish the major fluid inclusion release (500°C to 800°C) from contamination (≤ 400°C), late stage fluid inclusions (400 to 500°C) and graphite (900°C to 1200°C). In some cases the fluid inclusion release will coincide with a carbonate break down temperature (600°C to 700°C), adequate precautions during sample selection and preparation will ensure that samples are essentially carbonate-free. The similarity between release patterns for garnet and quartz confirms the suggestion that fluid inclusion decrepitation temperature is strongly dependent on entrapment conditions.

The isotopic data obtained for charnockite formation in South India have been divided into two groups on the basis of radiometric evidence of two periods of charnockite formation. The earlier period (2.5 Ga) is characterised by a wide range of isotopic compositions for inclusion-CO_2 (-4‰ to -13‰). These compositions may be related to local crustal modification of mantle CO_2, but the model prefered here involves charnockite formation above a subduction zone. In such an environment the carbon isotopic composition will be variable when released from subducted sediments or magmas.

There is less constraint on the age of the second charnockite formation episode which probably occurred at around 500 Ma. In general the carbon isotope data argue strongly for a sub-continental mantle origin of the CO_2 during rifting and uplift. Locally where incipient charnockites are formed in graphitic sediments isotopic data argue against an internal graphite oxidation processes, prefering an external source of isotopically heavy CO_2.

Chapter 6

NULIYAM - A STUDY OF FLUID-ROCK INTERACTION

6.1 INTRODUCTION

It has been concluded that CO_2 is vital in virtually all charnockite formations in South India. In some cases clear evidence exists for a sub-solidus transformation, but the discussion has so far avoided identifying the mechanisms of fluid movement and fluid-rock interaction. These problems are the subject of this Chapter, which presents a case study from a calc-silicate locality in the Kerala Khondalite Belt.

There are two major methods of identifying the involvement of a fluid phase during mineral equilibration; solid phase equilibria and stable isotope studies of minerals and fluid inclusions. These methods have been used to study both lower crustal interactions and convective hydrothermal aureoles associated with high level intrusions. Although estimates of the total volume of fluid which has passed through a rock have been obtained, confusion over what is actually being measured by such fluid-rock ratios often make these estimates difficult to interpret. To determine whether fluids are capable of transporting heat and material over sufficient distances to be important in processes of crustal stabilisation and modification it is vital to improve our understanding of fluid/rock interaction.

Theories based on continuum mechanics (applicable to the deep crust) have recently been developed to model geochemical, stable isotope and heat transport during single pass fluid movements. Although Litchner (1985) provides a complete mathematical treatment of chemical reactions and mass transport, the derived equations are prohibitively complicated to solve without using simplifying assumptions. Baumgartner and Rumble III (1988) and Bickle and McKenzie (1987), using

appropriate boundary conditions and assuming local grain-scale equilibrium between fluid and solid, model one dimensional transport of stable isotopes and heat and matter respectively. The most important concept derived from these models is that fluid driven processes give rise to reaction and geochemical fronts. These fronts mark the boundaries between transformed and untransformed rock and move at different rates with respect to the fluid flux rate and each other.

Sharp fronts are expected for fluid transport driven purely by advection, but with the increasing influence of diffusion or dispersion these fronts will broaden. Advection implies that the fluid phase moves relative to the rock matrix, whereas diffusive movement is driven by chemical or potential gradients with the fluid static with respect to the rock matrix. Dispersion involves mixing or heterogeneous flow in a pore fluid and can disrupt purely advective transport. Identification of the relative importance of these processes is vital for understanding fluid flow because diffusion is a slower and a less effective means of heat and matter transportation. Thus, evidence for diffusion without advection is not consistent with the regional transport of components by fluid processes. Identification of the topology and relative position of reaction and isotopic fronts in a fluid-affected rock can constrain the processes and rate of fluid transport, as well as total fluid abundance.

Bickle and Baker (1990) have extended this theory by modelling the relative positions of reaction and stable isotope fronts for a series of infiltration controlled reactions involving CO_2-H_2O fluids and a calc-silicate rock. Harris and Bickle (1989) have applied the simplified continuum mechanics theory to incipient charnockite formation at Ponmudi, and concluded that the data cited in Jackson *et al.* (1988a) are consistent with advective fluid transport, albeit, over limited distances (< 1 m).

This chapter presents a case study involving reaction progress and stable isotope studies on rocks from a quarry near Nuliyam (KKB) (location on Figure 3.3b). This

locality preserves, in a continuous exposure, the complete transformation from gneiss to biotite-free charnockite which allows the applicability of the continuum mechanics model to be tested. The gneiss-charnockite transformation is a simple fluid infiltration driven process, involving sub-solidus destruction of biotite and formation of orthopyroxene. Nuliyam is an excellent locality for this type of study due to the precise field control, where both a potential fluid source (calc-silicate) and its furthest extent of penetration can be observed. Reaction mineralogy and carbon isotopic composition of co-existing graphite, carbonate and fluid inclusion bound-CO_2 for a suite of samples across the transition have been analysed.

6.2 FIELD RELATIONS

The samples for this study were collected near the village of Nuliyam 50 km SE of Trivandrum (Figure 3.3b). Figure 6.1 shows the field relations from a section of continuous exposure (80 m) on a steep hillside. There are three lithological units; calc-silicate, charnockite and gneiss. At the base of the quarry 1.5 m of a calc-silicate horizon of unknown thickness is exposed. The calc-silicate assemblage is essentially quartz and diopside. (Common calc-silicate phases such as forsterite, scapolite, tremolite and wollastonite were not observed). Carbonate grains are seen to be highly corroded in thin section.

The calc-silicate is immediately overlain by coarse charnockite (massive charnockite type (c)) which is both biotite and garnet-free but contains coarse (1 cm) flakes of graphite. Completely anhydrous conditions of formation are indicated by the pristine nature of the orthopyroxene in the biotite-free charnockite. The great majority of southern Indian charnockites are characterised by low temperature hydrous retrogression which converts orthopyroxene grains to a dark mush of clay minerals. Plates 6.1a and b illustrate a comparison between common retrogressed orthopyroxene

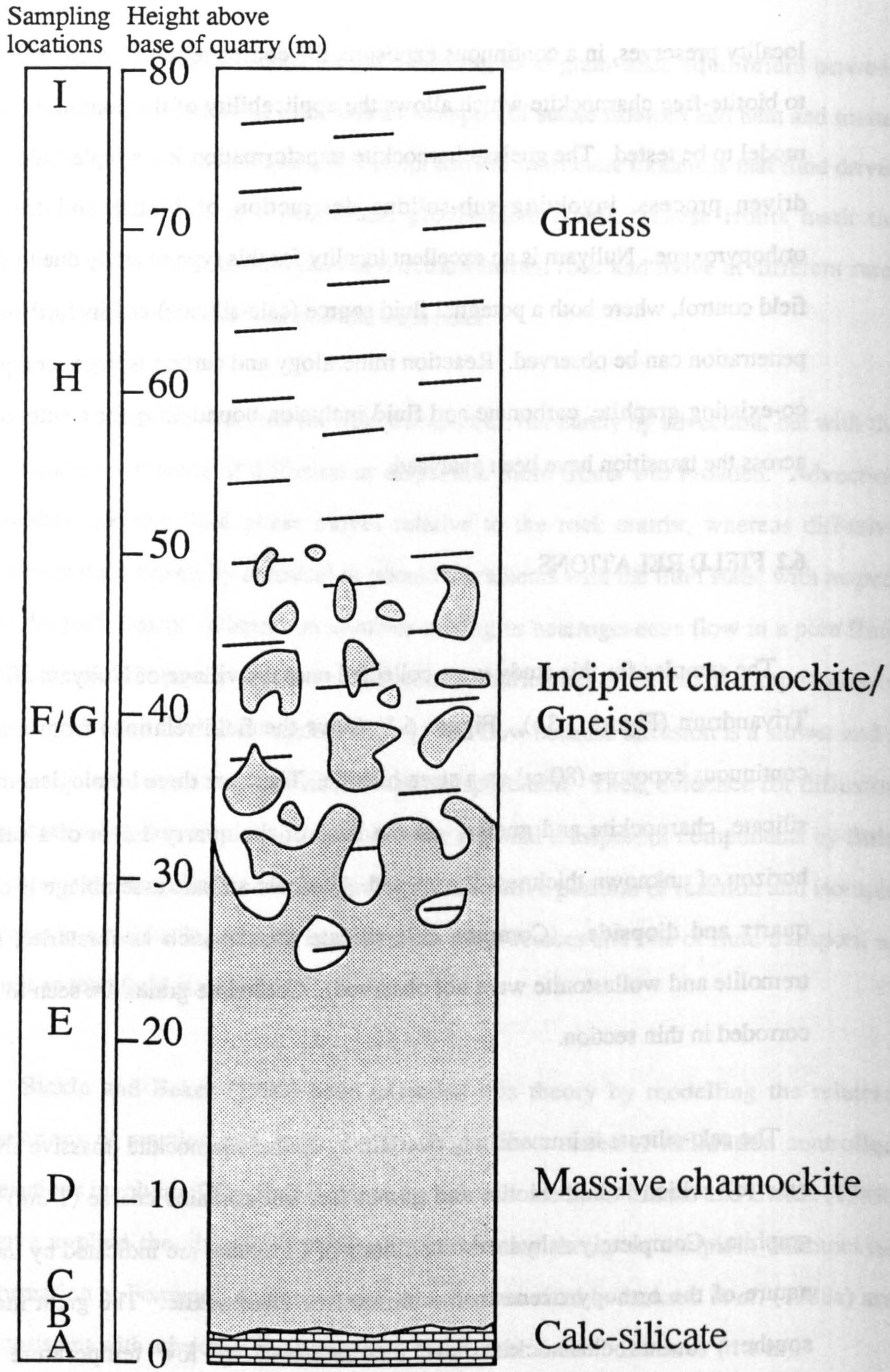

Figure 6.1. Diagramatic representation of the field relations observed at Nuliyam, see text for description.

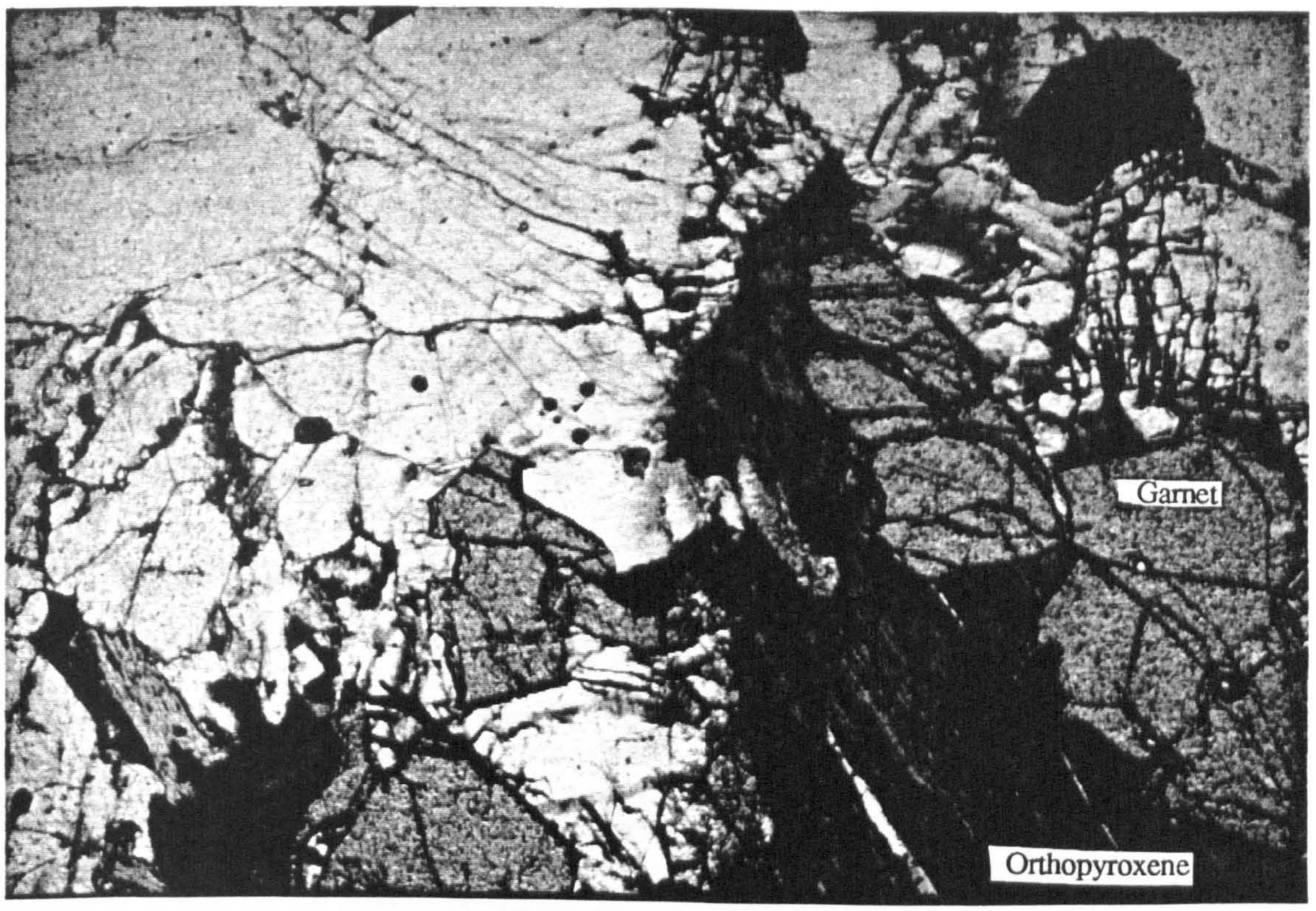

Plate 6.1a. Photomicrograph of an incipient charnockite from Ponmudi (TR15B), showing a heavily retrogressed orthopyroxene grain. Plate is 2.23mm across.

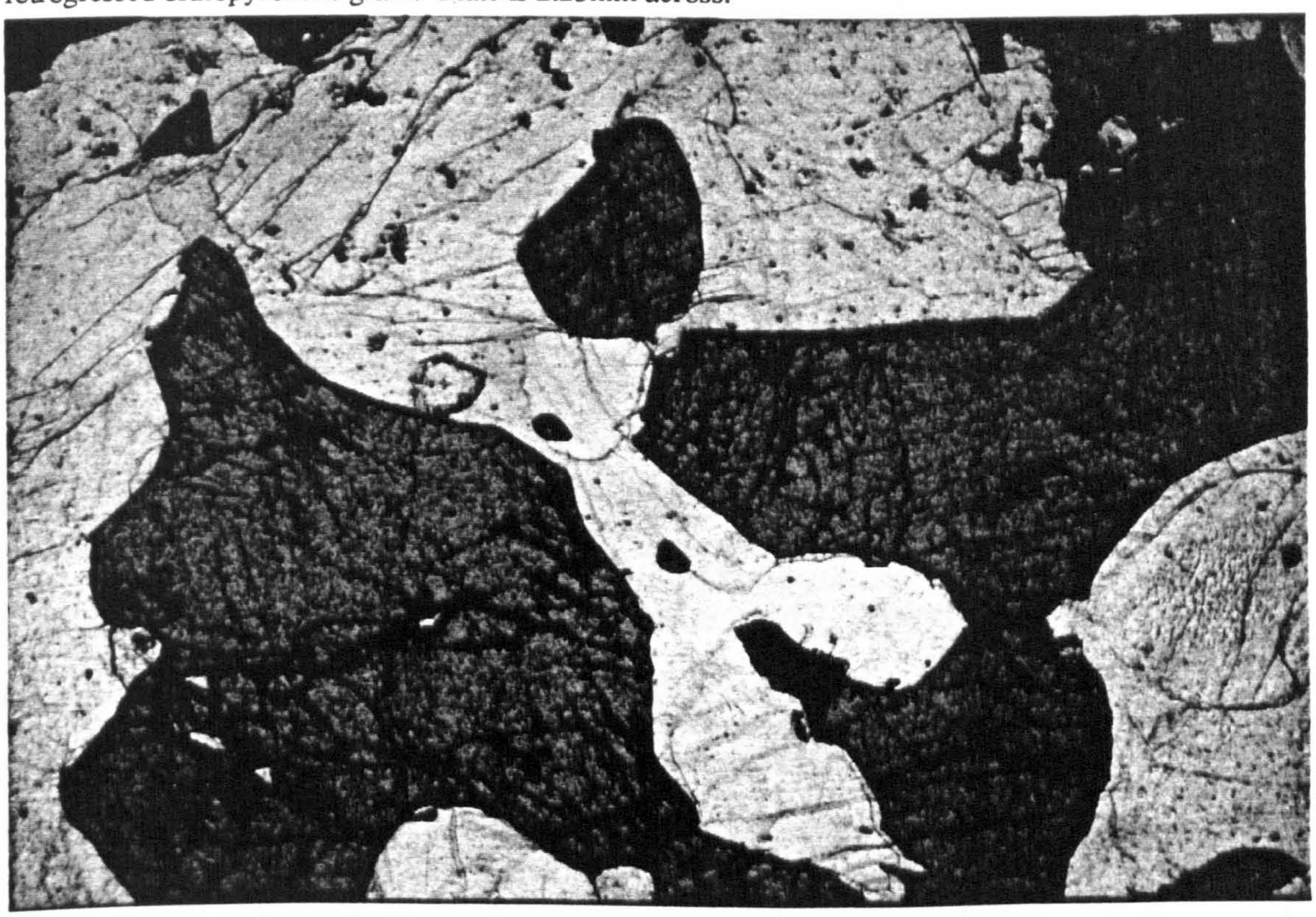

Plate 6.1b. Photomicrograph of sample TR27D from Nuliyam where garnet and biotite are absent and the orthopyroxene in pristine. Plate is 2.23mm across.

taken from an incipient charnockite at Ponmudi with that from sample TR27D (Nuliyam). At Ponmudi and indeed in TR27E and TR27F the activity of water is lowered sufficiently to stabilise orthopyroxene during charnockite formation but some water remains in the rock and during cooling it back reacts with the orthopyroxene. At Nuliyam the water appears to have been expelled completely by flushing with copious quantities of pure CO_2, a theory which will be discussed in more detail later.

Away from the calc-silicate, the abundance of graphite appears to decrease (this may simply be an artifact of decreasing grain size, **6.5.3**), and biotite and garnet appear about 10 m from the charnockite/calc-silicate contact (between localities TR27D and E (Figure 6.1)). The charnockite is a coarse equigranular rock with a typical green colouration and no distinct foliation even when the biotite is present. The abundance of garnet and biotite increases, with a sympathetic decrease in orthopyroxene further away from the calc-silcate. Rafts and selvedges of untransformed garnet-biotite gneiss begin to appear in the charnockite 25 m from the calc-silicate. At about 30 m from the contact, the gneiss enclaves have become the dominant rock type with only patches of graphite-bearing incipient charnockite remaining over the next 15 m. These charnockitic blobs appear to be completely isolated in the quarry face and are absent from the top 30 m of the section which exposes only charnockite-free gneiss.

The gneiss shows segregations of leucocratic layers of feldspar and quartz from more mafic layers. There is, however, no evidence of whole rock melting as is documented from Kadamakod (Plate 3.12). The mafic phases are predominantly biotite and garnet with some ore minerals and occasional graphite flakes. No aluminosilicate minerals were identified in the field or thin section.

6.3 MECHANISM OF FLUID MOVEMENT

6.3.1 Introduction

Harris and Bickle (1989) have discussed and attempted to distinguish diffusive and advective fluid motion during incipient charnockite formation. Their approach argues that the topology of reaction and isotope fronts can distinguish the two mechanisms of fluid transport, assuming local grain-scale equilibrium between rock and fluid on either side of the front. They argue that advective movement will generate sharp fronts, whereas diffusion will tend to smear out the fronts. Harris and Bickle (1989) identify a sharp reaction front (< 1 cm) between gneiss and biotite-bearing charnockite and cite this as evidence for an advective mechanism for fluid transport.

Several mechanisms of fluid transport in the crust are encompassed by the processes of diffusion and advection, these are discussed in more detail below.

6.3.2 Diffusion

Diffusive transport within a fluid occurs if driven by a chemical potential gradient. Transport by diffusion can occur by three different pathways, shown diagramatically on Figure 6.2, approximate diffusion coefficients for each case are given in Table 6.1 below.

	Path	Diffusion Coefficient (500°C,5 kb)	Time taken to move 10 m	Reference
A	Volume diffusion via lattice defects	10^{-18}-10^{-20} m^2s^{-1}	10^7-10^9 yrs	Cole and Ohmoto (1986)
B	Grain boundary diffusion	?		
C	Self diffusion through a static pore fluid	10^{-8} m^2s^{-1}	10 yrs*	Bickle and McKenzie (1987)

Table 6.1. The rates for the diffusion pathways illustrated in Figure 6.3. (* Time doesn't allow for fluid-solid equilibrium)

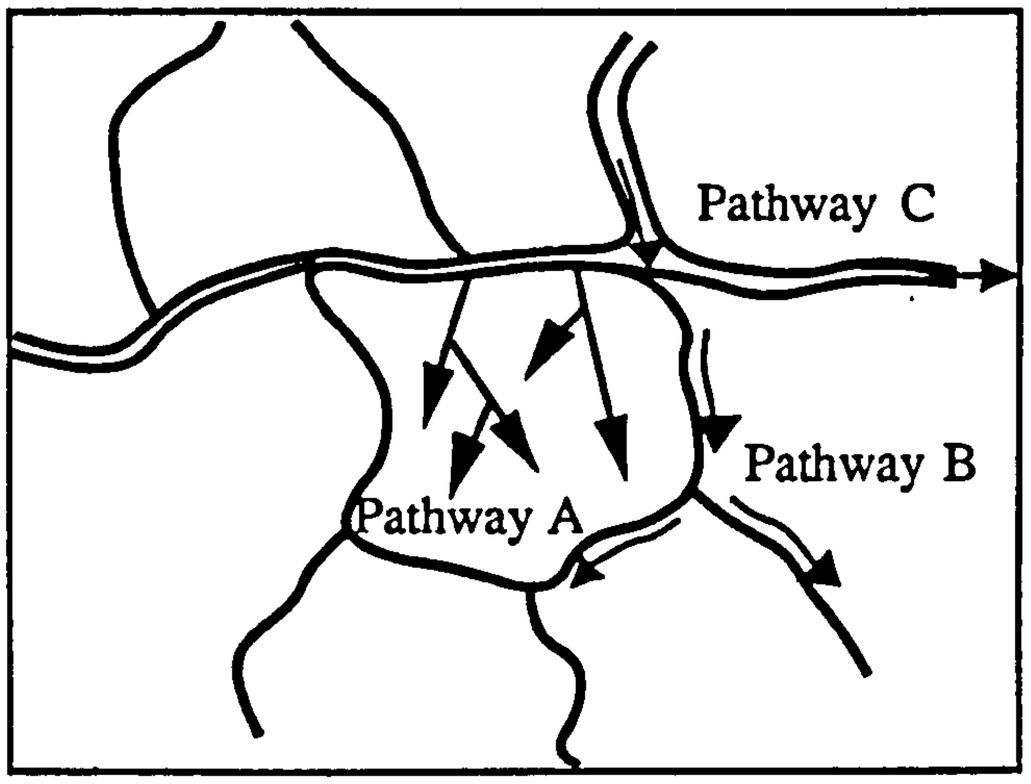

Figure 6.2. Possible diffusion pathways through (A) and around mineral grains (B and C), for a description of each see Table 6.1 (below).

Although the diffusion coefficient for pathway B is lower than that for A, there are a multitude of different A paths so at high temperatures volume diffusion may dominate over grain boundary diffusion. Solid-state diffusion rates are slow and probably only effective on a millimeter scale over the duration of fluid influx (*eg*. Cole and Ohmoto, 1986). Table 6.1 shows that the time taken for a fluid to diffuse 10 m via path A is unrealistically long for a metamorphic event. Walther and Orville (1982) conclude that grain boundary diffusion (path B) is wholly inadequate to explain observed metamorphic fluid fluxes. Although 'self' diffusion through an interconnected pore fluid (path C) is much more rapid and may be an effective fluid transport mechanism, it is argued below that such an continuous fluid did not exist.

6.3.3 Advection

Advective movement requires a mechanical potential gradient as a driving force and involves movement of a fluid with respect to the rock matrix. Advection can occur by the two mechanisms given below.

A. Fluid movement through an interconnected pore network.

B. Hydraulic fracture of the rock and fluid-filled crack propagation.

Beere (1975) has shown that the existence of an interconnected pore network is solely dependent on the 'dihedral angle' Θ[1] (illustated in Figure 6.3). The dihedral angle is different for each combination of fluid and solid species, and also depends on the orientation of anisotropic minerals. Smith (1964) has shown that if the dihedral angle is less than 60° then the grain-edge channels will form a continuous network; the pore spaces will remain unconnected if $\Theta > 60°$.

Watson and Brenan (1987) have carried out a series of experimental determinations of the dihedral angle for CO_2-H_2O fluids in pure quartzites and dunites. The experiments were conducted at 10 kb and > 900°C with mono- and poly-mineralic solid phases. Their results appear to be sufficiently consistent for the range of fluid and solid

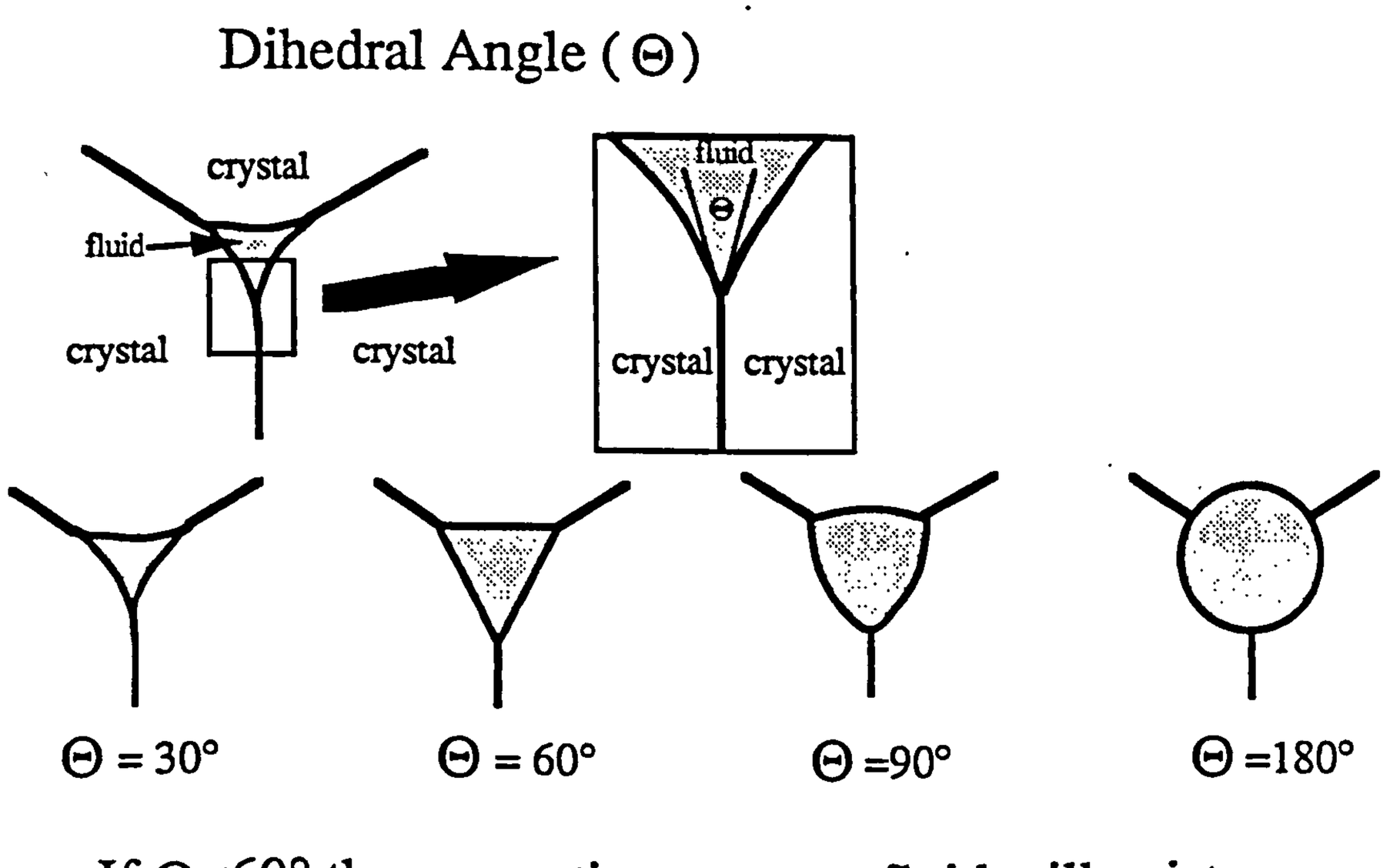

Figure 6.3. Diagram showing the formation of the dihedral angle between two mineral grains and a pore fluid and the appearance of some dihedral angles.

---

[1] The dihedral angle (Θ) is given by $\Theta = 2\arccos(\gamma_{S\text{-}S}/2\gamma_{S\text{-}f})$, where $\gamma_{S\text{-}S}$ is the energy per unit area of the solid-solid interface and $\gamma_{S\text{-}f}$ is that of the solid-fluid interface.

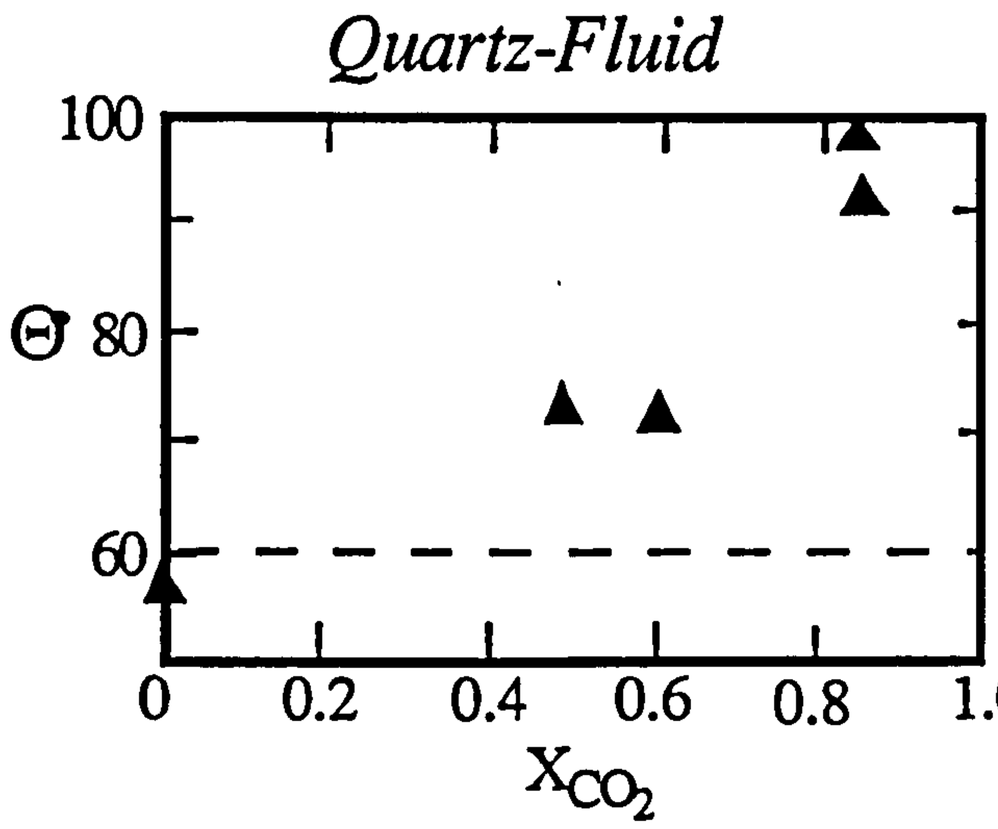

Figure 6.4. Graph reproduced from Watson and Brenan (1987) showing the variation of dihedral angle with pore fluid composition. Fluids with X_{CO_2}>0.1 will not form a continuous pore fluid.

compositions studied to be generally applicable to most high temperature (> 300°C) geological situations. They conclude that aqueous (and particularly saline fluids) have $\Theta < 60°$ for crustal rocks, although CO_2-H_2O mixtures of $X_{CO_2} > 0.5$ have $\Theta > 60°$ for all rock types and therefore can not exist as an interconnected pore fluid. Although they have no experimental data on fluids richer in water they extrapolate their results to at least $X_{CO_2} = 0.2$ before the critical $\Theta = 60°$ is reached (Figure 6.4). These results have crucial implications for flow of CO_2-rich fluids and carbonic metamorphism. A carbonic fluid may not form an interconnected pore network, consequently if it occurs, advective fluid movement will be by a hydraulic fracture mechanism.

Figure 6.5 shows the Mohr envelope for rock failure and examples of stress circles, when such a circle intersects the failure envelope the rock will undergo brittle failure. If the circle intersects the envelope at position A this failure will be tensional, and anywhere between A and B there will be a tensile component. If the gneiss is initially stable with a principal stresses σ_1 and σ_3 (circle I Figure 6.5) and a fluid is influxed, then the Mohr failure envelope will be intersected if $P_f - \sigma_3 > T_0$ (circle II), where T_0 is the tensile strength of the rock (Figure 6.5) and P_f is the pore fluid pressure. For the

gneiss T_0 will be «1 kb (depending slightly on the orientation of the gneissic foliation) (Walther and Orville, 1982).

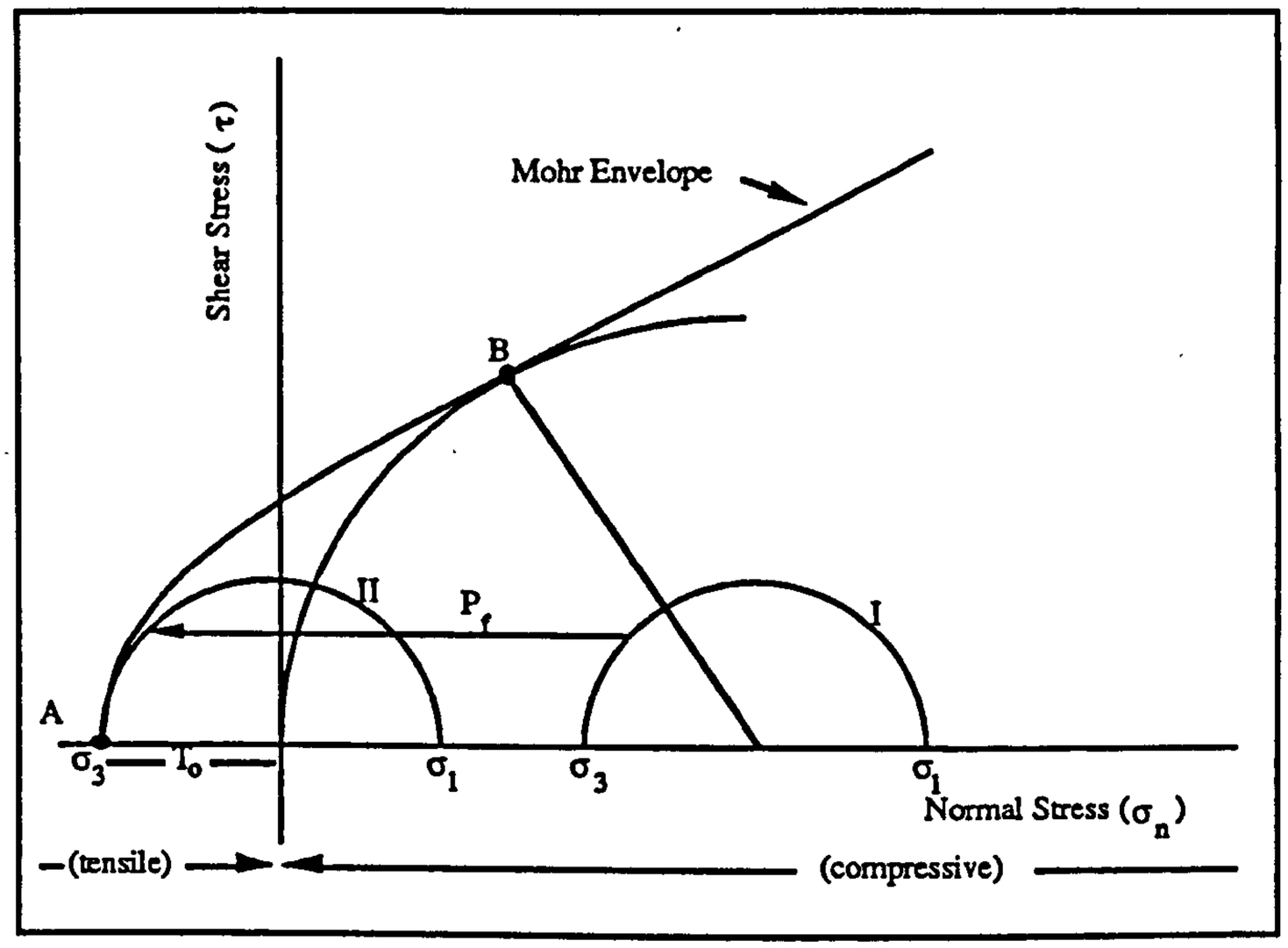

Figure 6.5. Diagram of a Mohr failure envelope to illustrate the conditions under which a rock will undergo hydraulic fracture, see text for discussion.

The porosity of granulites is low and during decarbonation there is a large total volume increase of 40% (Valley, 1986), so the required fluid over-pressure (P_f) could rapidly build up and cause failure by tensile hydraulic fracturing. This will cause a process of continuous fluid release in a series of small batches or 'burps'. A fluid-filled crack will develop and move down the fluid pressure gradient (away from the calc-silicate). Planar arrays of fluid inclusions which cross-cut mineral grains are thought to be healed fluid-filled fractures and provide the best evidence of hydraulic fracturing. In most metamorphic situations the dihedral angle for a give fluid phase is not important because during a fluid-flow event the rock is continually recrystallising and undergoing deformation. These processes will allow pockets of fluid to move sporadically through the rock. In South India, the evidence of charnockite formation along distinct pathways suggests that areas of gneiss were only undergoing deformation along specific horizons, which are zones of enhanced fluid flow.

The distance travelled and size of these cracks will depend on a number of variables. Walther and Orville (1982) estimated their size by calculating the volume of fluid preserved in inclusions and, assuming no fluid was lost, they deduced a typical crack diameter to be 0.02 μm. The grain size of the rocks is 0.5 - 5 mm and consequently these fluid-filled cracks are sufficiently narrow for the fluid flow to be modelled as a continuous pervasive process, with the fluid interacting with the entire rock. Brenan and Watson (1987) studied experimentally the propagation of CO_2 through olivine by hydraulic fracture and found a sharp fluid front and pervasive fluid interaction behind this front. This is an important conclusion as the continuum mechanical approach (discussed in 6.4 below) treats the fluid and rock as continuous pervasive phases.

6.4 APPLICATION OF CONTINUUM MECHANICS TO CHARNOCKITE FORMATION AT NULIYAM

6.4.1 Introduction

In a porous rock all points are either solid phase or pore space, so an assessment of the rock's physical properties on the microscopic scale is complex. Continuum mechanical theory simplifies the real situation with a hypothetical continua of pore space and solid rock. By modelling the physical properties of each point in the rock as the average of a large volume around that point, microscopic heterogeneities are eliminated. This approach allows the absolute definition of the physical properties of a porous rock which are pertinent to the modelling of fluid flow.

Although the full equations are complex (see Litchner, 1985) they can be simplified through the use of boundary conditions and by assuming local grain-scale fluid-rock equilibrium (Bickle and McKenzie, 1987 and Baumgartner and Rumble III, 1988); the modelling then predicts that an infiltration-driven univariant reaction will move through a rock with a sharp front. Although the front will be spread out by diffusive and

dispersive effects, these are often estimated to be small even in high grade metamorphic situations (Harris and Bickle, 1989 and Bickle and McKenzie, 1987). Isotopic studies have attempted to identify such fronts in the field (*eg*. Baker and Bickle, 1989 and Ganor *et al*. 1989). Diffusion appears to be the dominant transport mechanism indentified by these studies; they were, however, conducted perpendicular to the principal flow direction. The outstanding field control of a fluid infiltration driven reaction available at Nuliyam makes it an ideal locality for testing an advective flow model based on continuum mechanics against field data.

6.4.2 Initial assumptions

In the subsequent sections the following initial conditions are assumed before the fluid infiltration event at Nuliyam:

1) The calc-silicate was originally interlayered with gneiss, with the contact lying perpendicular to the surface exposure so ground measurements give true distances from the calc-silicate.

2) The gneiss is initially under vapour-absent conditions (see discussion in Chapter 3).

3) The temperature and pressure remain constant during the transformation event.

4) The input fluid phase is pure CO_2.

5) All fluids can be described as mixtures of two components (CO_2-H_2O).

6.4.3 Gneiss - charnockite transformation

The charnockite-forming reaction involves the breakdown of garnet and biotite and formation of orthopyroxene. The equilibrium mineral assemblage is determined by the ambient pressure and temperature conditions, the Fe-Mg chemistry of the biotite and the fluid composition. In subsequent modelling the first two are estimated from the data in Table 6.3 (see below) and the variation of fluid and mineral chemistry with time is

assessed. Orthopyroxene is absent from the analysed sections of samples TR27E and F, hence to obtain thermobarometric estimates the orthopyroxene analysis from TR27D has been used in conjunction with those from TR27E. The results obtained by making this assumption are in broad agreement with P-T conditions measured regionally by Chacko *et al.* (1987). The Hodges and Spear (1982) and Ganguly and Saxena (1984) biotite-garnet geothermometers give 680°C and 674°C respectively and the Perkins and Newton orthopyroxene-garnet-plagioclase-quartz geobarometer gives 5.37 kb for 700°C and 5.34 kb for 600°C. The Powell and Holland (1985) database gives 680 ± 50°C and 4.8 ± 1.4 kb at X_{H_2O} = 0.1 calculated in the CKMASH system for the assemblage garnet-biotite-orthopyroxene-quartz-K-feldspar-plagioclase.

Sample	Quartz	K-feldspar	Plagioclase	Garnet	Biotite	Orthopyroxene	Ore	Graphite
TR27C	47	37	1	-	-	4	+	+
TR27D	22	47	24	-	-	7	1	-
TR27E	41	41	7	7	1	1	1	+
TR27F	33	43	15	5	2	-	-	+
TR27G	32	53	13	+	1	-	+	-
TR27H	32	53	8	4	2	-	1	-
TR27I	38	38	4	13	4	-	+	-

Table 6.2. Modal analysis across the gneiss-charnockite transition, taking 1000 points covering the whole of one section from each sample. The analysis was performed using a step size of 0.5 mm and the grain size between 1 and 5 mm. (+) and (-) imply the presence in trace amounts and absence of the mineral respectively. See Figure 6.1 for sample locations.

To quantify the changes in mineralogy during progressive transformation, modal analyses were obtained and the results are given in Table 6.2. The mineralogy confirms the qualitative field observations that there is a decrease of biotite and garnet and increase in orthopyroxene and graphite when passing from the gneiss down through the charnockite, but no quantitative conclusions can be drawn from the data for two major reasons.

(1) The errors involved in point counting are large, particularly in the absence orthogonally-oriented sections. The grain size of the charnockite (1-5 mm) means that the rock is heterogenous on thin-section scale thus increasing errors from point counting on a single section. (For a full discussion of the errors involved with point counting see Solomon (1963)).

(2) The extent of original sedimentary heterogeneity is unknown (*eg*. samples TR27D and I come from sedimentary layers which preserve distinct oxygen fugacities (**6.5.3**)).

The gneiss-charnockite transformation reaction is;

$$\text{garnet + biotite + quartz = orthopyroxene + K-feldspar + plagioclase + ilmenite + } H_2O$$

For the purposes of modelling the simplification to:-

$$\text{biotite + quartz = orthopyroxene + K-feldspar + } H_2O$$

is justified because biotite is the only phase contributing to the fluid. The destruction of garnet does however suggest that charnockite formation occurred during a decompressional regime after the peak pressure conditions.

The dehydration reaction is illustrated on a T-a_{H_2O} plot (Figure 6.6). The gneiss is assumed to be fluid-absent because no evidence of partial melting, expected in the presence of a water-rich pore fluid, was observed (see Chapter 3). On influx of CO_2, a_{H_2O} is controlled by the fluid composition and will initially drop to point A (Figure 6.6). The mineral assemblage is then unstable and orthopyroxene will grow at the expense of biotite. This liberates water into the pore fluid, so a_{H_2O} increases to B. When B is reached the system has regained a stable equilibrium position, with the water activity (0.64) buffered by the composition of the biotite.

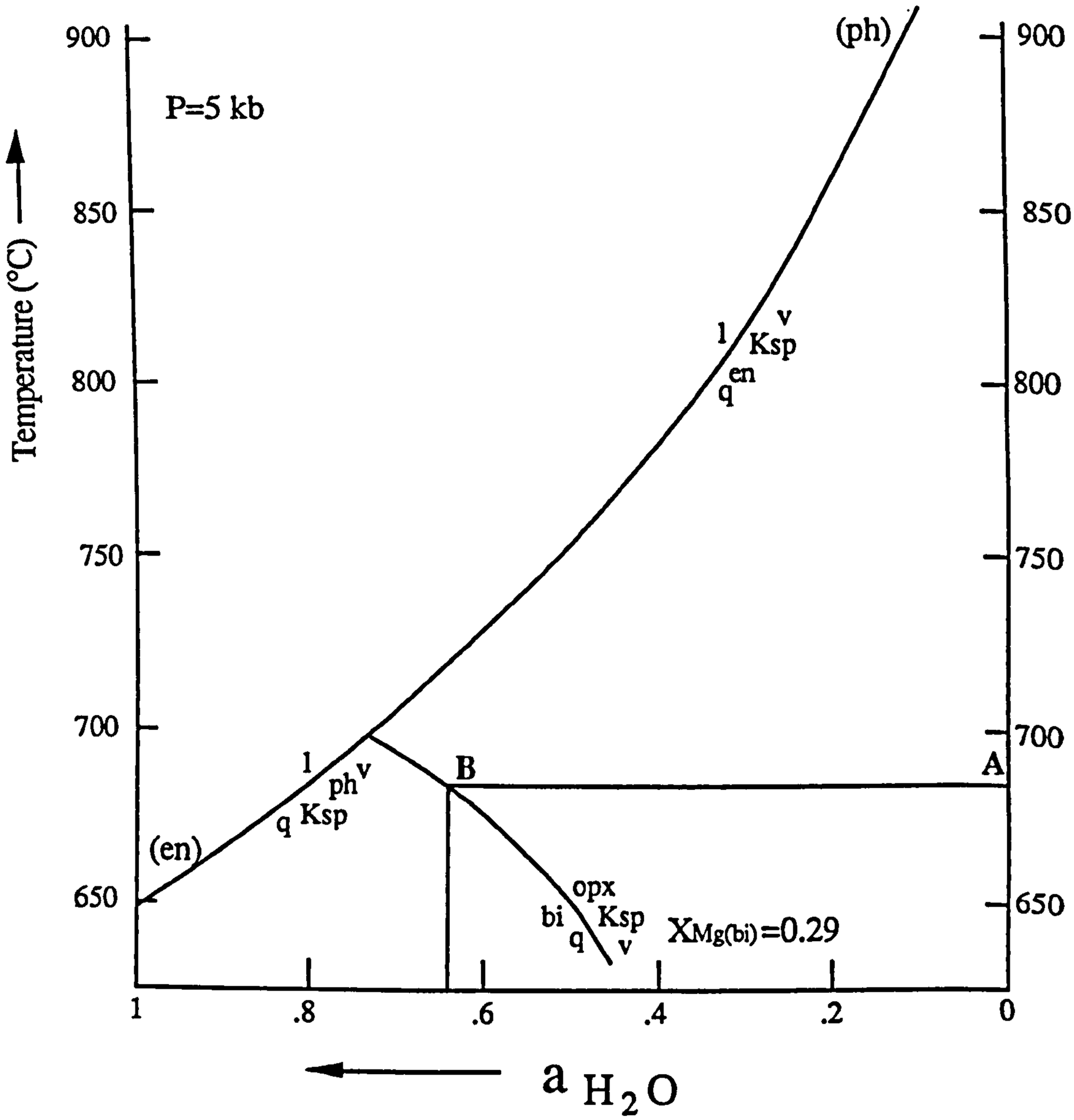

Figure 6.6. Plot of T-a_{H_2O} for 5 kb pressure (see Figure 2.3 for details of construction) and illustrates how the pore fluid composition changes during vapour influx. The sub-solidus dehydration curve is plotted using Holland and Powell's (1985) self-consistent data set which takes into account non-ideal mixing between H_2O and CO_2. Its position depends on the Mg content of the mafic phases, the line (X_{Mg}= 0.29) is for a biotite composition from the gneiss at Nuliyam.

6.4.4 Reaction Front Profile

In order to model the transport of the reaction front it is assumed that pure CO_2 is influxed into the base of the gneiss (above the calc-silicate horizon) and the biotite breakdown reaction (**6.4.3**) occurs. Fluid with X_{H_2O} = 0.64 (*ie.* not rich enough in CO_2 to cause further biotite breakdown in the overlying gneiss) is expelled from the top

of the charnockite. Assuming local equilibrium is attained, a reaction front (the boundary between gneiss and biotite-free charnockite) will propagate away from the calc-silicate. If fluid transport is an advective process the reaction front will be a sharp boundary and will move to a distance away from the calc-silicate which is fixed by the total volume of CO_2 input at the base. Since the influxing fluid is pure CO_2 a biotite-bearing charnockite should not be seen at Nuliyam. The situation envisaged by Harris and Bickle (1989) of a reaction front between gneiss and biotite-bearing charnockite only exists where fluid of a mixed CO_2-H_2O composition infiltrates.

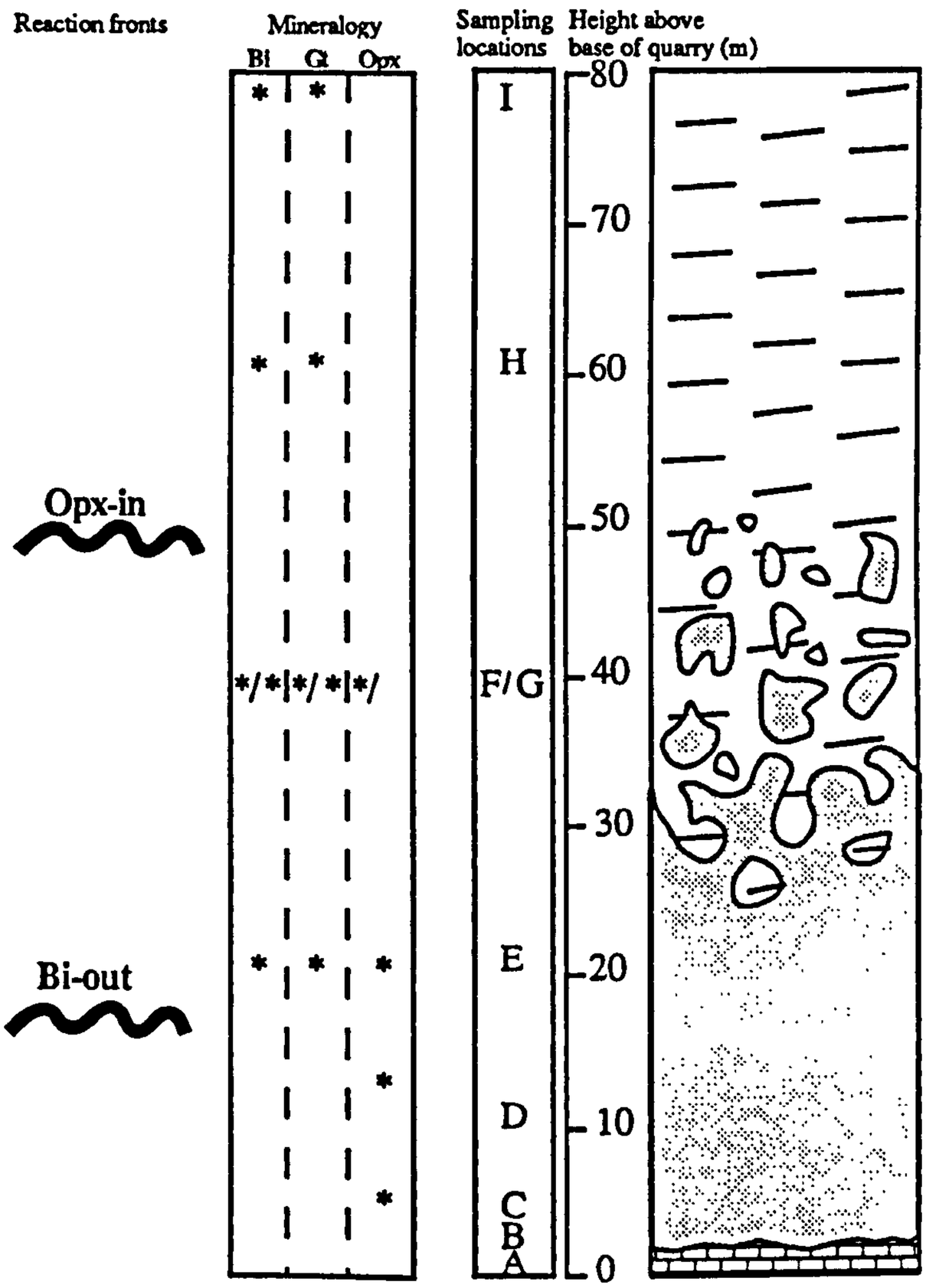

Figure 6.7. Diagram showing the distribution of mafic phases and position of the fronts discussed in the text at Nuliyam.

Samples TR27E and F are biotite-bearing charnockites, so the sharp front anticipated by the continuum mechanical theory is not observed. Bickle and Baker (1990) have argued that diffusion is the major mechanism for broadening some reaction fronts. In the Nuliyam example broadening on the scale of 35 m cannot be diffusion controlled (6.3.4), so another explanation is needed. Two fronts are identified on Figure 6.7; the 'opx-in' front at the onset of charnockite and 'bi-out' front where the last vestige of the biotite is destroyed. Two explanations may account for the separation of these fronts;

1) The reaction is not univariant.

2) Local fluid-rock equilibrium is not achieved.

6.4.5 Divariant reaction

The charnockite forming reaction has been assumed to be a simple univariant reaction, but biotite, garnet and orthopyroxene are all solid solutions between iron and magnesium (amongst other) end-members. The position of the biotite dehydration equilibrium curve in T-X_{CO_2} space depends on the Fe-Mg composition of the mafic phases (see Figure 6.6). If the reaction for the iron and magnesium end-members occur at different rates then an 'Fe-front' and 'Mg-front' will progress through the rock at different speeds causing a separation between the opx-in and bi-out fronts. Figure 6.8 is a theoretical illustration of this process occuring displayed in aluminium-iron-magnesium (AFM) space.

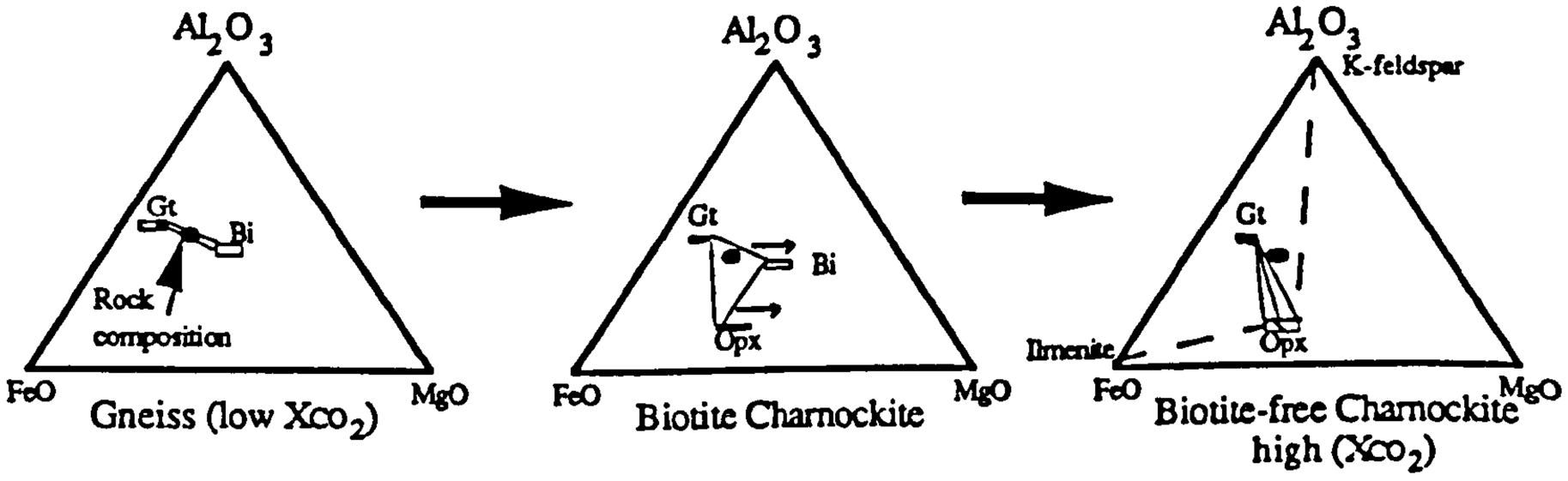

6.8a 6.8b 6.8c

Figure 6.8. Theoretical Al_2O_3-FeO-MgO plots showing how divariant nature of the biotite breakdown reaction can cause the stabilisation of a biotite-bearing charnockite.

Figure 6.8a shows the configuration in the gneiss, with a possible rock composition illustrated. When a CO_2-rich fluid is introduced Fe-rich orthopyroxene is stabilised and both the biotite and garnet compositions become richer in magnesium and a biotite-garnet-orthopyroxene triangle moves towards the magnesium apex (Figure 6.8b). The last vestige of biotite is destroyed when the garnet-orthopyroxene tie-line cuts the bulk rock composition (Figure 6.8c). This scenario is over-simplified since garnet is also destroyed; this is illustrated by the dotted tie-lines joining K-feldspar, ilmenite and orthopyroxene on Figure 6.8c.

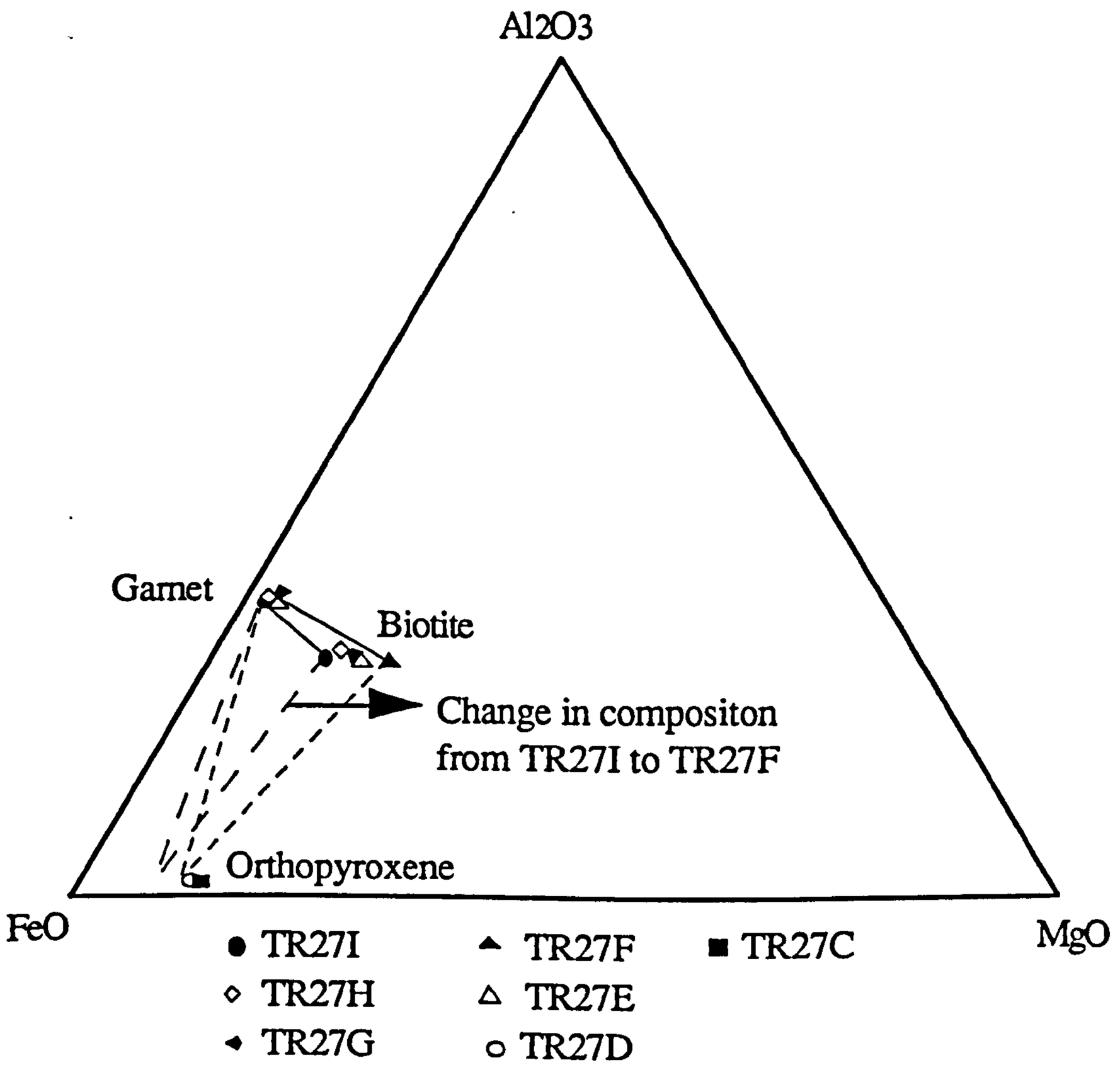

Figure 6.9. AFM plot of the change in chemistry of the mafic phases through the sample traverse at Nuliyam. The tie-lines connecting pyroxene to the other phases are dotted as the pyroxene composition is unknown or absent from these samples.

Mineral	Biotite					Garnet					Pyroxene	
Sample	TR27I	TR27H	TR27G	TR27F	TR27E	TR27I	TR27H	TR27G	TR27F	TR27E	TR27D	TR27C
SiO2	35.68	36.40	35.77	35.74	35.81	37.30	37.47	37.53	36.97	36.62	47.66	47.73
TiO2	5.00	4.84	5.43	4.45	5.37	0.06	0.08	0.04	0.07	1.14	0.21	
Al2O3	13.05	13.20	12.84	12.79	12.76	20.91	21.08	21.25	21.30	20.79	0.88	0.75
FeO	27.48	26.24	25.76	24.13	25.48	37.45	37.04	36.16	36.18	36.40	45.06	44.23
MnO	0.05	0.06	0.05	0.04	0.05	0.74	0.73	0.72	0.73	0.75	0.62	0.48
MgO	5.40	5.98	6.52	8.22	6.96	1.26	1.46	1.88	1.96	2.05	5.84	6.27
CaO						3.06	3.41	3.46	3.45	3.26	0.62	0.76
Na2O												
K2O	9.58	9.43	9.46	9.23	9.28							
F	2.89	2.74	2.50	2.93	2.31							
Cl	0.80	0.56	0.75	0.69	1.11							
Total	99.91	99.44	99.09	98.20	99.12	100.78	101.27	101.03	100.67	101.01	100.89	100.34
Mg/Mg+Fe	0.259	0.289	0.311	0.377	0.327	0.056	0.066	0.085	0.088	0.092	0.188	0.202
Formula Oxygens	22	22	22	22	22	12	12	12	12	12	6	6
Si	5.64	5.70	5.62	5.65	5.63	3.01	3.00	3.00	2.97	2.94	1.98	1.98
Ti	0.59	0.57	0.64	0.53	0.63	0.00	0.00	0.00	0.00	0.07	0.01	
Al	2.43	2.44	2.38	2.38	2.37	1.99	1.99	2.00	2.02	1.97	0.04	0.04
Fe	3.63	3.44	3.39	3.19	3.35	2.53	2.48	2.42	2.43	2.45	1.56	1.54
Mn	0.01	0.01	0.01	0.00	0.01	0.05	0.05	0.05	0.05	0.05	0.02	0.02
Mg	1.27	1.40	1.53	1.94	1.63	0.15	0.17	0.22	0.24	0.25	0.36	0.39
Ca						0.26	0.29	0.30	0.30	0.28	0.03	0.03
Na												
K	1.93	1.89	1.90	1.86	1.86							
F	1.44	1.36	1.24	1.47	1.15							
Cl	0.22	0.15	0.20	0.18	0.30							
H2O	2.34	2.49	2.56	2.35	2.55							
Total	17.18	16.96	16.94	17.21	16.93	7.99	8.00	7.99	8.01	8.00	3.99	4.00

Table 6.3. Average chemical analyses of mafic phases at Nuliyam (Appendix C gives full analyses).
Oxide analyses given in weight per cent. All Fe expressed as Fe(II).

Previous studies of the gneiss-charnockite transformation have only found small and variable compositional differences in biotite or garnet across the reaction front (Hansen *et al.* 1987 and Srikantappa *et al.* 1985). Harris and Bickle (1989) use a 2% increase in $\frac{Mg}{Fe+Mg}$ ratio in biotite to derive the change in fluid composition across the gneiss-charnockite boundary to model an infiltration driven reaction. The chemical change (taken from the data in Hansen *et al.* (1987)) is within the error of other biotite analyses from neighbouring charnockites (± 5%), indeed in some cases the $\frac{Mg}{Fe+Mg}$ ratio in

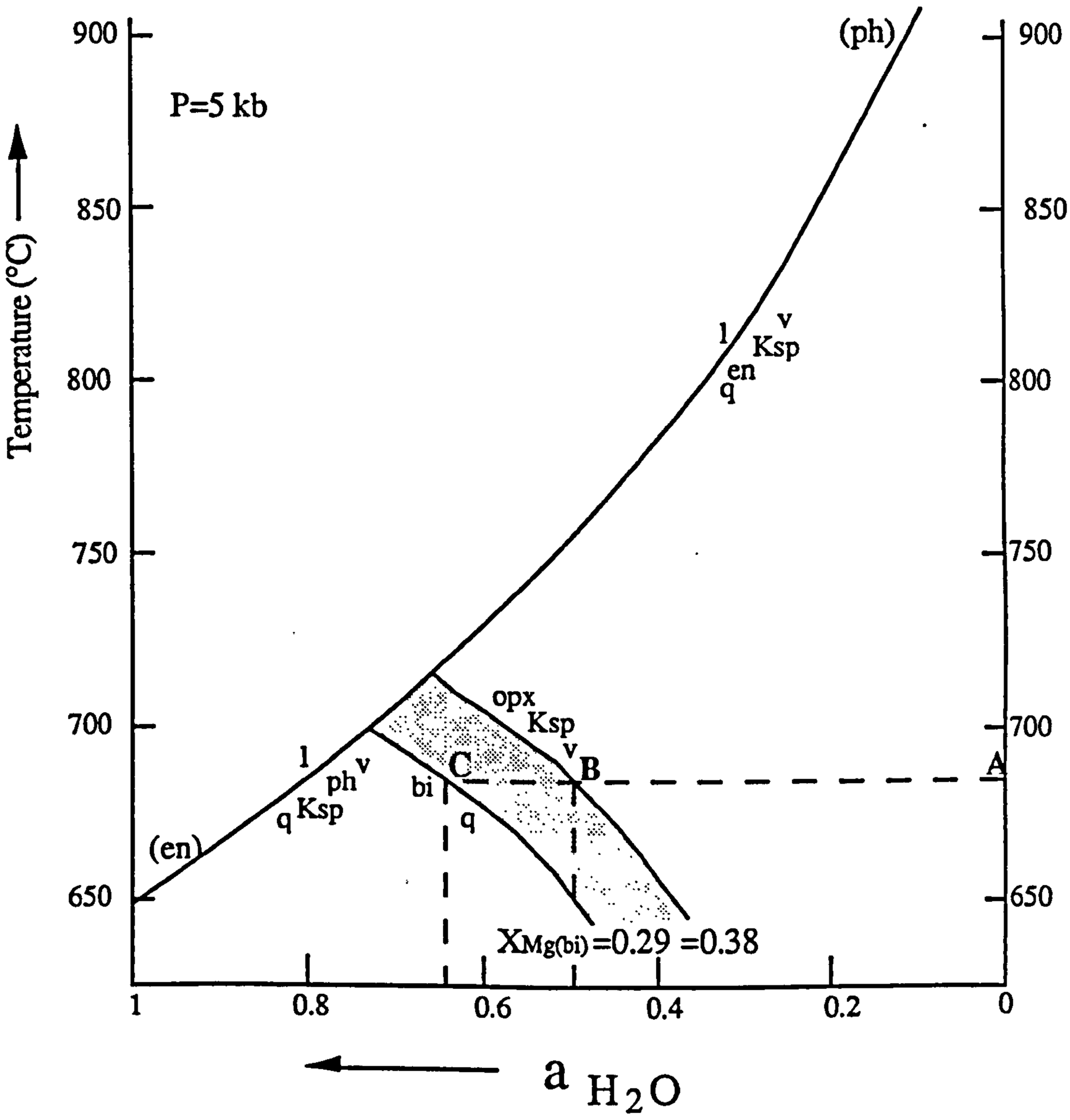

Figure 6.10. Plot of T-a_{H_2O} for 5 kb pressure in the K_2O-FeO-MgO-Al_2O_3-SiO_2-Vapour system. The sub-solidus dehydration curves are plotted using Holland and Powell's (1985) self-consistent data set which takes into account non-ideal mixing between H_2O and CO_2. The effect of different rates of iron and magnesium end-member reactions is illustrated.

biotite actually decreases across the reaction front. At Nuliyam, where biotite is exhausted, any change in mineral chemistry should be more pronounced towards the 'bi-out' front. Microprobe analyses of biotite, garnet and orthopyroxene are given in Table 6.3 and illustrated in AFM space in Figure 6.9 (full analyses are given in Appendix C.2).

The results show a significant shift to more magnesium-rich compositions in samples closer to the calc-silicate (Figure 6.9), with $\frac{Mg}{Fe+Mg}$ (bi) changing from 0.26 to 0.37. Due to the magnesium-poor nature of these rocks the bulk composition is likely to lie near the garnet apex of the three phase triangle (Figure 6.9), so only a small change in X_{Mg} may be necessary for the biotite to become unstable. The effect of this divariant nature on the univariant equilibrium line in T-X_{CO_2} space is illustrated on Figure 6.10, where a zone replaces the line. The equilibrium fluid composition is now buffered between X_{CO_2}= 0.64 and X_{CO_2}= 0.5 for the Mg-rich and Fe-rich mineral compositions respectively.

Figure 6.11 shows how the fluid composition evolves over time against distance from the calc-silicate horizon. In the final position (t_2), as preserved in the field, the 'iron-rich reaction' has progressed four times the distance of the 'magnesium-rich reaction'. Either the thermodynamic properties of iron and magnesium end-members are sufficiently different to cause such a dramatic separation of reaction fronts, or an alternative explanation is required. Non-attainment of local equilibrium is the most plausible alternative. As explained below non-equilibrium conditions will cause a variation in fluid composition and consequently stabilise the divariant mineral assemblages.

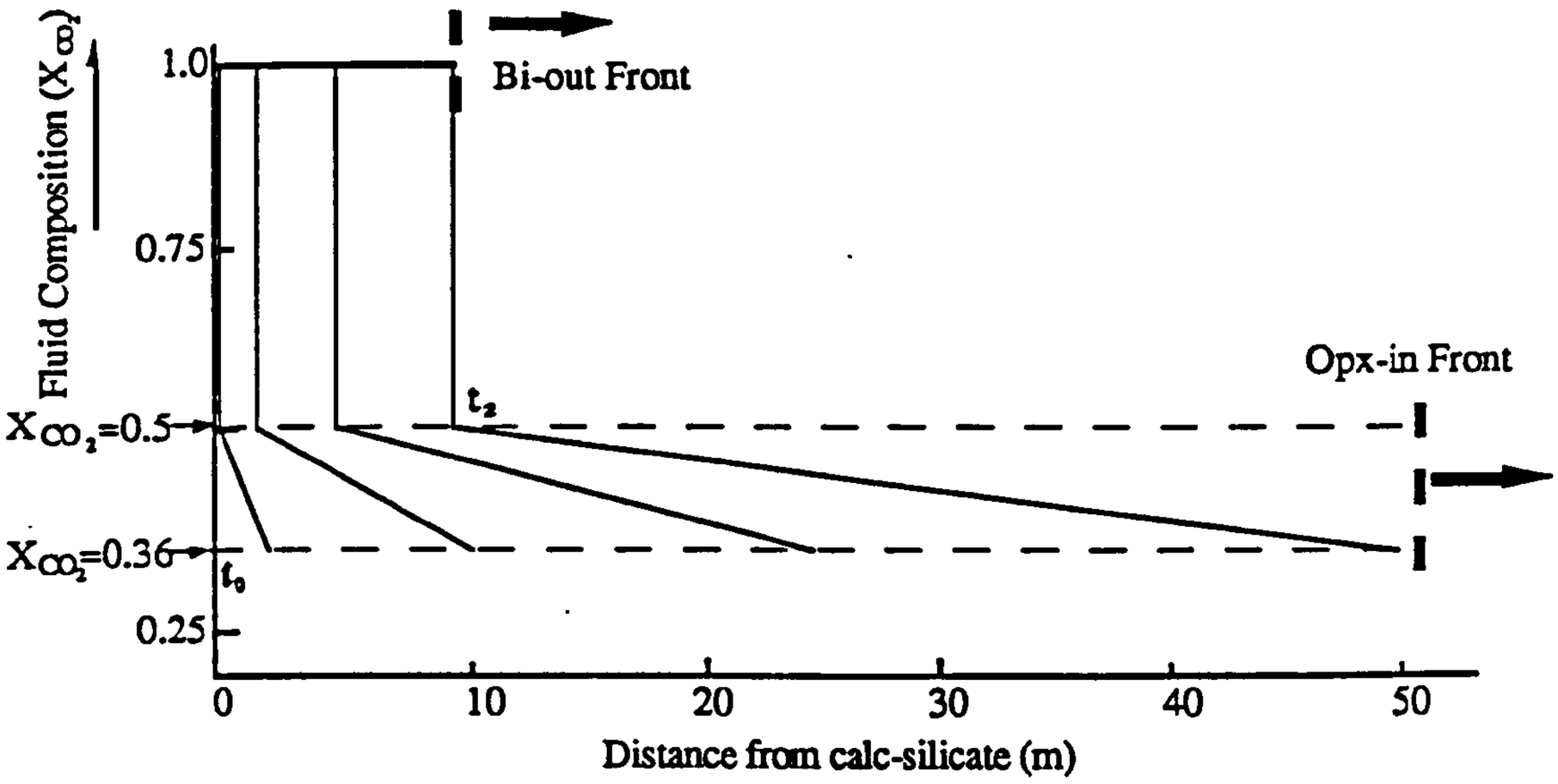

Figure 6.11. The evolution of the fluid composition in equilibrium with the rock over time, plotted against distance from the calc-silicate (*cf.* Figure 6.7). There is a gradual change in fluid composition which is in equilibrium with increasing magnesium-rich biotite compositions, until the biotite disappears whence the fluid becomes externally buffered and jumps to the influx composition. The gradient of the fluid composition in the biotite-bearing charnockite is controlled by the relative rates of the iron and magnesium reactions.

6.4.6 Fluid - rock disequilibrium

Rock re-equilibration, which is a kinetically controlled process, may be slower than fluid flow. If this is the case the rock will only 'see' a fraction of the potential disequilibrium effect of the fluid. This implies that the rock reaction will lag behind its potential position, hence the bi-out and opx-in fronts will become separated.

In some circumstances the distance over which re-equilibration occurs may be estimated by a study of the size of corona structures that form around unstable minerals. In fluid-absent granulites such corona structures seldom reach 0.5 cm wide, under fluid-present conditions, which are likely to be shorter lived, diffusion rates are more rapid; for instance Santosh (1987) reports coronas of cordierite growing up to 1 cm around garnet during incipient charnockite formation in the Kerala Khondalite Belt. Diffusion rates through fluids are faster (see Table 6.1) and dissolution or nucleation and growth kinetics may be the rate controlling step during mineral reactions. In general time constants for these processes are poorly known, but Wood and Walther

(1986) report one estimate of dissolution; 2 mm quartz grains taking 1000 years to dissolve at 600°C in pure water. Rates of nucleation and growth are highly dependent on ambient conditions, but they are even less well known, so currently the rate of rock re-equilibration remains an unknown parameter.

The assumption of local fluid-rock equilibrium is made in several studies of fluid/rock interaction mainly because it simplifies the mathematics of the continuum mechanical theory. Although attempting to solve the equations without this simplification is beyond the scope of this thesis, a semi-quantitative model for the processes observed has been derived.

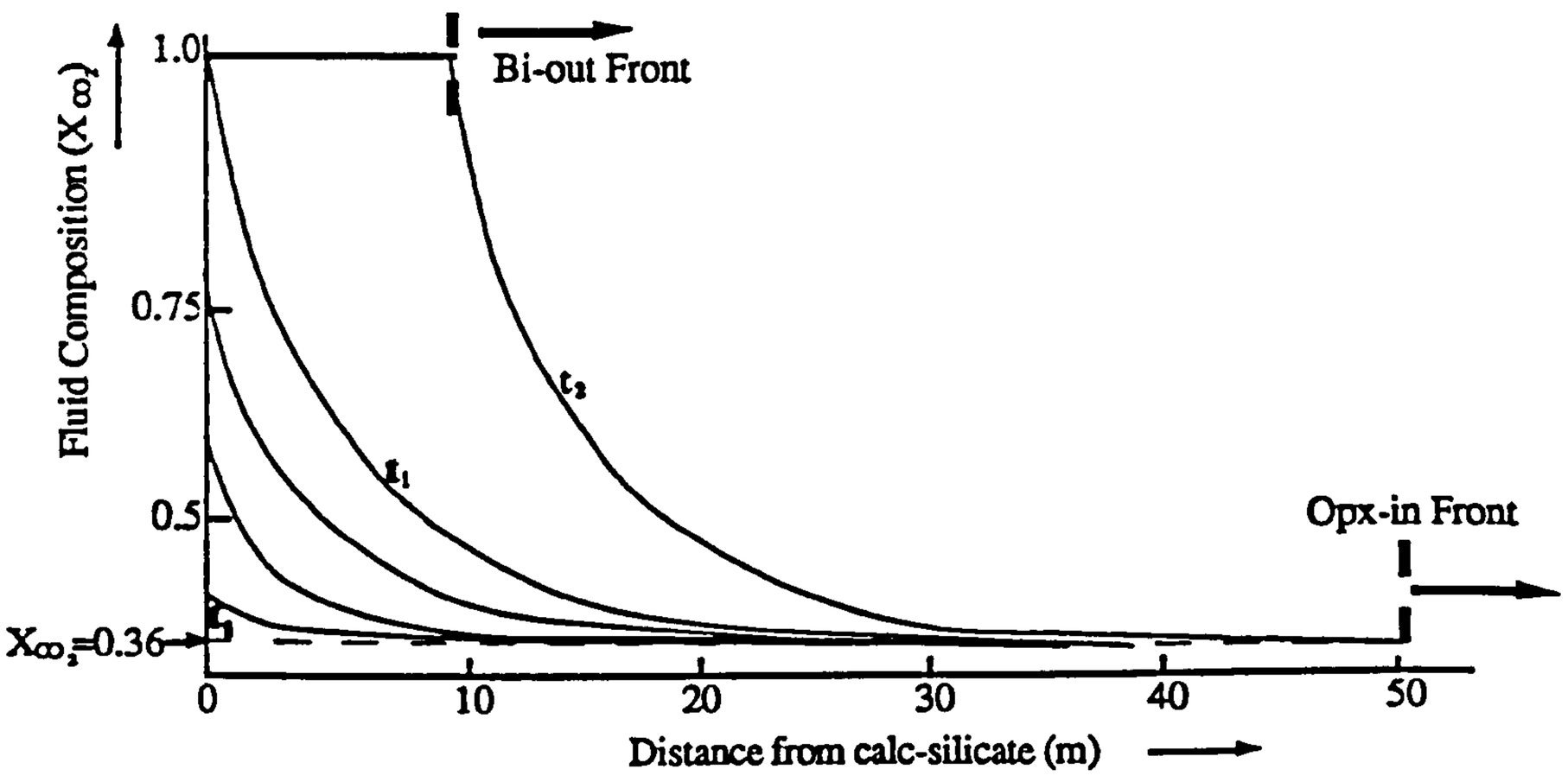

Figure 6.12. Evolution of the fluid composition profile through time, plotted against distance from the calc-silicate assuming that local fluid-rock equilibrium is not attained (*cf.* Figure 6.11). The limiting fluid composition X_{CO_2}= 0.36 is taken from Figure 6.6.

Figure 6.12 shows a possible profile of fluid composition plotted against distance away from the calc-silicate for a number of different times after the beginning of fluid infiltration ($t = t_0$). The fluid composition profile (Figure 6.12) is controlled by the amount of biotite which breaks down. The fraction of the potential amount of biotite which can be destroyed for a given volume of influxing fluid (of given composition) depends on the relative rates of fluid flow and rock re-equilibration. As the fluid

becomes more dilute away from the calc-silicate, the potential amount of biotite it is capable of dehydrating drops. Nevertheless the fraction of potentially destroyable biotite which is dehydrated remains the same. These combined effects result in an exponential decrease in the amount of biotite destroyed and hence X_{CO_2} (Figure 6.12) with distance from the calc-silicate.

When the last of the biotite is exhausted from the first element of rock ($t = t_1$) the bi-out front will begin to move away from the calc-silicate and the fluid composition profile will remain constant, until the observed situation in the field is reached ($t = t_2$ on Figure 6.12). The fluid rapidly becomes depleted in CO_2 (to $X_{CO_2} < 0.5$) over the first 15 m beyond the bi-out front. This 15 m constitutes the biotite-bearing charnockite (Figure 6.7). Beyond this distance the fluid is close to the equilibrium composition ($X_{CO_2} = 0.36$), so the driving force for the reaction is low and other factors which control charnockite formation may become important. Over the next 20 m of the section; charnockite occurs as increasingly isolated patches whose location appear to lack any control. In this area the driving potential for the transformation is small, so minor fluid or rock heterogeneities may influence charnockite formation in specific areas. The patchy nature of incipient charnockite suggests that nucleation energy is an important controlling factor.

6.4.7 Front velocities

Harris and Bickle (1989) derive equations which define the velocity of fluid driven reaction and isotope fronts in terms of the fluid velocity and rock porosity. These equations are based on the assumption that local equilibrium is attained between fluid and rock on either side of the reaction front. Although there is a large separation between the bi-out and opx-in fronts at Nuliyam the fluid and rock on either side 'appear' to be in equilibrium, hence the equation derived by Harris and Bickle (1989) can be used on either side of these fronts, to give the velocity of the reaction front (V_f).

$$V_f = \frac{\omega_1\phi_1[X_{V_1}^{CO_2}.X_{V_2}^{H_2O} - X_{V_2}^{CO_2}.X_{V_1}^{H_2O}]}{\phi_1[X_{V_1}^{CO_2}.X_{V_2}^{H_2O} - X_{V_2}^{CO_2}.X_{V_1}^{H_2O}] + X_{V_2}^{CO_2}.X_R^{H_2O}}$$

Where:- ω and ϕ are the fluid velocity and porosity.

$X_V^{CO_2}$ is the fluid composition.

$X_R^{CO_2}$ is the abundance of CO_2 released in the reaction.

1 and 2 refer to the charnockite and gneiss respectively.

In this case $X_{V_1}^{CO_2}= 1$, $X_{V_2}^{CO_2} = 0.44$, $X_R^{CO_2}= 0$, $X_R^{H_2O}= 2.7x10^{-3}g/cm^3$ of gneiss, assuming that $\phi = 0.2\%$:

$$V_f = 0.53\ \omega_1$$

The velocity of an isotope front is given by:

$$V_i = \frac{\omega_1\phi_1}{[(\rho_s/\rho_f)K_D + \phi_1]}$$

(Harris and Bickle, 1989)

Where:- ρ_s and ρ_f are the densities of the rock (2.8 gcm^{-3}) and fluid (1 gcm^{-3}) respectively and K_D is the distribution coefficient of the element in question between the rock and fluid.

For a carbon isotope front, assuming 0.1% graphite in the rock (6.5.3) $K_D= 2.9 \times 10^{-3}$, and

$$V_C = 0.25\ \omega_1$$

For an oxygen isotope front, $K_D = 1.1$, and

$$V_O = 6.5 \times 10^{-4}\ \omega_1$$

Hence if the reaction front has moved 50 m away from the calc-silicate, the carbon isotope front is expected to have travelled 24 m and the oxygen isotope front just 6 cm, assuming fluid-rock equilibrium is generally attained. In this case the sampling is insufficiently detailed to attempt to identify an oxygen front, but the next section investigates the carbon isotope systematics and attempts to identify a carbon isotope front.

6.5 CARBON ISOTOPE STUDY AT NULIYAM

6.5.1 Introduction

The location of an isotope front with respect to the reaction front is predicted by the kinetic continuum isotope theory (KCIT) (Baumgartner and Rumble III, 1988) and provides an important constraint on the fluid flux rate. The propagation rate of an isotope front is inversely proportional to the abundance of that element in the rock (Bickle and McKenzie, 1987), so a carbon front should propagate faster through the gneiss than an oxygen front. Bickle and Baker (1990) discuss the possible configurations of reaction and isotope fronts for different rock and fluid characteristics.

At Nuliyam the carbon isotopic composition of both the graphite and inclusion-bound CO_2 has been analysed for each sample (Table 6.4 and Figure 6.13). This was intended to provide two estimates of the position of the isotope front and an assessment of the extent of equilibrium between the two phases. It has already been argued that the fluid is moving too fast to be in local equilibrium with the mineral phases, but isotopic exchange maybe significantly more rapid than whole rock re-equilibration as no mineral dissolution and nucleation is involved. Isotopic exchange is however controlled by solid state diffusion within graphite grains so path A (Table 6.1) rates apply. Hence the graphite isotopic front is expected to be diffuse, but the fluid inclusion-CO_2 which involves no such exchange and advective flow may produce a sharp isotope front.

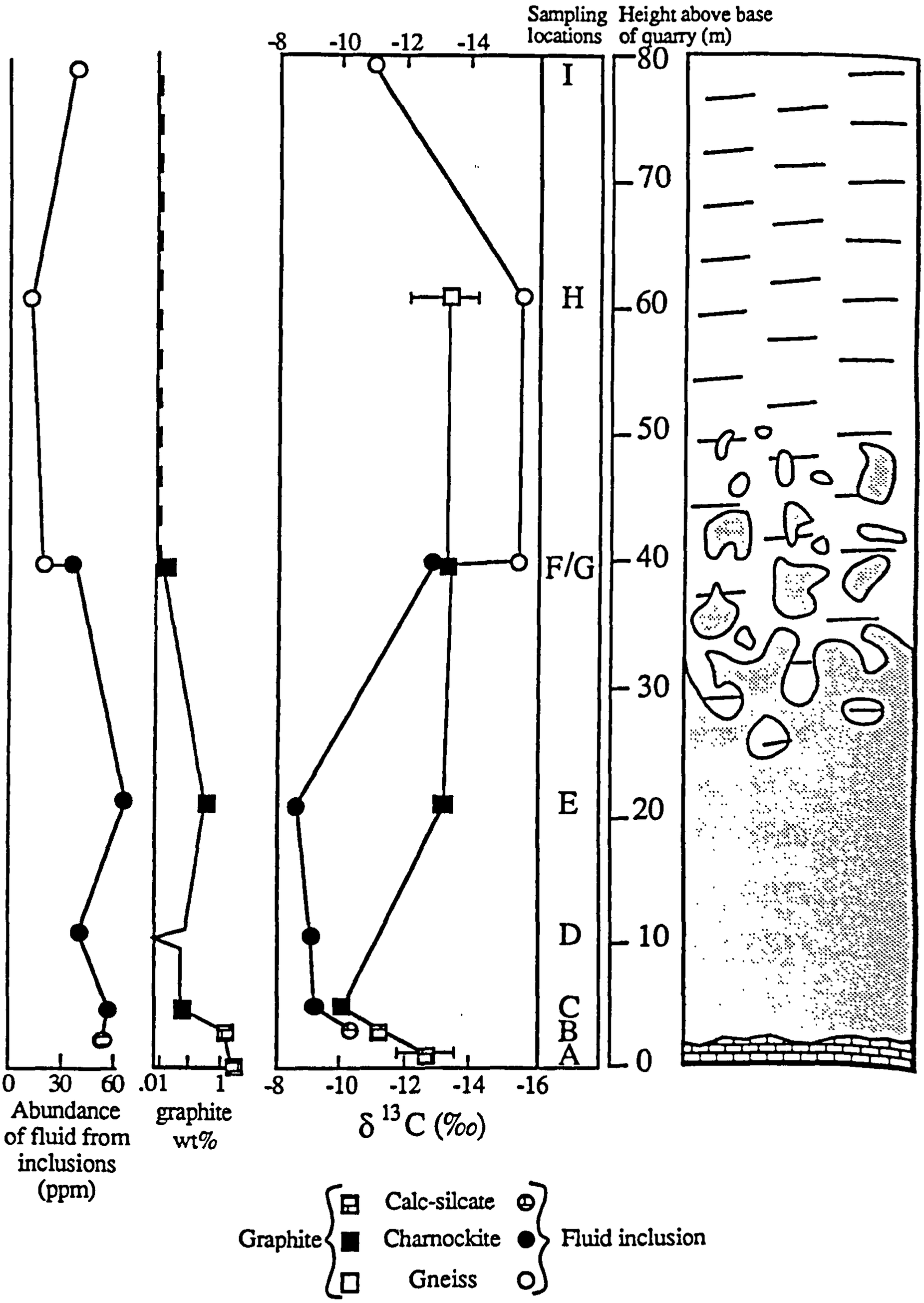

Figure 6.13. The variation of the carbon isotopic composition and carbon abundance of graphite and fluid inclusion-CO_2 from the section exposed at Nuliyam.

Sample	$\delta^{13}C$ calcite	$\delta^{13}C$ graphite	$\delta^{13}C$ inclusion-CO_2	Average $\Delta_{gr\text{-}cc}$	Average $\Delta_{gr\text{-}CO_2}$[3]	Abundance calcite[2]	Abundance graphite[2]	Abundance CO_2
TR27A	-10.2‰ -9.9‰	-13.5‰ -11.7‰ -12.0‰[1]	-	3.3‰ 1.8‰	-	4.5% 4.2%	1.2%	-
TR27B	-7.2‰ -7.9‰	-11.1‰ -11.3‰ -13.5‰[1]	-10.4‰	3.9‰ 3.4‰	0.8‰	1.6% 1.7%	1.0%	42ppm
TR27C	-	-9.9‰ -10.1‰ -12.3‰[1]	-9.2‰	-	0.8‰	-	0.09%	53ppm
TR27D	-	-	-9.5‰	-	-	-	-	51ppm
TR27E	-	-13.1‰ -13.6‰ -15.5‰[1]	-8.3‰	-	5.0‰	-	0.15%	75ppm
TR27F	-	-12.9‰ -12.9‰	-13.3‰	-	0.4‰	-	0.05%	50ppm
TR27G	-	-	-15.9‰	-	-	-	-	23ppm
TR27H	-	-14.3‰[4] -12.1‰[4]	-16.3‰	-	-3.1‰	-	-	24ppm
TR27I	-	-	-10.6‰	-	-	-	-	47ppm

Table 6.4. Carbon isotope and abundance data for carbonate, graphite and inclusion-CO_2 from Nuliyam. Notes: [1] Graphite isotopic compositions taken from stepped heating abundance determination experiments (see Figure 6.13). [2] Graphite and calcite abundances given in weight per cent. [3] $\Delta_{gr\text{-}CO_2}$ taken as the average of graphite values. [4] Yield from graphite combustion below 95%, so these results may be unreliable.

Initially the isotopic compositions of the carbon-bearing phases in the calc-silicate will be discussed to assess its plausibility as the sole fluid source. A carbon budget calculation is presented to ascertain the thickness of calc-silicate required to release sufficient CO_2 to cause charnockite formation in the overlying gneiss. Finally a qualitative model which has more general applicability is developed to explain the carbon isotopic results obtained from Nuliyam.

6.5.2 Calc-silicate horizon

The KKB has been shown to be a large metasedimentary terrain and is thought to be deposited in a shallow marine environment (Chacko *et al.* 1987). The calc-silicate is probably derived from an impure dolomitic limestone. As such the isotopic composition of the carbonate on deposition is expected to be $\delta^{13}C = 0 \pm 2‰$. There is nothing to suggest that the $\delta^{13}C$ value recorded in the carbonate phases (see Table 6.4) is due to an unusual depositional environment, but is more likely to be a post-diagenetic

effect.

Evidence of decarbonation reactions have already been documented from thin section observation (**6.2**). When CO_2 and calcite are in isotopic equilibrium the carbon in the CO_2 is about 2‰ heavier (at 700°C) (Bottinga, 1969), consequently during a decarbonation reaction the remaining calcite will equilibrate to lighter values of $\delta^{13}C$. If during decarbonation the CO_2 remains in contact with the carbonate then the isotopic composition of the carbonate will follow a batch fractionation path. Alternatively, if the CO_2 is constantly removed it will obey a Rayleigh distillation law. Valley (1986) outlines the principle behind these two processes and demonstrates that both carbon and oxygen isotopic compositions change with gradual decarbonation (Figure 6.14 illustrates these processes).

The carbonate from samples TR27A and B and a carbonatite box (after Valley, 1986) are also plotted on Figure 6.14. Samples TR27A and B plot between the normal Rayleigh decarbonation trend and the carbonatite box. Although the carbonate may have had an unusual initial oxygen isotopic composition, its $\delta^{18}O$ value is probably derived from mixing with an isotopically distinct source. A mantle-derived fluid is possible, but it is more probable that isotopic exchange occurred with local silicate minerals (initial $\delta^{18}O \sim +10‰$).

In order to produce the isotopically light carbon remaining in the calc-silicate it would be necessary to volatilise more than 95% of the carbonate by a Rayleigh process. About 5% carbonate remains in the sample (Table 6.4) so such a process cannot be ruled out but mixing with an isotopically light source is the prefered mechanism. The source of light carbon may either be an externally derived CO_2 fluid of mantle origin or organic matter already present within the rock (now as graphite). Again although the external fluid cannot be dismissed, 1-2% graphite (Table 6.4) is present and this option is prefered. Isotopic equilibration between co-existing graphite and carbonate has been

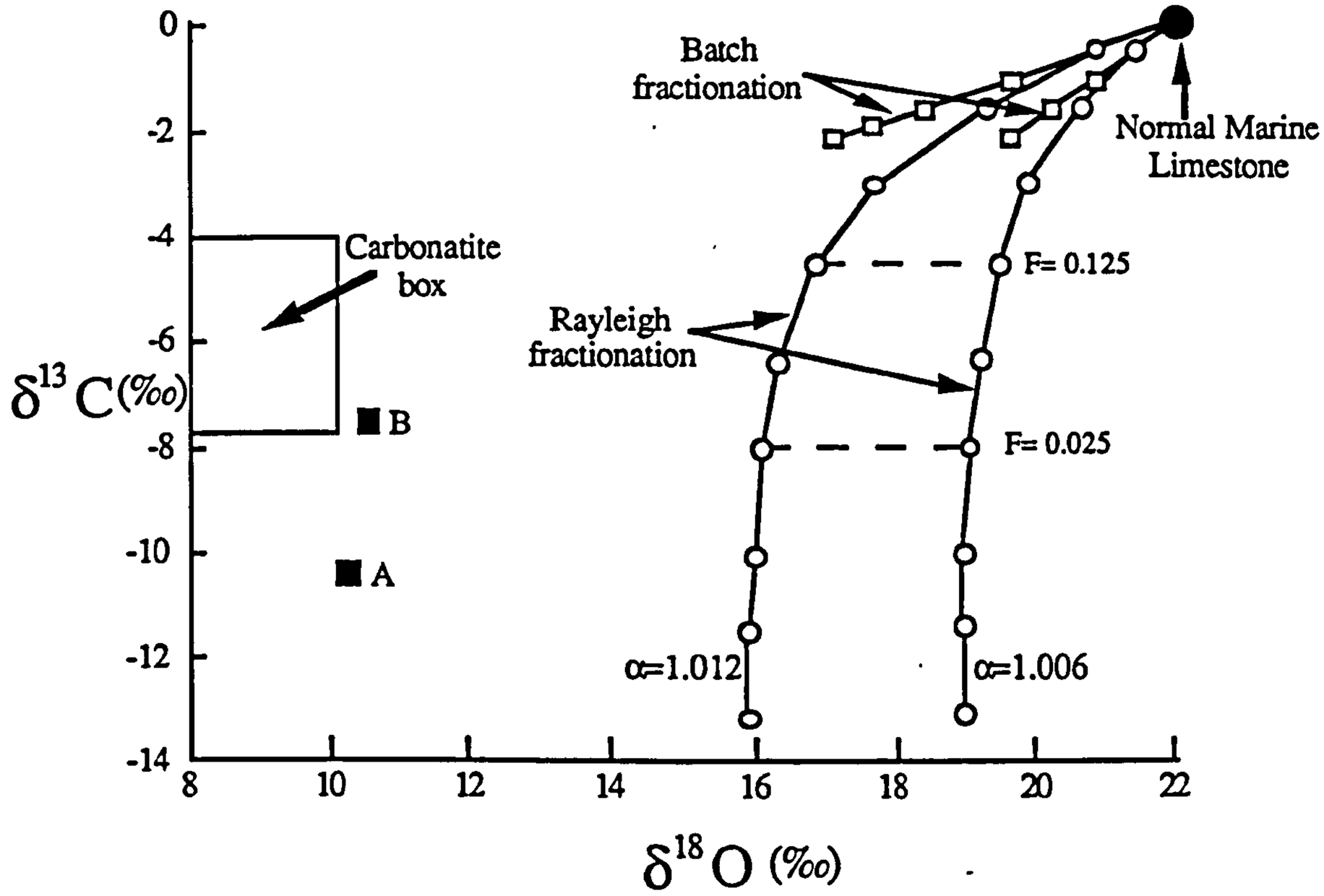

Figure 6.14. Carbon and oxygen isotopic composition of the remaining carbonate changes during decarbonation of a marine limestone of initial composition $\delta^{13}C = 0‰$ and $\delta^{18}O = +20‰$ by both Rayleigh and batch processes. The fractionation curves were calculated using $\delta_f - \delta_i = 1000(F^{(\alpha-1)}-1)$ and $\delta_f = \delta_i-(1-F)1000\ln\alpha$ respectively. Where $_i$ and $_f$ refer to the final and initial values, F is the fraction of the element remaining and α is the fractionation factor in this case between calcite and CO_2 at 700°C; α values for carbon (1.002) and oxygen (1.006 and 1.012) have been used (modified after Valley, 1986).

discussed in **5.4.2.** In **6.6.4** a carbon isotope budget calculation is presented to determine the thickness of calc-silicate which, when decarbonated, will provide sufficient CO_2 to cause the observed charnockite formation in the overlying gneiss.

The isotopic composition of both calcite and graphite have been measured in the calc-silicate and the $\Delta_{cc\text{-}gr}$ determined as $3.3 \pm 1.5‰$ (Table 6.4). Valley and O'Neil (1984) have reviewed the variation of $\Delta_{cc\text{-}gr}$ with temperature from both theoretical calculations and measured samples. They conclude that theoretical estimates of $\Delta_{cc\text{-}gr}$ give a larger fractionation than that observed in natural samples, and they base a thermometer on natural samples. Based on this calibration the measured $\Delta_{cc\text{-}gr}$ for the calc-silicate at Nuliyam gives a temperature estimate of 720°C ± 50°C which is within the range estimated using Fe-Mg exchange thermometers.

6.5.3 Carbon in the gneiss and charnockite

Field observations suggest that although graphite exists in the gneiss it only occurs as small and disperate flakes. There appears to be an increase in graphite abundance across the reaction front, with most patches of incipient charnockite containing coarse graphite flakes. Lamb and Valley (1984) have shown that if the oxidation state of the rock is below the graphite stability curve then an influx of a CO_2-rich fluid would cause graphite precipitation. Consequently it is important to ascertain whether the graphite in the rock is precipitated at the time of charnockite formation or is recrystallised organic matter already present in the rock. A stepped combustion method for quantifying graphite abundance was developed and used on whole rock powders (see Chapter 4 for experimental details).

Carbon released between 300°C and 500°C is derived from sample contamination, that released between 600°C and 700°C is from carbonate breakdown and that given off from 900°C to 1200°C is collected as the graphite combustion fraction (5.2.4). Figure 6.15 shows the stepwise plots obtained; samples TR27C, E and F show clearly distinct contamination and graphite release peaks, with no carbonate release. Surprisingly TR27A didn't show a clear carbonate release, but in sample TR27B a substantial carbonate yield (0.25%) is recorded at 600°C with $\delta^{13}C = -9‰$ (1-2‰ lighter than the estimate obtained by acid extraction). This peak is distinct from the graphite release at 900°C and a large release at 1200°C. This latter release is similar to that obtained during stepped heating of quartz separates from the same sample (5.2.4). The isotopic composition of the graphite released by this method is consistently 1-2‰ heavier than that obtained by bulk analysis of single flakes (Table 6.4). The reason for this discrepancy is unclear, but sample contamination during powdering cannot be ruled out. Due to its malleable properties graphite is likely to be lost during sample preparation, so results are minimum estimates of the graphite content of the rock (Figure 6.13). In general the data obtained using this technique are consistent, so it can

be assumed that the yields and estimates of graphite abundance although minimums are reliable. The average isotopic composition of the graphite can be taken from these plots and they are listed in Table 6.4 for comparison with composition obtained from individual flakes.

No graphite was detected in samples TR27D and I under the microscope or microprobe which may be a reflection of original sedimentary conditions. This implies that graphite absent strata were laid down under relatively oxidising conditions in comparison with the rest of the gneiss which formed under more reducing conditions. The high oxidation state puts this band of rock above the QFM buffer preventing graphite formation either during diagenesis or by precipitation from CO_2-rich fluids (Lamb and Valley, 1984). This original sedimentary difference has been masked in the field by the charnockitic recrystallisation, but is still defined by the mineralogy. Its existence confirms that solid-state diffusion cannot be effective on a large scale and that the fluid flow was insufficient to overcome the internal oxidation buffering capacity of the rock. A similar preservation of original sedimentary oxidation state has been documented in the Scottish Dalradian (Chinner, 1960).

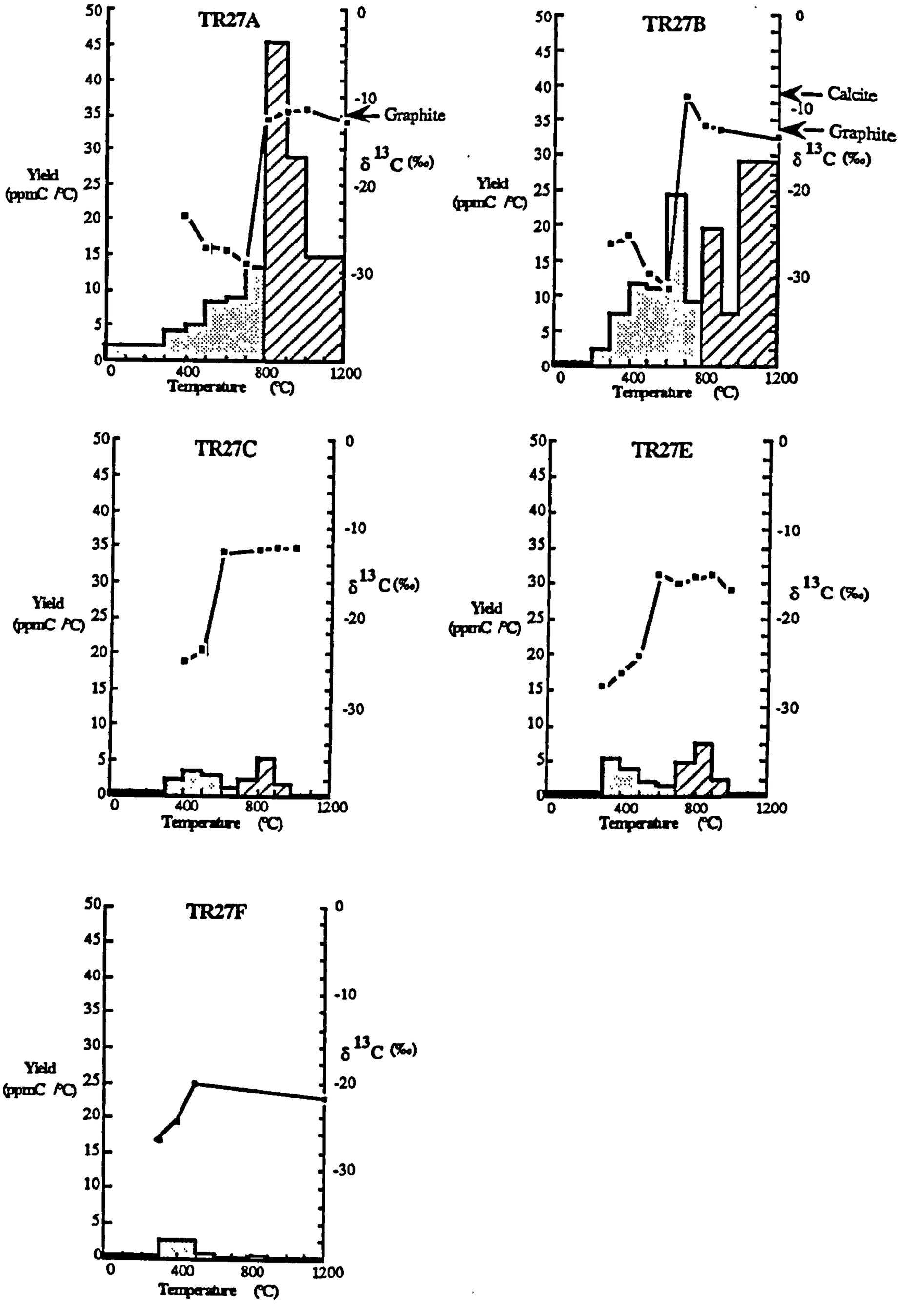

Figure 6.15. Stepwise plots obtained for powdered samples of TR27A, B, C, E and F, used to determine the abundance of graphite in each sample. The part used as the graphite release is hatched. The results are given in Table 6.4.

Apart from these samples there are two major discontinuities in the graphite abundance profile (Figure 6.13); one at the boundary between the calc-silcate and charnockite and the other at the gneiss-charnockite reaction front. Although the first of these is lithologically controlled, the second, which appears to follow the inter-associated gneiss-incipient charnockite boundary, is reaction controlled. Figure 6.13 shows an increase in carbon as both inclusion-CO_2 and graphite across the transition from gneiss to charnockite. The green colouration of the charnockite also suggests an increase in grain margin calcite across the boundary. These increases suggest that the 'opx-in' front approximates the extent of fluid penetration (fluid-front).

At Nuliyam most of the graphite is precipitated from the CO_2-rich fluid, so little carbon is present in the untransformed gneiss. A carbon isotope front, recorded by the fluid inclusion-CO_2, is coincidental with the drop in CO_2 abundance at the gneiss-charnockite transition (Figure 6.13). These observations suggest that the gneiss-charnockite reaction boundary marks the position of maximum penetration of the fluid into the gneiss. The stepwise plots for the fluid inclusion release from all samples are illustrated on Figure 6.16. The inclusions in the gneiss samples contain isotopically lighter CO_2 and in general decrepitate at lower temperatures (500-600°C) than those in the charnockite (600-800°C). The latter show the normal release for charnockitic quartz, so it is suspected that the gneiss either contains a few early or late inclusions formed at lower temperatures.

The equilibrium fractionation between CO_2 and graphite at 700°C lies between 5‰ (Valley and O'Neil, 1984) and 8‰ (Bottinga, 1969). Isotopic equilibrium is only approached in sample TR27E (Figure 6.13). Other samples show a fractionation smaller than the equilibrium value and in the gneiss samples the graphite is isotopically heavier than the CO_2. Hence it is deduced that fluid flow was too rapid for isotopic equilibrium to be attained between CO_2 and graphite. The model developed below includes an assessment of the position of the fluid front and attempts to account for the reaction and isotopic disequilibrium assemblages.

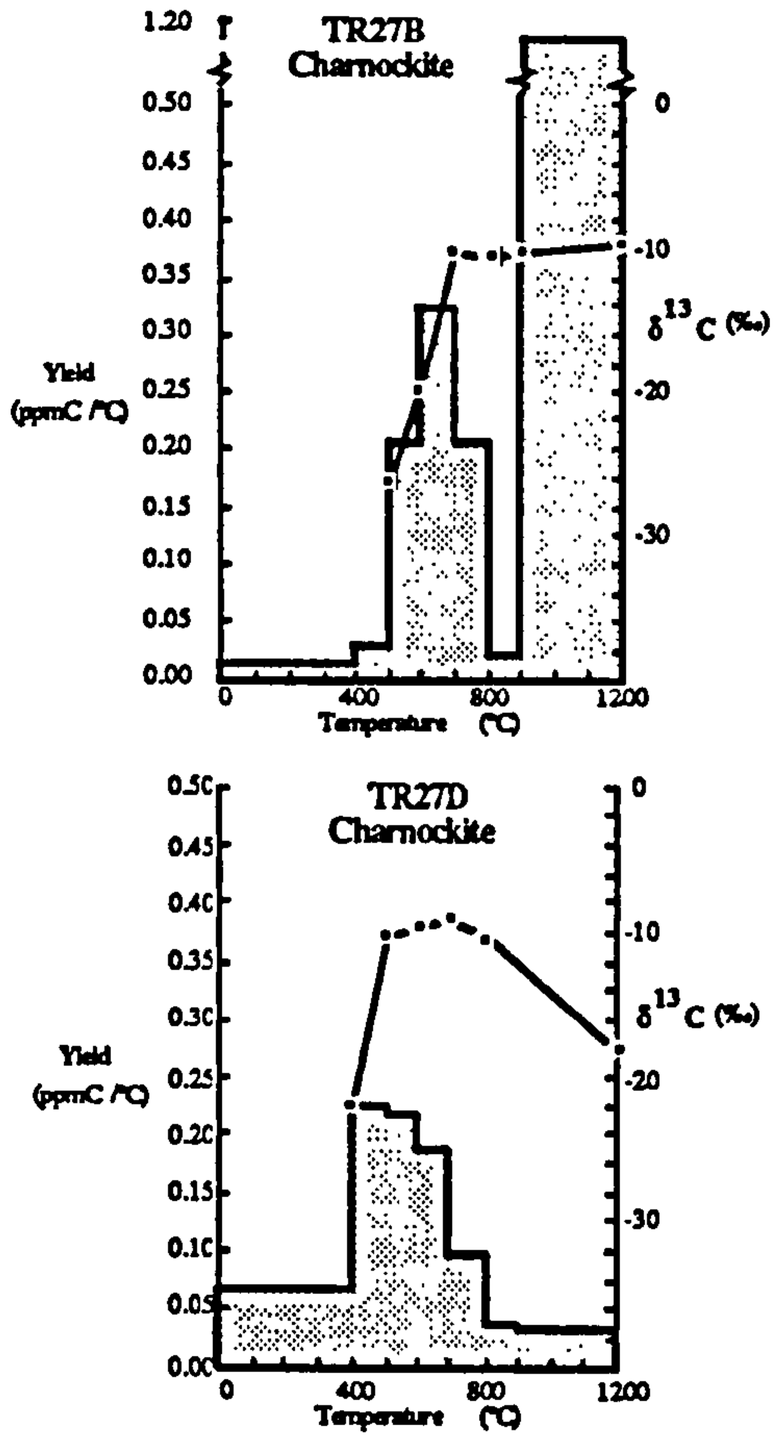

Figure 6.16. Stepwise plots of quartz separates from samples TR27B-I, used to obtain the isotopic composition and abundance of CO_2 entrapped in fluid inclusions given in Table 6.4. See text for discussion.

6.5.4 Carbon budget

In this section the abundance of carbon and isotopic budget spresent at Nuliyam are calculated to determine if the calc-silicate is a sufficient source of carbon, or whether an external source is required. Table 6.5 shows the total abundance of carbon present in the calc-silicate and charnockite and the average isotopic composition of each reservoir.

	Mass (wt%)	Abundance($molCm^{-2}$)	Average $\delta^{13}C$
Carbon in charnockite:-			
Graphite in massive charnockite (15m)	0.1%	3.75	-10‰
Graphite in incipient charnockite (15m)	0.025%	.94	-13‰
CO_2 required for gneiss-charnockite transformation	$2.2x10^{-3}$ rock vols	3.41	-9‰
Total carbon in charnockite		8.10	-9.7‰
Carbon in calc-silicate			
Graphite in calc-silicate	1%	2.50 m^{-1}	-12‰
Carbonate in calc-silicate	5%	1.5 m^{-1}	-10‰
Total carbon in calc-silicate		4.0 m^{-1}	-11.3‰

Table 6.5. Shows abundances and isotopic compositions of carbon-bearing phases for a unit cross-section perpendicular to the gneiss-calc-silicate boundary. Density of carbonate = density of gneiss = $3x10^3$ kgm^{-3}, density of the CO_2 fluid at the time of charnockite formation = $1x10^3$ kgm^{-3}.

It is assumed that no carbon is lost or gained by the system and the only carbon movement is perpendicular to the original gneiss-calc-silicate contact. The total carbon content of the charnockite is now 8.1 $molCm^{-2}$ and assuming it was initially carbon-free, all this must be derived from the calc-silicate. A pure carbonate contains 30 $molCm^{-3}$, so 27% decarbonation of a 1 m thick pure marble layer would evolve 8.1 $molCm^{-2}$. The calc-silicate is, however, assumed to be initially impure, containing both organic matter and silicates. If only 1 m of calc-silicate had been available it must have originally contained 32% carbonate (of which only 5% carbonate remains, Table 6.4). From a consideration of the isotopic budget the thickness of calc-silicate, and its initially proportion of carbonate, may be estimated.

The average isotopic composition of the carbon in the charnockite is -9.7‰. This must be the average isotopic composition of the CO_2 released by the calc-silicate. The

isotopic composition of the carbon remaining in the calc-silicate is -11.3‰, so the average isotopic composition of the carbon preserved at Nuliyam is -10.2‰. This must be the same as the initial isotopic composition of the carbon in the calc-silicate. Assuming that the graphite and carbonate in the calc-silicate have initial isotopic compositions of -25‰ and 0‰ respectively, the initial abundance of carbonate in the calc-silicate (X) can be estimated:-

$$\frac{[-25x2.5]+[0x0.3X]}{[2.5+0.3X]} = -10.2‰$$

and X = 12.1%.

This means that a calc-silicate (originally containing 1% organic matter and 12.1% carbonate) of 4 m thickness must undergo decarbonation to provide the carbon preserved at Nuliyam. Only 1.5 m of the calc-silicate unit are exposed at the quarry base, but it is not considered unreasonable for at least a further 3 m to exist unexposed.

6.5.5 Modelling carbon isotope distribution at Nuliyam

The model outlined below is a qualitative extension to the (kinetic continuum isotope theory) KCIT (Baumgartner and Rumble III, 1988) taking into account the concept of a fluid front and both fluid-rock and isotopic disequilibrium. Although developed specifically to explain the field relations and carbon isotopic compositions recorded from Nuliyam, the principals should be generally applicable to other isotope systems and reaction types. It is assumed that isotopic equilibration within each graphite flake is instantaneous. Isotopic measurements made by bulk analysis of graphite flakes will average any isotopic zoning.

Figure 6.17a is a cartoon of $\delta^{13}C$ against time showing profiles for both graphite and fluid CO_2 (preserved as inclusions) as viewed from a position in the gneiss, for instance 1 m, above the calc-silicate. The gneiss initially contains graphite and a few CO_2-rich fluid inclusions, which were formed during an earlier recrystallisation episode with carbon isotopic equilibrium between graphite and fluid ($\Delta_{CO_2\text{-}Gr}$) achieved. At the time $t = t_o$ pure CO_2 fluids being given off the calc-silicate reach this point, *ie.* the fluid front passes. This is recorded by a sharp step in the isotopic composition of inclusion-CO_2 from its initial value CO_2^i to the influx value CO_2^f.

The isotope front (defined by the increase in fluid inclusion abundance) may lag behind the fluid front due to the build up of fluid originally present of $\delta^{13}C = CO_2^i$ ahead of the infiltrating fluid, this effect will become enhanced with distance from the fluid source. The sharpness of this front depends on the relative effects of advection and diffusion or dispersion as predicted by the continuum mechanical theory. A slight tailing on this curve is shown (Figure 6.17a) which can be caused by dispersion or diffusion, but is included here mainly to add clarity to the cartoon. At $t = t_1$ the opx-in front is illustrated (Figure 6.17a). If fluid-rock equilibration is instantaneous the opx-in front will lag behind the fluid front, increasingly with distance away from the fluid source. As fluid flow is faster than rock re-equilibration less water is released (by biotite breakdown) to dilute the CO_2 and the opx-in front will not fall so far behind the fluid front. It is shown lagging slightly to account for charnockite nucleation problems. The position of the bi-out front is of little interest to this discussion.

If local isotopic equilibrium between CO_2 and graphite does not exist, the graphite's isotopic composition will respond more slowly to the influx (Figure 6.17a). The rate at which the graphite reaches isotopic equilibrium depends on the relative abundance of graphite in the rock to fluid passing through the rock and the fluid velocity. An isotope front is shown at the position where the two phases regain isotopic equilibrium. The

displacement between this and the sharp isotopic jump recorded by the fluid CO_2 gives a measure of the degree of disequilibrium.

Figure 6.17b presents a cartoon of $\delta^{13}C$ against distance from the calc-silicate, oriented identically to Figure 6.13 for easy comparison. As the fluid moves away from its source it exchanges isotopically with the light graphite and is buffered towards lighter compositions. Near to the fluid source the graphite will approach equilibrium with the influx CO_2 composition, but the fluid reaching more distant gneiss will already be isotopically light and will have little effect on the graphite composition. As the cartoon (6.18b) is plotted sharp isotopic fronts are not seen in the field for either graphite or inclusion CO_2. By varying the relative abundances of fluid and graphite and extent of disequilibrium sharp fronts may be generated. In the limiting cases of (a) complete local equilibrium, the inclusion CO_2 and graphite would have coincidental sharp fronts and (b) complete disequilibrium and/or high graphite to fluid abundance, a sharp front for CO_2 near the fluid front and no variation in graphite from its initial composition would be observed.

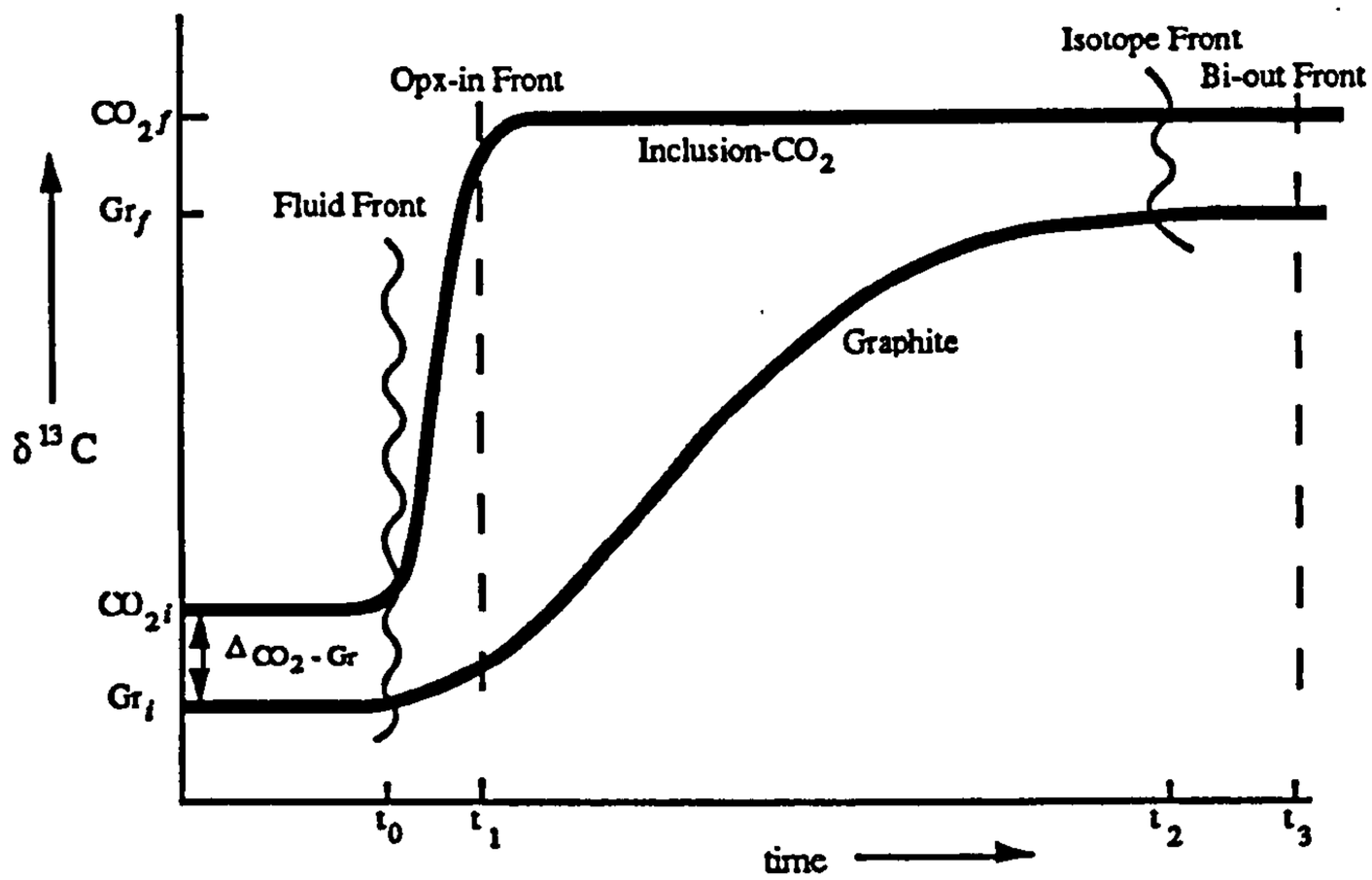

6.17a Graphite present originally

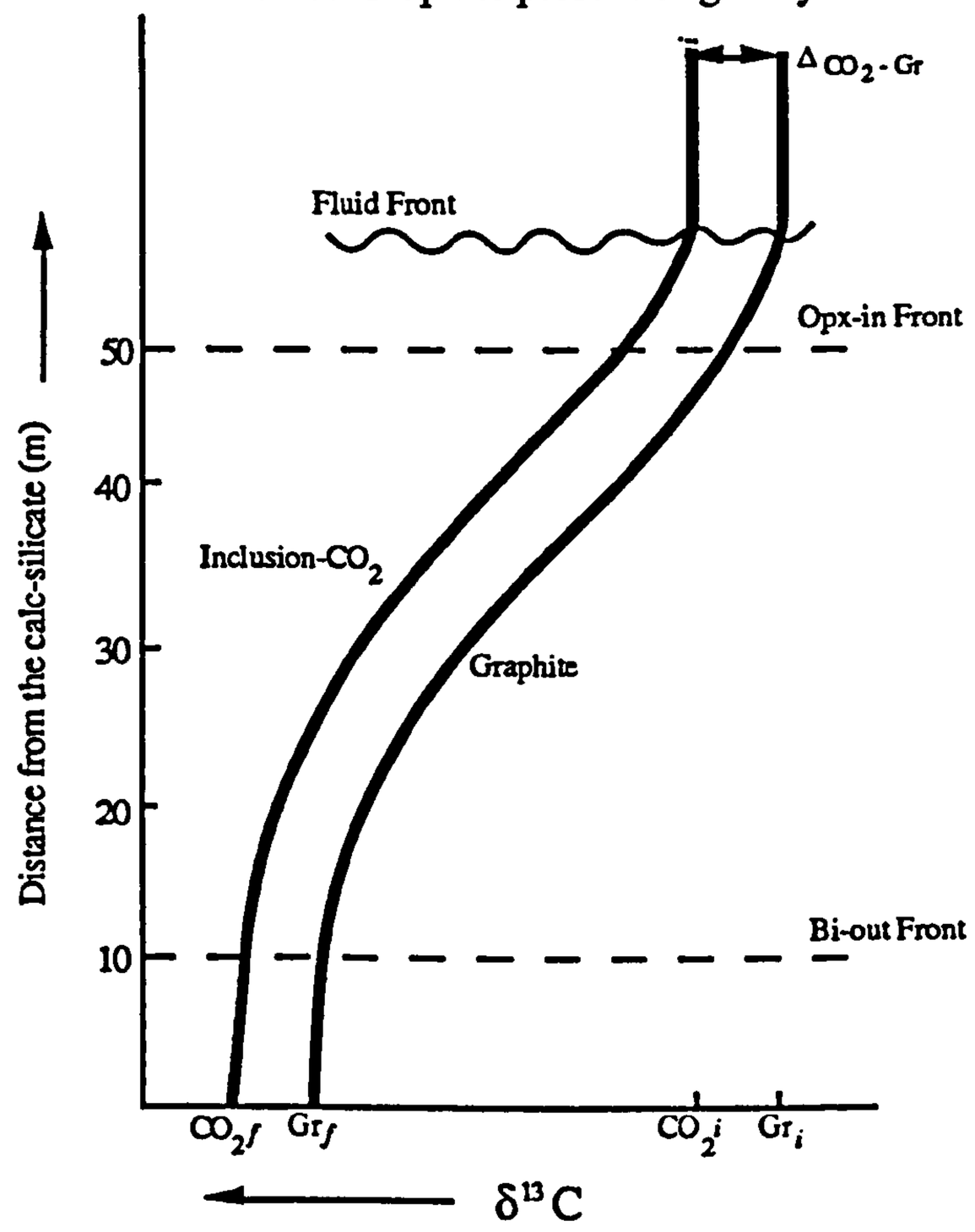

6.17b Graphite present originally

Figure 6.17. Cartoons showing predicted variations in the isotopic compositions of graphite and fluid inclusion-CO_2 during the influx event at Nuliyam. Local fluid-rock equilibrium is assumed not to be obtained. Graphite and fluid have initial compositions in the gneiss of Gr^i and CO_2^i respectively. In this, initially, simple case it is assumed that no graphite is precipitated and that the fluid is influxing with a constant isotopic composition (CO_2^f). Figure 6.17a (applicable to 6.18a and 6.19a also) is a view of the change of $\delta^{13}C$ through time from a point in the gneiss just above the boundary with the calc-silicate. Figure 6.17b (also 6.18b and 6.19b) is a plot of $\delta^{13}C$ against distance from the calc-silicate at the end of the flushing event (*ie.* as preserved in the field), and is directly comparable with the observed isotopic profiles (Figure 6.13).

Now the case where no graphite is present in the gneiss (with it all being precipitated during the fluid flow event) is considered and the situation is simplified (Figure 6.18a). The graphite is always in equilibrium with the fluid from which it is precipitated. The relations immediately behind the fluid front are the same as in the case discussed above. The abundance of fluid passing a given volume of rock controls the abundance of graphite that is precipitated.

The fluid becomes isotopically heavier away from the calc-silicate because it is continually precipitating light graphite (Figure 6.18b). This effect emphasises the isotopic front as recorded by both the graphite and CO_2 (Figure 6.18b). In this case the fluid is used up, precipitating graphite, and because the CO_2 is continually flowing away from the graphite it has just precipitated a Rayleigh fractionation curve is followed. The graphite has no option but to follow a parallel path.

The data obtained from Nuliyam suggest that graphite is being precipitated, but the isotopic composition of the influxing fluid may not be constant, consequently the graphite may find itself out of equilibrium with the fluid some time after it is precipitated. Figures 6.19a and b present the case which is thought to be most realistic for Nuliyam; all the graphite is precipitated and the isotopic composition of the influxing fluid (derived from decarbonation) changes over time. The fluid precipitates graphite in the overlying rock but as the influx fluid composition changes CO_2-graphite disequilibrium results. Now; close to the calc-silicate layer the isotopic compositions of the graphite and fluid inclusions will have less than an equilibriun value (Figure 6.19b). Where there is a small, but finite, quantity of graphite present in the original gneiss the 'hump' near the opx-in front (Figure 6.18b) caused by Rayleigh precipitation of graphite will be eliminated (Figure 6.19b). A sharp front is still expected in the inclusion-CO_2, but the isotope front described in Figure 6.17a will no longer be seen.

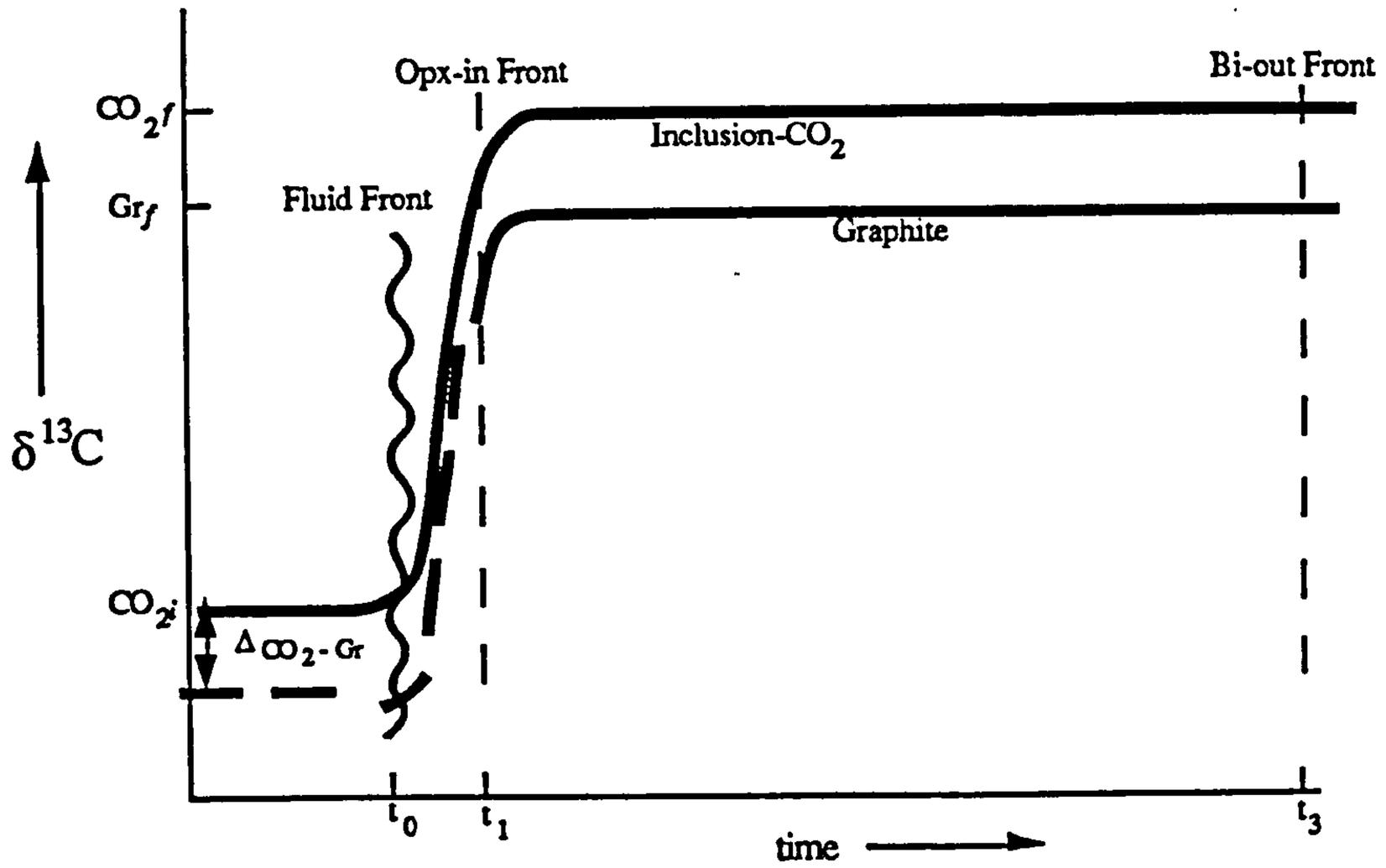

6.18a Graphite precipitated from fluid

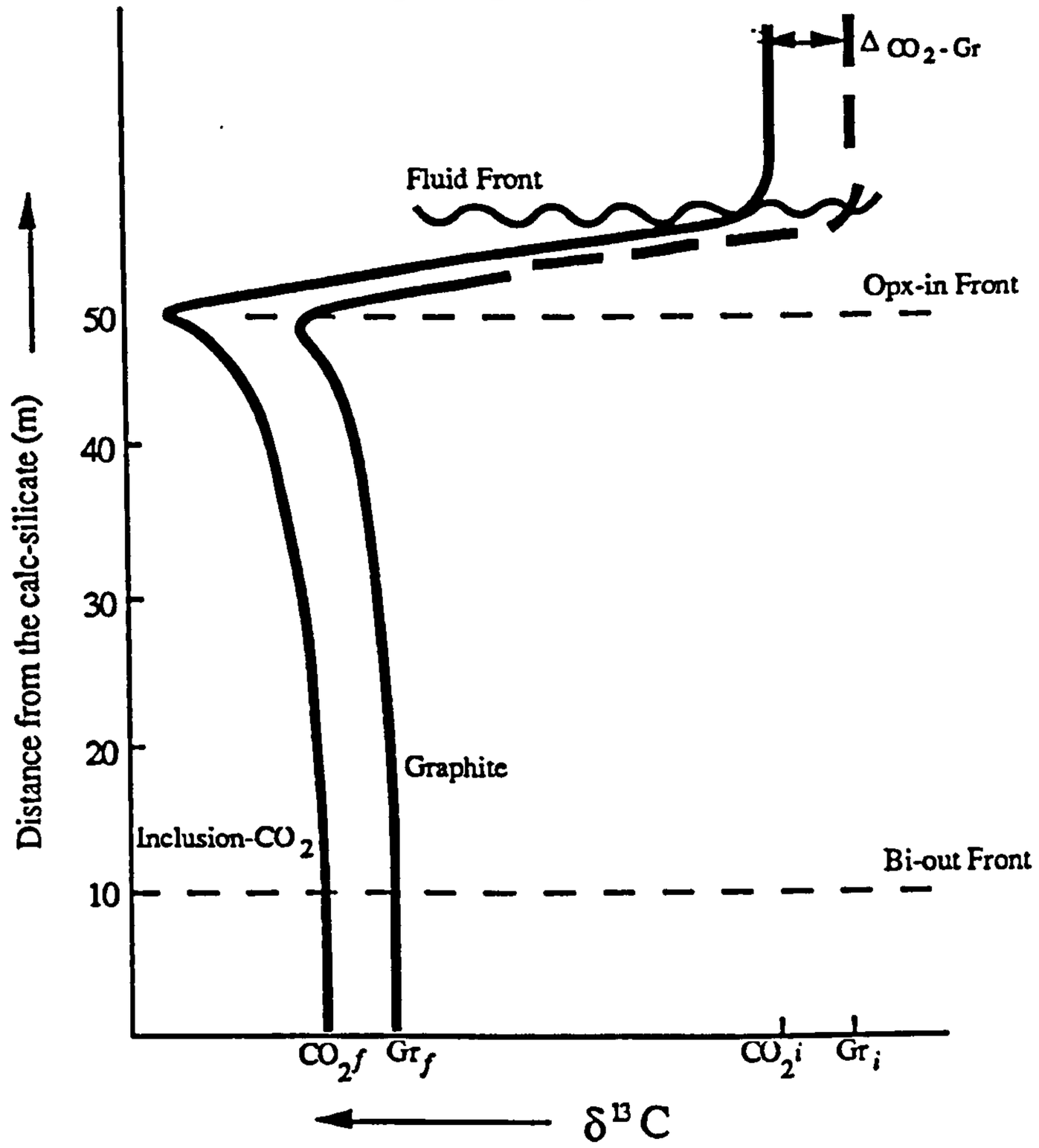

6.18b Graphite precipitated from fluid

Figure 6.18. Cartoons as described for Figure 6.17, but assuming all graphite is precipitated during CO_2-influx with none present in the original gneiss. The isotopic composition of the influxing fluid is constant at CO_2^f.

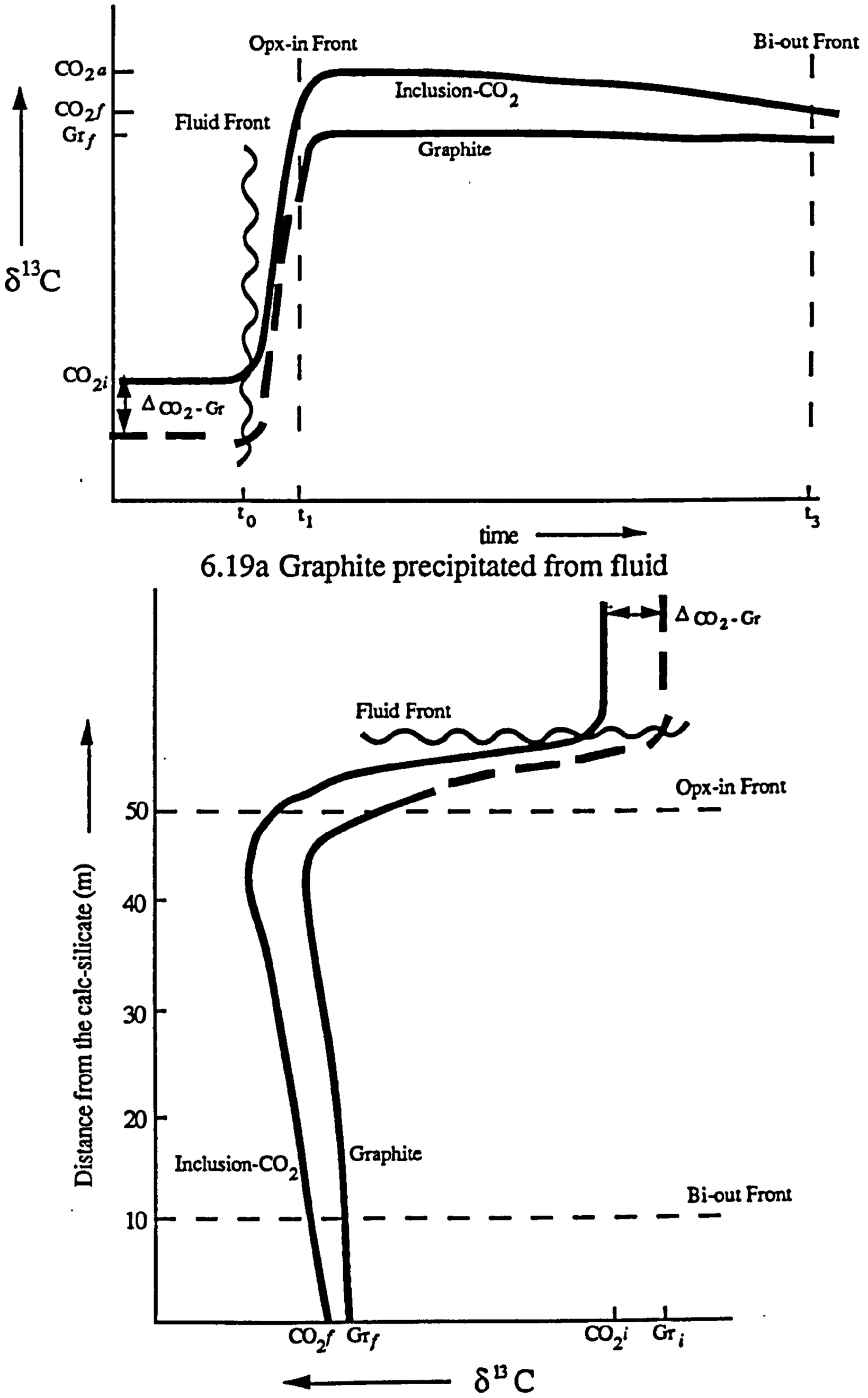

6.19a Graphite precipitated from fluid

6.19b Graphite present originally

Figure 6.19. Cartoons as described for Figure 6.17, assuming all the graphite is precipitated from the fluid, but the fluid composition changes between CO_2a (at the start of fluxing) to CO_2f (at the end), this simulates a decarbonating source. The results based on these assumptions most closely imitate those preserved at Nuliyam (Figure 6.13).

Within the Nuliyam section (Figure 6.13) the graphite at the base of the gneiss (TR27C) will be precipitated from the initial fluid flux and its final isotopic composition will tend towards later fluid compositions. In contrast the graphite in the incipient charnockite (TR27F) will only precipitate at the end of the fluxing event from the last increment of fluid, so should have a composition in equilibrium with that fluid. Although not clear cut, these general relations are picked out in Figure 6.13. In sample TR27E the fluid and graphite are close to equilibrium, suggesting that the graphite was precipitated relatively late and has not subsequently seen much change in the fluid's isotopic composition. In contrast in sample TR27C the graphite and CO_2 are out of equilibrium, with the graphite being precipitated earlier from an isotopically heavier fluid than that finally trapped in inclusions. For the reason outlined above the hump which may be expected in TR27F is not seen.

6.6 FLUID - ROCK RATIOS

Normally the area over which fluid flow has occurred is difficult to estimate so it has become conventional to calculate fluid-rock ratios rather than total fluid abundances in fluid-related studies. At Nuliyam the apparent extent of fluid flow is preserved in the field, making a more reliable estimate of absolute fluid abundance possible. Fluid-rock ratios have been used in studies of fluid-rock interaction to emphasise the abundance of fluid which has passed through a rock. The results are however generally ambiguous due to confusion over exactly what is being measured. Two main methods have been used to estimate fluid-rock ratios; one uses a phase equilibrium approach using fluid controlled mineral reactions (*eg*. Ferry, 1980 and 1986), the other is based on changes in stable isotope compositions of mineral phases or whole rocks (*eg*. Kreulen, 1988, Wickham and Taylor, 1986). Rumble *et al.* (1982) combine both methods to produce an estimate of the abundance of fluid to have interacted with the rock at the Beaver Brooke fossil locality, New Hampshire.

Although at Nuliyam the stable isotope data are not suitable for this second method, the abundance of CO_2 which has entered the gneiss can be calculated using a phase equilibrium approach (**5.6.3**). Initially it is assumed that local equilibrium was achieved between the fluid and rock, so a sharp reaction front between biotite-free charnockite and gneiss will have penetrated a certain distance from the calc-silicate. The proportion of the biotite to breakdown at any point during the tranformation depends on the abundance of fluid and its composition (X_{CO_2}) influxed to a given volume of gneiss. Assuming that pure CO_2 is infiltrating the gneiss the distance travelled by the reaction front is directly dependent on the abundance of CO_2 infiltrating the rock.

Using the method outlined in **5.6.3** and the analyses in Tables 6.2 and 6.3 the fluid-rock volume ratio can be estimated. While some biotite remains, the fluid composition is buffered at point A (Figure 6.6) where $X_{CO_2} = 0.36$, so CO_2 must have entered the rock in only (0.36/0.64) times the volume of H_2O released. The estimate obtained using this closed system model at Nuliyam gives a fluid-rock volume ratio of 0.0015 (equivalent to about 0.05 wt%). This estimate is equally valid when local equilibrium is not achieved. An identical amount of biotite will be destroyed by this volume of CO_2, it will just be spread over a larger volume of rock, so biotite-bearing charnockite remains. Using the method outlined in Harris and Bickle (1989), a fluid-rock volume ratio of 0.002 is obtained. The fact that these two methods provide similar estimates is not surprising as they are both based on the same assumptions, but to obtain meaningful estimates from either method the full extent of fluid flow must be known.

If an average value of 30 m of gneiss at Nuliyam is transformed to biotite-free charnockite, with a fluid-rock volume ratio of 0.0015, then 4.5 cc (measured at formation conditions) of pure CO_2 must enter the gneiss per unit cross-sectional area. All this fluid must have passed through the basal centimeter of gneiss, giving it a fluid-rock volume ratio of 4.5. Most fluid-rock ratio estimates using either the stable isotopic or phase equilibria approaches will record this type of estimate, rather than the more

realistic total fluid abundance calculated above. Consequently a fluid-rock ratio estimating the volume of fluid to have passed a particular point has very little meaning unless the regional extent of fluid flow can be inferred. The implication is that fluid abundance estimates may be distorted to high values masking an estimate of true fluid abundance.

6.7 CONCLUSIONS

1) Fluid flow is an advective process occurring by microhydraulic fracture. The fluid may still be treated as continuous because the size of the fluid-filled cracks produced is very small in comparison with the mineral grain size.

2) The reaction front is not sharp (as predicted by advection fluid flow theory) which is due to two effects:

a) The divariant nature of the reaction; Fe-biotite reacts more rapidly than Mg-biotite.

b) Local grain scale equilibrium is not achieved because the kinetics of the reaction are slow compared to fluid flow.

The second of these is believed to be the major cause of front broadening due to the thermodynamic similarity between Fe and Mg ions. This kinetic control on the front profile is in agreement with that predicted by Lasaga (1989) for this type of reaction.

3) The porosity induced in the charnockite during the fluid flux event is calculated to be 0.2%.

4) Carbon isotopic budget calculations suggest that sufficient CO_2 is released by decarbonation of 50% of the carbonate from about 4 m of calc-silicate (initially 10% carbonate) to account for all the carbon which has entered the gneiss. Nonetheless interaction with an externally derived fluid infiltrating along the gneiss - calc-silicate boundary cannot be dismissed.

5) The concept of a fluid front is introduced as the furthest extent to which the fluid has penetrated.

6) A sharp carbon isotope front is observed for inclusion-CO_2, but not for graphite, also because local fluid-solid equilibrium is not attained.

7) The carbon isotopic profile in both inclusion-CO_2 and graphite is qualitatively modelled and a broad agreement with the measured field data is obtained. Closer-spaced sampling is required to constrain the geometry of the reaction and the isotopic fronts.

Chapter 7

SUMMARY

7.1 STEPPED HEATING

Stepped heating techniques are in routine use for extracting carbon from a variety of materials, notably basalt glasses and mantle diopsides (Mattey *et al.* 1989). In this study these techniques have been successfully adapted to extraction of CO_2 from fluid inclusions in mineral grains from granulites and associated rocks. This technique represents a significant advance in the analysis of fluid inclusions since virtually all inclusion fluids are released allowing reliable yield measurements (compared to crushing which gives variable and low yields). It also overcomes the major disadvantage of contamination by CO_2 released from sources other than inclusions. The experimental method outlined here has the added advantage that gas released from small samples (100 mg of host mineral) can be accurately measured, which allows for much tighter sample control and hence more reliable results. For instance if sample TR10A (illustrated in Figure 5.1) had been measured using a single step heating procedure the yield of gas would have been identical, but the isotopic composition of the gas collected would be about - 8.8‰, in contrast to the result obtained for the peak release by stepped heating - 7.1‰. The discrepancy results from mixing with isotopically light contamination. This sample gave a relatively sharp peak with little low or high temperature release, a similar comparison for other samples would show a more marked agreement.

One of the major conclusions which can be drawn from the stepped heating experiments is that the temperature range at which the inclusions were trapped broadly controls the temperature at which they will decrepitate. Stepped heating can successfully distinguish the major fluid inclusion release (500°C to 800°C) from

contamination (≤ 400°C), from late stage fluid inclusions (400 to 500°C) and from graphite oxidation (900°C to 1200°C). A stepped heating technique has also been applied to the determination of the abundance of graphite in small samples of powdered rock.

7.2 THE SOURCE OF CO_2

The isotopic composition of the CO_2 trapped in inclusions can help to constrain its source. In southern India geochronological studies have shown that at least two periods of charnockite formation have occurred. The first of these is associated with regional granulite facies metamorphism along the southern margin of the Northern block at about 2500 Ma. This event resulted in the massive charnockites of the Nilgiris and Madras blocks as well as incipient charnockite formations in the granulite/amphibolite transition zone. The isotopic composition of the CO_2 from these charnockites is variable, between - 4‰ and - 13‰, with no spatial or lithological control. Although a large area is covered by relatively few measuements, it is concluded that these variations are geologically significant and in the absence of calc-silicate and graphite-bearing metasediments, they are interpreted as indicative of a deep-seated, but heterogeneous, source of the CO_2. Available isotopic data from deep-seated sources suggest that isotopic heterogeneity is most likely to be found above a subduction zone. In such a setting CO_2 is released from both organic and carbonate sediments during subduction. The range of isotopic compostions preserved in these charnockites results from the relative proportion of such sediments and perhaps the depth of release of CO_2.

The terrains to the south of the Palghat-Cauvery shear zone were metamorphosed in at least one younger event at about 500 Ma, although an earlier amphibolite/granulite metamorphism may have occurred. Detailed isotopic analysis of locations in the Kerala Khondalite Belt and from selected areas in the Tamil Nadu block argue for an influx of

CO_2 during uplift following the peak of metamorphism from a source characterised by $\delta^{13}C$ of -6‰ to -8‰. This is typical of sub-continental mantle. The association of uplift with within-plate syenites and charnockites suggests that charnockite formation and CO_2 influx occurred during attenuation of continental lithosphere.

The composition of these fluids has locally been modified by isotopically light organic matter in the metasediments to values between - 9‰ and - 13‰. The isotopic data are able to refute the suggestion that in these areas CO_2 was generated by oxidation of the graphite. An isotopically heavy (external) source is required, although in localities with calc-silicate localities they may provide a sufficient source of CO_2. Nevertheless the isotopically light CO_2 preserved in some gneisses and intercalated massive charnockites (type b) may have formed during an earlier part of the metamorphic cycle (or a previous event), being partly or wholly dervied from metasedimentary sources of carbon.

7.3 MECHANISM OF FLUID FLOW AND FLUID - ROCK INTERACTION

A carbon isotope and theoretical study of a charnockite-gneiss-calc-silicate locality (Nuliyam) allowed constraints to be placed on fluid flow and fluid-rock interaction. CO_2 fluid flow within these charnockites is an advective process, but in the absence of deformation enhanced pathways, the failure of CO_2-rich fluids to form a continuous grain boundary phase implies that fluid propagation must occur by microhydraulic fracture. Nevertheless the fluid may still be treated as a pervasive phase because the size of the fluid-filled cracks produced is very small in comparison with the mineral grain size.

The field relations and carbon isotope systematics do not conform to predictions, of sharp reaction and isotopic fronts that propagate outwards from the fluid source, made by advection fluid flow theory. Both reaction and isotopic fronts are diffuse over at

least half the total fluid penetration distance (50 m). In the case of the propagation of the charnockite-forming reaction this may be due to the divariant nature of the reaction (Fe-biotite reacts more rapidly than Mg-biotite). The same hypothesis cannot be applied to the isotopic distribution, which is probably caused by the lack of local fluid-rock equilibrium. It is reasonable to assume that this lack of equilibrium also causes the diffuse nature of the gneiss-charnockite reaction front. This kinetic control on the front profile is in accordance with that predicted theoretically for this type of reaction (Lasaga. 1989).

The porosity induced in the charnockite during the fluid flux event is calculated to be 0.2%, which is equivalent to the abundance of fluid which has been influxed. assuming that fluid has been retained between the source and fluid front. Fluid-rock ratio calculations have been discussed and shown to give meaningful results only when the entire distance of fluid penetration is preserved in the field.

Carbon isotopic budget calculations suggest that sufficient CO_2 is released by decarbonation of 50% of the carbonate from about 4 m of calc-silicate (initially 10% carbonate) to account for all the carbon which has entered the gneiss in this locality. Nonetheless an externally derived fluid infiltrating along the gneiss-calc-silicate boundary cannot be dismissed as a potential fluid source.

The carbon isotopic profiles for both inclusion-CO_2 and graphite can qualitatively modelled with a broad agreement with the measured field data, assuming fluid-rock isotopic disequilibrium and precipitation of most of the graphite from the fluid. One major conclusion of this study is that future stable isotope studies that identify fluid-rock interaction must allow for fluid/rock disequilibrium. This precipitation of graphite from a CO_2-rich fluid infiltrating rocks with f_{O_2} below the QMF buffer confirm the theoretical considerations of Lamb and Valley (1984).

7.4 CHARNOCKITE FORMATION IN SOUTHERN INDIA

The data presented in this thesis show that all incipient charnockites contain significantly more CO_2 than the precursor gneiss. Similarly high abundances are also recorded in massive charnockites, suggesting that CO_2 is integral to the formation of all types of charnockite. Nevertheless field evidence argues that a number of different mechanisms are responsible for charnockite production.

7.4.1 Incipient charnockite at the orthopyroxene isograd

The pressure-temperature conditions recorded at the orthopyroxene isograd are between those of the vapour-absent and water-present melting curves. Clearly if a water-rich pore fluid had been present the gneisses would have under gone partial melting. Hence it is assumed they were vapour-absent prior to an influx of both water and CO_2 in variable proportions, related to the formation of massive charnockites at deeper levels.

Influx of water will cause migmatisation of the gneisses, whereas influx of CO_2 will cause subsolidus dehydration. Depending of the ambient temperature conditions, melting at the fluid-present invariant point (FAMIPOF) may occur and a charnockitic magma may be produced. Field evidence for all these processes can be found at Kabbaldurga from the pervasive migmatisation of the gneisses, from the sub-solidus transformation of gneiss to charnockite, with preservation of gneissic foliation and from the veins of intrusive charnockite and granite. The different morphologies of migmatisation and sub-solidus charnockite formation result from water forming a pervasive grain boundary fluid, but CO_2 only flowing along zone of deformation enhanced permeability. The isochemical nature of the subsolidus transformation argues for a predominantly closed system. In more heavily charnockitised patches where gneissic foliation is obliterated the geochemistry of charnockite has a minimum melt

composition indicating an igneous origin. Although this is attributed to FAMIPOF melting, invasion of a granitic melt by CO_2 is an alternative mechanism. The low temperature retrogression of orthopyroxene suggests that all water is not lost from the system, but retained as inclusions which rupture during uplift.

7.4.2 Incipient charnockite south of the Palghat-Cauvery shear zone

The incipient charnockite formation from south of the P-C shear zone involves biotite rather than hornblende breakdown, but the clearest distinction between these charnockites and those found at the orthopyroxene isograd (7.4.1) is the absence of migmatisation in this younger event. The reason for this difference is not clear, but is probably related to the precursor rocks. In the Northern block charnockite formation is the culmination of a metamorphic sequence, all apparently related to the same event, hence the pecursor rocks were initially of a low grade and hence fertile and relatively rich in water (present in hornblende and biotite). To the south the precursor rocks are interbanded gneisses and charnockites, the charnockites already in the granulte facies and the gneisses exhibiting considerable partial melting in some areas. This suggests that the precursor rocks were already relatively dry, so little water was released during charnockite formation and no associated migmatisation occurred.

In the Kerala Khondalite Belt different types of incipient charnockite formation have been documented:

(1) Charnockite formation around calc-silicate lithologies.

(2) Charnockite formation around pegmatites and cracks.

(3) Patchy charnockite formation in graphite-bearing gneiss, with evidence for melting.

(4) Patchy charnockite formation in graphite-bearing gneiss, with no evidence for melting.

(5) Charnockite associated with cordierite formation.

(6) Charnockite formation in zones of enhanced permeability in the absence of graphite.

Type (1) charnockite is a result of CO_2 influx into a gneiss which was initially vapour-absent or contained a water-rich pore fluid, the subsolidus dehydration reaction proceeds and charnockite is formed. No melting may be expected in such occurrences because the continual influx of pure CO_2 causes complete biotite destruction at very low water activities. Coarse recrystallisation, graphite precipitation and complete destruction of biotite accompany this type of charnockite formation (see Chapter 6 for an isotope and fluid-rock interaction study from this type of locality at Nuliyam).

Type (2) charnockite was described by Ravindra Kumar and Chacko (1986) as resulting from a decompression reaction, but margins of intrusives (*eg.* Kalanjur) (Plate 3.15) are not obviously zones of decompression. This model also fails to explain some vital features, such as the increase in CO_2 content in charnockite (Figure 5.12b), enrichment in LILE (Ravindra Kumar and Chacko, 1986) and most importantly the observation that an influx of water-rich fluids causes an identical reverse reaction (Plate 3.15). A simple change in pore fluid composition explains all these observations. A crack provides an easy path for CO_2 fluids which cause a reduction in the water activity and the subsolidus dehydration reaction. Similarly granitic or pegmatitic intrusions bring with them dissolved H_2O and may 'carry' CO_2 as an associated vapour. The CO_2 is 'released' initially which causes charnockite formation and subsequent crystallisation of the magma releases water which rehydrates some of the charnockite.

For type (3) and (4) charnockite formations Srikantappa *et al.* (1985) suggested 'pore fluid release', Ravindra Kumar and Chacko (1986) prefered CO_2-influx and Hansen *et al.* (1987) opted for internal pore fluid modification by graphite oxidation, although all authors failed to distinguish between them. In Chapter 2 the 'pore fluid release' model was shown to be invalid, nevertheless the clear structural control on this charnockite formation (Plate 3.13) requires explanation. The isochemical nature of the

transformation argues against any melt mobility if melting occurred. Garnet is commonly destroyed during the reaction, implying a decompressive regime.

Type (3) charnockite formation occurs in localities where there is no evidence for an earlier migmatisation episode (Kottavatom and Manali). Small scale element mobility in these localities is suggested by the presence of bleached areas surrounding the charnockite patches which completely obliterate gneissic structure (Plate 3.17). In these situations although subsolidus reaction cannot be ruled out, the evidence is more compatible with a FAMIPOF melting reaction, induced by CO_2 influx, and subsequent recrystallisation without melt loss.

Type (4) charnockite formation shows evidence of a sub-solidus transformation with ghost foliation preserved, and charnockite formation in zones of deformationally enhanced fluid flow (Ponmudi). In both these types the transformation appears to be isochemical which is compatible with subsolidus transformation or melting and no melt migration.

Type (5) charnockite formation is associated with cordierite replacement of garnet along the Achan Kovil shear zone. The symplectite intergrowth of cordierite and hypersthene surrounding garnet is clearly indicative of a decompression reaction, in fluid present conditions such a reaction could produce charnockite, during rapid uplift on the Achan Kovil lineament. Although abundant CO_2-rich inclusions are reported from these charnockites (Santosh, 1987) it is not clear whether these are coincidental, being present in the precursor lithologies or introduced during charnockite formation.

In graphite-free locations that are heavily migmatised by an earlier event (*eg.* Kadamakad) subsequent charnockite formation (type (6)) either follows the unmelted portions or cuts across the leucosome pods in shear zones (Plate 3.12). Fluid inclusion studies (Hansen *et al.* 1987) suggest the precursor is fluid-absent whilst the charnockite

has a limited number of CO_2-rich inclusions. For such charnockites subsolidus dehydration caused by influx of CO_2-rich fluids and decompression reactions accelerated by the presence of fluid cause charnockite formation in the unmelted and coarse melt patches respectively.

7.4.3 Massive charnockites

Three types of massive charnockites have been differentiated on the basis of their outcrop patterns, they may nevertheless all form by the same mechanism. Two possible mechanisms were suggested: (a) they are igneous bodies crystallising directly from water-deficient CO_2-rich magmas (b) they form by a regional extension of the incipient charnockite processes described above.

Clear evidence for an igneous origin of type (c) massive charnockites exists, but such localities appear to be of very limited extent. The 'gneissic' foliation and geochemical depletions of type (a) charnockites argue against an igneous origin. Nevertheless protolith and metamorphic ages are generally indistinguishable, and although biotite-free massive charnockites may be the result of extensive flushing by pure CO_2, it is difficult to produce biotite-bearing massive charnockites, which record conditions above the FAMIPOF melting temperature without crystallising directly from a water deficient, CO_2-rich magma.

O'Nions and Oxburgh (1988) have argued that insufficient CO_2 is released from the mantle to cause crustal scale, sub-solidus dehydration. By crystallising massive charnockites directly from magmas the volumes of CO_2 required may be considerably reduced. Wickham (1988) proposed that intrusion of a basic sill would cause widespread melting in the overlying crust and any carbonate bodies would not melt, but sink through into the basic magma and devolatilise. Such a mechanism would release CO_2 into the basic sill and overlying granitic melt, causing it to crystallise as a

charnockite. The $\delta^{13}C$ data available suggests that this is not a likely source for the CO_2, unless it is mixed with organic carbon, also present in the melt. Although the data are unable to prove it the author prefers an igneous origin for all massive charnockites.

7.5 CONCLUDING STATEMENT

Although a number of different mechanisms for charnockite formation have been identified on a local scale, they all have CO_2 (generally from an external source) as a common factor. Carbon isotopes are capable of constraining the source under favourable circumstances. This is the case with the younger event in southern India during which the CO_2 has very strong affinities with a sub-continental lithospheric source. The earlier event is less well constrained, although a mantle source is one possibility. In general charnockite formation is closely related to availability of CO_2, whether it is locally derived on a small scale (*eg*. Nuliyam) or on a regional scale (the southern margin of the Northern Block).

One interesting problem is why charnockites are so abundant in India, whereas, although they are common in many granulite terrains, they are normally only a minor constituent. It may suggest that there is something unusual about the lower crust or continental lithosphere below southern India, that has caused it to be enriched in carbon. This, combined with the existence of large areas of acidic crust of suitable composition for charnockite production may have caused two or more charnockite forming events in this area over 2000 Ma of earth history.

References

Allen, P., Condie, K.C. and Narayana, B.L. (1985) The geochemistry of prograde and retrograde charnockite-gneiss reactions in southern India. *Geochim. Cosmochim. Acta.* **49** 323-336.

Annamalai, (1987) Geology and geochemistry of the rock formation around Andipatti, Madurai, Tamil Nadu. *Unpublished PhD Thesis (Anna University, Madras).*

Ashwal, L.D. (1978) Petrogenesis of Massif-type Anorthosites: Crystallisation history and liquid line of descent of the Adirondack and Morin complexes. *Unpublished PhD Thesis (Princeton University).*

Baker, A.J. and Fallick, A.E. (1988) Evidence for CO_2 infiltration in granulite facies marbles from Lofoten-Vesteralen, Norway. *Earth Planet. Sci. Letts.* **91** 132-140.

Barker, C. and Sommer, M.A. (1973) Mass spectrometric analysis of the volatiles released by heating or crushing rocks. *A.S.T.M. Publication STP* **539** 56-70.

Barker, C. and Torkleson, B.E. (1974) Gas absorption on crushed quartz and basalt. *Geochim. Cosmochim. Acta.* **39** 212-218.

Battachayra, A. and Sen, S.K. (1986) Granulite metamorphism, fluid buffering and dehydration melting in the Madras charnockites and metapelites. *J. Petrol.* **27** 1119-1141.

Baumgartner, L.P. and Rumble III, D. (1988) Transport of stable isotopes-I: Development of a kinetic continuum theory for stable isotope transport. *Contrib. Mineral. Petrol.* **98** 417-430.

Baur, N., Kroner, A. and Todt, W. (1987) Prograde and retrograde metamorphic reactions in high-grade gneisses of Sri Lanka: structural control and U-Pb zircon data. *Terra Cognita* **7** 133-134.

Becker, R.H. and Clayton, R.N. (1975) Nitrogen abundances and isotopic compositions in lunar samples. *Proc. Lunar Sci. Conf.* **6th** 2131-2149.

Beckinsale, R.D., Reeves-Smith, G., Gale, N.H., Holt, R.W. and Thompson, B. (1982) Rb-Sr and Pb-Pb whole rock isochron ages and REE data for Archæan gneisses and granulites, Karnataka State, South India. *Indo-U.S. Workshop on Precambrians of South India, NGRI, Hyderabad. Abstracts vol.* 35-36.

Beere, W. (1975) A unifying theory of the stability of penetrating liquid phases and sintering pores. *Acta Metall.* **23** 131-138.

Bernard-Griffiths, J., Jahn, B-M. and Sen, S.K. (1987) Sm-Nd isotopes and REE geochemistry of Madras granulites: an introductory statement. *Precamb. Res.* **37** 343-355.

Bhaskar Rao, Y.J., Beck, W., Rama Murthy, V., Nirmal Charan, S. and Naqvi, S.M. (1983) Geology, geochemistry and age of metamorphism of the Archæan grey gneisses around Channarayanapatna, Hassan District, Karnataka, South India. *Geol. Soc. India Mem.* **4** 115-125.

Bickle, M.J. and Baker, J. (1990) Infiltration, reaction progress, stable isotope transport and fractionation in meta-carbonate rocks. *Geochim. Cosmochim. Acta.* **in press.**

Bickle, M.J. and McKenzie, D.P. (1987) The transport of heat and matter by fluids during metamorphism. *Contrib. Mineral. Petrol.* **95** 384-392.

Blattner, P. (1976) Replacement of hornblende by garnet in granulite-facies assemblages near Milford Sound, New Zealand. *Contrib. Mineral. Petrol.* **55** 181-190.

Bodnar, R.J., Binns, P.R. and Hall, D.L. (1989) Synthetic fluid inclusions-VI. Quantitative evaluation of the decrepitation behaviour of fluid inclusions in quartz at one atmosphere confining pressure. *J. Metamorphic Geol.* **7** 229-242.

Bohlen, S.R. (1987) Pressure-Temperature-Time paths and a tectonic model for the evolution of granulites. *J. Geol.* **95** 617-632.

Bohlen, S.R., Boettcher, A.L., Wall, V.J. and Clemens, J.D. (1983) Stability of phlogopite-quartz and sanadine-quartz: A model for melting in the lower crust. *Contrib. Mineral. Petrol.* **83** 270-277.

Bottinga, Y. (1969) Calculated fractionation factors for carbon and hydrogen isotope exchange in the system calcite-carbon dioxide-graphite-methane-hydrogen-water vapour. *Geochim. Cosmochim. Acta.* **3** 49-64.

Bowen, N.L. and Tuttle, O.F. (1950) The system $NaAlSi_3O_8$-H_2O. *J.Geol.* **58** 489-511.

Boyd, S.R. (1988) A study of carbon and nitrogen isotopes in the earth's mantle. *Unpublished Thesis (Open Unversity).*

Brenan, J.M. and Watson, E.B. (1987b) Transport of CO_2 in polycrystalline olivine at elevated P-T conditions. *EOS* **68** 466.

Brophy, J.G. and Marsh, B.D. (1986) On the origin of high alumina arc basalt and the mechanics of melt extraction. *J. Petrol.* **27** 763-789.

Brown, G.C. and Fyfe, W.S. (1970) The production of granite melts during ultrametamorphism. *Contrib. Mineral. Petrol.* **28** 310-318.

Buhl, D. (1987) U-Pb und Rb-Sr altersbestimmungen und untersuchungen zum strontiumisotopenaustausch an granuliten sudindiens. *Unpublished PhD Thesis (University of Munster, FRG).*

Buhl, D., Grauert, B. and Raith, M. (1983) U-Pb zircon dating of Archæan rocks from the South India craton: results from the amphibolite to granulite facies transition zone at Kabbal quarry, southern Karnataka. *Fortschr. Mineral.* **61** 43-45.

Burton, K.W. and O'Nions, R.K. (1988) Isotope systematics and chronology of granulite genesis in Sri Lanka. *Chem. Geol.* **70** 5.

Chacko, T. (1987) Petrologic, geochemical and isotopic studies in the charnockite-khondalite terrain of southern Kerala, India: The deposition and granulite-facies metamorphism of a Precambrian sedimentary sequence. *Unpublished PhD Thesis (University of North Carolina, Chapel Hill).*

Chacko, T., Ravindra Kumar, G.R. and Newton, R.C. (1987) Metamorphic P-T conditions of the Kerala (South India) khondalite belt. A granulite facies terrain. *J. Geol.* **95** 343-358.

Chacko, T., Ravindra Kumar, G.R. and Peterson, J.W. (1988) Water activities in the Kerala Khondalite Belt. *J. Geol. Soc. India* **31** 16-18.

Chang, S., Lawless, J., Romiez, M., Kaplan, I.R., Petrowski, C., Sakai, H. and Smith, J.W. (1974) Carbon, nitrogen and sulphur in lunar fines 15012 and 15013: abundances, distribution and isotopic compositions. *Geochim. Cosmochim. Acta.* **38** 853-872.

Chayes, F. (1955) Potash feldspar as a by-product of the biotite-chlorite transformation. *Journal of Geology* **63** 75-84.

Chinner, G.C. (1960) Oxidised and reduced gneisses, Glen Clova. *J. Petrol.* **1** 178-217.

Clark, S.P. and Ringwood, A.E. (1964) Density distribution and constitution of the mantle. *Rev. Geophys. Space Phys.* **2** 35-88.

Clemens, J.D. (1984) Water contents of intermediate to silicic magmas. *Lithos* **17** 273-287.

Clemens, J.D. and Vielzeuf, D. (1987) Constraints on melting and magma production in the crust. *Earth Planet. Sci. Letts.* **86** 287-306.

Clemens, J.D. and Wall, V.J. (1981) Crystallisation and origin of some peraluminous (S-type) granitic magmas. *Can. Mineral.* **19** 111-132.

Cole, D.R. and Ohmoto, H. (1986) Kinetics of isotope exchange at elevated temperatures and pressures. *in Stable isotopes in high temperature geological processes. (eds. Valley, J.W., Taylor, H.P. and O'Neil, J.R.) Rev. Mineral.* **16** 41-87.

Compton, P.R. (1960) Charnockitic rocks of the Santa Lucia Range, California. *Am. J. Sci.* **258** 609-639.

Condie, K.C. and Allen, P. (1984) Origin of Archæan charnockites from southern India. In *Archæan Geochemistry, The Origin and Evolution of the Archæan Continental Crust (ed. Kroner, A., Goodwin, A.M. and Hanson, G.N.)* 182-203.

Condie, K.C., Allen, P. and Narayana, B.L. (1982) Geochemistry of the Archæan low- to high-grade transition zone, southern India. *Contrib. Mineral. Petrol.* **81** 157-167.

Coolen, J.J.M. (1981) Carbonic fluid inclusions in granulites from Tanzania - a comparison of geobarometric methods based on fluid density and mineral chemistry. *Chem. Geol.* **37** 59-77.

Cooray, P.G. (1969) Charnockites as metamorphic rocks. *Am. J. Sci.* **267** 969-982.

Crawford, A.R. (1969) Reconnaissance Rb-Sr dating of the Precambrian rocks of southern Peninsular India. *J. Geol. Soc. India* **10** 117-166.

Crawford, A.R. and Compston, W. (1973) The age of the Cuddapah and Kurnool systems, southern India. *J. Geol. Soc. India* **19** 453-464.

Crawford, M.L. and Hollister, L.S. (1986) Metamorphic fluids: The evidence from fluid inclusions. *in Fluid-rock interactions during metamorphism. (eds Walther, J.V. and Wood, B.J.)* 1-35.

Deans, T. and Powell, J.L. (1968) Trace elements and strontium isotopes in carbonatites, fluorites and limestones from India and Pakistan. *Nature* **218** 750-752.

Deines, P., Gurney, J.J. and Harris, J.W. (1986) On the existence of ^{13}C depleted carbon in the mantle, evidence from diamond studies. *4th Inter. Kimberlite Conference, Extended abstracts, Geol. Soc. Austral.* **16** 383-385.

Des Marais, D.J. (1986) Carbon abundance measurements in oceanic basalts: the need for concensus. *Earth Planet. Sci. Letts.* **79** 21-26.

Drury, S. A., Harris, N.B.W., Holt, R.W., Reeves-Smith, G.J. and Wightman, R.T. (1984) Precambrian tectonics and crustal evolution in South India. *J. Geol.* **92** 3-20.

Drury, S.A. and Holt, R.W. (1980) The tectonic framework of the south Indian craton: a reconnaissance involving LANDSAT imagery. *Tectonophysics* **65** T1-T15.

Eskola, P. (1920) The mineral facies of rocks. *Nor. Geol. Tidsskr.* **6** 143-158.

Ferry, J.M. (1980) A case study of the amount and distribution of heat and fluid during metamorphism. *Contrib. Mineral. Petrol.* **71** 373-385.

Ferry, J.M. (1986) Reaction progress: a monitor of fluid-rock interactions during metamorphic and hydrothermal events. *in Fluid-rock interactions during metamorphism. (eds. Walther, J.V. and Wood, B.J.)* 60-88.

Forbes, W.C. and Flowers, M.F.J. (1974) Phase relations of titan-phlogopite, $K_2Mg_4TiAl_2Si_6O_{20}(OH)_4$: a refractory phase in the upper mantle? *Earth Planet. Sci. Letts.* **22** 60-66.

Friend, C.R.L. (1981) Charnockite and granite formation and influx of CO_2 at Kabbaldurga. *Nature* **294** 550-552.

Friend, C.R.L. (1983) The link between charnockite formation and granite production: evidence from Kabbaldurga, Karnataka, South India. In *Migmatites, Melting and Metamorphism (eds. Atherton, M.P. and Gribble, C.D.)* 264-276.

Frost, B.R. and Frost, C.D. (1987) CO_2, melts and granulite metamorphism. *Nature* **327** 503-506.

Frost, B.R., Frost, C.D. and Touret, J.L.R. (1989) Magmas as a source of heat and fluids in granulite facies metamorphism. *in NATO ASI vol. C281 (ed. Bridgewater, D.)* 19-28.

Frost, B.R., Fyfe, W.S., Tazaki, K. and Chan, T. (1989) Grain-boundary graphite in rocks and implications for high electrical conductivity in the lower crust. *Nature* **340** 134-136.

Frost, R.B. and Chacko, T. (1989) The granulite uncertainty principle: limitations on thermobarometry in granulites. *J. Geol.* **97** 435-450.

Fyfe, W.S. (1973) The granulite facies, partial melting and the Archæan crust. *Phil. Trans. R. Soc.* **A273** 457-461.

Ganguly, J. and Saxena, S. (1984) Mixing properties of aluminosilicate garnets: constraints from natural and experimental data, and applications to geothermobarometry. *Am. Mineral.* **69** 88-97.

Ganor, J., Matthews, A. and Paldor, N. (1989) Constraints on effective diffusivity during oxygen isotope exchange at a marble-schist contact, Sifnos (Cyclades), Greece. *Earth Planet. Sci. Letts.* **94** 208-216.

Glassley, W.E. (1983) The contribution of carbonates to deep crustal CO_2: evidence from metasomatic reaction zones. *Contrib. Mineral. Petrol.* **84** 15-24.

Grady, M.M. (1987) Acid-dissolution of carbonates: an outline of the technique used at the Open University. *P.S.U. Internal Report (3).*

Grant, J.A. (1981) Orthoamphibole and orthopyroxene relations in high-grade metamorphism of pelitic rocks. *Am. Jour. Sci.* **281** 1127-1143.

Grant, J.A. (1986) Quartz-phlogopite-liquid equilibria and origins of charnockite. *Am. Mineral.* **71** 1071-1075.

Grew, E.S. and Manton, W.J. (1984) Age of allanite from Kabbaldurga quarry, Karnataka. *J. Geol. Soc. India* **25** 193-195.

Hansen, E.C., Hickman, M.H., Grant, N.K. and Newton, R.C. (1985) Pan-African age of "Peninsular Gneiss" near Madurai, S. India. *EOS* **66** 419-420.

Hansen, E.C., Hunt, W., Jacob, S.C., Morden, K., Reddi, R. and Tacy, P. (1988) Evidence for CO_2-rich fluids in rocks from the "type" charnockite area near Pallavaram, Tamil Nadu. *J. Geol. Soc. India* **31** 37-39.

Hansen, E.C., Janardhan, A.S., Newton, R.C., Prame, W.H.B.N. and Ravindra Kumar, G. R. (1987) Arrested charnockite formation in southern India and Sri Lanka. *Contrib. Mineral. Petrol.* **96** 225-244.

Hansen, E.C., Newton, R.C. and Janardhan, A.S. (1984) Pressures, temperatures and metamorphic fluids across an unbroken amphibolite facies to granulite facies transition in southern Karnataka, India. In *Archæan Geochemistry, The Origin and Evolution of the Archæan Continental Crust (ed. Kroner, A., Goodwin, A.M. and Hanson, G.N.)* 161-181.

Harley, S.L. (1989) The origins of granulites: a metamorphic perspective. *Geol. Mag.* **126** 215-247.

Harris, N.B.W. and Bickle, M.J. (1989) Advective fluid transport during charnockite formation; an example from southern India. *Earth Planet. Sci. Letts.* **93** 151-156.

Harris, N.B.W., Holt, R.W. and Drury, S.A. (1982) Geobarometry, geothermometry and late Archæan geotherms from the granulite facies terrain of South India. *J. Geol.* **90** 509-528.

Harris, N.B.W. and Jayaram, S. (1982) Metamorphism of cordierite gneisses from the Bangalore region of the Indian Archæan. *Lithos* **15** 89-97.

Heier, K.S. (1960) Petrology and geochemistry of high-grade metamorphic and igneous rocks on Langoy, northern Norway. *Norges Geol. Undersok* **207** 7-246.

Hodges, K.V. and Spear, F.S. (1982) Geothermometry, geobarometry and the Al_2SiO_5 triple point at Mt. Moosilauke, New Hampshire. *Am. Mineral.* **67** 1118-1134.

Hoefs, J. and Touret, J. (1975) Fluid inclusion and carbon isotope study from Bamble granulites (S. Norway). *Contrib. Mineral. Petrol.* **52** 165-174.

Hoefs, J., Coolen, J.J.M. and Touret, J. (1981) The sulfur and carbon isotope composition of scapolite-rich granulites from Southern Tanzania. *Contrib. Mineral. Petrol.* **78** 332-336.

Holland, T.H. (1900) The charnockite series, a group of Archæan hypersthenic rocks in peninsular India. *Geol. Surv. India Mem.* **28 (Pt 2)** 192-249.

Holland, T.J.B. and Powell, R. (1985) An internally consistent thermodynamic dataset with uncertainties and correlations, 2. Data and results. *J. Metamorphic Geol.* **3** 343-370.

Hollister, L.A. and Burruss, R.C. (1976) Phase equilibria in fluid inclusions from the Khada Lake complex. *Geochim. Cosmochim. Acta.* **40** 163-175.

Hollister, L.S. (1988) On the origin of CO_2-rich fluid inclusions in migmatites. *J. Metamorphic Geol.* **6** 467-474.

Holloway, J.R. (1977) Fugacity and activity of molecular species in supercritical fluids. *in Thermodynamics in Geology (ed. Fraser, D.G.)* 161-182.

Holloway, J.R. and Ford, C.E. (1975) Fluid-absent melting of the fluoro-hydroxy amphibole paragasite to 35 kilobars. *Earth Planet. Sci. Letts.* **25** 44-48.

Holt, R.W. and Wightman, R.T. (1983) The role of fluids in the development of a granulite facies transition zone in South India. *J. Geol. Soc. London* **140** 651-656.

Howie, R.A. (1955) The geochemistry of the charnockite series of Madras, India. *Trans. R. Soc. Edinburgh* **62** 725-768.

Howie, R.A. (1967) Charnockites and their colour. *J. Geol. Soc. India* **8** 1-7.

Hubbard, F.H. (1978) Geochemistry of the Varberg granite gneisses. *Geol. For. Stock. Forh.* **100** 31-38.

Jackson, D.H., Mattey, D.P. and Harris, N.B.W. (1988a) Carbon isotope compositions of fluid inclusions in charnockites from southern India *Nature* **333** 167-170.

Jackson, D.H., Mattey, D.P., Santosh, M. and Harris, N.B.W. (1988b) Carbon stable isotope analysis of fluid inclusions by stepped heating *Memoirs of the Geological Survey of India* **11** 149-158.

Janardhan, A.S., Newton, R.C. and Hansen, E.C. (1982) The transformation of amphibolite facies gneiss to charnockite in southern Karnataka and northern Tamil Nadu, India. *Contrib. Mineral. Petrol.* **79** 130-149.

Janardhan, A.S., Newton, R.C. and Smith, J.C. (1979) Ancient crustal metamorphism at low P_{H_2O}: charnockite formation from Kabbaldurga, South India. *Nature* **278** 511-514.

Jansen, J.B.H. and Schuiling, R.D. (1976) Metamorphism on Naxos: petrology and geothermal gradients. *Am. J. Sci.* **276** 1225-1253.

Jansen, J.B.H., Van der Rijst, H., Rye, R.O., Andriessen, P.A.M. and Rye, D.M. (1989) High integrated fluid-rock ratios during metamorphism at Naxos: evidence from carbon isotopes of calcite in schists and fluid inclusions. (A discussion of the paper by Kreulen (1988) (Contrib. Mineral. Petrol. 98: 28-32)). *Contrib. Mineral. Petrol.* **103** 123-126.

Javoy, M., Pineau, F. and Delorme, H. (1986) Carbon and nitrogen isotopes in the mantle *Chem. Geol.* **57** 41-62.

Jiang, J., Clayton, R.N. and Newton, R.C. (1988) Fluids in granulite facies metamorphism: a comparative oxygen isotope study on the South India and Adirondack high-grade terrains. *J. Geol.* **96** 517-533.

Keppler, H. (1989) The influence of the fluid phase composition on the solidus temperatures in the haplogranite system $NaAlSi_3O_8$-$KAlSi_3O_8$-SiO_2-H_2O-CO_2. *Contrib. Mineral. Petrol.* **102** 321-327.

Kerrick, D.M. and Jacobs, G.K. (1981) A modified Redlich-Kwong equation for H_2O, CO_2 and H_2O-CO_2 mixtures at elevated pressures and temperatures. *Am. J. Sci.* **281** 735-767.

Klatt, E., Hoernes, S. and Raith, M. (1988) Characterisation of fluids involved in the gneiss-charnockite transformation in southern Kerala (India). *J. Geol. Soc. India* **31** 57-59.

Konnerup-Madsen, J. (1979) Fluid inclusions in quartz from deep-seated granitic intrusions, South Norway. *Lithos* **12** 13-23.

Kreulen, R. (1980) CO_2-rich fluids during regional metamorphism on Naxos (Greece): carbon isotopes and fluid inclusions. *Am. J. Sci.* **280** 745-771.

Kroner, A., Williams, I.S., Compston, W., Baur, N., Vitanage, P.W. and Perera, L.R.K. (1987) Zircon ion microprobe dating of high-grade rocks in Sri Lanka. *J. Geol.* **95** 775-791.

Lamb, W. and Valley, J.W. (1984) Metamorphism of reduced granulites in low-CO_2 vapour-free environments *Nature* **312** 56-58.

Lamb, W., Valley, J.W. and Brown, P.E. (1987) Post-metamorphic CO_2-rich fluid inclusions in granulites *Contrib. Mineral. Petrol.* **96** 485-495.

Lamb, W.M. (1988) CO_2-rich fluid inclusions in granulites: evidence for entrapment after the peak of metamorphism. *Memoirs of the Geological Survey of India* **11** 101-115.

Lasaga, A.C. (1989) Fluid flow and chemical reaction kinetics in metamorphic systems: a new simple model. *Earth Planet. Sci. Lett.* **94** 417-424.

Leroy, J. (1979) Contribution a l'etalonnage de la pression interne des inclusions fluides lors de leur decrepitation. *Bull. Soc. francaise Mineral. et Cristall.* **102** 584-593.

Lichtner, P.C. (1985) Continuum model for simultaneous chemical reactions and mass transport in hydrothermal systems. *Geochim. Cosmochim. Acta.* **49** 779-800.

Luth, R.W. and Boettcher, A.L. (1986) Hydrogen and the melting of silicates. *Am. Mineral.* **71** 264-276.

McCrea, W.S. (1950) On the isotopic chemistry of carbonates and a palæotemperature scale *J. Chem. Phys.* **18** 849-857.

Macrae, N.D. and Nesbitt, H.W. (1980) Partial melting of common metasedimentary rocks: a mass balance approach. *Contrib. Mineral. Petrol.* **75** 21-26.

Mattey, D.P. (1987) Carbon isotopes in the mantle. *Terra Cognita* **7** 31-37.

Mattey, D.P., Exley, R.A. and Pillinger, C.T. (1989) Isotopic composition of CO_2 and dissolved carbon species in basalt glass. *Geochim. Cosmochim. Acta.* **53** 2377-2386.

McKenzie, D.P. (1987) The compaction of igneous and sedimentary rocks. *J. Geol. Soc. London* **144** 299-307.

McKirdy, D.M. and Powell, T.G. (1974) Metamorphic alteration of carbon isotopic composition in ancient sedimentary organic matter: New evidence from Australia and South Africa. *Geology* **2** 591-595.

Morrison, J. and Valley J.W. (1988) Post-metamorphic fluid infiltration into granulites from the Adirondack mountains. *J. Geol. Soc. India* **31** 91-93.

Morrison, J. and Valley J.W. (1988) Post-granulite facies fluid infiltration in the Adirondack Mountains. *Geology* **16** 513-516.

Naney, M.T. (1983) Phase equilibria of rock-forming ferromagnesian silicates in granitic systems. *Am. J. Sci.* **283** 993-1033.

Newton, R.C. and Hansen, E.C. (1986) The South India-Sri Lanka high-grade terrain as a possible deep-crust section. in *The Nature of the Lower Continental Crust (ed. Dawson J.B.) Geol. Soc. Special Publication No. 25*. 297-307.

Newton, R.C., Smith, J.V. and Windley, B.F. (1980) Carbonic metamorphism, granulites and crustal growth. *Nature* **288** 45-50.

O'nions, R.K. and Oxburgh, E.R. (1988) Helium, volatile fluxes and the development of continental crust. *Earth Planet. Sci. Letts.* **90** 331-347.

Ormaasen, D.E. (1977) Petrology of the Hopen mangerite-charnockite intrusion, Lofoten, north Norway. *Lithos* **10** 291-310.

Perkins, D., III and Newton, R.C. (1981) Charnockite geobarometers based on coexisting garnet-pyroxene-plagioclase-quartz. *Nature* **292** 144-146.

Peterson, J.W. and Newton, R.C. (1989a) Reversed experiments on biotite-quartz-feldspar melting in the system KMASH: Implications for crustal anatexis. *J. Geol.* **97** 465-485.

Peterson, J.W. and Newton, R.C. (1989b) CO_2-enhanced melting of biotite-bearing rocks at deep-crustal pressure-temperature conditions. *Nature* **340** 378-380.

Peucat, J.J., Vidal, P., Bernard-Griffiths, J. and Condie, K.C. (1989) Sr, Nd and Pb isotopic systematics in the Archæan low- to high-grade transition zone of southern India: syn-accretion vs. post-accretion granulites. *J. Geol.* **97** 537-550.

Pichamuthu, C.S. (1953) "The charnockite problem" *Spec. Publ. Mysore Geologists' Assoc.*

Pichamuthu, C.S. (1960) Charnockite in the making. *Nature* **188** 135-136.

Pichamuthu, C.S. (1965) Regional metamorphism and charnockitisation in Mysore State, India. *Ind. Mineral.* **6** 119-126.

Pichamuthu, C.S. (1972) Job Charnock and charnockite. *J. Geol. Soc. India* **13** 86-91.

Pineau, F., Javoy, M., Behar, F. and Touret, J. (1981) La géochimie isotopique du faciès granulite du Bamble (Norvège) et l'origine des fluides carbonés dans la croûte profonde. *Bull. Minéral.* **104** 630-641.

Piperov, N.B. and Penchev, N.B. (1973) A study on gas inclusions in minerals. Analyses of the gases from micro-inclusions in allanite. *Geochim. Cosmochim. Acta.* **37** 2075-2086.

Powell, R. (1983) Processes in granulite-facies metamorphism. In *Migmatites, Melting and Metamorphism (eds. Atherton, M.P. and Gribble, C.D.)* 127-139.

Powell, R. and Holland, T.J.B. (1985) An internally consistent thermodynamic dataset with uncertainties and correlations, 1. Methods and a worked example. *J. Metamorphic Geol.* **3** 327-342.

Raase, P., Raith, M., Ackermand, D. and Lal, R.K. (1986) Progressive metamorphism of mafic rocks from greenschist to granulite facies in the Dharwar Craton of South India. *J. Geology* **94** 261-282.

Raith, M. (1988) The granulite terrane of the Nilgiri Hills (South India). *Terra Cognita* **8** 253.

Raith, M., Hoernes, S., Klatt, E. and Stahle, H.J. (1989) Contrasting mechanisms of charnockite formation in the amphibolite to granulite grade transition zones of southern India. *in NATO ASI vol. C281 (ed. Bridgewater, D.).*

Raith, M., Raase, P., Ackermand, D. and Lal, R.K. (1983) Regional geothermobarometry in the granulite facies terrane of South India. *Royal Soc. (Edinburgh) Earth Sci. Trans.* **73** 221-244.

Rama Rao, B. (1940) The Archæan complex of Mysore. *Mysore Geol. Dept. Bull.* **17** 1-101.

Ramiengar, A.S., Ramakrishnan, M. and Viswanatha, M.N. (1978) Charnockite-gneiss complex relationship in southern Karnataka. *J. Geol. Soc. India* **19** 411-419.

Ravindra Kumar, G.P., Srikantappa, C. and Hansen, E.C. (1985) Charnockite in the making at Ponmudi, Kerala, South India. *Nature* **313** 207-209.

Ravindra Kumar, G.R. and Chacko, T. (1986) Mechanisms of charnockite formation and breakdown in southern Kerala: implications for the origin of the southern Indian granulite terrain. *J. Geol. Soc. India* **28** 277-288.

Richardson, S. H., Gurney, J.J., Erlank, A.J. and Harris, J.W. (1984) Origin of diamonds in old enriched mantle. *Nature* **310** 198-202.

Roedder, E. (1984) Fluid Inclusions. *Reviews in Mineralogy 12, Mineralogical Society of America, Washigton D.C.*

Rumble III, D., Ferry, J.M., Hoering,T.C. and Boucot, A.J. (1982) Fluid flow during metamorphism at the Beaver Brook fossil locality. *Am. J. Sci.* **282** 886-919.

Rye, R.O., Schuiling, R.D., Rye, D.M. and Jansen, J.B.H. (1976) Carbon, hydrogen and oxygen isotope studies of the regional metamorphic complex at Naxos, Greece. *Geochim. Cosmochim. Acta.* **40** 1031-1049.

Sandiford, M. and Powell, R. (1986) Deep crustal metamorphism during continental extension: modern and ancient examples. *Earth Planet. Sci. Letts.* **79** 151-158.

Santosh, M. (1985) Fluid evolution characteristics and piezothermic array of south Indian charnockites. *Geology* **13** 361-363.

Santosh, M. (1986) Carbonic metamorphism of charnockites in the S.W. Indian shield. A fluid inclusion study. *Lithos* **19** 1-10.

Santosh, M. (1987) Cordierite gneisses of southern Kerala, India: petrology, fluid inclusions and implications for crustal uplift history. *Contrib. Mineral. Petrol.* **96** 343-356.

Santosh, M. and Drury, S.A. (1988) Alkali granites with Pan-African affinities from Kerala, S.India. *J. Geol.* **96** 616-626.

Schidlowski, M., Eichmann, R. and Junge, C.E. (1975) Precambrian sedimentary carbonates: carbon and oxygen isotope geochemistry and implications for the terrestrial oxygen budget. *Precamb. Res.* **2** 1-69.

Sen, S.K. (1974) A review of some geochemical characters of the type area (Pallavaram, India) charnockites. *J. Geol. Soc. India* **15** 413-420.

Sen, S.K. and Battachayra, A. (1988) Granulites of Satnuru and Madras: a study in different styles of fluid-melt interaction. *Terra Cognita* **8** 253.

Smith, C.S. (1964) Some elementary principles of polycrystalline microstructure. *Met. Rev.* **9** 1-47.

Solomon, (1963) Counting and sampling errors in modal analyses by point counter. *J. Petrol.* **4** 367-382.

Srikantappa, C., Raith, M. and Spiering, B. (1985) Progressive charnockitisation of a leptynite-khondalite suite in southern Kerala, India-evidence for formation of charnockites through decrease in fluid pressure? *J. Geol. Soc. India* **26** 849-872.

Stähle, H.J., Raith, M., Hoernes, S. and Delfs, A. (1987) Element mobility during incipient granulite formation at Kabbaldurga, southern India. *J. Petrol.* **28** 803-834.

Sterner, S.M. and Bodnar, R.J. (1989) Synthetic fluid inclusions - VII. Re-equilibration of fluid inclusions in quartz during laboratory-simulated metamorphic burial and uplift. *J. Metamorphic Geol.* **7** 243-260.

Subramaniam, A.P. (1959) Charnockites of the type area near Madras - a reinterpretation. *Am. J. Sci.* **257** 321-353.

Subramanian, A.P. (1967) Charnockites and granulites of India: A review. *Medd. Dansk. Geol. Foren.* **17** 473-493.

Subramanian, V. (1983) Geology and geochemistry of the carbonatites of Tamil Nadu, India. *Unpublished PhD Thesis (Indian Inst. Sci. Bangalore).*

Swanenberg, H.E.C. (1980) Fluid inclusions in high-grade metamorphic rocks from S.W. Norway. *Geologica Ultraiectina, University of Utrecht* **25** 147.

Swart, P.K., Grady, M.M. and Pillinger, C.T. (1983) A method for the identification and elimination of contamination during carbon isotopic analysis of extraterrestrial samples. *Meteoritics* **18** 137-154.

Taylor, P.N., Chadwick, B., Friend, C.L.R., Ramakrishnan, M., Moorbath, S. and Viswanatha, M.N. (1984) Petrography, chemistry and isotopic ages of Peninsular gneiss, Dharwar acid volcanic rocks and the Chitradurga Granite with special reference to the late Archæan evolution of the Karnataka Craton, southern India. *Precamb. Res.* **23** 349-375.

Taylor, P.N., Chadwick, B., Moorbath, S., Ramakrishnan, M. and Viswanatha, M.N. (1988) New age data on the geological evolution of southern India. *J. Geol. Soc. India* **31** 155-157.

Taylor, S.R. and McLennan, S.M. (1985) The continental crust: Its composition and evolution. *Blackwells, Oxford.*

Thompson, A.B. (1983) Fluid-absent metamorphism. *J. Geol. Soc. London* **140** 533-547.

Touret, J.L.R. (1971) Le facies granulite en Norvege meridionale II. Les inclusions fluides. *Lithos* **4** 423-436.

Touret, J.L.R. and Bottinga, Y. (1979) Equation d'etat pour le CO_2: application aux inclusions carboniques. *Bull. Mineral.* **102** 635-649.

Touret, J.L.R. and Hansteen, T.H. (1988) Geothermobarometry and fluid inclusions in a rock from the Doddabetta charnockite complex, Southwest India. *Rend. Soc Ital. Mineral. Petrol.* **43** 65-82.

Valley, J.W. (1985) Polymetamorphism in the Adirondacks: Wollastonite at contacts of shallowly intruded anorthosite. In *The Deep Proterozoic Crust of the North Atlantic Provinces (eds. Tobi, A.C. and Touret, J.L.R.) (NATO ASI Series C, 158)* 217-236.

Valley, J.W. (1986) Stable isotope geochemistry of metamorphic rocks. In *Stable isotopes in high temperature geological processes. (eds. Valley, J.W., Taylor, H.P. and O'Neil, J.R.) Rev. Mineral.* **16** 445-481.

Valley, J.W. and O'Neil, J.R. (1984) Fluid heterogeneity during granulite facies metamorphism in the Adirondacks, stable isotope evidence. *Contrib. Mineral. Petrol.* **85** 158-173.

Valley, J.W., Petersen, E.U., Essene, E.J., Lamb, W.M. (1982) Fluorphlogopite and fluortremolite in Adirondack marbles and calculated C-O-H-F fluid compositions. *Am. Mineral.* **67** 545-557.

Vielzeuf, D. and Holloway, J.R. (1988) Experimental determination of the fluid-absent melting reactions in the pelitic system. *Contrib. Mineral. Petrol.* **98** 257-276.

Vry, J., Brown, P.E., Valley, J.W. and Morrison, J. (1988) Constraints on granulite genesis from carbon isotope compositions of cordierite and graphite. *Nature* **332** 66-68.

Walther, J.V. and Orville, P.M. (1982) Volatile production and transport in regional metamorphism *Contrib. Mineral. Petrol.* **79** 252-257.

Waters, D.J. (1988) Partial melting and the formation of granulite facies assemblages in Namaqualand, South Africa. *J. Metamorphic Geol.* **6** 387-404.

Waters, D.J. and Whales, C.J. (1984) Dehydration melting and the granulite transition in metapelites from southern Namaqualand, S. Africa. *Contrib. Mineral. Petrol.* **88** 269-275.

Watson, E.B. and Brenan, J.M. (1987) Fluids in the lithosphere, 1. Experimentally-determined wetting characteristics of CO_2-H_2O fluids and their implications for fluid transport, host-rock physical properties, and fluid inclusion formation. *Earth Planet. Sci. Letts.* **85** 497-515.

Weaver, B.L. (1980) Rare earth element geochemistry of Madras granulites. *Contrib. Mineral. Petrol.* **71** 271-279.

Weis, P.L., Friedman, I. and Gleason, J.P. (1981) The origin of epigenetic graphite: evidence from isotopes. *Geochim. Cosmochim. Acta.* **45** 2325-2332.

Wells, P.R.A. (1979) Chemical and thermal evolution of Archæan sialic crust, southern West Greenland. *J. Petrology* **20** 187-226.

Wendlandt, R.F. (1981) Influence of CO_2 on melting of modal granulite facies assemblages: a model for the genesis of charnockites. *Am. Mineral.* **66** 1164-1174.

Wickham, S.P. (1988) Evolution of the lower crust. *Nature* **333** 127.

Wickham, S.P. and Taylor, H.P. Jr. (1987) Stable isotopic evidence for the origin and depth of penetration of hydrothermal fluid associated with Hercynian regional metamorphism and crustal anatexis in the Pyrenees. *Contrib. Mineral. Petrol.* **95** 255-268.

Wightman, R.T. (1986) Constraints on crustal development and tectonics in the Archæan rocks of South India. *Unpublished PhD Thesis (Open University).*

Wones, D.R. & Dodge, F.C.W. (1977) The stability of phlogopite in the presence of quartz and diopside. *in Thermodynamics in Geology (ed. Fraser, D.G.)* 229-247.

Wood, B.J. (1976) The reaction phlogopite + quartz = enstatite + sanidine + H_2O. *Prog. Exper. Petrol. Water Enviromental Resources Council* **6** 17-19.

Wood, B.J. and Walther, J.V. (1986) Fluid flow during metamorphism and its implications for fluid-rock ratios. *in Fluid-rock interactions during metamorphism. (eds. Walther, J.V. and Wood, B.J.)* 89-108.

APPENDIX A

ANALYTICAL TECHNIQUES

A.1 STABLE ISOTOPE ANALYSIS OF CARBONATES

CO_2 was extracted from carbonates by acid dissolution, using the technique outlined in Planetary Sciences Unit Internal Report No. 3 (Grady, 1987), which is based on McCrea (1950). The acid (100% orthophosphoric acid) was evacuated for at least five hours, to a pressure below 10^{-4} mbars, before reaction with the sample. Sample reaction was carried out at 25.2°C in a water bath for at least two hours and the CO_2 was extracted and purified in the usual way and analysed using the SIRA 24 mass spectrometer (4.2). Particular care was exercised during acid degassing and sample reaction in carbonate-poor samples. The fractionation factor (α) used for the oxygen isotopic analysis of calcite at 25.2°C was 1.01025 (Sharma and Clayton, 1965). Carbonate-rich samples gave results reproducible to ± 0.2‰

A.2 STABLE ISOTOPE ANALYSIS OF GRAPHITE

Graphite was converted to CO_2 by reaction with CuO at 1000°C. Graphite flakes were hand picked from a crushed rock sample, weighed and loaded into a prebaked quartz bucket with an excess of CuO. The vessel was sealed under vacuum and allowed to react for at least two hours at 1000°C, then held for a further two hours at 450°C to resorb any oxygen. The capsule was crushed under vacuum and the CO_2 purified and its volume measured to check for complete conversion of the graphite. The gas was then analysed using the SIRA 24 mass spectrometer (4.2). The reproducibility of $\delta^{13}C$ graphite analyses (except where stated) is within 0.2‰.

A.3 WAVELENGTH DISPERSIVE ELECTRON MICROPROBE ANALYSIS

Microprobe mineral analyses were carried out on polished carbon-coated thin sections using a Cambridge instruments Microscan 9 (M9) microprobe. The M9 incorportaes a fully automated computerised system which controls spectrometer angles, count times, crystal selection and specimen position. In addition on-line ZAF corrections are performed automatically.

An accelerating potential of 20 kV and a probe current of 30 nA were used for all wavelength dispersive analyses using a defocused 15 μm diameter electron beam. The instrument was calibrated daily using mineral standards and operating conditions listed in Table A1. An "in-house" standard (ABG - a basaltic glass) was analysed several times each day to moniter instrument precision.

					Count time (s)	
Element	Mineral	Concentration (%)	Crystal	Peak angles	Std.	Unk.
Si	wollastonite	24.05	TAP	16.04	20	30
Ti	rutile	5.95	PET	18.232	15	30
Al	jadeite	3.28	TAP	18.851	30	30
Fe	fayalite	52.95	LIF	28.72	30	50
Mn	metal	100.00	LIF	31.45	20	50
Mg	forsterite	25.52	TAP	22.579	30	30
Ca	wollastonite	34.16	PET	22.494	20	30
Na	jadeite	11.20	TAP	27.573	40	30
K	KCl	52.45	PET	25.24	15	30
Ba	barite	57.11	PET	18.413	20	50
F	LIF	73.25	TAP	45.36	50	50
Cl	KCl	47.55	PET	32.64	20	30

Table A.1. Standards and calibration conditions used for wavelength dispersive microprobe analysis.

Appendix B

SAMPLE CATALOGUE

The sample catalogue gives the following information: **Sample No.**, brief sample description, sampling location, (and area), locality on sample map (Figure 3.3), source of the sample (D.H.J.= author; M.S.= Dr. M. Santosh; C.U.H.C.= Cambridge University Harker Collection; R.W.H.= Dr. Richard Holt; R.T.W.= Dr. Roger Wightman) and the type of sample/separate analysed for carbon isotopic composition (W.R.= whole rock powder, qtz = quartz, gt = garnet, gr = graphite).

KA1-Hornblende-biotite (Peninsular) gneiss from Channapatna, (Kabbal) (1) D.H.J. qtz.

KA2-Hornblende-biotite (Peninsular) gneiss from Kabbaldurga (1) D.H.J. qtz.

KA5-Incipient charnockite from Kabbaldurga (1) D.H.J. qtz.

SA3-Incipient charnockite from Satnuru, (Kabbal) (1) D.H.J. qtz.

I633-Hornblende-biotite (Peninsular) gneiss from Mercera (23 km north), (Coorg) (2) R.T.W.qtz.

CO8D-Incipient charnockite from Mercera (17 km north), (Coorg) (2) D.H.J. qtz.

I648-Massive (type a) charnockite from Mercera (15 km north), (Coorg) (2) R.T.W qtz.

146061-Massive (type a) charnockite from Kodaikanal (38 km north), (Palni) (3) C.U.H.C. qtz.

H43-Massive (type a) charnockite from Kodaikanal, (Palni) (3) R.W.H. qtz.

MA5A-Massive (type b) charnockite from Pallavaram, (Madras) (4) D.H.J. qtz.

I685-Massive (type a) charnockite from Wellington, (Nilgiris) (5) R.T.W. qtz.

IU6-Massive (type a) charnockite from Doddabetta, (Nilgiris) (5) D.H.J. qtz, gt.

PC6A-Biotite gneiss (graphite-free) from Koddakad, (Palghat) (6) D.H.J. qtz.

PC6C-Incipient charnockite from Koddakad, (Palghat) (6) D.H.J. qtz.

AN11A-Gneiss/incipient charnockite (graphite-free) from Andipatti, (Madurai) (8) D.H.J. qtz.

146059-Massive (type b) Charnockite from Andipatti, (Madurai) (8) C.U.H.C. qtz.

SH/QF/11-Biotite gneiss (graphite-bearing) from Kottavatom, (KKB) (9) M.S. qtz, gr.

SH/QF/12-Incipient charnockite from Kottavatom, (KKB) (9) M.S. qtz, gr.

IU13A-Incipient charnockite from Kottavatom, (KKB) (9) D.H.J. qtz; WR.

SH/QF/4-Massive (type b) charnockite from Manali, (KKB) (10) M.S. qtz.

SH/QF/5-Biotite gneiss (graphite-bearing) from Manali, (KKB) (10) M.S. qtz.

SH/QF/6-Incipient charnockite from Manali, (KKB) (10) M.S. qtz.

TR10A-Biotite gneiss (graphite-free) from Kalanjur, (KKB) (11) D.H.J. qtz.

TR10D-Incipient charnockite from Kalanjur, (KKB) (11) D.H.J. qtz, gt.

146057-Incipient charnockite from Kuttalam, (Madurai) (12) C.U.H.C. qtz.

146060-Incipient charnockite from Panaikkudi, (KKB) (13) C.U.H.C. qtz.

SH/CS/1-Calc-silicate from Kadakaman, (KKB) (14) M.S. WR.

SH/QF/10-Massive (type b) charnockite from Kadakaman, (KKB) (14) M.S. qtz.

TR20A-Massive (type c) charnockite from Kottaram, (Nagerkoil) (15) D.H.J. qtz.

TR20B-Sillimanite-bearing metapelite (graphite-free) from Kottaram, (Nagerkoil) (15) D.H.J. qtz, gt.

TR20D-Massive (type c) charnockite from Kottaram, (Nagerkoil) (15) D.H.J. qtz,gt.

146058-Massive (type b) charnockite from Rajapalayam, (Madurai) (16) C.U.H.C. qtz.

SH/QF/3B-Biotite gneiss (graphite-bearing) from Ponmudi, (KKB) (17) M.S. qtz, gt, gr.

SH/QF/3-Incipient charnockite from Ponmudi, (KKB) (17) M.S. qtz, gt, gr.

TR15A-Incipient charnockite from Ponmudi, (KKB) (17) D.H.J. qtz.

IU10A-Incipient charnockite from Ponmudi, (KKB) (17) D.H.J. qtz, WR.

TR27A-Calc-silicate from Nuliyam, (KKB) (18) D.H.J. cc, gr, WR.

TR27B-Calc-silicate from Nuliyam, (KKB) (18) D.H.J. qtz, cc, gr, WR.

TR27C-Massive (type d) charnockite from Nuliyam, (KKB) (18) D.H.J. qtz, gr, WR.

TR27D-Massive (type d) charnockite from Nuliyam, (KKB) (18) D.H.J. qtz.

TR27E-Massive (type d) charnockite from Nuliyam, (KKB) (18) D.H.J. qtz, gt, gr, WR.

TR27F-Incipient charnockite from Nuliyam, (KKB) (18) D.H.J. qtz, gt, gr, WR.

TR27G-Biotite gneiss (graphite-bearing) from Nuliyam, (KKB) (18) D.H.J. qtz.

TR27H-Biotite gneiss (graphite-free) from Nuliyam, (KKB) (18) D.H.J. qtz, gr.

TR27I-Biotite gneiss (graphite-bearing) from Nuliyam, (KKB) (18) D.H.J. qtz.

Appendix C

ANALYTICAL DATA

C.1 STEPPED HEATING DATA

ic = incipient charnockite, gn = gneiss, mca = massive charnockite type (a), cs = calc-silicate, q = quartz, (qp = powdered quartz separate), gt = garnet, WR = whole rock powder. (Samples are quartz separates unless stated otherwise)

C.1.1 Combustion line blank runs

Sample Weight (mg)	Blank 1 100**		Blank 2 100**		Blank 3 185.68*		Blank 4 72.3*	
T(°C)	Yield (ppm)	$\delta^{13}C$ (‰)	Yield (ppm)	$\delta^{13}C$ (‰)	Yield (ppm)	$\delta^{13}C$ (‰)	Yield (ppm)	$\delta^{13}C$ (‰)
300	0.29	N.D.	-	-	-	-	1.20	N.D.
400	0.07	N.D.	0.73	N.D.	5.65	-23.4	2.01	-26.1
500	0.19	N.D.	-	-	-	-	0.77	N.D.
600	0.12	N.D.	0.63	-33.7	7.00	-22.9	0.66	N.D.
700	0.10	N.D.	0.27	N.D.	-	-	0.59	N.D.
800	0.10	N.D.	0.19	N.D.	1.88	-27.4	0.66	N.D.
900	0.05	N.D.	-	-	-	-	-	-
1200	0.24	N.D.	0.22	N.D.	1.40	-33.0	1.67	-27.1

(*= Weight of crushed and prebaked (1000°C for 12 hours) quartz glass; **= blank conducted with empty sample vessel - arbitrary weight to allow yield calculation.)

C.1.2 Gneisses and incipient charnockites from near the orthopyroxene isograd.

Sample Weight (mg)	Pen Gn (gn) 161.94		KA2 (gn) 109.90		KA5 (ic) 107.10		KA5 (ic) 85.00	
T(°C)	Yield (ppm)	$\delta^{13}C$ (‰)	Yield (ppm)	$\delta^{13}C$ (‰)	Yield (ppm)	$\delta^{13}C$ (‰)	Yield (ppm)	$\delta^{13}C$ (‰)
300	0.45	N.D.	-	-	-	-	4.59	-15.9
400	0.61	N.D.	0.97	N.D.	6.82	-11.7	2.65	N.D.
500	1.11	-24.1	3.09	-14.0	1.88	N.D.	4.35	-18.6
600	0.36	N.D.	3.46	-13.5	6.26	-12.3	8.94	-12.2
700	-	-	4.28	-13.1	10.27	-11.6	9.88	-10.7
800	0.22	N.D.	-	-	2.52	-10.2	3.88	-13.1
1200	0.40	-25.0	4.19	-22.9	3.08	-13.4	11.88	-12.0

Sample Weight (mg)	I 633 (gn) 86.87		CO8D (ic) 75.36		I648 (mca) 117.80		SA3 (ic) 137.10	
T(°C)	Yield (ppm)	$\delta^{13}C$ (‰)	Yield (ppm)	$\delta^{13}C$ (‰)	Yield (ppm)	$\delta^{13}C$ (‰)	Yield (ppm)	$\delta^{13}C$ (‰)
300	-	-	3.60	N.D.	-	-	-	-
400	0.71	-25.6	7.10	-22.4	13.50	-21	7.06	-21.3
500	0.19	N.D.	5.84	N.D.	10.95	-10.8	3.06	-18.2
600	0.28	-21.7	9.62	-11.7	38.88	-5.1	25.24	-9
700	-	-	20.70	-7.5	51.44	-4.4	44.64	-9.4
800	0.15	N.D.	10.18	-9.9	15.11	-4.3	8.61	-9.9
900	-	-	2.31	N.D.	7.13	-5.8	-	-
1200	0.05	N.D.	4.21	N.D.	14.43	-10.7	14.81	-9.6

C.1.3 Northern massive charnockites

Sample Weight (mg)	146061q (mca) 139.02		H43 (mca) 109.33		MA5A (mcb) 130.15	
T(°C)	Yield (ppm)	$\delta^{13}C$ (‰)	Yield (ppm)	$\delta^{13}C$ (‰)	Yield (ppm)	$\delta^{13}C$ (‰)
300	3.24	-30.0	-	-	18.29	-10.8
400	5.68	-28.1	6.40	-33.1	13.06	-15.1
500	6.69	-26.0	7.68	-17.4	11.76	-16.6
600	19.21	-11.5	9.15	-11.3	11.91	-14.8
700	38.12	-6.7	11.98	-10.6	21.28	-10.3
800	34.74	-7.1	8.14	-11.8	21.21	-8.9
900	-	-	-	-	8.45	-9.9
1200	2.37	-24.6	5.12	-23.3	6.61	-9.9

Sample Weight (mg)	I 685 (mca) 159.40		IU6 (q) (mca) 118.04		IU6 (gt) (mca) 148.90	
T(°C)	Yield (ppm)	$\delta^{13}C$ (‰)	Yield (ppm)	$\delta^{13}C$ (‰)	Yield (ppm)	$\delta^{13}C$ (‰)
400	8.53	-14.3	8.22	-41.2	-	-
500	9.16	-11.9	5.10	-44.8	41.50	-17.6
600	18.32	-9.0	9.31	-9.3	86.77	-10.5
700	13.43	-8.8	13.51	-6.9	125.92	-9.0
800	17.44	-9	2.89	N.D.	48.35	-11.4
900	8.78	-10.8	-	-	32.03	-14.1
1200	17.25	-11.9	6.03	-19.5	151.24	-20.7

C.1.4 Gneiss-incipient charnockite pairs from south of the Palghat-Cauvery shear zone.

Sample Weight (mg)	PC6A (gn) 110.10		PC6C (ic) 111.73		AN11A 2 (gn) 77.62		AN11A 1 (ic) 88.97	
T(°C)	Yield (ppm)	$\delta^{13}C$ (‰)	Yield (ppm)	$\delta^{13}C$ (‰)	Yield (ppm)	$\delta^{13}C$ (‰)	Yield (ppm)	$\delta^{13}C$ (‰)
400	2.52	-28.0	5.98	-13.7	14.69	-27.5	12.59	-28.1
500	-	-	2.96	-11.1	3.61	-22.7	4.38	-24.0
600	5.80	-11.1	14.03	-7.4	12.75	-8.1	10.34	-9.9
700	8.42	-6.9	29.78	-6.8	24.74	-6.2	20.91	-6.6
800	3.30	-7.8	5.17	-10.0	15.07	-6.4	17.42	-5.9
900	-	-	4.20	-12.6	-	-	2.47	-9.6
1200	1.49	-17.4	8.19	-11.4	7.60	-14.0	5.51	-14.8

Sample Weight (mg)	SH/QF/12 (gn) 85.65		SH/QF/11 (ic) 111.20		SH/QF/6 (gn) 131.12		SH/QF/5 (ic) 167.67	
T(°C)	Yield (ppm)	$\delta^{13}C$ (‰)	Yield (ppm)	$\delta^{13}C$ (‰)	Yield (ppm)	$\delta^{13}C$ (‰)	Yield (ppm)	$\delta^{13}C$ (‰)
300	-	-	6.03	-15.7	-	-	3.64	-21.4
400	15.39	-17.3	8.36	-16.4	4.58	-27.1	5.55	-22.7
500	8.56	-19.4	11.15	-13.4	11.06	-26.4	9.07	-17.7
600	5.20	-16.8	18.71	-9.5	12.74	-19.5	27.26	-9.2
700	6.16	-10.8	7.46	-11.2	21.20	-12.1	86.12	-7.6
800	5.79	-11.2	16.01	-10.1	23.41	-11.3	64.05	-7.7
900	-	-	6.12	-14.6	2.97	-10.0	6.32	-9.0
1200	5.56	-17.2	6.12	-14.3	1.11	N.D.	6.44	-14.6

C.1.5 Gneisses, incipient charnockites and calc-silicate from the KKB.

Sample Weight (mg)	TR10A (gn) 139.20		TR10D (q) (ic) 131.60		TR10A (gn) 135.20		TR10D (gt) (ic) 122.60	
T(°C)	Yield (ppm)	$\delta^{13}C$ (‰)	Yield (ppm)	$\delta^{13}C$ (‰)	Yield (ppm)	$\delta^{13}C$ (‰)	Yield (ppm)	$\delta^{13}C$ (‰)
400	5.67	-24.2	9.42	-25.4	6.71	-15.6	9.14	-31.9
500	2.23	-18.6	4.26	-16.1	4.79	-11.0	5.46	-14.3
600	10.03	-8.5	28.42	-6.8	14.35	-7.5	7.01	-9.4
700	21.98	-7.3	38.45	-6.2	28.62	-7.1	20.96	-6.6
800	5.75	-9.1	14.21	-7.4	16.05	-7.1	7.10	-7.9
900	-	-	4.10	-10.8	4.14	-8.8	1.47	-5.8
1200	4.71	-21.5	4.86	-15.1	4.08	-16.2	N.D.	N.D.

Sample Weight (mg)	146057 (ic) 113.45		146060 (ic) 127.89		SH/CS/1 (wr) (cs) 2.10		SH/QF/10 (mcb) 113.37	
T(°C)	Yield (ppm)	$\delta^{13}C$ (‰)	Yield (ppm)	$\delta^{13}C$ (‰)	Yield (ppm)	$\delta^{13}C$ (‰)	Yield (ppm)	$\delta^{13}C$ (‰)
300	8.11	-18.5	2.97	0.0	-	-	3.18	-18.6
400	10.31	-17.9	6.18	-8.6	1264	-24.9	6.62	-20.3
500	38.52	-6.2	7.74	-15.5	1017	-19.8	7.06	-22.1
600	15.16	-13.9	19.24	-9.8	8097	0.0	9.97	-17.3
700	-	-	45.59	-7.3	6547	1.2	20.02	-10.8
800	5.46	-21.0	14.07	-8.6	218	-18.0	18.88	-10.7
900	-	-	-	-	-	-	6.44	-14.1
1200	3.35	-27.6	5.40	-24.4	252	-27.6	7.85	-17.8

C.1.6 Kottaram and type (b) massive charnockites.

Sample Weight (mg)	TR20B (q) (gn) 128.50		TR20B (gt) (gn) 145.97		TR20D (q) (mcc) 101.30		TR20D (gt) (mcc) 151.01	
T(°C)	Yield (ppm)	$\delta^{13}C$ (‰)	Yield (ppm)	$\delta^{13}C$ (‰)	Yield (ppm)	$\delta^{13}C$ (‰)	Yield (ppm)	$\delta^{13}C$ (‰)
300	-	-	6.86	-29.1	-	-	4.37	-25.7
400	8.79	-12.7	10.41	-16.3	56.37	-8.3	59.44	-7.46
500	5.14	-9.9	7.14	-16.2	91.71	-6.2	109.27	-6.4
600	24.67	-7.7	26.16	-8.3	49.46	-7.4	55.43	-6.2
700	24.98	-7.8	16.78	-7.8	59.03	-8.0	71.52	-6.1
800	1.25	-13.8	-	-	5.33	-11.5	5.23	-14.8
1200	1.25	-25.3	1.58	-33.3	3.55	-16.4	7.48	-10.3

Sample Weight (mg)	TR20D (q) (mcc) 123.36		TR20A (mcc) 89.70		146058b (mcb) 129.91		146059 (mcb) 128.78	
T(°C)	Yield (ppm)	$\delta^{13}C$ (‰)	Yield (ppm)	$\delta^{13}C$ (‰)	Yield (ppm)	$\delta^{13}C$ (‰)	Yield (ppm)	$\delta^{13}C$ (‰)
cr	6.18	-4.7	-	-	-	-	-	-
300	12.26	-14.6	-	-	3.62	-27.6	5.90	-10.5
400	103.36	-9.6	24.97	-8.4	8.39	-26.2	6.45	-16.9
500	200.06	0.0	31.77	-5.2	14.32	-19.4	4.74	-19.4
600	184.91	-6.8	17.73	-7.9	26.56	-19.9	5.67	-16.2
700	59.58	-7.6	3.57	-14.2	18.09	-11.3	9.32	-9.9
800	6.96	-9.0	-	-	16.55	-9.5	8.54	-9.3
1000	-	-	-	-	6.62	-20.7	-	-
1200	4.02	-9.8	2.56	-13.7	5.77	-25.8	2.33	-25.3

C.1.7 Other samples from the KKB

Sample Weight (mg)	IU13A (qp) (ic) 115.84	
T(°C)	Yield (ppm)	$\delta^{13}C$ (‰)
250	8.86	-30.1
300	63.18	-25.1
350	27.43	-22.9
400	26.48	-25.7
450	15.92	-11.4
500	15.73	-11.2
550	27.45	-6.7
600	24.29	-8.9
650	3.87	0.0
1100	24.52	-29.5

Sample Weight (mg)	SH/QF/4 (mcb) 129.33	
T(°C)	Yield (ppm)	$\delta^{13}C$ (‰)
300	10.83	-18.9
400	11.91	-22.0
500	10.59	-19.7
600	8.12	-17.0
700	25.44	-12.4
800	23.43	-12.5
900	4.87	-18.8
1200	4.79	-20.3

C.1.8 Quartz and garnet samples from Ponmudi.

Sample Weight (mg)	SH/QF/3 (ic) 111.04		SH/QF/3 (ic) 103.63		TR15B (q) (ic) 66.93		TR15B (gt) (ic) 245.73	
T(°C)	Yield (ppm)	$\delta^{13}C$ (‰)	Yield (ppm)	$\delta^{13}C$ (‰)	Yield (ppm)	$\delta^{13}C$ (‰)	Yield (ppm)	$\delta^{13}C$ (‰)
300	6.39	-18.2	4.73	-22.0	12.55	-21.2	-	-
400	3.96	-18.7	9.26	-24.0	16.70	-20.4	5.53	-29.5
500	5.13	-14.0	12.16	-21.2	8.02	-4.9	-	-
600	14.05	-11.0	18.72	-14.8	6.54	-12.1	10.26	-11.6
700	31.07	-10.3	54.42	-10.5	9.68	-12.2	47.86	-8.6
800	19.36	-10.3	22.29	-10.4	7.69	-11.6	12.11	-8.5
900	9.46	-11.0	9.36	-11.1	-	-	3.78	-10.0
1200	8.20	-14.1	8.78	-13.7	4.48	N.D.	3.16	-13.9

Sample Weight (mg)	SH/QF/3B (q) (gn) 113.29		SH/QF/3B (gt) (gn) 134.90		IU10A (q) (ic) 79.88		IU10A (qp) (ic) 91.40	
T(°C)	Yield (ppm)	$\delta^{13}C$ (‰)	Yield (ppm)	$\delta^{13}C$ (‰)	Yield (ppm)	$\delta^{13}C$ (‰)	Yield (ppm)	$\delta^{13}C$ (‰)
300	3.62	-16.2	5.40	-25.4	0.66	N.D.	84.70	-26.9
400	7.59	-14.5	2.67	-19.1	8.73	-14.8	145.05	-24.7
500	5.56	-22.1	4.59	-16.9	10.14	-22.4	25.65	-14.0
600	7.24	-16.1	11.33	-12.6	8.48	-12.4	47.25	-5.6
700	16.24	-10.7	3.41	-15.0	53.20	-10.3	1.40	N.D.
800	6.18	-12.4	13.57	-19.5	16.35	-8.1	1.16	N.D.
900	4.68	-14.6	-	-	10.12	-11.1	-	-
1200	4.15	-20.8	-	-	4.48	N.D.	4.72	-12.9

C.1.9 Results from 50°C stepped heating experiments.

Sample Weight (mg)	IU10A (q) (ic) 237.09		IU6 (gt) (mca) 80.17	
T(°C)	Yield (ppm)	$\delta^{13}C$ (‰)	Yield (ppm)	$\delta^{13}C$ (‰)
200	0.89	N.D.	-	-
250	1.73	-15.3	-	-
300	2.02	-8.5	-	-
350	1.77	-10.3	-	-
400	2.28	-12.8	23.57	-16.8
450	2.49	-5.1	17.59	-14.2
500	1.73	-12.6	12.22	-13.5
550	1.98	-12.7	35.55	-12.4
600	4.50	-12.4	52.01	-10.9
650	5.44	-11.2	95.55	-9.8
700	6.28	-11.0	53.26	-11.1
750	5.65	-11.4	25.57	-12.4
800	1.29	N.D.	18.21	-13.4
850	-	-	15.72	-13.7
900	-	-	19.96	-13.5
950	-	-	17.09	-14.7
1000	-	-	19.58	-15.9
1050	-	-	17.77	-16.9
1100	-	-	63.53	-18.0
1200	-	-	213.06	-18.7

C.1.10 Quartz separates from Nuliyam.

Sample Weight (mg)	TR27I (gn) 76.20		TR27H (gn) 78.78		TR27G (gn) 79.50		TR27F (ic) 49.97	
T(°C)	Yield (ppm)	$\delta^{13}C$ (‰)	Yield (ppm)	$\delta^{13}C$ (‰)	Yield (ppm)	$\delta^{13}C$ (‰)	Yield (ppm)	$\delta^{13}C$ (‰)
400	10.25	-17.2	17.07	-15.0	14.21	-26.8	11.63	-22.0
500	7.24	-13.3	17.78	-16.9	19.42	-16.0	42.91	-13.3
600	15.88	-11.1	7.71	-15.3	4.33	-15.3	7.12	-13.1
700	20.92	-11.2	3.35	N.D.	2.59	N.D.	2.86	N.D.
800	10.25	-9.0	6.32	-18.4	5.75	-18.0	-	-
900	1.94	N.D.	-	-	-	-	-	-
1200	6.18	-18.5	-	-	4.50	-16.0	15.47	-14.3

Sample Weight (mg)	TR27E (mcd) 96.48		TR27D (mcd) 54.68		TR27C (mcd) 73.66		TR27B (cs) 102.18	
T(°C)	Yield (ppm)	$\delta^{13}C$ (‰)	Yield (ppm)	$\delta^{13}C$ (‰)	Yield (ppm)	$\delta^{13}C$ (‰)	Yield (ppm)	$\delta^{13}C$ (‰)
300	2.91	N.D.	-	-	-	-	-	-
400	7.22	-24.8	26.41	-21.9	24.04	-25.2	4.36	N.D.
500	6.24	-23.5	22.44	-10.3	13.27	-17.3	3.05	-26.2
600	12.33	-13.6	21.51	-9.6	15.70	-12.4	20.34	-19.8
700	33.20	-8.8	18.58	-9.0	33.34	-9.0	32.15	-10.2
800	42.88	-7.9	9.82	-10.4	20.82	-9.6	20.39	-10.7
900	3.96	-13.2	3.49	N.D.	4.53	-14.7	2.22	N.D.
1200	4.47	-24.1	9.82	-18.1	6.11	-21.3	336.17	-9.7

C.1.11 Garnet separates and powdered whole rock samples from Nuliyam.

Sample Weight (mg)	TR27F (gt) (ic) 144.50		TR27E (gt) (mcd) 90.58		TR27A(wr) (cs) 4.62		TR27B (wr)(cs) 4.84	
T(°C)	Yield (ppm)	$\delta^{13}C$ (‰)	Yield (ppm)	$\delta^{13}C$ (‰)	Yield (ppm)	$\delta^{13}C$ (‰)	Yield (ppm)	$\delta^{13}C$ (‰)
200	-	-	-	-	-	-	75	N.D.
300	-	-	-	-	634	-2.1	253	-26.1
400	6.23	-19.3	7.26	-25.5	417	-23.8	752	-25.3
500	96.11	-12.9	3.50	N.D.	497	-27.2	1172	-29.3
600	36.06	-12.7	5.61	-15.3	818	-27.5	1097	-30.9
700	1.25	0.0	8.47	-10.4	898	-28.9	2446	-9.2
800	0.64	-18.6	4.46	-12.2	1309	-12.6	912	-12.7
900	-	-	-	-	4541	-11.6	1972	-13.0
1000	-	-	-	-	2900	-11.4	754	N.D.
1200	1.94	-25.3	2.30	N.D.	2885	-12.8	5855	-13.8

Sample Weight (mg)	TR27C (wr) (mcd) 5.77		TR27E (wr) (mcd) 4.06		TR27F (wr) (ic) 6.04	
T(°C)	Yield (ppm)	$\delta^{13}C$ (‰)	Yield (ppm)	$\delta^{13}C$ (‰)	Yield (ppm)	$\delta^{13}C$ (‰)
300	112.7	N.D.	219.2	-27.8	158.6	-26.8
400	254.8	-25.0	512.6	-26.1	238.4	-24.6
500	331.0	-23.7	391.6	-24.2	241.1	-20.4
600	301.6	-12.9	203.7	-15.0	56.1	N.D.
700	105.7	2.9	140.6	-16.0	22.8	N.D.
800	225.3	-12.5	469.5	-15.4	27.6	N.D.
900	521.7	-12.3	750.7	-15.0	49.3	N.D.
1000	171.6	-12.2	244.8	-16.8	-	-
1200	45.1	N.D.	38.2	N.D.	34.4	-21.8

C.2 MICROPROBE DATA

C.2.1 TR27I

Biotite

	IBB	IBC	IBD	IBE	IBF	IBG
SiO_2	35.79	35.66	35.72	35.50	35.86	35.55
TiO_2	5.51	5.33	4.05	5.33	4.42	5.33
Al_2O_3	13.03	12.87	13.16	13.00	13.10	13.11
FeO	27.44	28.14	28.16	27.64	25.69	27.81
MnO	0.05	0.05	0.05	0.05	0.02	0.08
MgO	4.82	4.90	5.53	5.22	6.99	4.92
CaO	-	-	-	-	-	-
K_2O	9.61	9.46	9.56	9.67	9.64	9.51
F	2.65	2.71	3.08	2.83	3.35	2.72
Cl	0.81	0.80	0.85	0.77	0.75	0.81
Total	99.71	99.92	100.16	100.01	99.82	99.84
Mg/Mg+Fe	0.239	0.237	0.259	0.252	0.327	0.240

Formula Oxygens	22	22	22	22	22	22
Si	5.65	5.64	5.66	5.61	5.65	5.62
Ti	0.65	0.63	0.48	0.63	0.52	0.63
Al	2.42	2.40	2.46	2.42	2.43	2.44
Fe	3.62	3.72	3.73	3.65	3.38	3.68
Mn	0.01	0.01	0.01	0.01	0.00	0.01
Mg	1.14	1.15	1.31	1.23	1.64	1.16
Ca	-	-	-	-	-	-
K	1.94	1.91	1.93	1.95	1.94	1.92
F	1.32	1.36	1.54	1.41	1.67	1.36
Cl	0.22	0.21	0.23	0.21	0.20	0.22
OH	2.46	2.43	2.23	2.38	2.13	2.42
Total	19.43	19.46	19.58	19.50	19.56	19.46

Garnet

	IGA	IGB	IGC	IGD	IGE	IGF
SiO_2	37.40	37.13	37.29	37.09	37.47	37.42
TiO_2	0.03	0.07	0.07	0.07	0.05	0.07
Al_2O_3	20.94	20.92	20.98	20.98	20.81	20.84
FeO	37.51	37.55	37.37	37.26	37.73	37.28
MnO	0.74	0.74	0.72	0.74	0.77	0.74
MgO	1.24	1.31	1.26	1.27	1.24	1.22
CaO	3.02	3.00	3.13	3.04	3.02	3.17
Total	100.88	100.72	100.82	100.45	101.09	100.74
Mg/Mg+Fe	0.056	0.059	0.057	0.057	0.055	0.055

Formula Oxygens	12	12	12	12	12	12
Si	3.01	3.00	3.01	3.00	3.02	3.02
Ti	0.00	0.00	0.00	0.00	0.00	0.00
Al	1.99	1.99	1.99	2.00	1.97	1.98
Fe	2.53	2.54	2.52	2.52	2.54	2.51
Mn	0.05	0.05	0.05	0.05	0.05	0.05
Mg	0.15	0.16	0.15	0.15	0.15	0.15
Ca	0.26	0.26	0.27	0.26	0.26	0.27
Total	7.99	8.00	7.99	7.98	7.99	7.98

C.2.2 TR27H

Biotite

	HBA	HBB	HBC	HBD	HBE	HBF
SiO_2	36.11	38.77	35.87	35.91	35.22	36.53
TiO_2	5.18	4.54	5.05	5.16	3.65	5.46
Al_2O_3	13.19	13.81	12.93	13.08	13.03	13.15
FeO	26.69	24.37	26.25	26.76	26.23	27.11
MnO	0.06	0.05	0.05	0.06	0.05	0.08
MgO	5.73	5.22	6.35	5.85	6.86	5.85
CaO	-	-	-	-	-	-
K_2O	9.43	9.62	9.35	9.31	9.45	9.44
F	2.50	2.37	2.96	2.73	3.24	2.63
Cl	0.57	0.51	0.56	0.56	0.58	0.59
Total	99.46	99.26	99.37	99.42	98.31	100.84
Mg/Mg+Fe	0.277	0.276	0.301	0.281	0.318	0.278

Formula Oxygens	22	22	22	22	22	22
Si	5.66	5.95	5.65	5.65	5.64	5.65
Ti	0.61	0.52	0.60	0.61	0.44	0.64
Al	2.44	2.50	2.40	2.42	2.46	2.40
Fe	3.50	3.13	3.46	3.52	3.51	3.51
Mn	0.01	0.01	0.01	0.01	0.01	0.01
Mg	1.34	1.19	1.49	1.37	1.64	1.35
Ca	-	-	-	-	-	-
K	1.89	1.89	1.88	1.87	1.93	1.86
F	1.24	1.15	1.47	1.36	1.64	1.29
Cl	0.15	0.13	0.15	0.15	0.16	0.16
OH	2.61	2.72	2.38	2.49	2.20	2.55
Total	19.45	19.19	19.49	19.45	19.63	19.42

Garnet

	HGA	HGB	HGC	HGD	HGE	HGF	HGG
SiO_2	37.50	37.59	37.46	37.59	37.33	37.44	37.37
TiO_2	0.07	0.07	0.07	0.09	0.05	0.09	0.09
Al_2O_3	20.90	21.27	20.97	21.04	20.99	21.42	20.99
FeO	36.93	37.27	36.92	36.93	37.55	36.76	36.95
MnO	0.71	0.74	0.69	0.71	0.75	0.74	0.74
MgO	1.50	1.50	1.54	1.46	1.31	1.40	1.54
CaO	3.42	3.28	3.39	3.53	3.32	3.53	3.39
Total	101.03	101.72	101.04	101.35	101.30	101.38	101.07
Mg/Mg+Fe	0.068	0.067	0.069	0.066	0.059	0.064	0.069

Formula Oxygens	12	12	12	12	12	12	12
Si	3.01	3.00	3.01	3.01	3.00	2.99	3.00
Ti	0.00	0.00	0.00	0.01	0.00	0.01	0.01
Al	1.98	2.00	1.98	1.98	1.99	2.02	1.99
Fe	2.48	2.49	2.48	2.47	2.52	2.46	2.48
Mn	0.05	0.05	0.05	0.05	0.05	0.05	0.05
Mg	0.18	0.18	0.18	0.17	0.16	0.17	0.18
Ca	0.29	0.28	0.29	0.30	0.29	0.30	0.29
Total	7.99	8.00	7.99	7.99	8.01	8.00	8.00

C.2.3 TR27G

Biotite

	GBB	GBC	GBD	GBE	GBF
SiO_2	35.64	35.62	35.66	35.59	36.36
TiO_2	5.19	5.47	5.61	5.49	5.39
Al_2O_3	12.71	12.74	12.87	12.89	12.97
FeO	25.67	25.87	25.95	25.76	25.53
MnO	0.06	0.05	0.05	0.05	0.05
MgO	6.53	6.56	6.30	6.44	6.77
CaO	-	-	-	-	-
K_2O	9.50	9.50	9.40	9.45	9.46
F	2.56	2.52	2.40	2.52	2.51
Cl	0.76	0.74	0.74	0.76	0.75
Total	98.62	99.07	98.98	98.95	99.79
Mg/Mg+Fe	0.312	0.311	0.302	0.308	0.321

Formula Oxygens	22	22	22	22	22
Si	5.64	5.61	5.61	5.61	5.66
Ti	0.62	0.65	0.66	0.65	0.63
Al	2.37	2.36	2.39	2.39	2.38
Fe	3.40	3.41	3.42	3.39	3.32
Mn	0.01	0.01	0.01	0.01	0.01
Mg	1.54	1.54	1.48	1.51	1.57
Ca	-	-	-	-	-
K	1.92	1.91	1.89	1.90	1.88
F	1.28	1.25	1.20	1.26	1.23
Cl	0.20	0.20	0.20	0.20	0.20
OH	2.52	2.55	2.60	2.54	2.57
Total	19.49	19.49	19.44	19.47	19.44

Garnet

	GGA	GGB	GGC	GGD	GGE	GGF
SiO_2	37.57	37.62	37.56	37.08	37.80	37.52
TiO_2	0.09	0.05	0.05	0.07	0.00	0.00
Al_2O_3	21.08	21.26	21.23	21.12	21.34	21.47
FeO	36.48	36.23	36.10	35.75	36.15	36.23
MnO	0.72	0.74	0.71	0.71	0.71	0.71
MgO	1.73	1.88	1.90	1.91	1.93	1.91
CaO	3.57	3.35	3.45	3.41	3.50	3.48
Total	101.24	101.13	101.00	100.05	101.43	101.32
Mg/Mg+Fe	0.078	0.085	0.086	0.087	0.087	0.086

Formula Oxygens	12	12	12	12	12	12
Si	3.00	3.01	3.00	2.99	3.01	2.99
Ti	0.01	0.00	0.00	0.00	0.00	0.00
Al	1.99	2.00	2.00	2.01	2.00	2.02
Fe	2.44	2.42	2.41	2.41	2.41	2.42
Mn	0.05	0.05	0.05	0.05	0.05	0.05
Mg	0.21	0.22	0.23	0.23	0.23	0.23
Ca	0.31	0.29	0.30	0.29	0.30	0.30
Total	8.01	7.99	7.99	7.98	7.99	8.00

C.2 4 TR27F

Biotite

	FBA	FBB	FBC	FBD	FBE	FBF
SiO_2	35.36	36.70	36.06	35.64	35.66	35.00
TiO_2	4.24	3.32	4.58	5.25	4.13	5.17
Al_2O_3	12.93	12.77	12.90	12.80	12.65	12.67
FeO	25.44	21.86	23.70	25.24	22.50	26.04
MnO	0.06	0.02	0.02	0.03	0.02	0.06
MgO	7.26	10.32	8.56	7.11	9.61	6.46
CaO	-	-	-	-	-	-
K_2O	9.14	9.38	9.25	9.23	9.35	9.02
F	2.81	3.61	2.98	2.48	3.30	2.41
Cl	0.75	0.65	0.62	0.75	0.64	0.71
Total	97.99	98.63	98.67	98.53	97.86	97.54
Mg/Mg+Fe	0.337	0.457	0.392	0.334	0.432	0.307

Formula Oxygens	22	22	22	22	22	22
Si	5.63	5.74	5.65	5.62	5.64	5.60
Ti	0.51	0.39	0.54	0.62	0.49	0.62
Al	2.43	2.35	2.38	2.38	2.36	2.39
Fe	3.39	2.86	3.10	3.33	2.97	3.48
Mn	0.01	0.00	0.00	0.00	0.00	0.01
Mg	1.72	2.41	2.00	1.67	2.27	1.54
Ca	-	-	-	-	-	-
K	1.86	1.87	1.85	1.86	1.89	1.84
F	1.42	1.78	1.48	1.24	1.65	1.22
Cl	0.20	0.17	0.16	0.20	0.17	0.19
OH	2.38	2.05	2.36	2.56	2.18	2.59
Total	19.55	19.62	19.52	19.48	19.62	19.48

Garnet

	FGA	FGB	FGC	FGD	FGE
SiO_2	36.72	36.81	37.23	36.94	37.16
TiO_2	0.09	0.05	0.07	0.09	0.07
Al_2O_3	21.17	21.08	21.41	21.38	21.44
FeO	36.28	35.84	36.30	36.05	36.43
MnO	0.75	0.74	0.74	0.69	0.74
MgO	1.96	1.88	1.99	2.05	1.94
CaO	3.53	3.23	3.42	3.58	3.49
Total	100.50	99.63	101.16	100.78	101.27
Mg/Mg+Fe	0.088	0.086	0.089	0.092	0.087

Formula Oxygens	12	12	12	12	12
Si	2.96	2.99	2.98	2.97	2.97
Ti	0.01	0.00	0.00	0.00	0.00
Al	2.01	2.02	2.02	2.02	2.02
Fe	2.45	2.43	2.43	2.42	2.44
Mn	0.05	0.05	0.05	0.05	0.05
Mg	0.24	0.23	0.24	0.25	0.23
Ca	0.31	0.28	0.29	0.31	0.30
Total	8.03	8.00	8.01	8.02	8.01

C.2.5 TR27E

Biotite

	EBA	EBB	EBC	EBD	EBE	EBF
SiO_2	35.25	35.28	35.94	36.30	35.99	36.07
TiO_2	5.63	5.58	5.76	5.64	5.51	4.09
Al_2O_3	12.70	12.75	12.93	12.67	12.74	12.78
FeO	26.14	25.80	25.67	25.80	25.81	23.64
MnO	0.05	0.05	0.05	0.05	0.06	0.02
MgO	6.65	6.66	6.39	6.65	6.59	8.83
CaO	-	-	-	-	-	-
K_2O	9.17	9.25	9.28	9.33	9.18	9.47
F	2.01	2.10	2.25	2.20	2.17	3.11
Cl	1.16	1.12	1.10	1.14	1.16	0.99
Total	98.76	98.59	99.37	99.78	99.21	99.00
Mg/Mg+Fe	0.312	0.315	0.308	0.315	0.313	0.400

Formula Oxygens	22	22	22	22	22	22
Si	5.57	5.58	5.63	5.66	5.65	5.67
Ti	0.67	0.66	0.68	0.66	0.65	0.48
Al	2.37	2.38	2.39	2.33	2.35	2.37
Fe	3.45	3.41	3.36	3.36	3.39	3.11
Mn	0.01	0.01	0.01	0.01	0.01	0.00
Mg	1.57	1.57	1.49	1.54	1.54	2.07
Ca	-	-	-	-	-	-
K	1.85	1.87	1.85	1.86	1.84	1.90
F	1.01	1.05	1.11	1.09	1.07	1.55
Cl	0.31	0.30	0.29	0.30	0.31	0.26
OH	2.68	2.65	2.60	2.61	2.62	2.19
Total	19.49	19.48	19.41	19.42	19.43	19.60

Garnet

	EGA	EGB	EGC	EGD	EGE
SiO_2	37.13	37.73	37.76	33.01	37.49
TiO_2	0.07	0.05	0.05	5.46	0.07
Al_2O_3	21.13	21.38	21.23	19.11	21.09
FeO	36.14	36.09	36.11	37.73	35.94
MnO	0.74	0.75	0.72	0.76	0.77
MgO	2.18	2.18	2.14	1.61	2.16
CaO	3.34	3.35	3.34	2.91	3.35
Total	100.73	101.53	101.35	100.59	100.87
Mg/Mg+Fe	0.097	0.097	0.096	0.071	0.097

Formula Oxygens	12	12	12	12	12
Si	2.98	3.00	3.01	2.72	3.00
Ti	0.00	0.00	0.00	0.34	0.00
Al	2.00	2.00	1.99	1.85	1.99
Fe	2.43	2.40	2.40	2.60	2.41
Mn	0.05	0.05	0.05	0.05	0.05
Mg	0.26	0.26	0.25	0.20	0.26
Ca	0.29	0.29	0.28	0.26	0.29
Total	8.01	8.00	7.98	8.02	8.00

C.2.6 TR27D

Orthopyroxene

	DPA	DPB	DPC	DPD	DPE
SiO_2	47.46	48.25	47.29	47.80	47.49
TiO_2	0.22	0.20	0.24	0.22	0.19
Al_2O_3	0.91	0.91	0.89	0.75	0.95
FeO	45.19	45.39	44.89	45.14	44.71
MnO	0.61	0.66	0.64	0.61	0.60
MgO	5.77	5.75	6.01	5.85	5.80
CaO	0.65	0.67	0.56	0.57	0.63
Total	100.81	101.83	100.52	100.94	100.37
Mg/Mg+Fe	0.186	0.184	0.193	0.188	0.188

Formula Oxygens	6	6	6	6	6
Si	1.97	1.98	1.97	1.98	1.98
Ti	0.01	0.01	0.01	0.01	0.01
Al	0.04	0.04	0.04	0.04	0.05
Fe	1.57	1.56	1.56	1.56	1.56
Mn	0.02	0.02	0.02	0.02	0.02
Mg	0.36	0.35	0.37	0.36	0.36
Ca	0.03	0.03	0.02	0.03	0.03
Total	4.00	3.99	4.00	3.99	3.99

C.2.7 TR27C

Orthopyroxene

	KPA	KPB	KPC	KPD	KPE
SiO_2	48.29	47.56	47.46	47.56	47.78
TiO_2	-	-	-	-	-
Al_2O_3	0.84	0.73	0.73	0.91	0.54
FeO	44.47	44.21	44.13	43.92	44.43
MnO	0.61	0.02	0.61	0.57	0.57
MgO	6.29	6.19	6.33	6.18	6.38
CaO	0.76	0.79	0.68	0.90	0.68
Total	101.26	99.50	99.94	100.04	100.38
Mg/Mg+Fe	0.202	0.200	0.204	0.201	0.204

Formula Oxygens	6	6	6	6	6
Si	1.98	1.98	1.98	1.98	1.99
Ti	-	-	-	-	-
Al	0.04	0.04	0.04	0.04	0.03
Fe	1.53	1.54	1.54	1.53	1.54
Mn	0.02	0.02	0.02	0.02	0.02
Mg	0.39	0.38	0.39	0.38	0.39
Ca	0.03	0.04	0.03	0.04	0.03
Total	3.99	4.00	4.00	4.00	4.00